DOT/FAA/TC-18/10

Federal Aviation Administration
William J. Hughes Technical Center
Aviation Research Division
Atlantic City International Airport
New Jersey 08405

Round-Robin Exercise for Tension Testing of Laminated Composites at Different Strain/Stroke Rates

July 2018

Final Report

U.S. Department of Transportation
Federal Aviation Administration

NOTICE

Technical Report Documentation Page

1. Report No.	2. Government Accession No.	3. Recipient's Catalog No.
DOT/FAA/TC-18/10		

4. Title and Subtitle	5. Report Date
ROUND-ROBIN EXERCISE FOR TENSION TESTING OF LAMINATED COMPOSITES AT DIFFERENT STRAIN/STROKE RATES	June 2018
	6. Performing Organization Code

7. Author(s)	8. Performing Organization Report No.
J. F. Acosta, G. Olivares, and S. K. Raju	

9. Performing Organization Name and Address	10. Work Unit No. (TRAIS)
National Institute for Aviation Research Wichita State University 1845 Fairmount Wichita, KS 67260-0093	
	11. Contract or Grant No.

12. Sponsoring Agency Name and Address	13. Type of Report and Period Covered
U.S. Department of Transportation Federal Aviation Administration Office of Aviation Research Washington, DC 20591	Final Report
	14. Sponsoring Agency Code AIR-600

15. Supplementary Notes

The FAA William J. Hughes Technical Center Aviation Research Division COR was Allan Abramowitz.

16. Abstract

There is a general lack of public domain information and data on the subject of the crashworthiness behavior of composite aircraft structures. More specifically, research on standardized protocols and data regarding high strain rate sensitivity and failure characteristics of continuous fiber-reinforced composite materials are limited.

The current investigation evaluated the test methods/apparatus and the force measurement methods employed by different laboratories when generating dynamic material properties. The tensile dynamic material response of Toray T700G/2510 plain weave carbon/epoxy fabric was the subject composite material characterized over a range of strain rates from 0.01 to 250 s-1. The work described herein was performed as a round-robin exercise by five participating research institutes.

Dynamic testing was conducted by various laboratories on a voluntary basis using either a high stroke servo-hydraulic testing machine or a Split Hopkinson Pressure Bar apparatus. Test methods/apparatus and load measurement methods employed by the participating laboratories were evaluated using extended tab 2024-T3 aluminum specimens.

The study developed a force signal correction methodology to correct for errant signal modulation caused by the response of the load frame of the servo-hydraulic testing machines during dynamic loading.

17. Key Words	18. Distribution Statement
Crashworthiness, Composites, Strain rate, Material models, Force signal correction, Errant signal modulation, Errant signal oscillation	This document is available to the U.S. public through the National Technical Information Service (NTIS), Springfield, Virginia 22161. This document is also available from the Federal Aviation Administration William J. Hughes Technical Center at actlibrary.tc.faa.gov.

19. Security Classif. (of this report)	20. Security Classif. (of this page)	21. No. of Pages	22. Price
Unclassified	Unclassified	203	

ACKNOWLEDGEMENTS

The authors would like to thank the following people for their support and participation in different activities of this round-robin exercise: coordination by FAA technical monitor A. Abramowitz; composite material donation by S. Tiam from Toray America; and testing by B. Mobasher, A. Bonakdar, and Y. Yao from Arizona State University, A. Johnson and M. David from the German Aerospace Center, M. Starbuck, D. Erdman and Y. Wang from Oak Ridge National Laboratory, A. Gilat from The Ohio State University, and graduate students Md Tareq Siddiqui and Iker Echavarri from the National Institute for Aviation Research/Wichita State University.

TABLE OF CONTENTS

LIST OF FIGURES

LIST OF TABLES

LIST OF ACRONYMS

ASU	Arizona State University
DIC	Digital image correlation
DLR	German Aerospace Center
FFT	Fast Fourier transform
NIAR	National Institute for Aviation Research
ORNL	Oak Ridge National Laboratory
OSU	Ohio State University
SHPB	Split Hopkinson Pressure Bar

EXECUTIVE SUMMARY

There is a general lack of public domain information and data on the subject of the crashworthiness behavior of composite aircraft structures. More specifically, research on standardized protocols and data regarding high strain rate sensitivity and failure characteristics of continuous fiber-reinforced composite materials are limited.

The current investigation evaluated the consistency of test methods/apparatus and the force-measurement methods employed by different laboratories when generating dynamic material properties. The tensile dynamic material response of Toray T700G/2510 plain-weave carbon/epoxy fabric was the subject composite material characterized over a range of strain rates from 0.01 to 250 s^{-1}. The work described herein was performed as a round-robin exercise by five participating research institutes.

Dynamic testing was conducted by various laboratories on a voluntary basis using either a high stroke servo-hydraulic testing machine or a Split Hopkinson Pressure Bar apparatus. Test methods/apparatus and load measurement methods employed by the participating laboratories were evaluated using extended tab 2024-T3 aluminum specimens.

The study developed a force signal correction methodology to correct for errant signal modulation caused by the response of the load frame of the servo-hydraulic testing machines during dynamic loading. Subsequently, the load measurement in the composite specimen tested using the servo-hydraulic machine was corrected for signal modulation and compared to the uncorrected data.

Data results and subsequent analysis from this combined effort tend to exhibit and reinforce the current limitations on material testing of this type. Evidence emerged that there is a lack of standardized methodology in pursuit of the subject testing, including equipment and terminology, thereby introducing undesirable results variability. The steps required to correct this situation are clear: an internationally recognized materials testing standard, at the coupon level, for high strain-rate testing of thermoset composite laminates should be created, so that systematic and repeatable material data can be generated.

The test results demonstrate both a test methodology for dynamic tension testing on servo-hydraulic machines and a correction methodology.

1. INTRODUCTION

There is a general lack of public domain information and data regarding the crashworthiness behavior of composite aircraft structures. More specifically, research on standardized protocols and data regarding high strain rate sensitivity and failure characteristics of continuous fiber-reinforced composite materials are limited. However, to design, evaluate, and optimize the crashworthiness behavior of composite structures to support the certification process—inclusive of numerical modeling techniques—it is necessary to first develop analytical methods and suitably predictive computational tools based on the building-block approach [1]. Consequent pursuit of the use of numerical tools based on this approach offers a cost-effective alternative to large or otherwise full-scale empirical testing.

Open literature reports variations in the material response of most materials when subjected to high strain rates. Examples of high strain rates are airplane/automobile accidents, impact or bird-strike events, plastic flow close to the tip of a fast propagating crack, high-speed metal forming [2]. Before including such effects in numerical modeling of structures, appropriate constitutive equations need to be developed.

However, characterizing the behavior of composites at the coupon level under dynamic loading conditions is not an easy task. Baselines for the stress-strain behavior of composites are generated at quasi-static to slow strain rates ($<1\ s^{-1}$) using traditional testing machines and load-sensing devices. However, at high strain rates, generating stress-strain curves represents a challenge; therefore, several test apparatuses are used to account for different strain rate ranges and different load measurement methods are used. However, no current standard exists for conducting such tests, only guidelines [3]. In addition, a standard procedure for extracting iso-strain-rate curves does not exist.

The current investigation evaluated the consistency of test methods/apparatus and the force measurement methods employed by different laboratories when generating dynamic material properties. The tensile dynamic material response of a subject composite material was characterized over a range of strain rates from 0.01 to 250 s^{-1}. The work described herein was performed as a round-robin exercise by five participating research institutes. The specific composite material was Toray - T700G/2510 plain weave carbon/epoxy fabric (F6273C-07M), whose selection was based on supporting the Composite Material Handbook organization (CMH-17) Crashworthiness Group activities. Test methods/apparatus and load measurement methods employed by the participating laboratories were comparatively evaluated using extended tab 2024-T3 aluminum (Al) specimens. The overall intent of inviting several laboratories to participate was to comparatively assess the level of homogeneity found in apparatus, method, and output data.

1.1 SCOPE

The primary objectives of the round-robin exercise were:

- Comparatively evaluate the test methods/apparatus employed by the participating laboratories.
- Evaluate load-measurement methods (load sensors) using aluminum specimens with extended tabs.

- Identify the limitations of dynamic material-testing techniques and their sources of variability.
- Generate tensile dynamic material properties of T700G/2510 plain weave carbon/epoxy fabric (F6273C-07M) from low-to-medium strain rates.

1.2 ROUND-ROBIN PARTICIPANTS AND PROCEDURE

Specimen fabrication, specimen instrumentation, and test fixture fabrication were performed by the National Institute of Aviation Research at Wichita State University (NIAR). NIAR also developed and distributed a test protocol to participating laboratories with instrumented test specimens. A preliminary quasi-static material characterization of the material systems was conducted first at NIAR. Subsequently, the following five laboratories conducted the subject dynamic testing:

- Arizona State University (ASU)
- German Aerospace Center (DLR)
- National Institute for Aviation Research (NIAR)
- Oak Ridge National Laboratory (ORNL)
- The Ohio State University (OSU)

Four laboratories conducted the subject dynamic tests using a high-stroke servo-hydraulic testing machine. The fifth laboratory used a Split Hopkinson Pressure Bar (SHPB) apparatus. Test results from the five labs were collected, analyzed, and summarized by NIAR using random generic identification IDs (Labs A to E). The repeatability and associated error analysis of experiments at each of the subject laboratories were quantified. Finally, a force signal correction methodology was developed and proposed to correct for errant signal oscillations (as read/indicated by the hydraulic load frame load cell) resulting from inherent load train inertial characteristics, wave propagations, and reflections.

2. TEST PROGRAM

The test methods described in this section summarize the test protocol and procedures distributed to all participants prior to conducting the tests. To reduce the variability associated with specimen preparation, all specimens were fabricated and instrumented by NIAR and then distributed to the participants. The specimen geometry per material is described with the corresponding instrumentation used to measure the material response. A preliminary quasi-static material characterization of all materials was conducted beforehand to generate baselines for evaluating strain rate sensitivity. Dynamic testing was conducted on an Al test specimen and one composite material system over a wide range of strain rates ranging between 0.01 to 250 s^{-1}. A brief description of the various test apparatuses used by the laboratories is included. A custom slack-inducer mechanism was used to enable the hydraulic systems to reach the desired speed prior to loading the test specimen.

2.1 MATERIAL SYSTEMS AND TEST SPECIMENS

Two material systems were employed in this round-robin exercise: 2024-T3 sheet Al (0.09 in/2.29 mm thick) [4] and Toray T700G/2510 plain weave/epoxy fabric [5]. Newport NB321/7781 fiberglass epoxy [6] was used for tabbing purposes on the composite specimens to protect the composite specimens from the grips during clamping.

The test specimens were fabricated, inspected, and instrumented at NIAR and shipped to participating labs. Laminates were fabricated using a single autoclave cycle and tabs bonded to subpanels from the same. The tabbed subpanels were machined to tolerance at NIAR. The nominal material properties of the above materials are summarized in table 1.

Table 1. Nominal mechanical properties of the material systems

Property	Material		
	2024-T3 bare [4]	Toray [5]	Newport [6]
Thickness/ply thickness (in)	0.010 – 0.128	0.0084	0.009
Young's Modulii (Msi)	E=10.5	E_1=8.12 E_2=7.97	E_1=4.19
Shear Modulus (Msi)	G=4.0	G_{12}=0.58	G_{12}=0.61
Poisson's Ratio	ν=0.33	ν_{12}=0.042	ν_{12}=0.138
Tensile Strength (ksi)	F_{TU}=65 (L)	F_{1t}=132 F_{2t}=112	F_t=63.5
Shear Strength (ksi)	F_{SU}=40	F_{12s}=22	F_{12s}=19

2.1.1 Metallic Specimen

2024-T3 Al was used as a control material to comparatively evaluate the capabilities of the different load-measurement systems. The dog-bone geometry, per ASTM E8 [7], of the Al specimens is shown in figure 1. Because it is well known that the elastic behavior of aluminum is insensitive to strain rates, the specimens were designed with an extended tab region, and strain gauges were mounted there to measure the load introduced into the specimen gauge region and therefore be able to compare it to the load cell measurement. This comparison was performed using frequency domain analysis, and signal modulations associated with the load cell measurements were quantified.

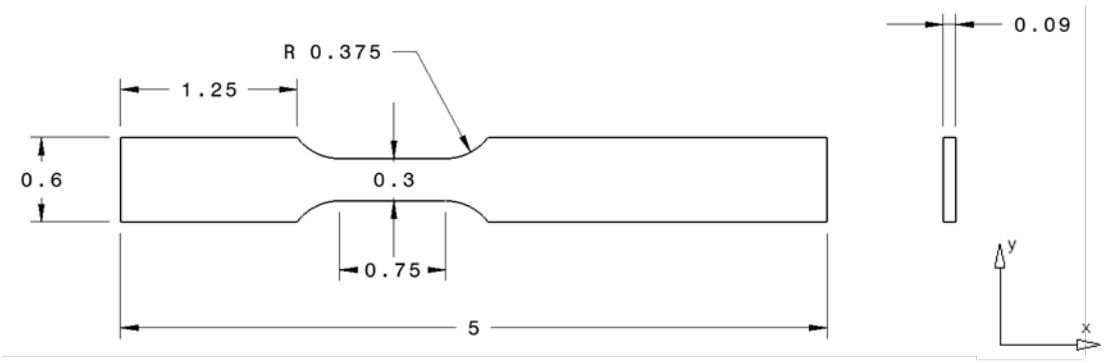

Figure 1. Geometry of 2024-T3 aluminum specimen with extended tab region [in]

2.1.2 Composite Specimen

The material system under evaluation was Toray-T700G/2510 Plain Weave carbon/epoxy fabric. Laminated composite panels were manufactured with traditional vacuum bag pre-preg lay-up and cured in an autoclave. Quality control was conducted on the panels by means of TTU C-Scans and fiber volume content measurements (47–53%). Composite specimens were extracted from the panels in three different orientations: $[0°]_4$, $[90°]_4$, and $[\pm45°]_4$. There was one stacking sequence along the principal material direction, another one perpendicular to it, and the last one with a balanced and symmetrical off-axis orientation at ±45°. The reference code used for the laminates is as follows:

1. $[0°]_N$
2. $[90°]_N$
3. $[+45°/-45°]_{NS}$

The geometry of the composite specimens is shown in figure 2. The specimens are straight-tabbed with reduced dimensions for high strain rate testing. Based on a previous study, this test geometry has been shown to produce material properties (strength and stiffness) equivalent to those generated using ASTM D3039 specimens [8]. The test specimens were tabbed using fiberglass tabs adhesively bonded. The nominal thickness of the tabs was 0.03 inches.

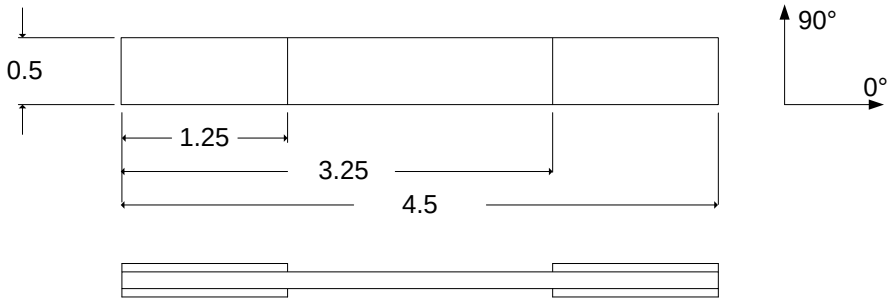

Figure 2. Geometry of laminated composite specimen [in]

2.2 SPECIMEN INSTRUMENTATION

The test specimens were instrumented with strain gauges at NIAR. Two axial strain gauges were attached to the Al specimens, one in the gauge region (Vishay model EP-08-250BG-120) and another in the extended tab region (Vishay model CEA-06-250UN-120). The composite specimens were also instrumented with two strain gauges, an axial gauge (Vishay model CEA-00-250UN-350) for the [0]n and [90]n specimens, and a biaxial gauge (Vishay model CEA-00-125UT-350) for the [+/-45] specimens, as shown in figure 3. In addition to strain gauges, one of the participating labs used photogrammetry as a secondary non-contact strain-measurement system. The grip region is also shown in figure 3; a 1.0-inch grip length was used. NIAR recommends a minimum grip length of 1.0 inch.

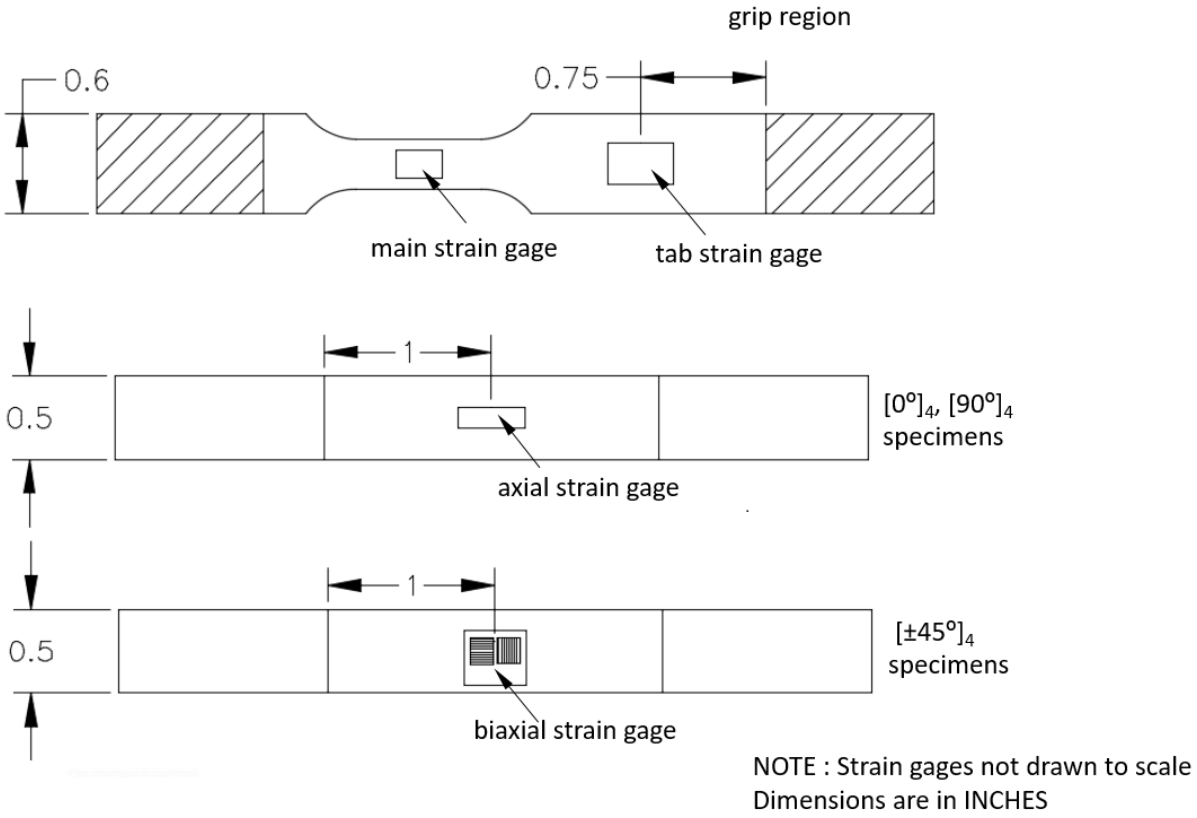

Figure 3. Strain gauge instrumentation for aluminum specimen and composite specimens [in]

2.3 DATA ACQUISITION SYSTEM AND DATA RECORDING

Data-acquisition rates commensurate with the associated stroke rate were specified in the test plan because each laboratory was permitted to use its acquisition system. However, data-acquisition cards in the data-acquisition systems were required to have a minimum resolution of 12 bits and be capable of simultaneous sampling on all channels. In addition, the application of any type of amplifier used to amplify the load or strain signals was required to be documented.

Labs A and B used a Vishay 2210 signal conditioner for the strain measurement. The data-acquisition system for Lab A was a National Instruments (NI) BNC-2090. Lab C used a Peekel Signalog 4000 signal conditioner for the strain measurement and a Gould Nicolet Technologies BE256XE data-acquisition system. Lab D used a Vishay 2310A signal conditioner for the strain measurement, an NI PXI 625 data-acquisition system for load and stroke, and an NI PXI 6259 data-acquisition system for the strain.

The minimum recommended data-acquisition rates and the recommended amplifier bandwidth at each nominal strain rate are summarized in table 2. Load, actuator displacement (if servo-hydraulic machines were used), and strain gauge readings for each test were recorded and submitted to NIAR for documentation and subsequent analysis. The displacement history is commonly measured in servo-hydraulic testing systems using linear positioning sensors, such as a linear variable differential transformer or a magnetostrictive sensor. The sensor is located in one end of the actuator.

Table 2. Recommended minimum data-acquisition rates and bandwidths

Nominal strain rate (1/s)	0.01	1	100	250
Recommended data acquisition rates	10^3 samples/sec	10^4 samples/sec	10^6 samples/sec	$3x10^6$ samples/sec
Amplifier bandwidth	10 kHz	10 kHz	100 kHz	100 kHz

The data acquisition for dynamic tests typically occurs over a time window larger than the duration of the specimen loading to failure, as shown in figure 4. Data points on either side of the loading pulse are required to correctly capture the system dynamics to facilitate frequency domain analysis using Fourier transforms. It was recommended to each lab that the minimum reported datasets consisted of data points spanning the window size shown in figure 4. This should include the load cell, the strain gauge, and the actuator displacement signals. The format for submitting the test data was provided in the form of a Microsoft® Excel® spreadsheet template.

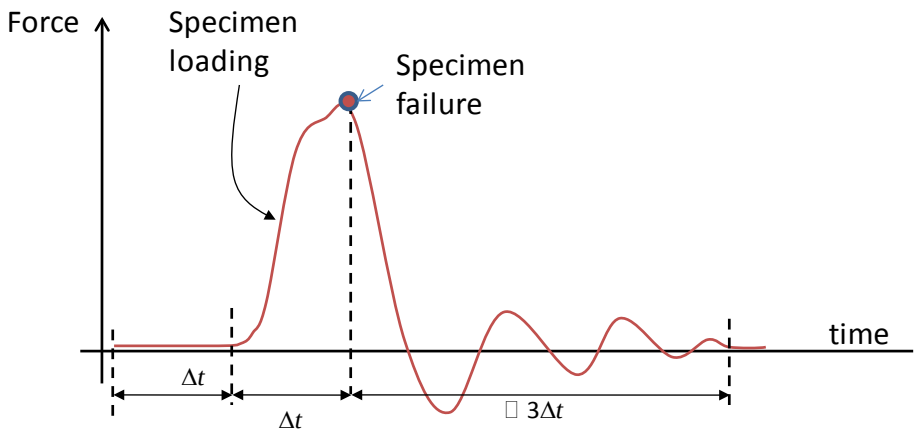

Figure 4. Typical time history of force during a tensile test

Labs D and E used ARAMIS, a non-contact digital image correlation (DIC) system, as an additional strain-measurement system. The DIC is a full-field measuring system that may increase accuracy of the strains measured and can be used as a valuable comparison against the strain gauge measurement.

2.4 TEST MATRIX

The test matrix is divided into quasi-static and dynamic testing. Because of the variability generally associated with composite material batches and processing, a limited number of quasi-static tests were performed at NIAR for each material to establish baseline properties and were sent to each laboratory with the instrumented specimens. The test matrix is shown in table 3. The tests were conducted three times for each of the four material types.

Table 3. Test matrix for quasi-static testing conducted at NIAR

Material System	Orientation	Nominal Strain Rate (1/s)
		Quasi-Static (0.000833)
2024-T3 Aluminum	[L]	×3
TORAY T700G/2510	$[0]_4$	×3
	$[90]_4$	×3
	$[\pm 45]_4$	×3

The test matrix for dynamic testing is summarized in table 4. Test specimens were intended for systematic testing at four nominal strain rates of 0.01, 1.0, 100, and 250 s^{-1} in each laboratory. The test plan called for three test runs of each material system and orientation at the predefined nominal

strain rates to obtain a measure of the statistics, while minimizing the number of tests. Extra specimens (×1 2024-T3 specimen and ×3 per material and stacking sequence) were provided to the labs to replace any errant tests.

Table 4. Test matrix for dynamic testing

Material System	Orientation	Nominal Strain Rate (1/s)			
		0.01	1	100	250
2024-T3 Aluminum	[L]	×3	×3	×3	×3
Toray T700G/2510	$[0]_4$	×3	×3	×3	×3
	$[90]_4$	×3	×3	×3	×3
	$[\pm 45]_4$	×3	×3	×3	×3

Because the tests using servo-hydraulic testing machines were conducted under stroke control rather than strain control, minimum stroke rates were recommended to each of the laboratories to achieve the desired strain rates, as shown in table 5. These values are based on the assumption that the actuator displacement translates directly into specimen elongation. Whereas this is true for the ideal case of rigid load frames, the recommended number was used as a starting point to achieve the strain rates desired in this program.

Table 5. Recommended stroke rates

Nominal strain rate (1/s)	0.01	1	100	250
Minimum recommended stroke rate (in/s)	0.02	2	200	500

2.5 QUASI-STATIC CHARACTERIZATION

The preliminary material characterization of the two material systems was conducted by NIAR using a standard 22 kip (100 kN) MTS servo-hydraulic machine with a 5.5 kip (25 kN) load sensor. Testing was conducted under displacement control at a rate of 0.00083 in/s (0.021 mm/s). The test control and data acquisition were carried out using MTS Basic TestWorks® software. Data acquired during testing included actuator displacement, force, and strain from the strain gauges mounted on the specimen. Strain gauge data were amplified using a Vishay 2210 signal conditioner. Testing was in accordance with standards ASTM E8 [7] for the Al specimens, and per ASTM D 3039 [8] for the composite specimens.

2.6 TESTING SYSTEMS FOR DYNAMIC CHARACTERIZATION

Two different types of systems were employed to conduct the subject dynamic material characterization: high-stroke servo-hydraulic testing machines and an SHPB. The machines used by the laboratories are not standard testing machines; rather, they are customized per laboratory requirements/specifications. Thus, capacity, control system, and parts and adaptors may differ in size and material. Laboratories also used their own gripping fixtures, load-measurement devices, data-acquisition systems, and strain-data conditioners. Details follow for each of the laboratories.

2.6.1 High-Stroke Servo-Hydraulic Testing Machine

Servo-hydraulic testing systems, as shown in figure 5, are frequently used for low-to-medium strain rates (0.000167 – 500 s^{-1}). Conventional servo-hydraulic systems are commonly used for quasi-static rates below 0.1 s^{-1}, and high-speed servo-hydraulic systems are used to examine the strain-rate regime between 0.1 and 500 s^{-1}. Higher actuator speeds are achieved with greater hydraulic power. The speed of this type of system is a function of the distance traveled by the actuator [1]. In addition, the ability to control the speed of the system is a function of the response capability of a servo-controlled system working in control-loop mode [9]. The open-loop control mode was used to meet the high-speed test requirements for the dynamic tests conducted. This allows maximum response to achieve the desired strain rate/speed and, by default, occurs before the specimen is loaded. The system shown in figure 5 includes a NIAR custom slack-inducer mechanism that allows the actuator to reach the desired speed before loading the specimen; the actuator accelerates over a predefined distance before engaging the slack rod attached to the bottom grip. Larger strain rates may be achieved using other test apparatuses, such as a drop-tower or drop-weight-impacts apparatus [10,11], a Charpy pendulum [12], an expanding ring [13,14], or a SHPB [15].

The test procedure for using the NIAR slack-inducer apparatus (appendix G) was sent to each of the labs. This was necessary to ensure that the use of the slack inducer of each laboratory was consistent and met specific requirements. A description of the four servo-hydraulic systems are described below.

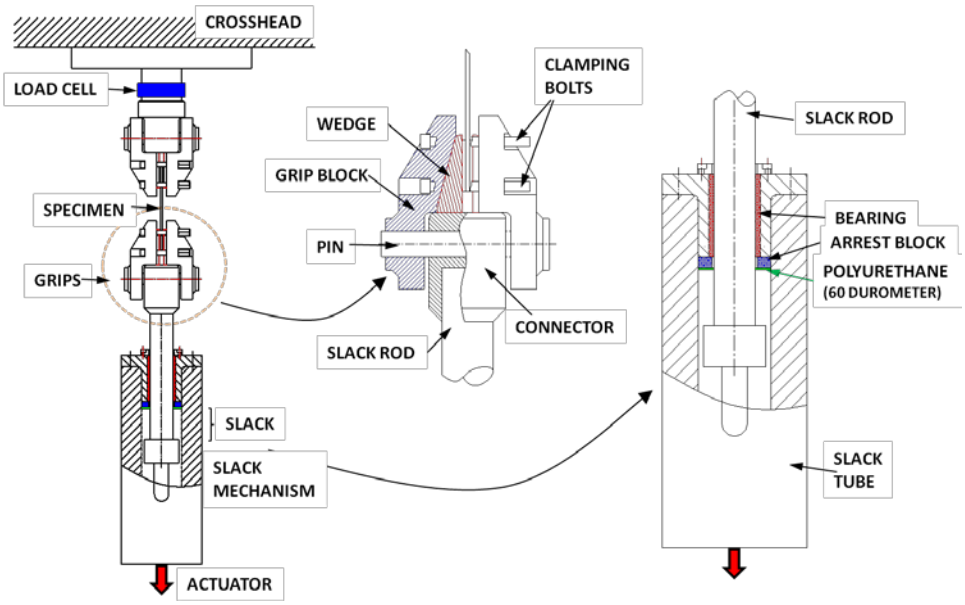

Figure 5. Schematic of servo-hydraulic testing system with custom slack inducer

System 1 used a MTS servo-hydraulic machine with a dynamic load capacity up to 5 kip, as shown in figure 6. The stroke rate ranges from 0.5 in/s to 550 in/s. Steel grips for high-rate testing were used. Load was measured using a Kistler 9041A piezoelectric load cell with a capacity up to 20.2 kip and a natural frequency of 33 KHz.

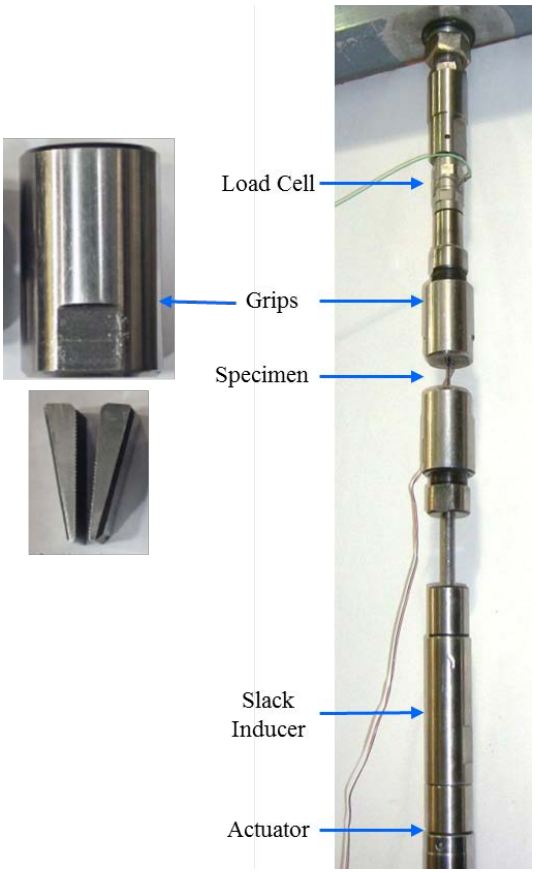

Figure 6. Servo-hydraulic testing system 1

System 2 used an Instron VHS 100/20 servo-hydraulic machine with a dynamic load capacity up to 22.5 kip and stroke rate capability of 780 in/s (see figure 7). Load was measured with a Kistler 9361B piezoelectric load cell, with a capacity up to 13.5 kip and a natural frequency of 28 KHz.

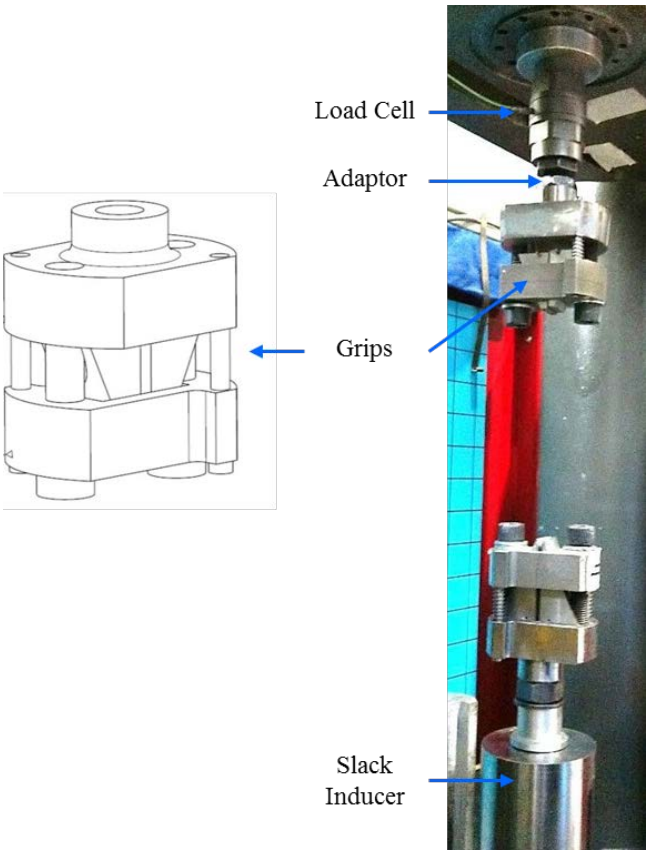

Figure 7. Servo-hydraulic testing system 2

System 3 used an MTS servo-hydraulic load frame with dynamic load capacity up to 5.5 kip and stroke rate capability of 700 in/s. The test apparatus was composed of a frame from a 100 kip MTS, driven with an MTS 407 servo-hydraulic controller, having an actuator with a single 400 gpm servo-valve supplied by two 5-gallon accumulators, as shown in figure 8. Low-mass titanium-alloy grips for high-rate testing were used. The moving mass between the sample and the load cell was reduced to increase the Eigen frequency of the test setup so that its effect on the stress-strain curves was minimized [15]. The load measurement was conducted with a Kistler 9051A piezoelectric load cell with a capacity of 9 kip and a natural frequency of 55 KHz.

System 4 used an MTS servo-hydraulic load frame that can provide dynamic loads up to 5 kip and stroke rates from 0.5–500 in/s. The test apparatus is shown in figure 9. Low-mass aluminum-alloy grips for high-rate testing were used. Load was measured using a PCB 206C piezoelectric load cell with a natural frequency of 40 KHz. The load cell was calibrated to 10 kip.

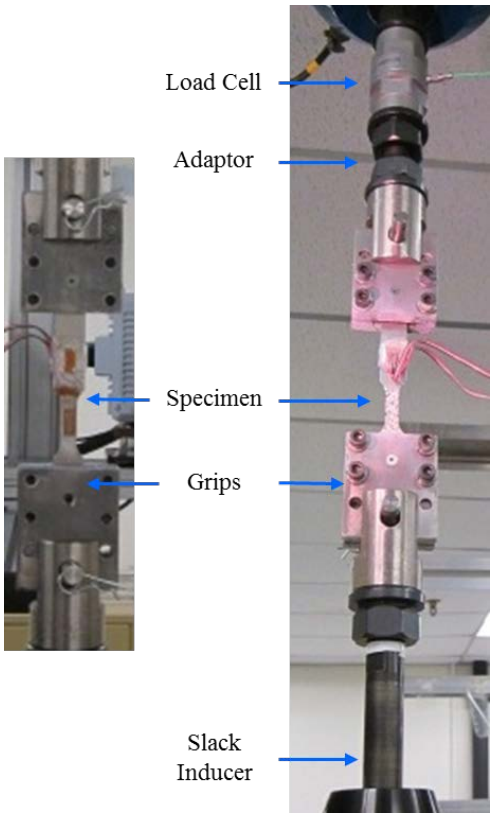

Figure 8. Servo-hydraulic testing system 3

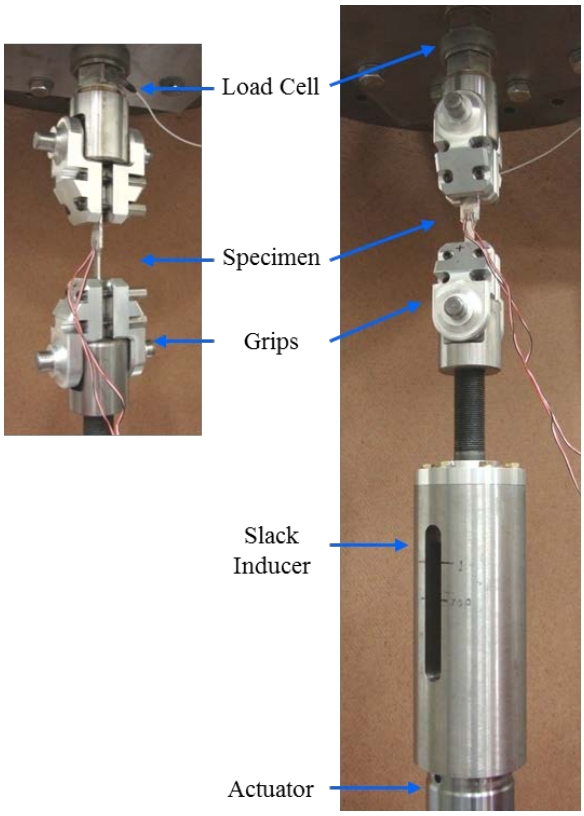

Figure 9. Servo-hydraulic testing system 4

2.6.2 SHPB

A tensile SHPB [16] was used to test the composite material Toray-T700G/2510 Plain Weave carbon/epoxy fabric. No metallic specimens were tested with this apparatus. A schematic of the apparatus is shown in figure 10. A SHPB for tensile-impact testing follows the same principles and data analysis methods as the classical compression SHPB. However, tensile and compression systems differ in the techniques used to grip the specimen, the methods for introducing the loading pulse, and the testing specimen geometry [17]. Details on the experimental technique are reported elsewhere [18].

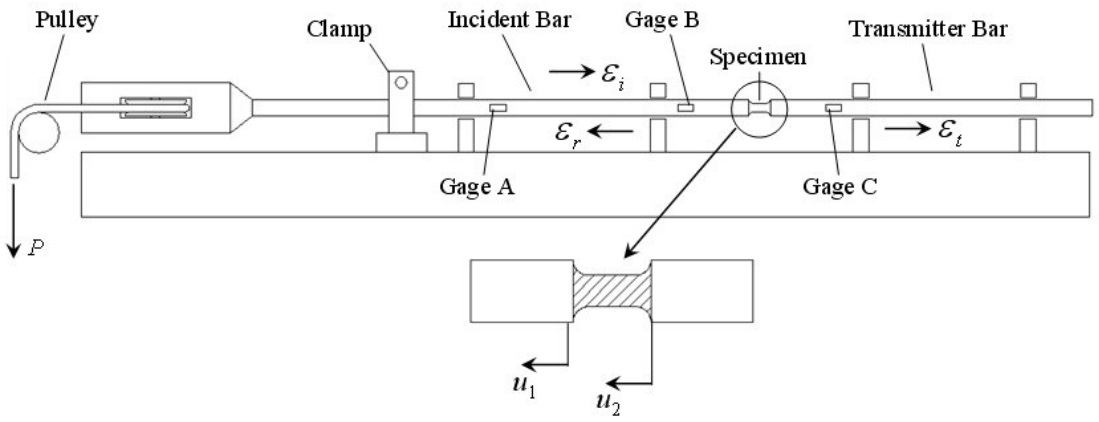

Figure 10. Tensile SHPB

Test results generated with the SHPB were suitable for comparison only at the high end of the strain rates generated with a servo-hydraulic machine (250 s^{-1}). Pressure-bar apparatuses are traditionally used to introduce a higher range of strain rates when compared to mechanical testing systems [19]. The apparatus not only differs from a servo-hydraulic machine in the strain rate range of application but also in the specimen size. It requires a significantly smaller size specimen than a standard specimen. The specimen geometry is shown in figure 11.

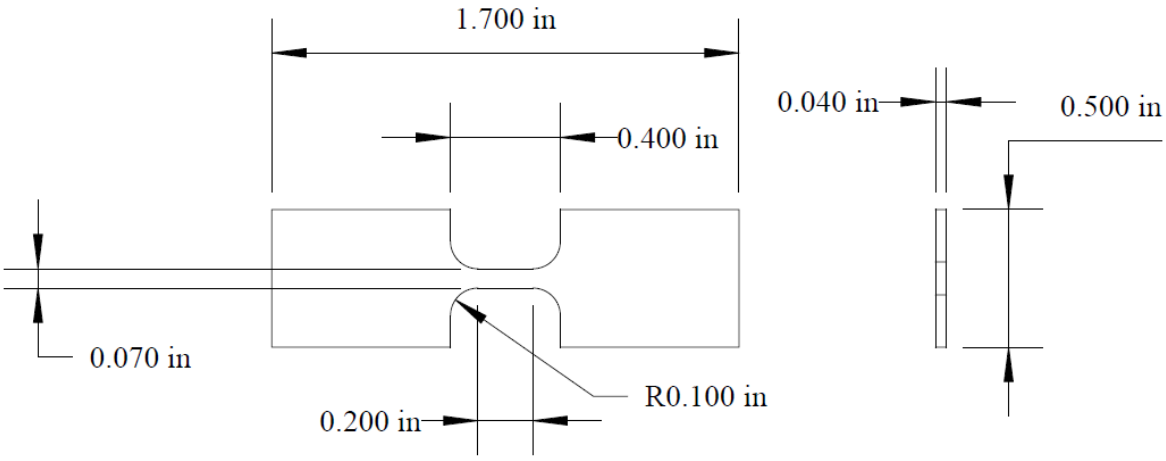

Figure 11. Sub-size composite specimen for SHPB

Strain histories were recorded in the incident bar and transmitted bar, and one-dimensional wave propagation theory was enforced to estimate average stress and average strain in the specimen. In addition, the strain in the specimen was measured directly over the specimen using digital image correlation, as shown in figure 12.

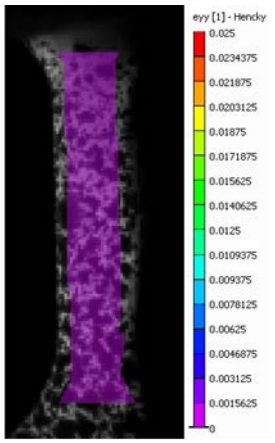

Figure 12. Example of ARAMIS image correlation strain distribution on a SHPB specimen

3. TEST RESULTS AND DATA ANALYSIS

Error analysis of experimentally generated materials properties reveals the cumulative effect of the inherent random variability of the material itself, and any random and systemic error of the measurement system. In the case of well-characterized common metals with consistent production qualities and associated well-defined moduli, typically precise and accurate properties measurements can be obtained within the elastic domain. However, composite materials routinely prove more difficult in the determination and separation of error bounds on material variability, and on measurement uncertainties, especially at high-strain rates encountered in dynamic tensile testing. The participating laboratories in this study were aware of this challenge, and this was a key reason for their involvement. Although there are other techniques to test at higher strain rates, in this exercise, data were obtained using high-speed servo-hydraulic machines and an SHPB. The test results for Laboratories A–D can be found in appendices A–D, respectively. The results of the SPHB tests are in appendix E, and the results of the quasi-static tests conducted by NIAR can be found in appendix F.

3.1 EXPERIMENTAL DATA ANALYSIS

Material properties including failure strength and strain rate were obtained for the material systems listed in section 2.1. All tests were conducted at nominal room temperatures. Target nominal strain rates for the subject composite material were: 0.00041, 0.01, 1.0, 100, and 250 s^{-1}.

The descriptive statistics used to evaluate the variability within the experimental data included the mean ($\bar{x}$), standard deviation (s), and coefficient of variation (CV), which are defined in equations 1–3, respectively [20]. The CV is defined as the residual variability in the data as a percentage of the mean. Error bars shown in the data histograms simply exhibit the max/min of the subject data range. In the current investigation, these statistics are estimated based on three samples only, and, therefore, they are used for reference only.

$$\bar{x} = \frac{\sum_{i=1}^{n} x_i}{n} \tag{1}$$

$$s = \sqrt{\frac{1}{n-1}\sum_{i=1}^{n}\left(x_i - \bar{x}\right)^2} \tag{2}$$

$$CV = \frac{s}{\bar{x}} \cdot 100\% \tag{3}$$

3.1.1 Quasi-Static Data Analysis

Quasi-static testing was conducted by NIAR with the specific intent of generating a baseline for a strain-rate effect comparative evaluation. Variability results are summarized in figures 13–15. The histograms show average material properties with error bars and the CV. As observed in figure 14 there is a difference/variation in the quasi-static strain rate. Quasi-static tests were conducted under displacement control in which the actuator speed is controlled. However the compliance of the components (slack adapter, grips, etc.,) between the actuator and the specimen contributes to the strain rate not being uniform. Since different specimens have different stiffnesses, they are affected differently by the compliance of the testing machine.

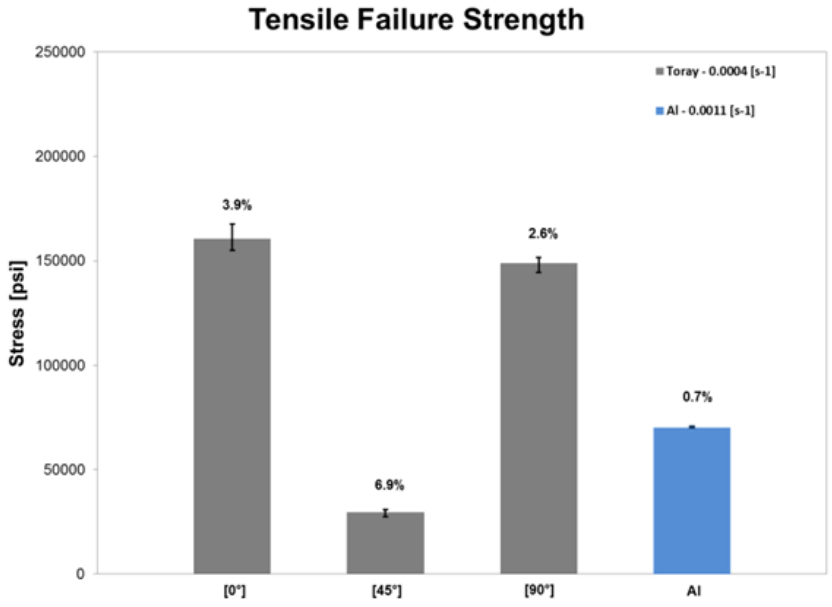

Figure 13. Average quasi-static tensile failure strength and CV of all material systems

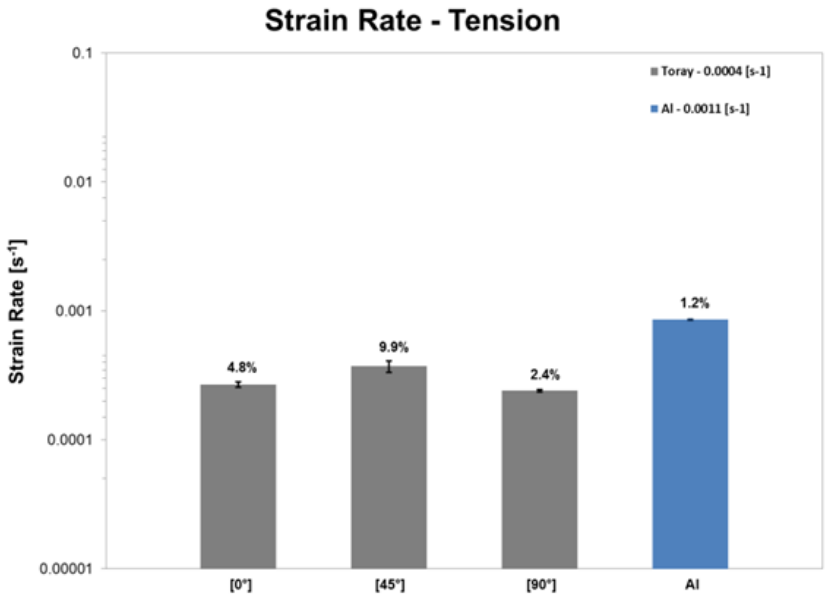

Figure 14. Average quasi-static strain rate and CV of all material systems

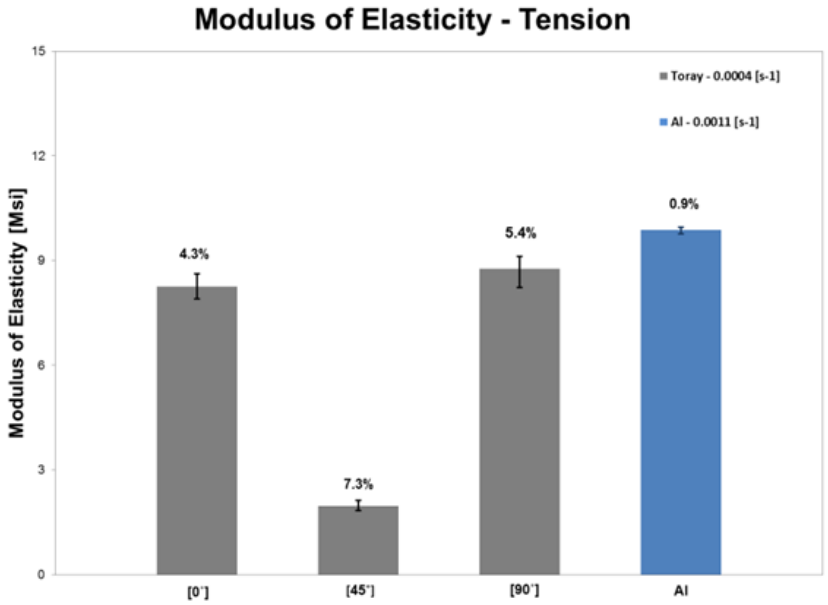

Figure 15. Average quasi-static modulus of elasticity of all material systems

3.1.2 Al 2024-T3 Dynamic Testing Results

Al 2024-T3 results are the control data for load-sensor evaluation. The modulus of elasticity for aluminum was essentially the same across the different stroke rates and was not plotted. Variability results are summarized in figures 16 and 17. The histograms show average material properties with respective error bars and coefficient of variation for only Laboratory A as a reference.

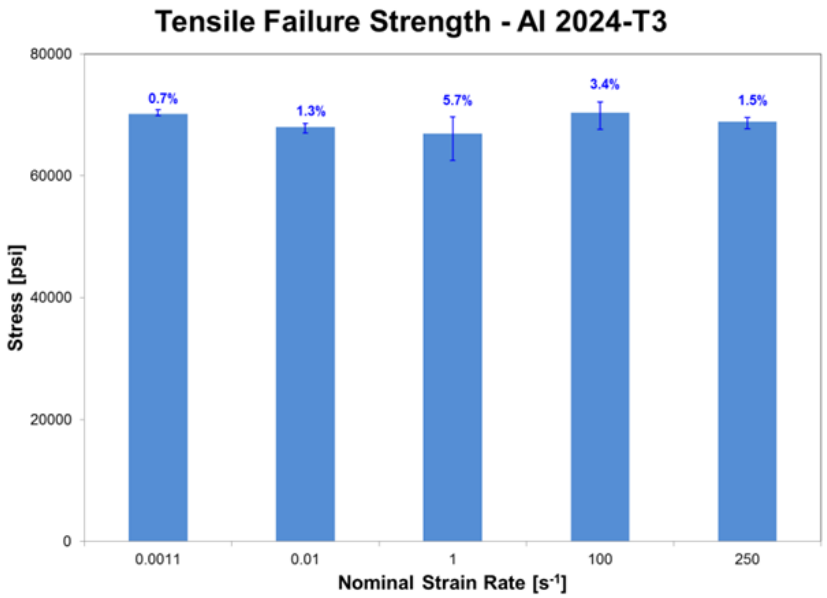

Figure 16. Average tensile failure strength of Al 2024-T3 at various nominal strain rates for Laboratory A

Average failure strength of the Al 2024-T3 in figure 16 suggests the material is insensitive to the evaluated strain rates. It is deemed that the coefficients of variation shown, falling within a few percent, are acceptable for the subject Al. Although data from the other labs are not shown, results analysis indicates comparable data correlation.

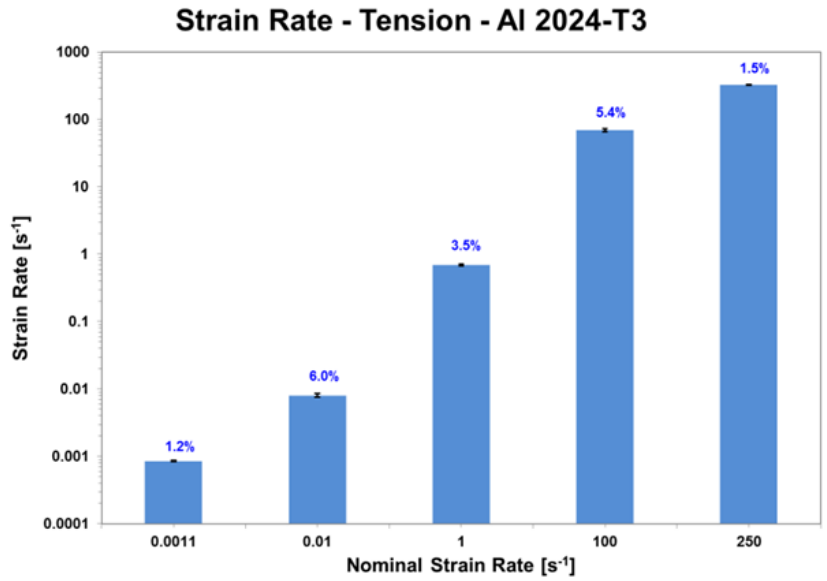

Figure 17. Average strain rate of Al 2024-T3 at various nominal strain rates for Laboratory A

3.1.3 Toray T700G/2510 Dynamic Testing Results

The variability of material properties for Toray T700G/2510 is summarized in figures 18–29 for all participating laboratories. Apparent tensile failure strength and average strain rate are summarized in histograms showing the average material properties, error bars, and coefficient of variation. All histograms show baseline quasi-static data generated by NIARU for comparison purposes. Plots showing the variation of apparent tensile failure strength with increasing strain rate are also presented for each laboratory. These plots provide an overview of the capability of generating repeatable results for each single laboratory.

Laboratory A results are shown in figures 18–20. Average strain rate results show the CV below 10% overall with a nominal strain rate of 1 s^{-1} having the smallest CV across all four nominal strain rates for all three material orientations. Conversely, apparent tensile failure strength shows more scatter in the results but below 10% CV. Note that although the results exhibit some unevenness in the coefficients of variation, the values, taken collectively, do not seem to exceed normative expectations of the subject material.

Apparent tensile failure strength in figure 20 may indicate an upward trend with increasing strain rate; this dependency is neither atypical nor unexpected. Note, these apparent values remain to be "corrected" via a signal correction methodology, which is presented in section 4.

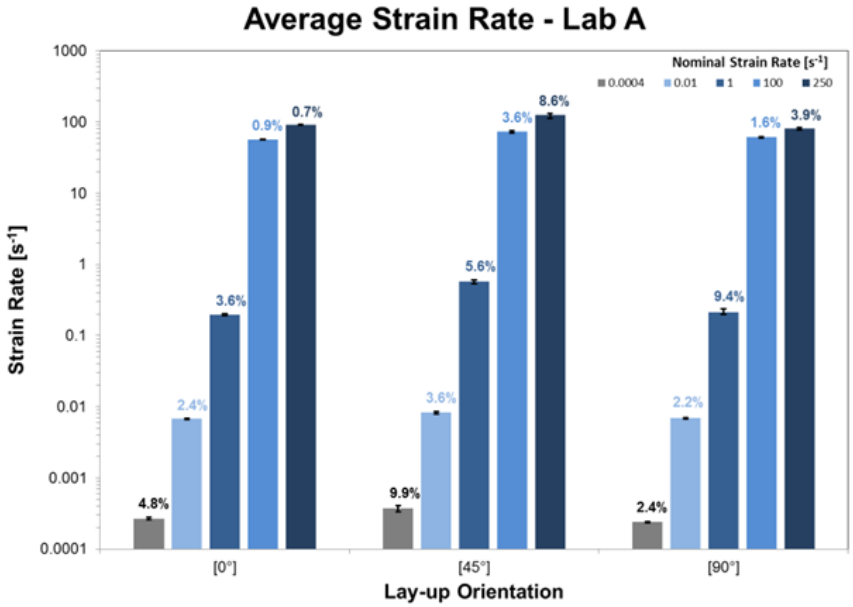

Figure 18. Variability of strain rate of Toray T700G/2510 at various nominal strain rates for Laboratory A

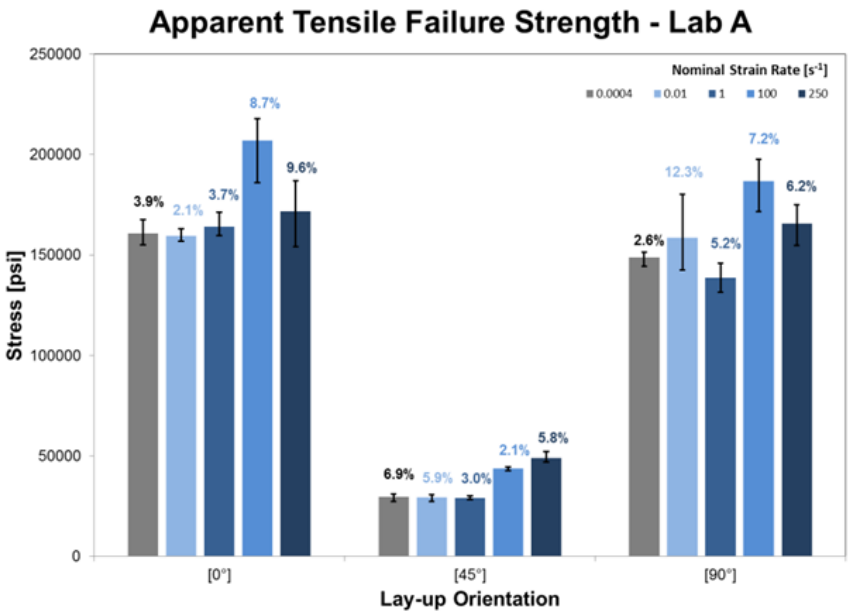

Figure 19. Variability of apparent tensile failure strength of Toray T700G/2510 at various nominal strain rates for Laboratory A

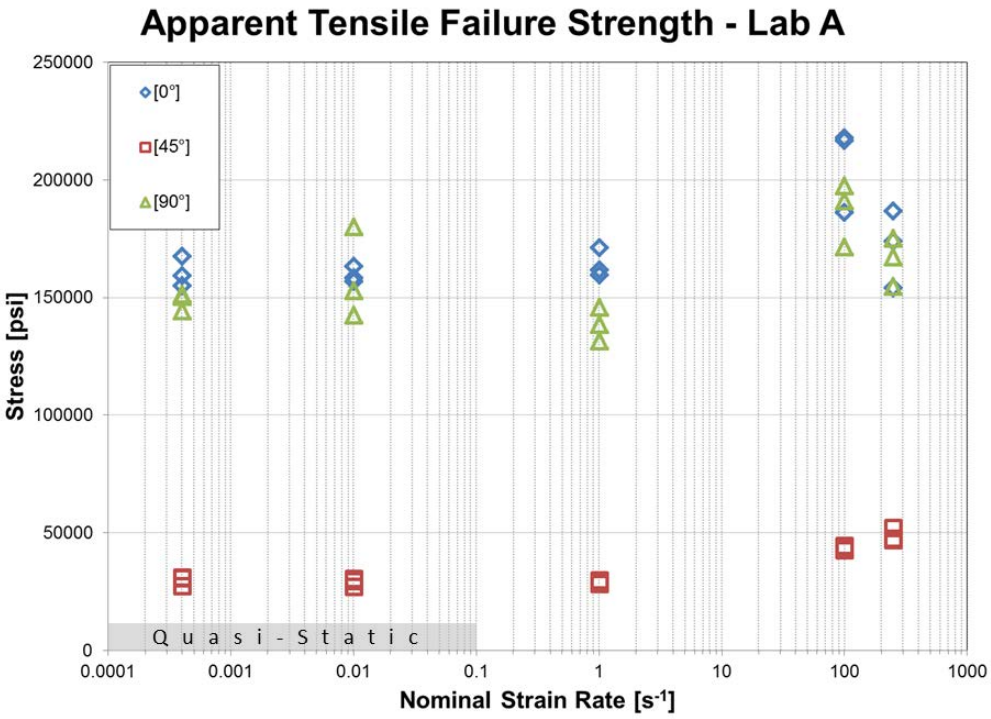

Figure 20. Apparent tensile failure strength of Toray T700G/2510 at various nominal strain rates for Laboratory A

Laboratory B results are summarized in figures 21–23. Note that only three of four rates were conducted; Laboratory B did not test for target nominal strain rate 250 s^{-1}, apparently having mixed

up the requested strain rate for stroke rate. Variability results show different levels of scatter for the various rates and material orientations, with CV not surpassing 11%.

The apparent tensile failure strength in figure 23 suggests a downward trend with increasing nominal strain rate. However, these are only apparent results before correction for signal modulation.

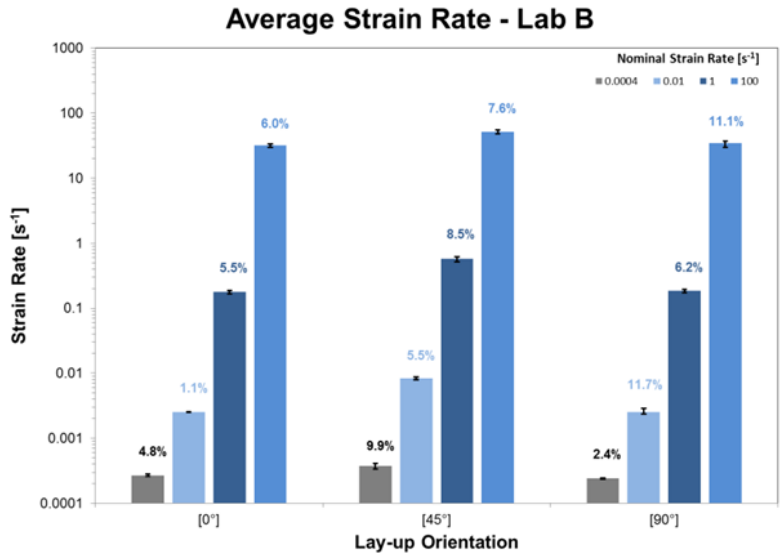

Figure 21. Variability of strain rate of Toray T700G/2510 at various nominal strain rates for Laboratory B

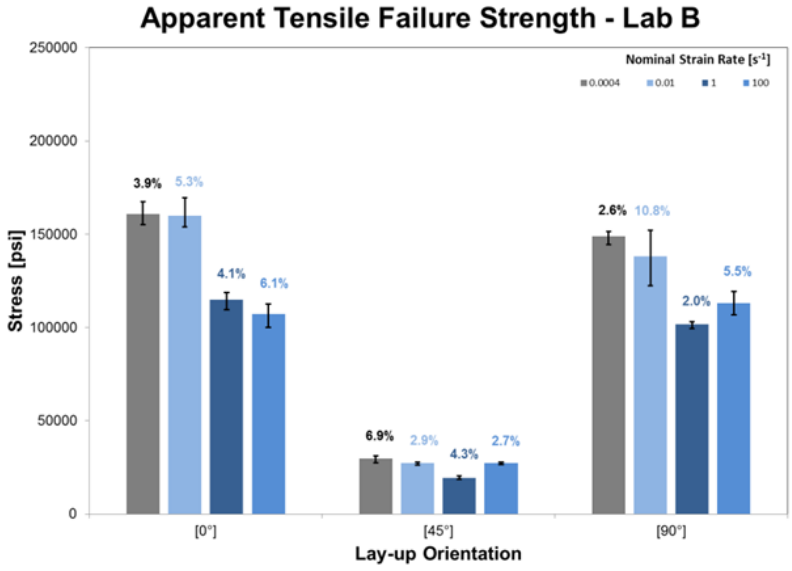

Figure 22. Variability of apparent tensile failure strength of Toray T700G/2510 at various nominal strain rates for Laboratory B

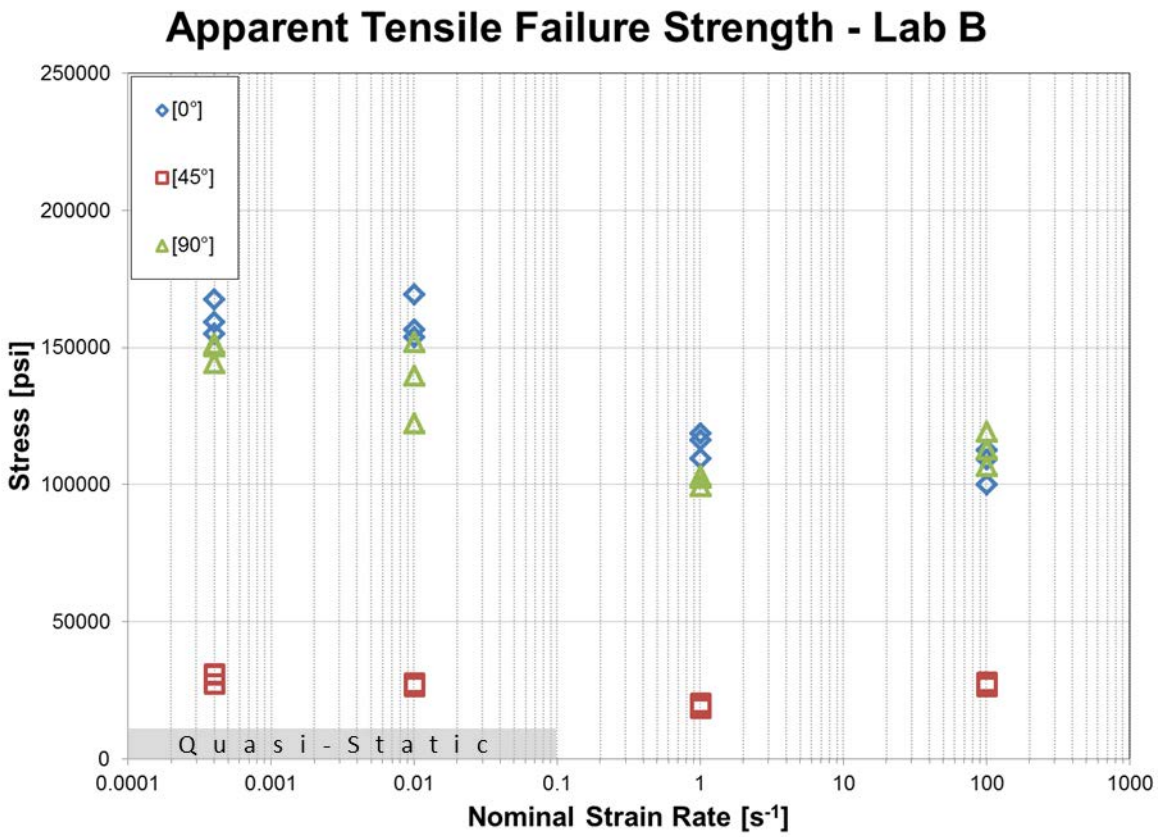

Figure 23. Apparent tensile failure strength of Toray T700G/2510 at various nominal strain rates for Laboratory B

Laboratory C results are summarized in figures 24–26. Results show few CV above 10% but no particular anomalies or surprises in the data. Average strain-rate results show a CV of [0°], slightly above 10%, for the various nominal strain rates. Average tensile failure strength also shows CV above 10% but for [90°] for two of the nominal strain rates.

The apparent tensile failure strength in figure 26 suggests an upward trend with an increasing nominal strain rate before load-signal modulation correction.

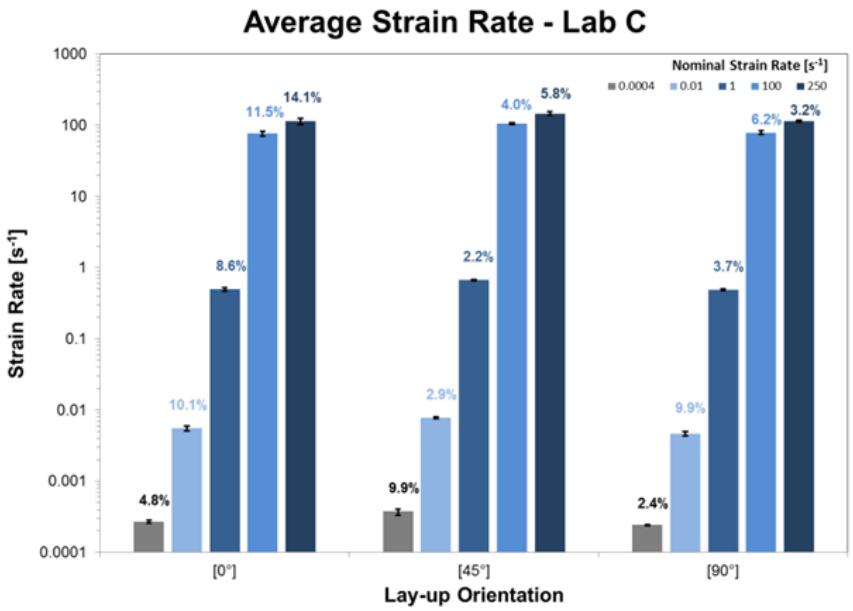

Figure 24. Variability of strain rate of Toray T700G/2510 at various nominal strain rates for Laboratory C

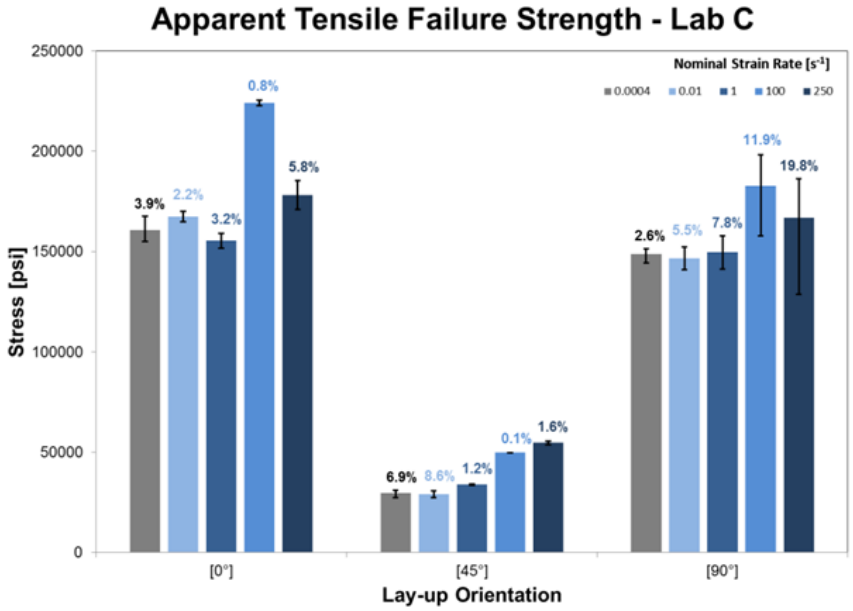

Figure 25. Variability of apparent tensile failure strength of Toray T700G/2510 at various nominal strain rates for Laboratory C

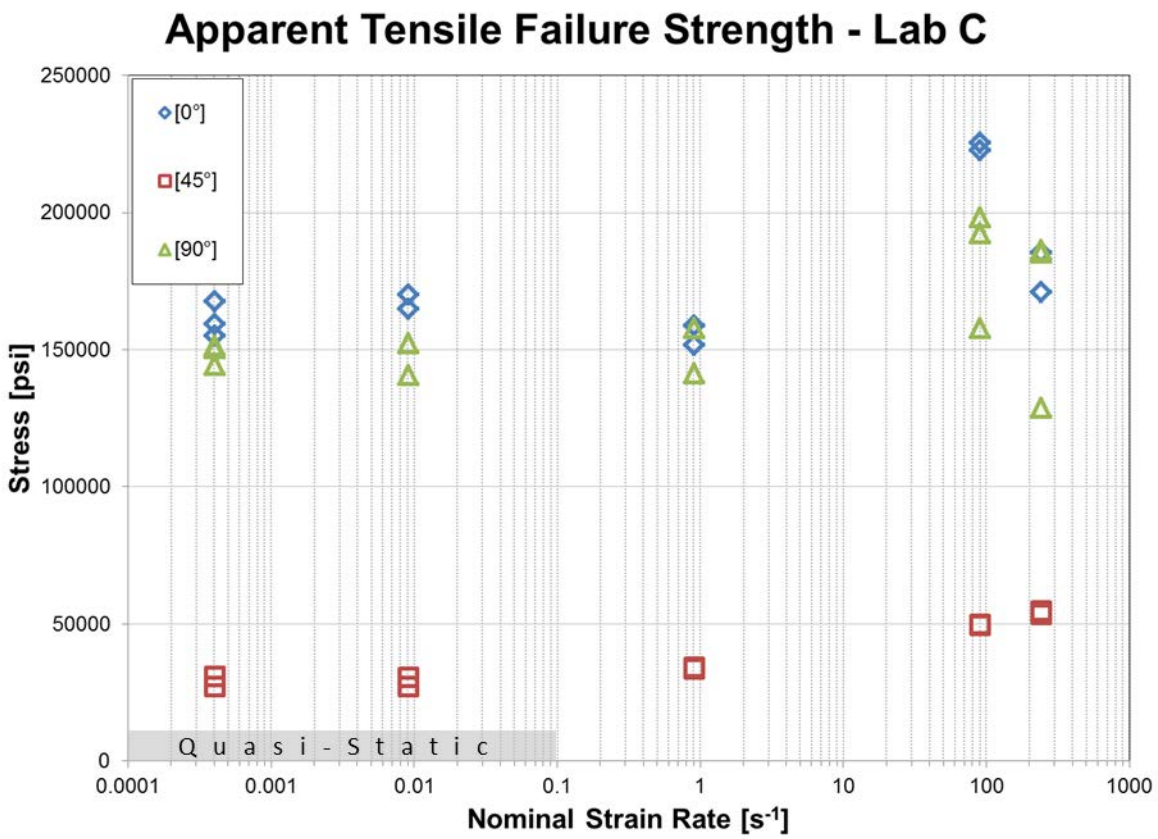

Figure 26. Apparent tensile failure strength of Toray T700G/2510 at various nominal strain rates for Laboratory C

Laboratory D results are summarized in figures 27–29. In general, results show slightly higher CV than the other laboratories but without particular anomalies or surprises in the data. Average strain-rate results show the CV of [45°] as high as 16.9% for a nominal strain rate of 0.01 s^{-1}. Average tensile failure strength also shows the CV as high as 16.7% for [45°] for nominal strain rate 250 s^{-1}.

The apparent tensile failure strength results shown in figure 29 exhibit some level of strain-rate sensitivity for the three material orientations until the nominal strain rate was 100 s^{-1}. However, these results remain to be corrected for load-signal modulation.

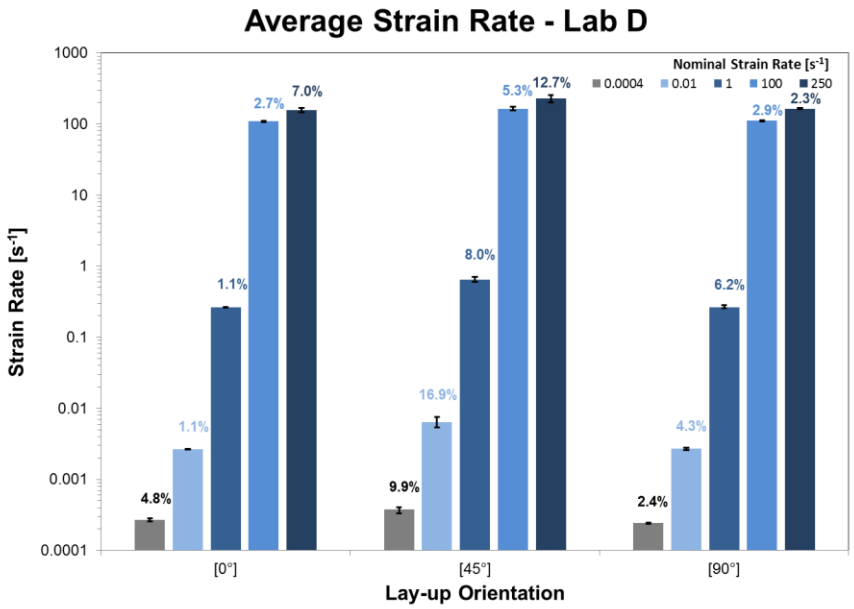

Figure 27. Variability of strain rate of Toray T700G/2510 at various nominal strain rates for Laboratory D

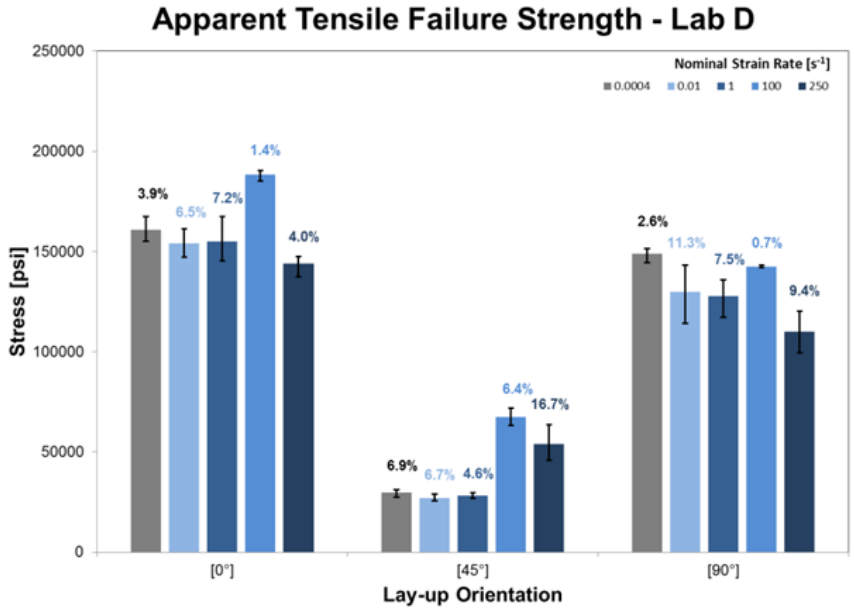

Figure 28. Variability of apparent tensile-failure strength of Toray T700G/2510 at various nominal strain rates for Laboratory D

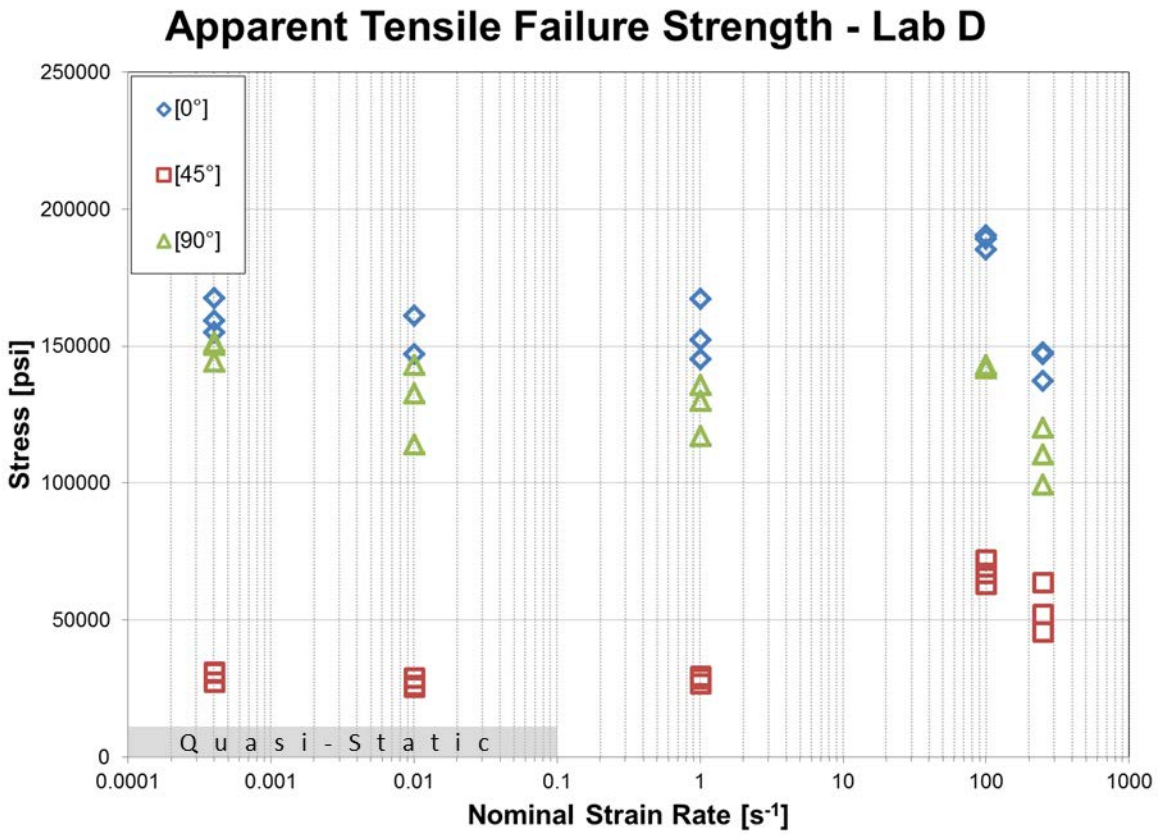

Figure 29. Apparent tensile-failure strength of Toray T700G/2510 at various nominal strain rates for Laboratory D

3.2 LAB-TO-LAB DATA VARIABILITY

Test results collected in the course of this investigation can also be evaluated by comparing laboratory results per material orientation. Beyond looking at each laboratory capability of generating repeatable results, comparing results between laboratories provides insight about the challenge that laboratories face when generating material properties at higher strain rates, even using equivalent test apparatus. Apparent tensile-failure strength results are shown collectively in figures 30–32 for each of the three material orientations before load signal correction. Note quasi-static results from NIAR as well as sub-size SHPB specimen data are included in these figures for reference. The side note "Conventional servo-machine" refers to the fact that sub-sized SHPB specimens were tested in a conventional servo-hydraulic machine to generate quasi-static data. To add clarity to the plots in figures 30–32, the strain-rate data were shifted around the nominal strain rates (0.01, 1.0, 100, and 250) for each lab.

Figure 30 shows the apparent tensile-failure strength results for [0°] orientation. The scatter in the results increases with increasing nominal strain rate. Note these are the apparent results, and no further conclusions should be deduced before comparing the corrected results.

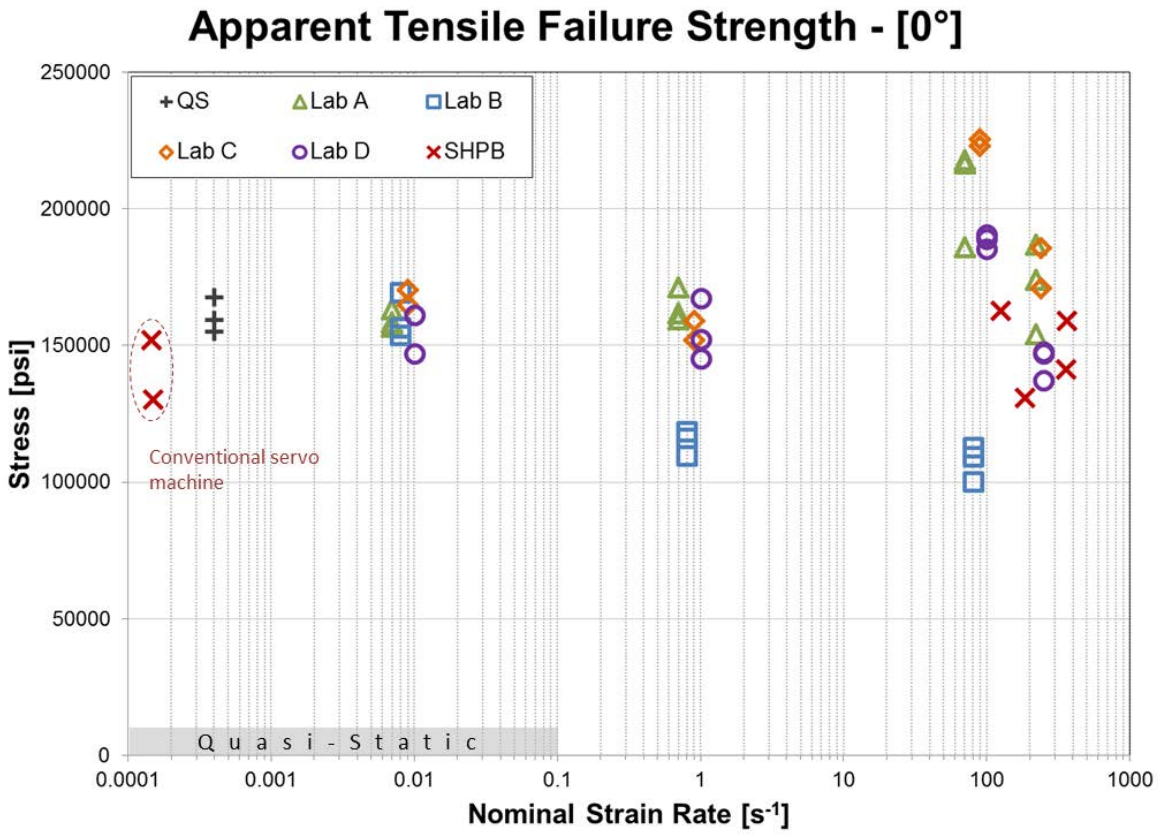

Figure 30. Apparent tensile-failure strength of [0°] orientation of Toray T700G/2510 at various nominal strain rates for all laboratories

Results for [90°] orientation are shown in figure 31. Similar levels of scatter are shown in the results with increasing nominal strain rate before load-signal correction.

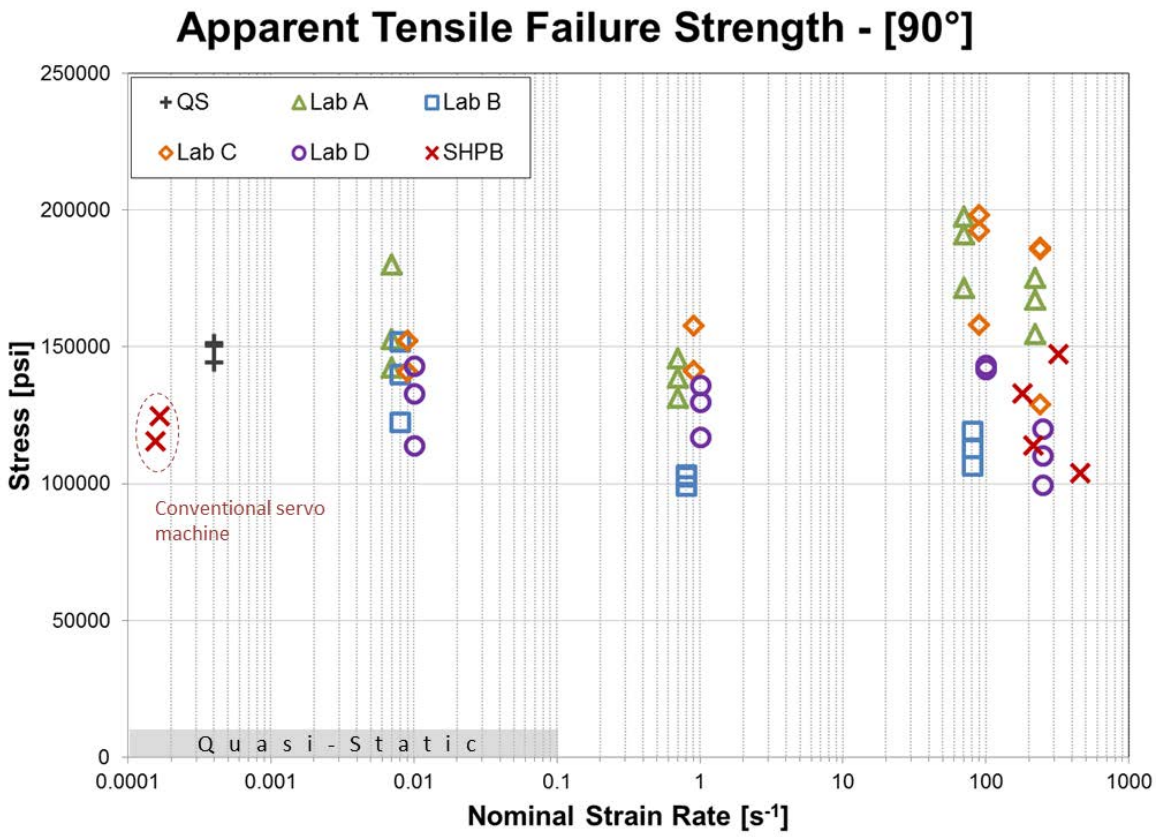

Figure 31. Apparent tensile failure strength of [90º] orientation of Toray T700G/2510 at various nominal strain rates for all laboratories

Figure 32 shows the apparent tensile failure strength for [45°] orientation. Scatter in the results increases with an increasing nominal strain rate before load signal correction. However, there seems to be lower scatter levels when compared with the other two material orientations.

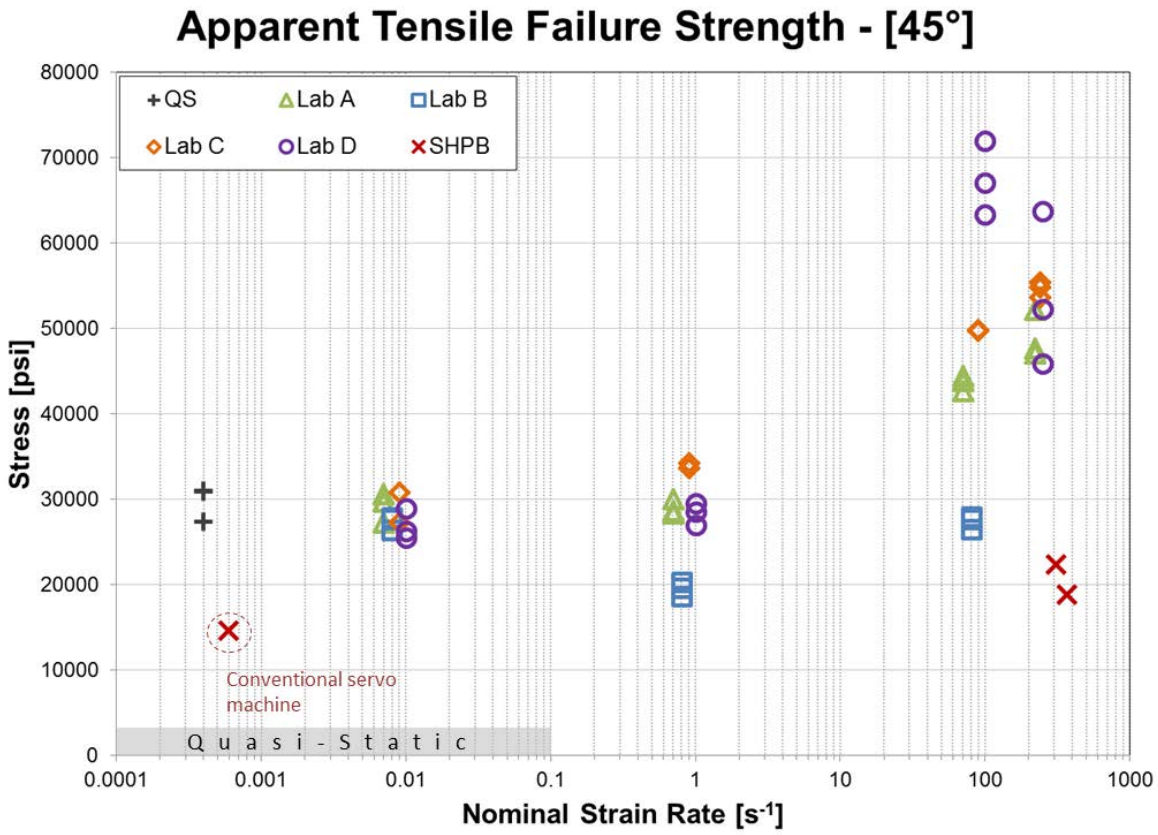

Figure 32. Apparent tensile failure strength of [45º] orientation of Toray T700G/2510 at various nominal strain rates for all laboratories

3.3 VELOCITY DROP ON SERVO-HYDRAULIC SYSTEMS

Incorporating slack inducers into servo-hydraulic load frames provides better means to reach higher stroke rates. However, results from this investigation suggest uncertainty about accurate control of the incident velocity on the test specimen. The actuator velocity drops when the slack inducer engages the lower grip of the testing device. This observation was common across laboratories.

Displacement histories of material orientation [0º] at a stroke rate of 2 in/s for each laboratory, which are shown in figure 33, reveal a drop in velocity at the time of engagement (t = 0). Note the actuator is moving at the indicated stroke rate prior to engaging the bottom end of the grip, but its velocity drops after encountering the grip. Such a velocity drop seems to be more pronounced for some laboratories, but deceleration is experienced to some degree by all test apparatuses.

The effect of the drop in the actuator velocity is also clear in other measurements of the test as the strain history, the strain rate history, and the force history shown in figures 34–36 for a stroke rate of 2 in/s. Table 6 summarizes the velocity before and after engagement of the slack inducer of each laboratory at a stroke rate of 2 in/s, and the percentage drop and the average strain rate. Each percentage drop is the result of a unique combination of load frame and fixtures.

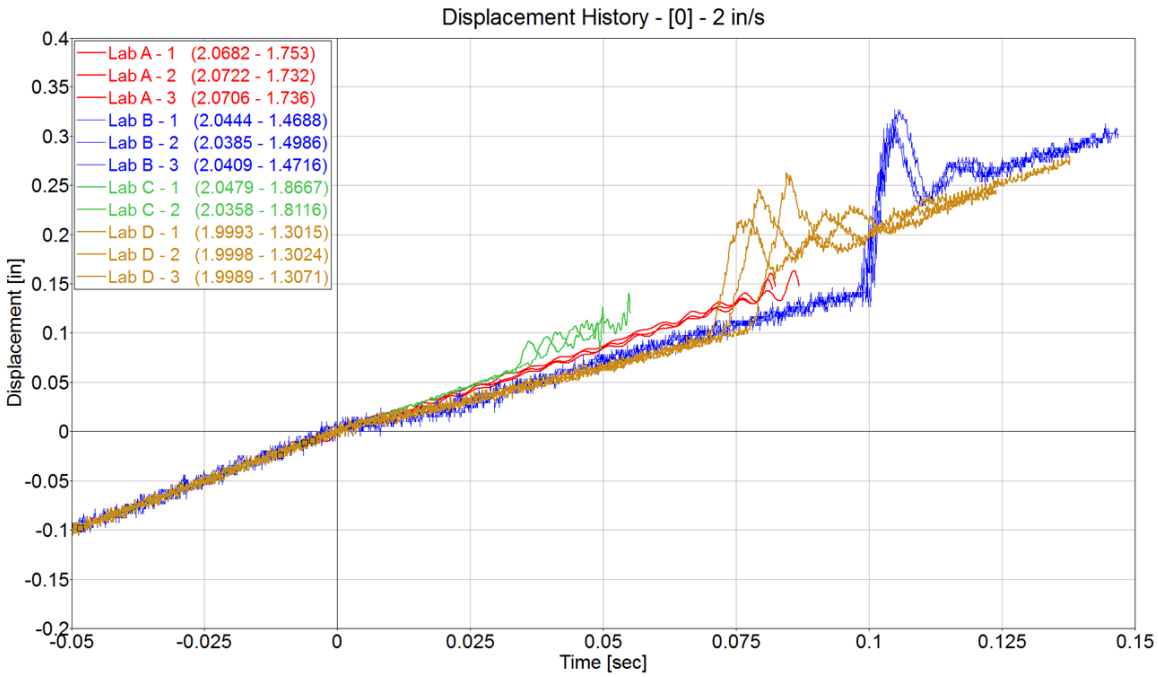

Figure 33. All laboratories' displacement history of [0º] orientation of Toray T700G/2510 at stroke rate of 2 in/s

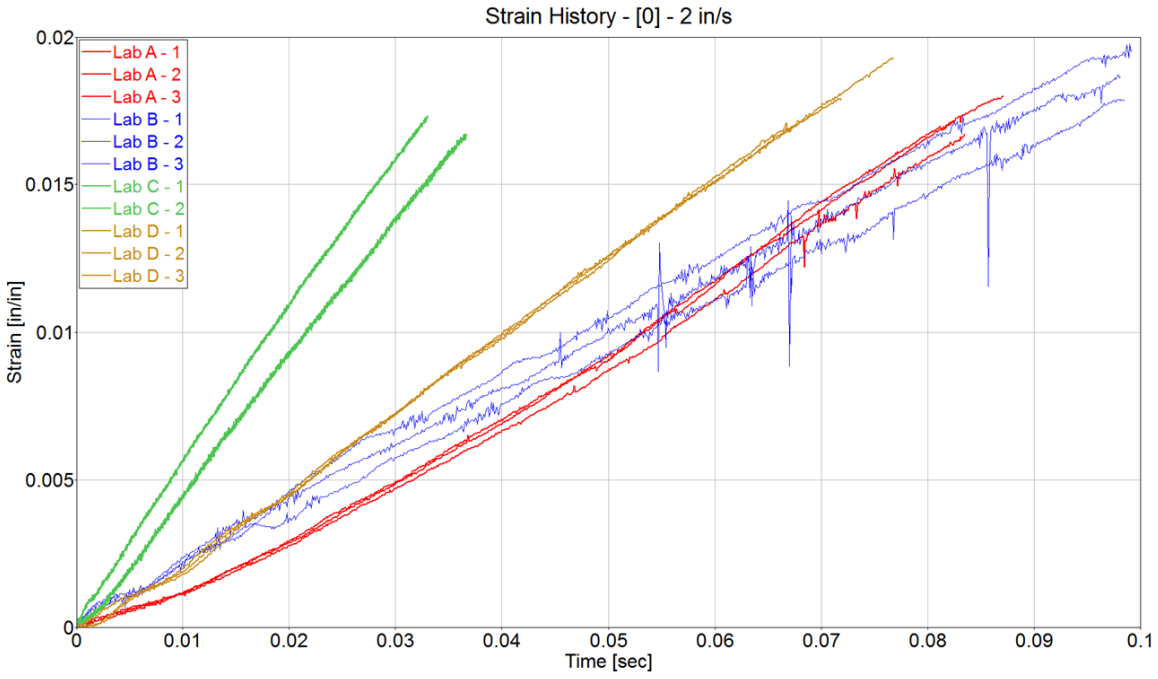

Figure 34. All laboratories' strain history of [0º] orientation of Toray T700G/2510 at stroke rate of 2 in/s

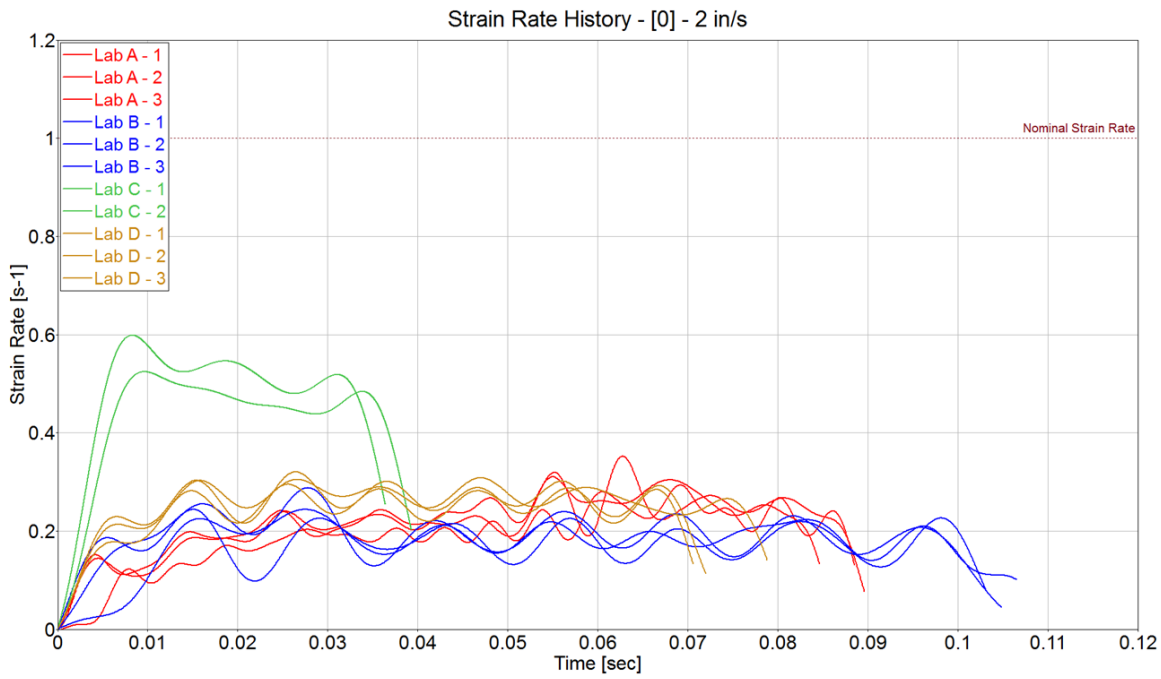

Figure 35. All laboratories' strain rate history of [0º] orientation of Toray T700G/2510 at stroke rate of 2 in/s

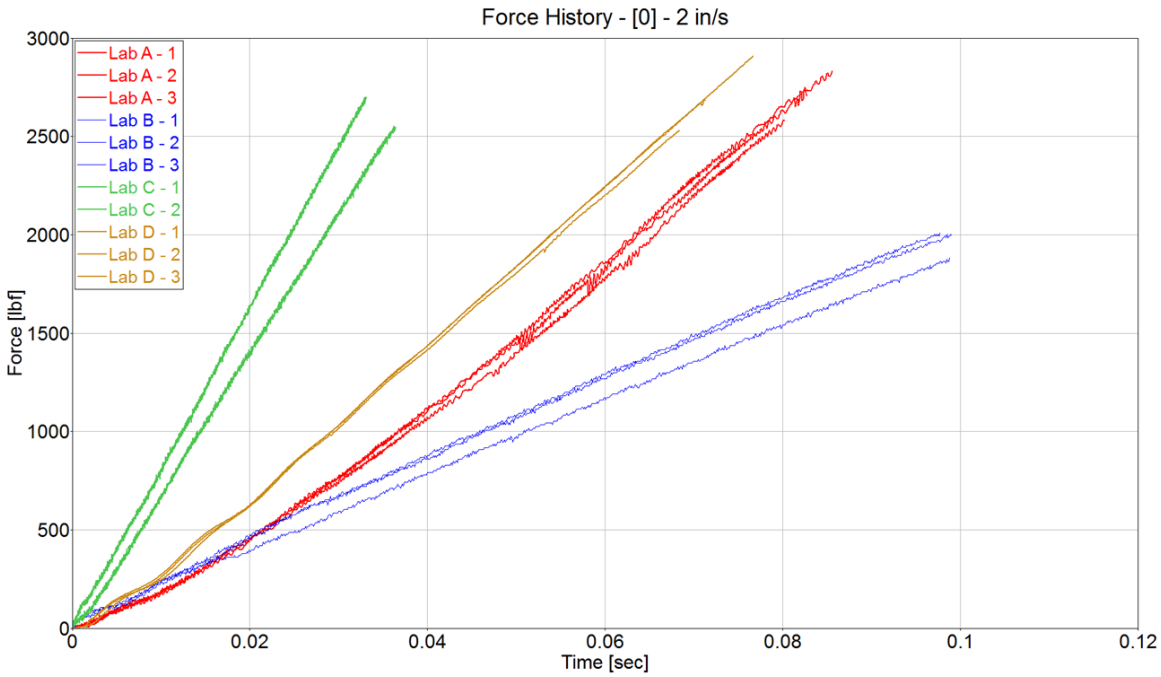

Figure 36. All laboratories' force history of [0º] orientation of Toray T700G/2510 at stroke rate of 2 in/s

Table 6. Actuator velocity drop of [0º] orientation of Toray T700G/2510 at stroke rate of 2 in/s

Lab	Avg. Pre-Test Velocity[in/s]	Avg. Test Velocity [in/s]	Velocity Drop [%]	Avg. Strain Rate [s^{-1}]
A	2.0703	1.7403	15.94	0.196
B	2.0413	1.4797	27.51	0.177
C	2.0419	1.8392	9.93	0.494
D	1.9993	1.3037	34.79	0.265

The velocity drop seems to be less pronounced as the stroke rate increases, as shown in the displacement history at the 200 in/s stroke rate shown in figure 37 for material orientation [0º]. The effect in other measured histories as the strain history, the strain-rate history, and the force history remains noticeable, as shown in figures 38–40, respectively. A summary in table 7 shows the velocity before and after the test and the percentage drop and average strain rate for each of the laboratories. Note Laboratory B results are included for reference because the tests were conducted at 100 in/s.

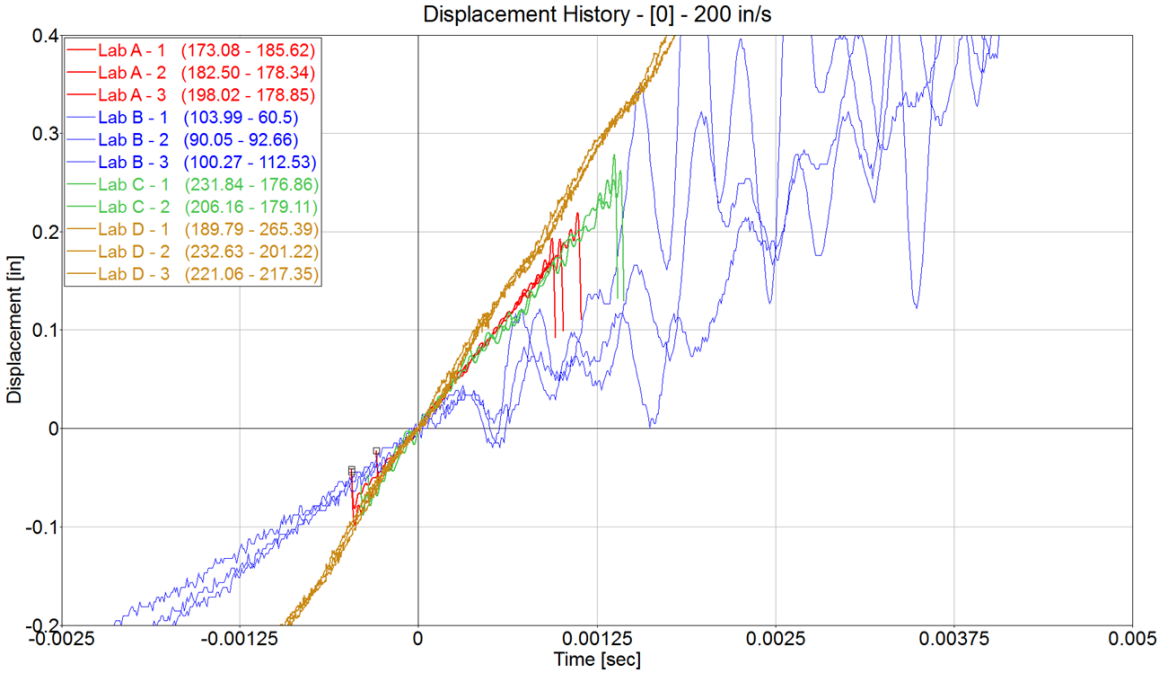

Figure 37. All laboratories' displacement history of [0º] orientation of Toray T700G/2510 at stroke rate of 200 in/s

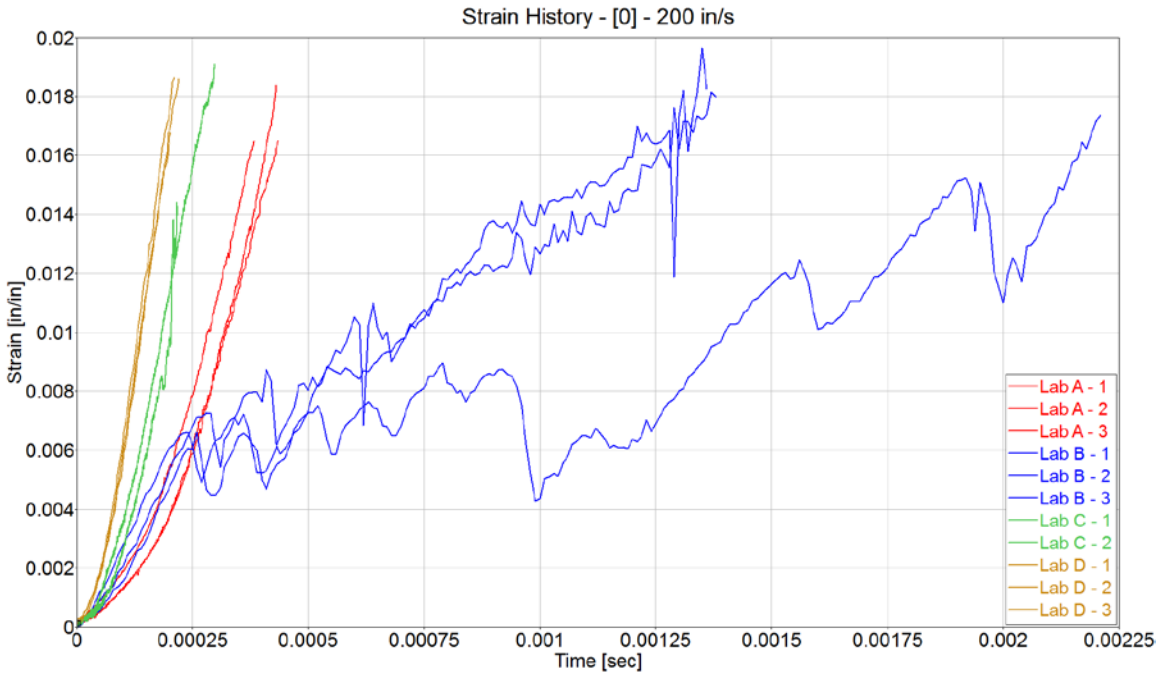

Figure 38. All laboratories' strain history of [0°] orientation of Toray T700G/2510 at stroke rate of 200 in/s

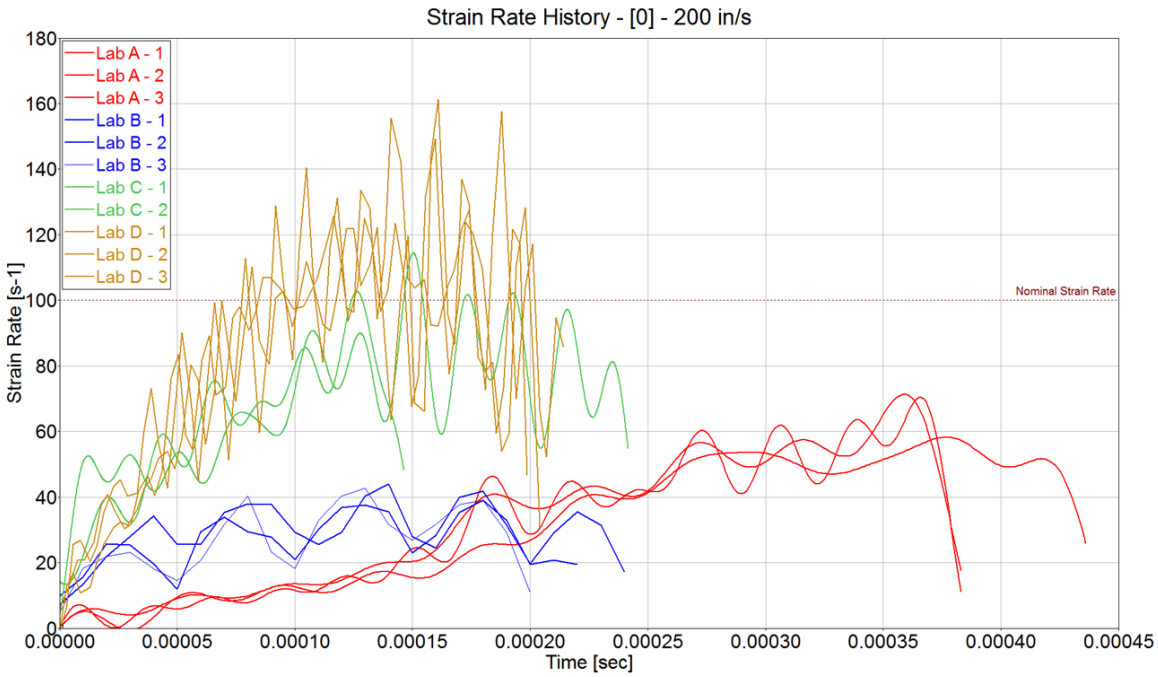

Figure 39. All laboratories' strain rate history of [0°] orientation of Toray T700G/2510 at stroke rate of 200 in/s

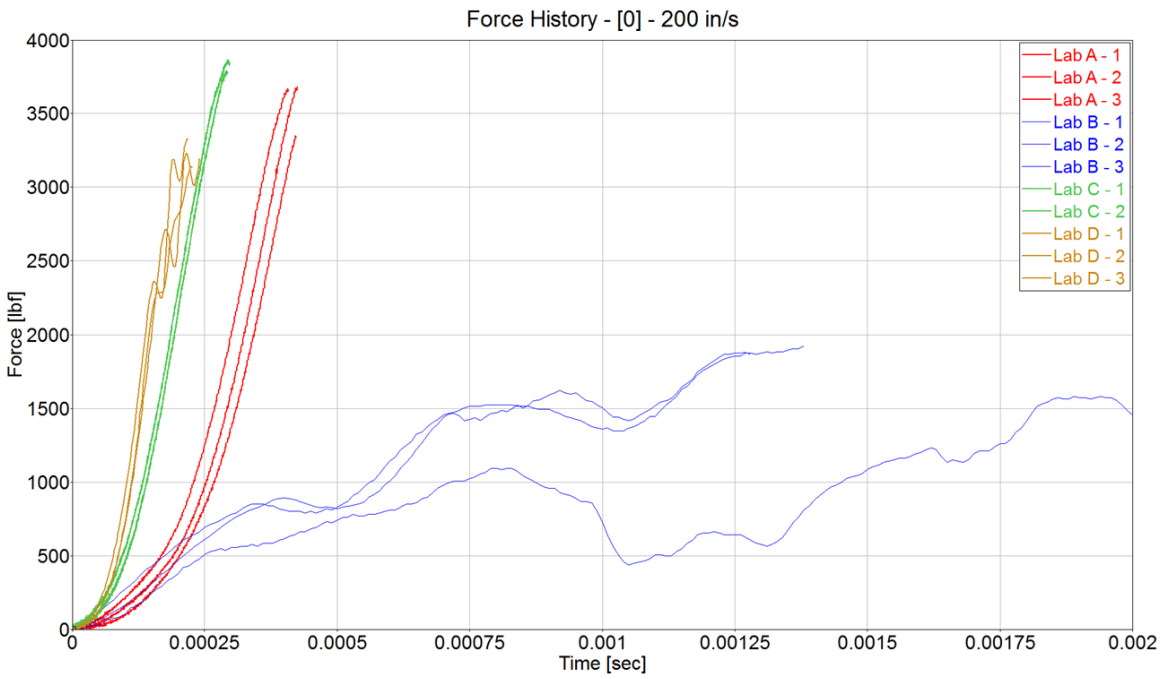

Figure 40. All laboratories' force history of [0º] orientation of Toray T700G/2510 at stroke rate of 200 in/s

Table 7. Actuator velocity drop of [0º] orientation of Toray T700G/2510 at stroke rate of 200 in/s

Lab	Avg. Pre-Test Velocity[in/s]	Avg. Test Velocity [in/s]	Velocity Drop [%]	Avg. Strain Rate [s^{-1}]
A	184.53	180.27	2.31	56.80
B	98.10	88.56	9.72	31.87
C	219.00	177.99	18.73	76.37
D	214.49	227.99	-6.29	109.13

With regard to servo-hydraulic test systems, as part of a comprehensive error analysis to improve repeatability (precision and accuracy) of the subject data gathering, each lab should conduct baseline sacrificial coupon tests to characterize their unique actuator velocity drop.

3.4 STRAIN MEASUREMENT

Laboratory D used an ARAMIS Digital Image Correlation (DIC) Measurement system (which, by definition, is a noncontact measurement system) and the strain gauges, as stated in section 2.3 and as shown in figure 41. Comparison of both measurements is presented in figures 42–figure 44 for all material orientations and stroke rates. The results are identical. However, the noncontact measurement system does not have the limitations of the strain gauges, so it can obtain meaningful strain measurements for a longer time window within each test. Here, the limitations are those associated with errors arising from the gauge's straddling of surface stress discontinuities as a result of its planar physical proximity to the roving(s) of the subject composite laminate. In

addition, there is much more motion of the fibers in the 45º specimens, creating localized dislocations.

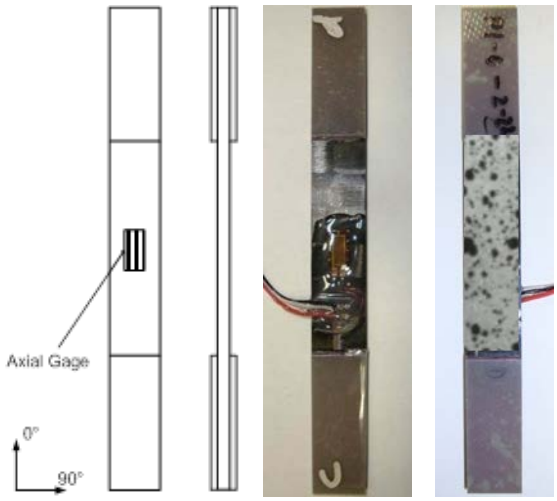

Figure 41. Specimen schematic and test specimen showing strain gauge on one side and speckle pattern on the other side for digital image correlation measurement

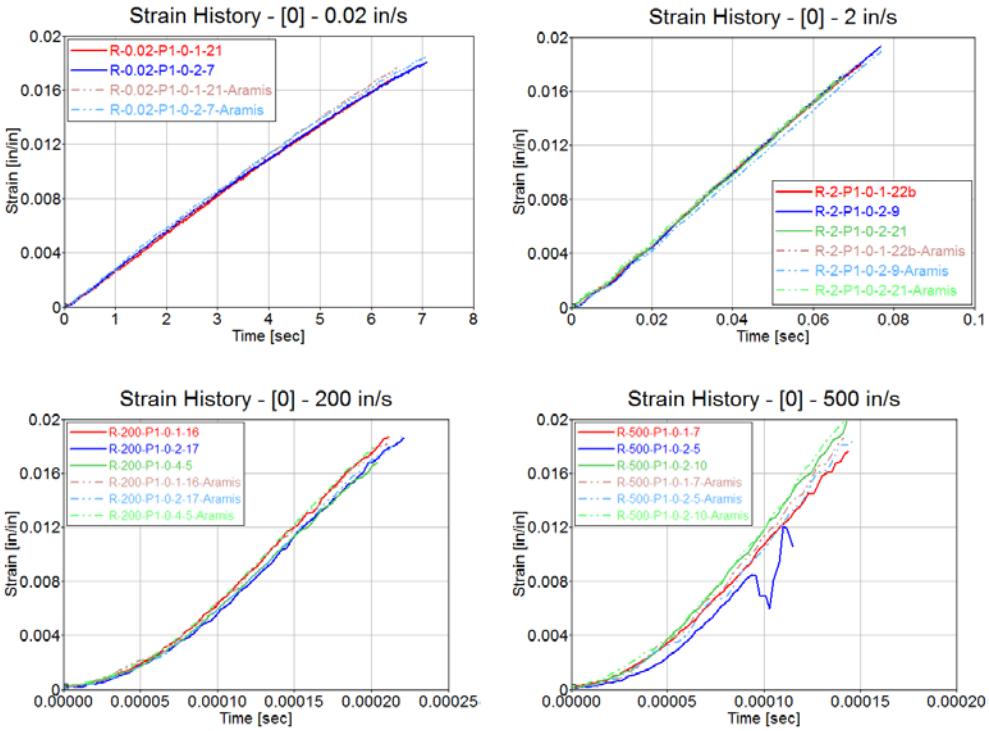

Figure 42. Strain history comparison between strain gauge and DIC of [0º] orientation of Toray T700G/2510 for all stroke rates for Laboratory D

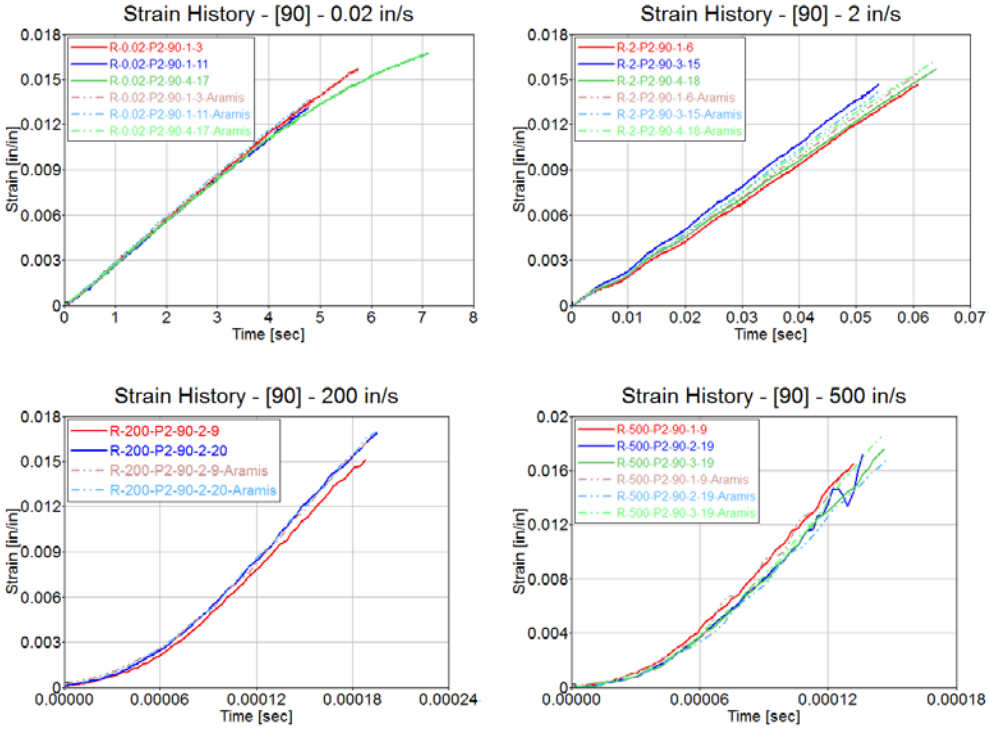

Figure 43. Strain history comparison between strain gauge and DIC of [90º] orientation of Toray T700G/2510 for all stroke rates for Laboratory D

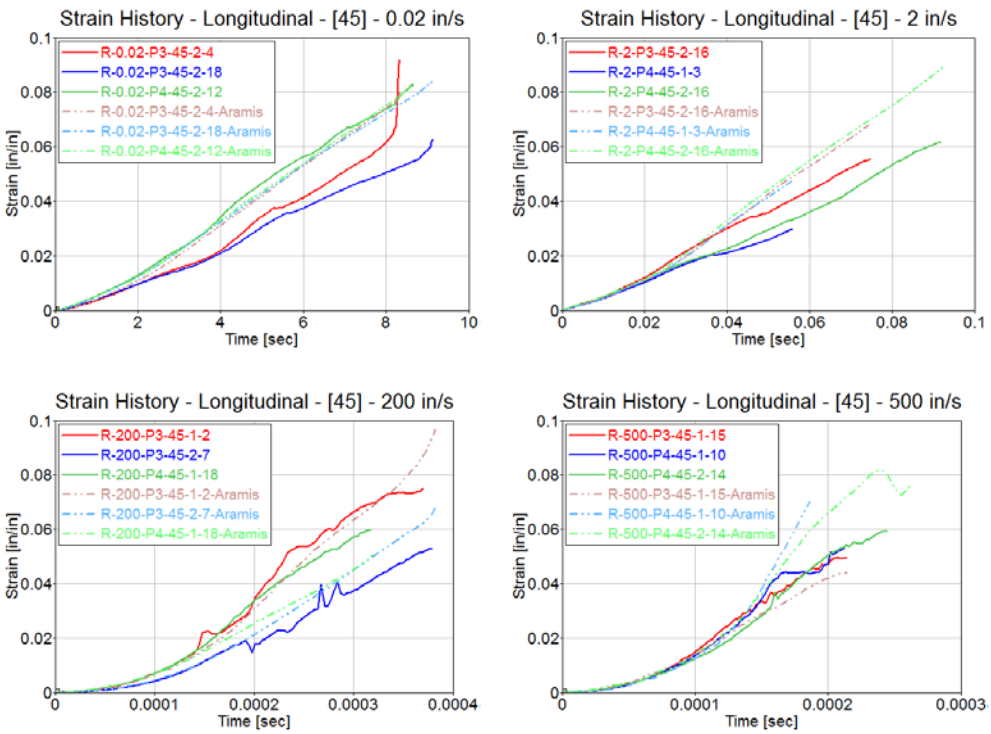

Figure 44. Strain history comparison between strain gauge and DIC of [45º] orientation of Toray T700G/2510 for all stroke rates for Laboratory D

4. LOAD-TRAIN-INDUCED MODULATION DATA CORRECTION

The test data recorded during the high-speed tests, specifically the force signal, cannot be used directly to generate the stress-strain curves for the material being tested. Whereas the strains measured using surface-mounted strain gauges provide an accurate measurement of the specimen strain along the loading direction, the force signals measured by the load frame load cell are contaminated by the oscillations of the load train. These oscillations are due to the finite stiffness and masses associated with the grips, connectors, and load frame. This is conceptually shown in figure 45. The signals may be corrected using modal information, as reported by Zhu et al. [21]. In this exercise, the deviation of the measured force signals from the true values was captured using dynamic tests on AL specimens with extended tab regions. The details of the force signal corrections and an evaluation of the force measurement apparatuses are presented in the following sections. The load oscillations at quasi-static rates are minimal and do not require additional correction.

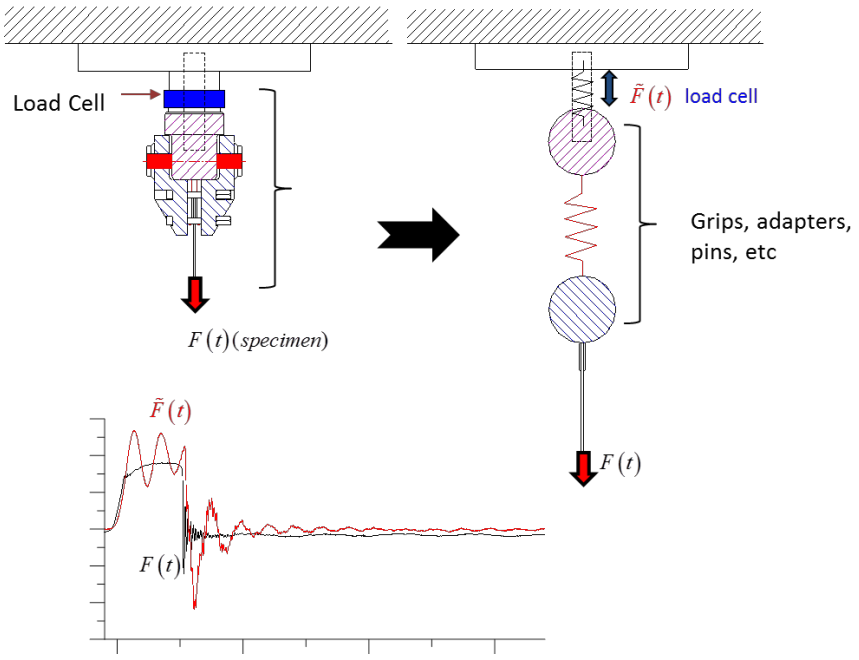

Figure 45. Differences in measured and actual force time histories due to load train vibrations

To evaluate the force measurement system, which includes the grips, load cell, and connectors, a reference force pulse is needed. Ideally, this force pulse should have sufficient bandwidth and should be repeatable. The fatigue cycling capability of servo-hydraulic machines to generate a repeatable dynamic load of known frequency could be used. However, most common servo-hydraulic load frames available today cannot exceed 30 Hz. The data obtained from such low-frequency tests will not be suitable to address issues with dynamic test data if the bandwidth of force signals could easily exceed 1 kHz. A comparison of the normalized amplitude spectra for a hypothetical brittle specimen tested at different nominal strain rates is shown in figure 46. In this idealized scenario, the force pulses resemble triangular pulses with different time durations. Based on this plot, to test the specimen at strain rates exceeding 100 s^{-1}, a force measurement system with a bandwidth in excess of 10 kHz is required. Therefore, to calibrate such force measurement systems, the only option would be to use a known force pulse whose spectrum spans the desired bandwidth. The force pulses can be generated by simply rupturing a specimen with known stress-strain behavior between the grips. If we are able to measure the force in the specimen without using a load cell, then we could use the specimen for the load pulse generation. A good candidate for this purpose would be specimens with extended tab regions. Because of the smaller cross-section area of the gauge region, failure of the specimen will be confined to this region, thereby guaranteeing an elastic loading in the extended tab region. The strains measured in the extended tab region using surface-mounted strain gauges may be calibrated against the load in the specimen. The force measurement using extended tabs is suitable for materials whose elastic response is known to be rate-insensitive. Such metals as aluminums and steels are well known to possess this attribute. These specimens are suitable for dynamic tests that are not dominated by stress-wave propagation. Extensive experimental [22] and finite element analyses [23] addressing the geometry of such specimens and the location of strain gauges has been reported in literature.

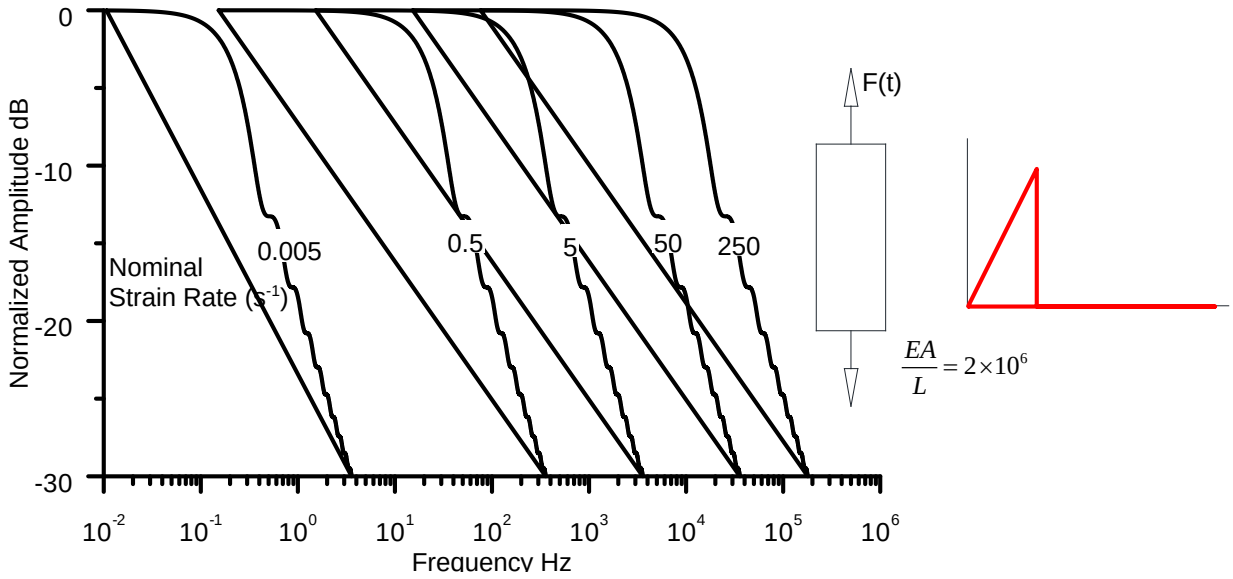

Figure 46. Normalized amplitude spectra for a rate-insensitive brittle specimen tested at different strain rates

In this investigation, 2024-T3 clad Al specimens of 0.09-inch thickness were used for generating the input or known force pulse. The geometry of the test specimens and the location of the strain gauge in the tab region are shown in figure 3 of section 2.2. Quasi-static calibration tests were performed by individual labs to correlate the tab strains to the applied force. The strains recorded using the tab strain gauges are plotted against the applied force, as shown in figure 47. The slopes of the curves are in good agreement with the theoretical value based on the tab area and Young's modulus of the specimen. The values of the slopes for individual labs were used to convert the tab strains recorded during dynamic testing to corresponding forces.

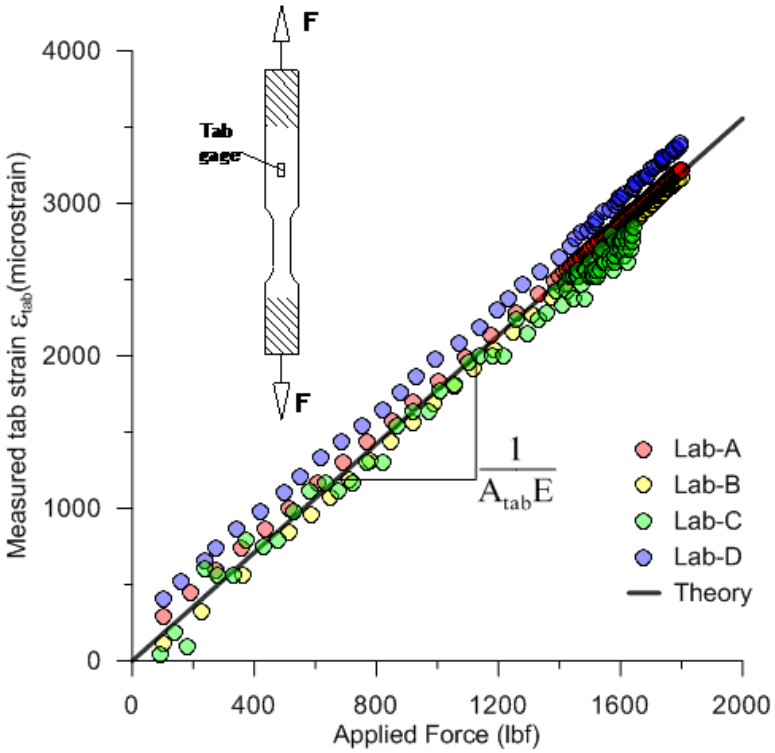

Figure 47. Quasi-static calibration tests on aluminum specimens

A sample of the data from dynamic tests conducted at different actuator speeds is shown in figure 48. It is evident from these figures that with increasing speeds, the load train oscillations tend to dominate the response measured using the load cell. The frequency and amplitude of the oscillations riding the elasto-plastic region of the response is characteristic of the test system. Whereas one may attempt to use bypass filters (low, high, or band pass) to alleviate the oscillations, it may not solve the problem completely. If the interest is only to capture the stress levels during plastic deformation, then such a solution would suffice. However, for brittle materials such as polymer composites, the stress-strain response seldom consists of an extended plastic region except for off-axis loading at certain orientations. Therefore, a correction method is sought that is not restricted to a certain portion of the stress-strain curve.

In this investigation, the corrections to the force signals as measured by the load cells were applied in the frequency domain. To accomplish this, calibration tests were conducted by each laboratory using aluminum specimens with extended tabs. These tests were conducted at speeds ranging between 187 in/s to 240 in/s.

Because both the input force (true force experienced by the specimen) and the output force (measured by the load cell) are available for these specimens, an empirical transfer function may be obtained by using the data. To accomplish this, the force signals in the time domain have to be transformed to corresponding signals in the frequency domain. The transfer functions are then computed in the frequency domain. Using these transfer functions, the force signals measured using load cells can be corrected for tests conducted on composite specimens. This process is shown in figure 49. The details of the generation of load pulses for calibration and assessment of

the force-measurement system, development of transfer functions, and application to composite test data are discussed in section 4.

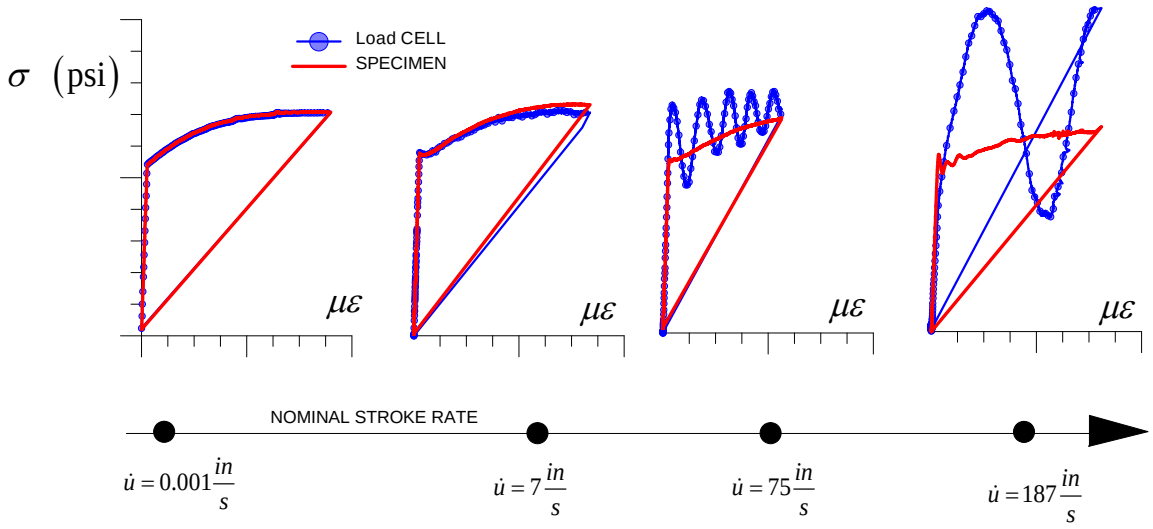

Figure 48. Comparison of stress-strain curves for Al specimens based on force measurements using load cells and tab gauges at different test speeds

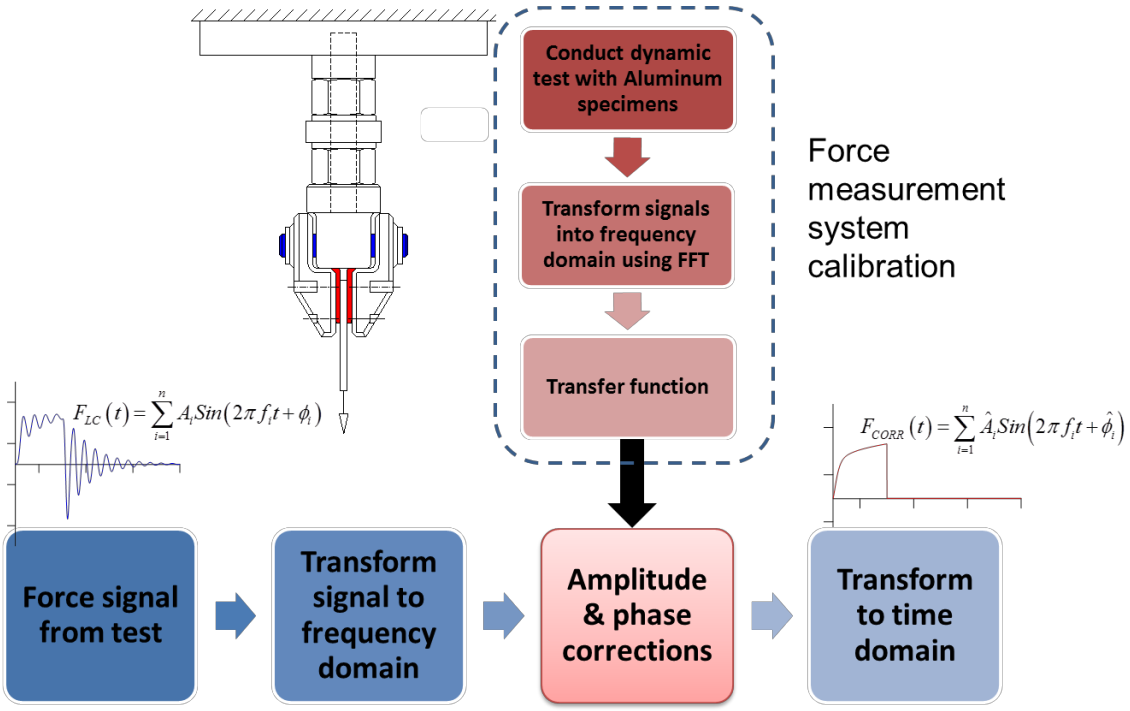

Figure 49. Methodology for development and application of corrections to force measurement

4.1 GENERATION OF LOAD PULSES FOR DEVELOPING CORRECTIONS

The force pulses required for the evaluation of the force measurement systems and the subsequent development of correction functions were generated by testing an extended tab Al specimen at nominal test speeds ranging between 187 in/s and 240 in/s. A sample of the test pulses obtained by converting the tab strains was compared over a duration of 6 milliseconds and is shown in figure 50. The force pulses consist of an initial trapezoidal pulse corresponding to the loading of the specimen followed by extended time duration of decaying small-amplitude oscillations. The decaying oscillations past the main pulse correspond to the multiple stress-wave reflections between the fractured end of the specimen and the grips. Whereas the overall force levels were somewhat similar, the time duration of the initial pulse and the oscillations following the same were markedly different and characteristic of the test apparatus used by the labs. Although the test was conducted at a speed of 200 in/s by Laboratory B, the pulse duration was longer because of the added compliance of their loading system. In addition, small oscillations (roughly $1/10^{th}$ the period of the main pulse) can be seen to ride the plateau portion of the main pulse recorded by Laboratory D. The decaying oscillations following the main pulse will be ignored for all subsequent analyses because this does not represent the force in the gauge region of the specimen (which is ruptured, so the force has to be zero). For analysis purposes, the force signals obtained from the tabs gauges were set to a value of zero past the main pulse.

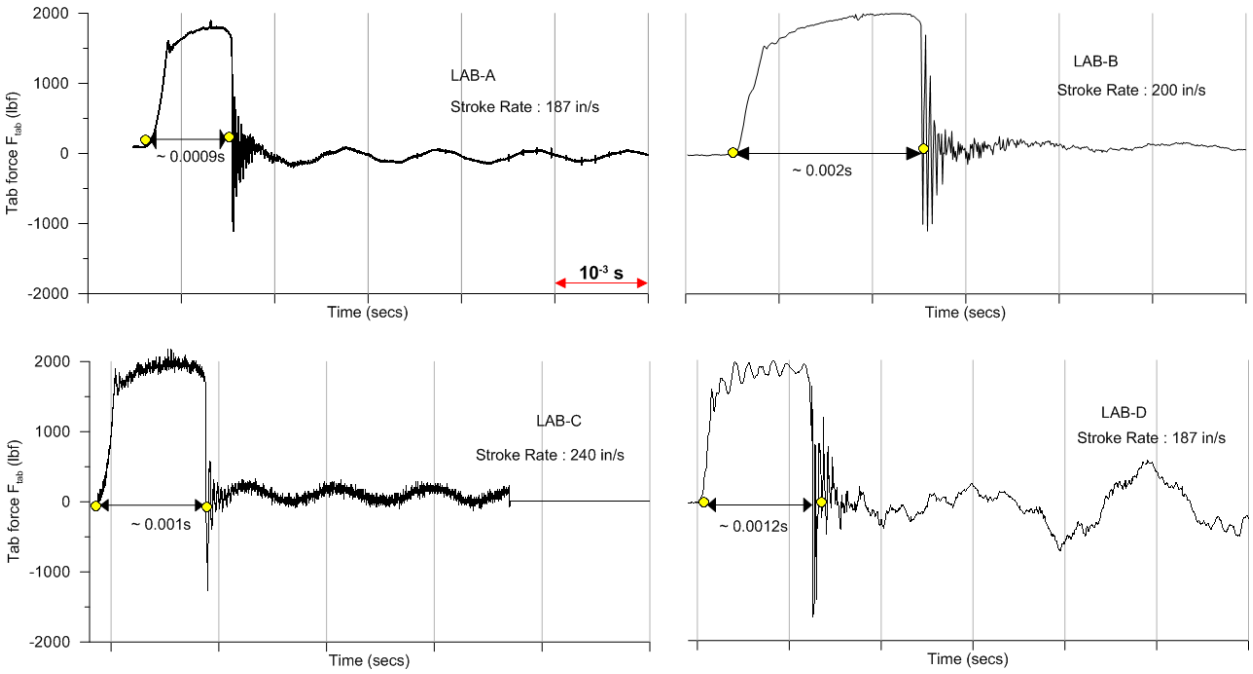

Figure 50. Comparison of initial portion of the force pulses generated by different laboratories using extended-tab aluminum specimens

The force time histories recorded using the force sensors during the same tests are shown in figure 51. Unlike the force time histories based on tab gauges, the load cells measure contrasting pulse shapes because of the particular configuration of the load train between the specimen and the load cell. The distinguishing features of the force time histories include large oscillations riding the

plateau region of the main pulse followed by a duration of pulse decay, both of which characterize the dynamic properties of the force-measurement apparatus. The test data reported by Laboratories A and B exhibit considerable damping, whereas that of Laboratory C indicates very little damping. Additional differences may be observed when the force signals are compared prior to specimen failure, as shown in figure 52. The amplitude and frequency of oscillations riding the plateau of the main pulse differ significantly. In addition, a time delay may be observed for the load-cell signal, especially for Laboratory D.

Whereas some features of the test system are obvious from the force time histories, additional information may be visualized in the frequency domain. The amplitude spectrums of the force pulses were generated using TableCurve 2D® [24]. The amplitude spectrums of the input signals, which are the force signals based on the tab gauge, are compared across the labs in figure 53. The normalized amplitudes on a decibel scale are plotted over a frequency range of 100 kHz. In the figure, a normalized amplitude value of -40 dB indicates that the signal has been reduced by 99% of the maximum value. The strength of the pulses can be compared in this plot by observing the first zero (dip in the curve) as highlighted by the corresponding frequencies. The longer the time duration of the load pulse, the lower the frequency corresponding to the first zero will be.

Ideally, for system evaluation, we would need a pulse of the shortest duration possible so that we have an almost horizontal line (corresponding to 0 dB) in the frequency domain. However, this would be hard to achieve because of practical constraints on the testing apparatus. For the participating labs, we observe that the first zero range is between 552 Hz and 1341 Hz. In addition, beyond 10 kHz, the amplitudes drop by more than 97% of the maximum amplitude. Keeping in mind that the full scale values of the tab gauge force measurement is approximately three times larger than the maximum force experienced by the specimen, the signals below -30 dB values (shown in figure 53) are not reliable measurements. This is because the force levels in this range are well below the smallest value (~1% of full scale) that can be measured.

The amplitude spectra of the force measurements using load cells are compared in figure 54. Ideally, these would be expected to match the spectra associated with the tab forces (shown as dotted lines in the figure). However, the spectra deviate significantly past the frequency corresponding to the first zeros. These frequency values are well below the natural frequencies of the load cells used by individual labs. Therefore, having a load cell with a high natural frequency would not suffice for dynamic load measurements. One must also design the rest of the force measurement apparatus, which includes the connectors and grips between the load cell and the specimen.

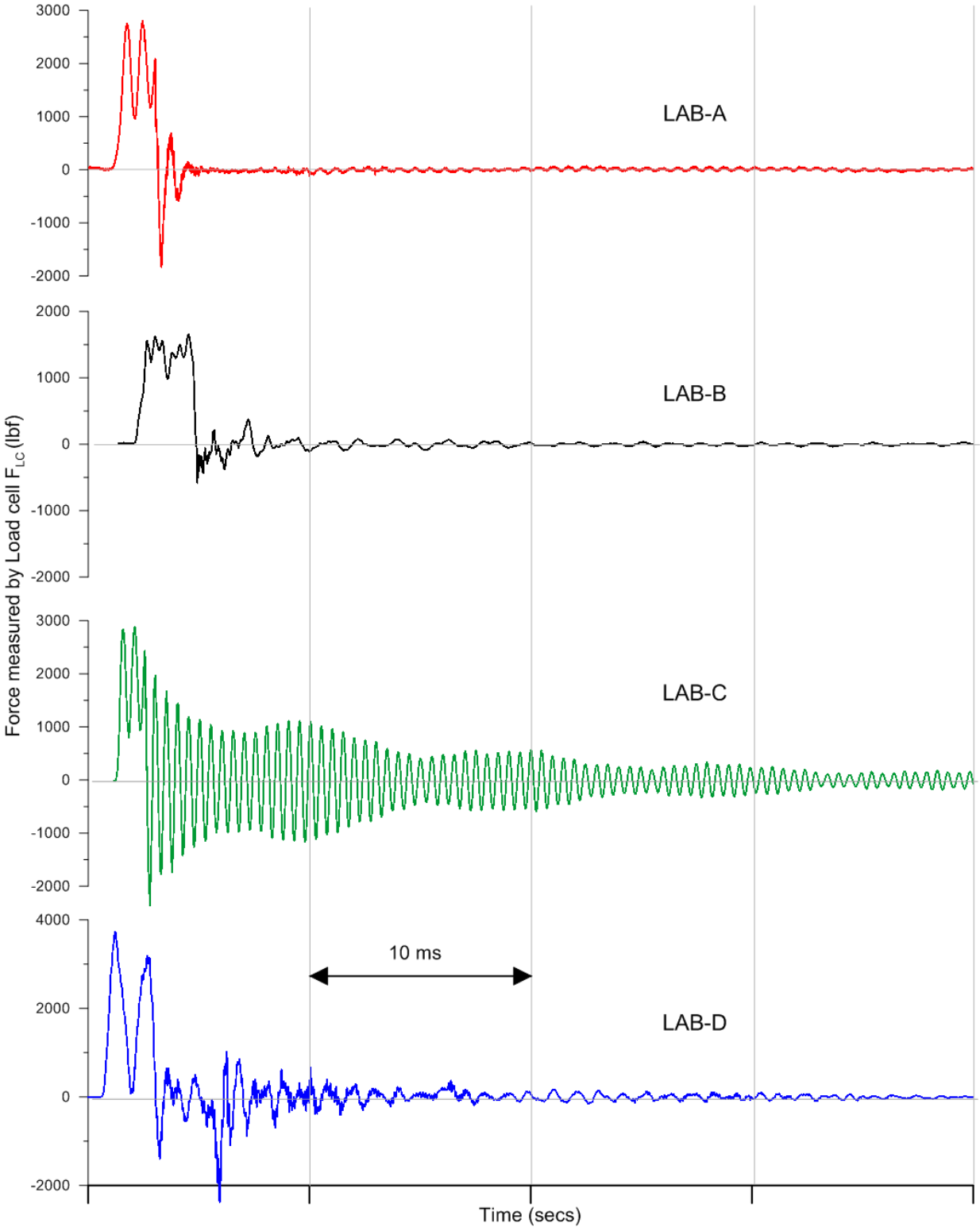

Figure 51. Comparison of force time history recorded by load cells

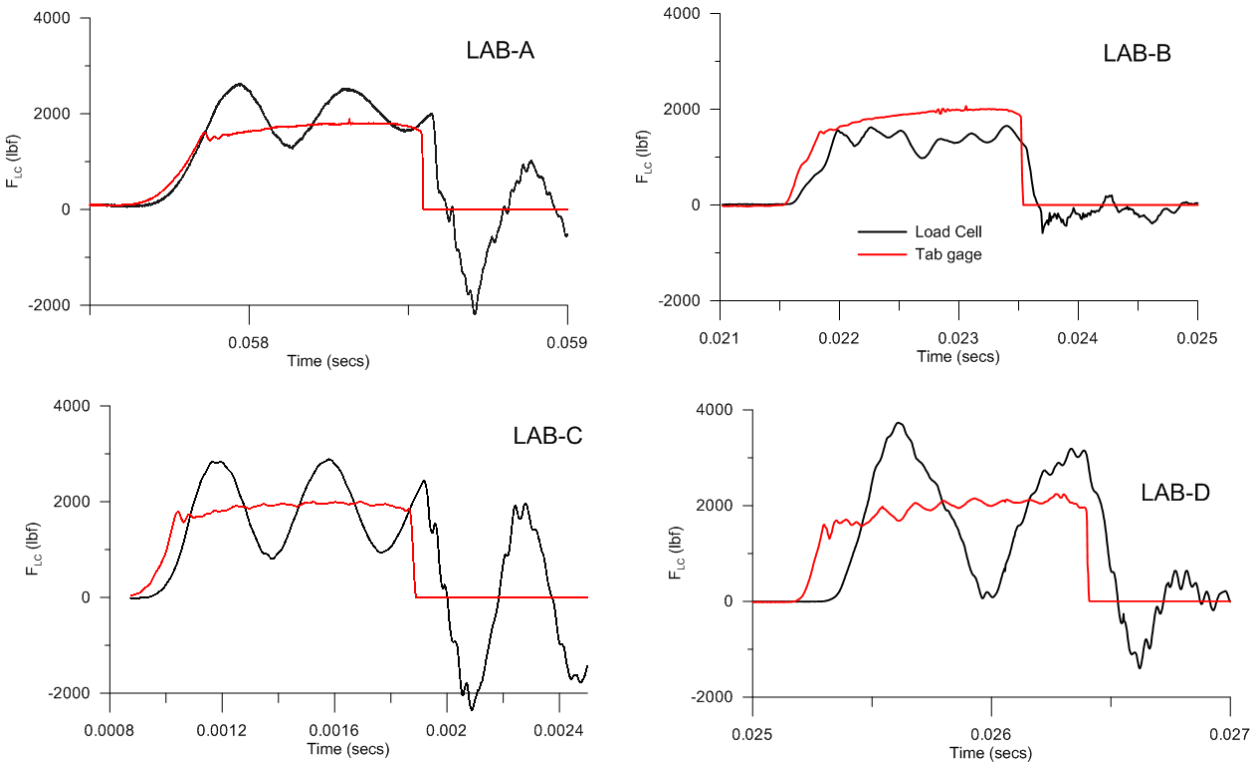

Figure 52. Comparison of the initial load pulses as recorded using the tab strain gauge and the load cell

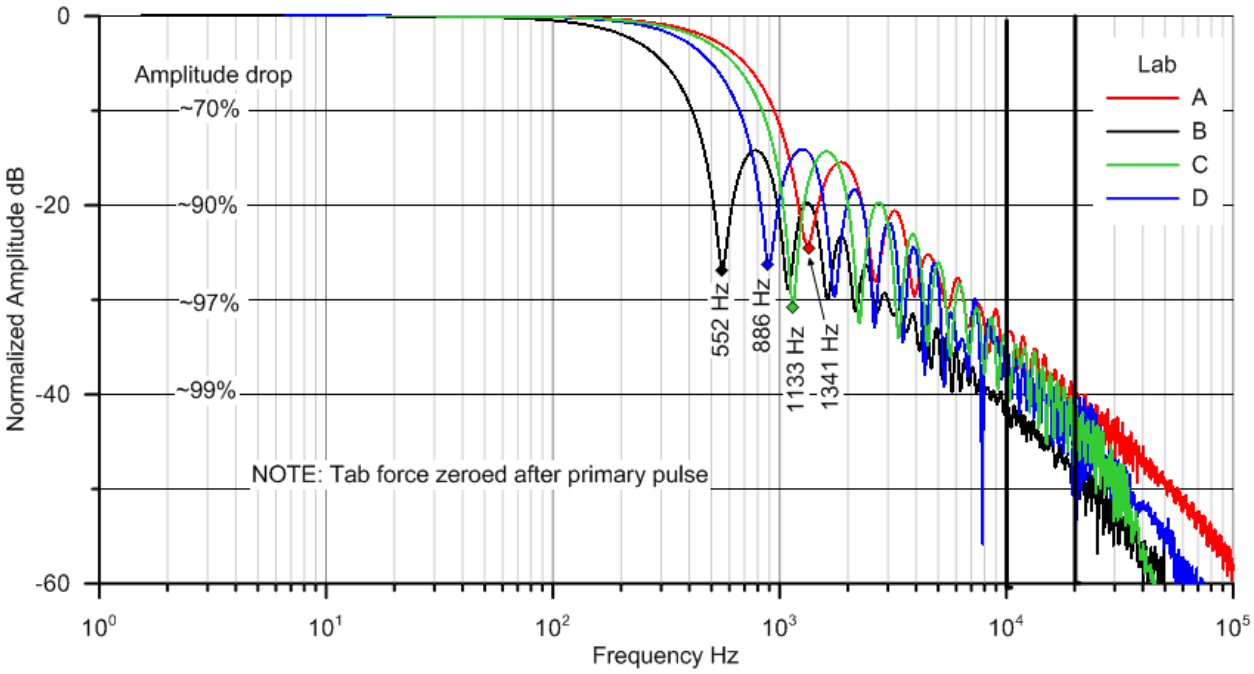

Figure 53. Comparison of tab force pulses in frequency domain

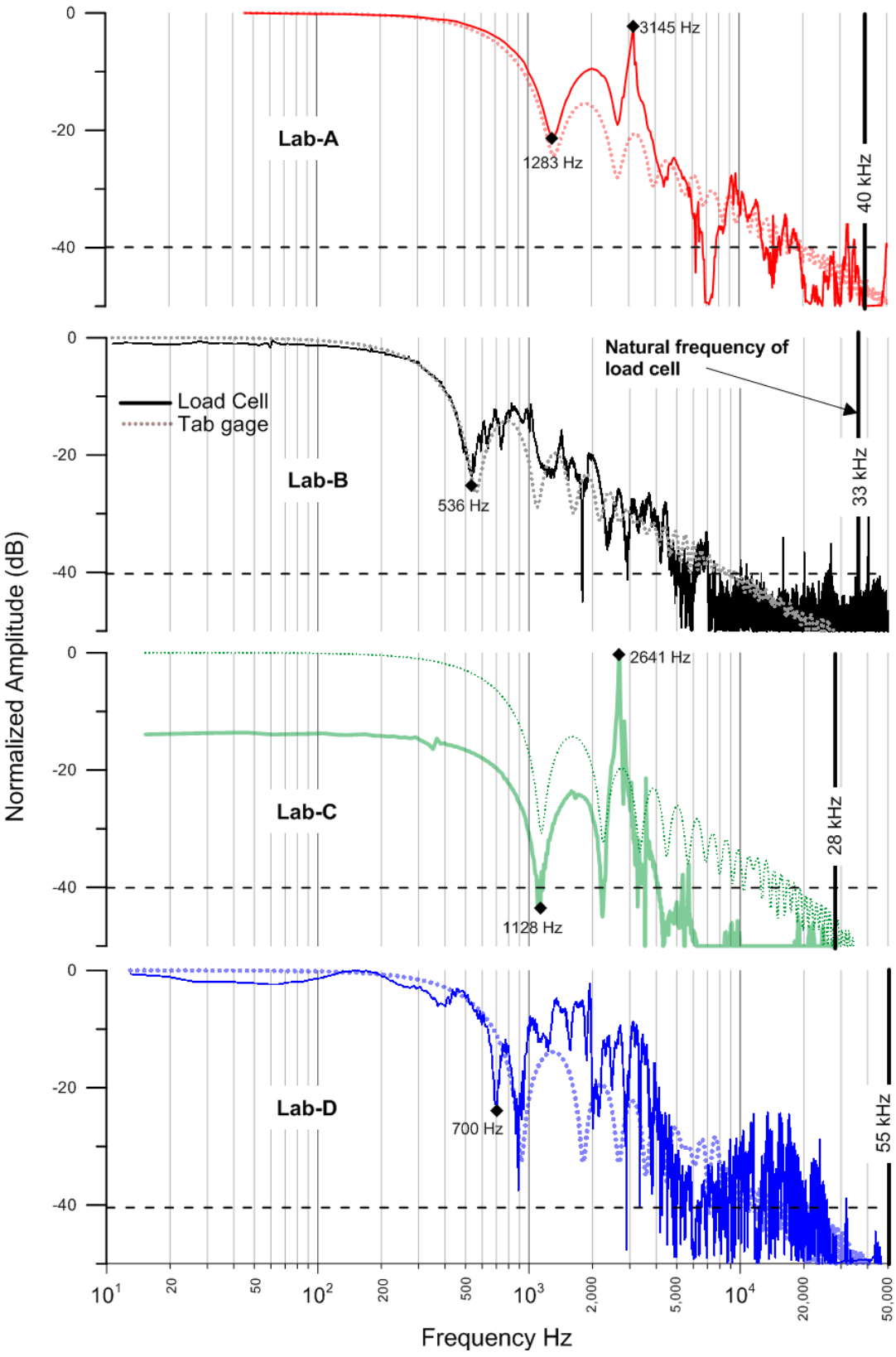

Figure 54. Comparison of load cell signals in the frequency domain

4.2 DEVELOPMENT OF EMPIRICAL TRANSFER FUNCTIONS

The frequency spectrum of the input load signal (tab force) and the output load signal (load cell) were obtained from the tests conducted on Al specimens at the highest actuator speed used by each individual lab. The input force signal was altered by clipping the signal past the initial pulse and padding it with zeros. The argument behind this is that the oscillations in the specimen following the main pulse are primarily due to multiple reflections of the stress wave generated at the rupture of the specimen. Conversely, the oscillations in the load-cell signal past the initial pulse are retained as they represent the residual oscillations of the load train. The fast Fourier transform (FFT) of the input and output signals were obtained using TableCurve 2D® curve fitting software [24]. The signals were further zero padded to a length of 2^{16} or 65,536 data points to facilitate the Fourier transform using the conventional "power of 2" FFT procedure [24]. This was done to increase the frequency resolution of the spectra. This is necessary because the signals to be corrected (e.g., composite specimens) may not have the same frequency content/resolution as the signals used for transfer-function generation. The spectra of the two signals were then used to generate the empirical transfer function as:

$$\text{Transfer Function} \quad \frac{1}{H(f)} = \frac{G_{xy}(f)}{G_{xx}(f)} \tag{4}$$

where

$G_{xy}(f) = S_{Tab}(f)\overline{S_{Load\_cell}}(f)$ ~ Cross-spectrum

$G_{xx}(f) = S_{Tab}(f)\overline{S_{Tab}}(f)$ ~ input Auto-spectrum

$S_{Tab}(f)$ ~ Fourier spectrum of input signal

$S_{Load\_cell}(f)$ ~ Fourier spectrum of output signal

The transfer function is expressed as a reciprocal of the frequency response function *H(f)* for convenience. The transfer function contains real and imaginary parts from which the functions associated with the amplitude and phase may be obtained as follows:

$$H_{Amp}(f) = \frac{2}{n_{data}}\sqrt{\left(\mathrm{Re}\left(1/H\right)\right)^2 + \left(\mathrm{Im}\left(1/H\right)\right)^2} \tag{5}$$

$$H_{Phase}(f) = \frac{\pi}{2} + \tan^{-1}\left(\frac{\mathrm{Im}\left(1/H\right)}{\mathrm{Re}\left(1/H\right)}\right) \tag{6}$$

In the above equations, the expression for phase is based on the assumptions that the Fourier series is based on "sine" terms. The transfer functions for Laboratory A, resolved into amplitude and phase components, are shown in figure 55. The figure shows the transfer functions based on two individual tests with their average value.

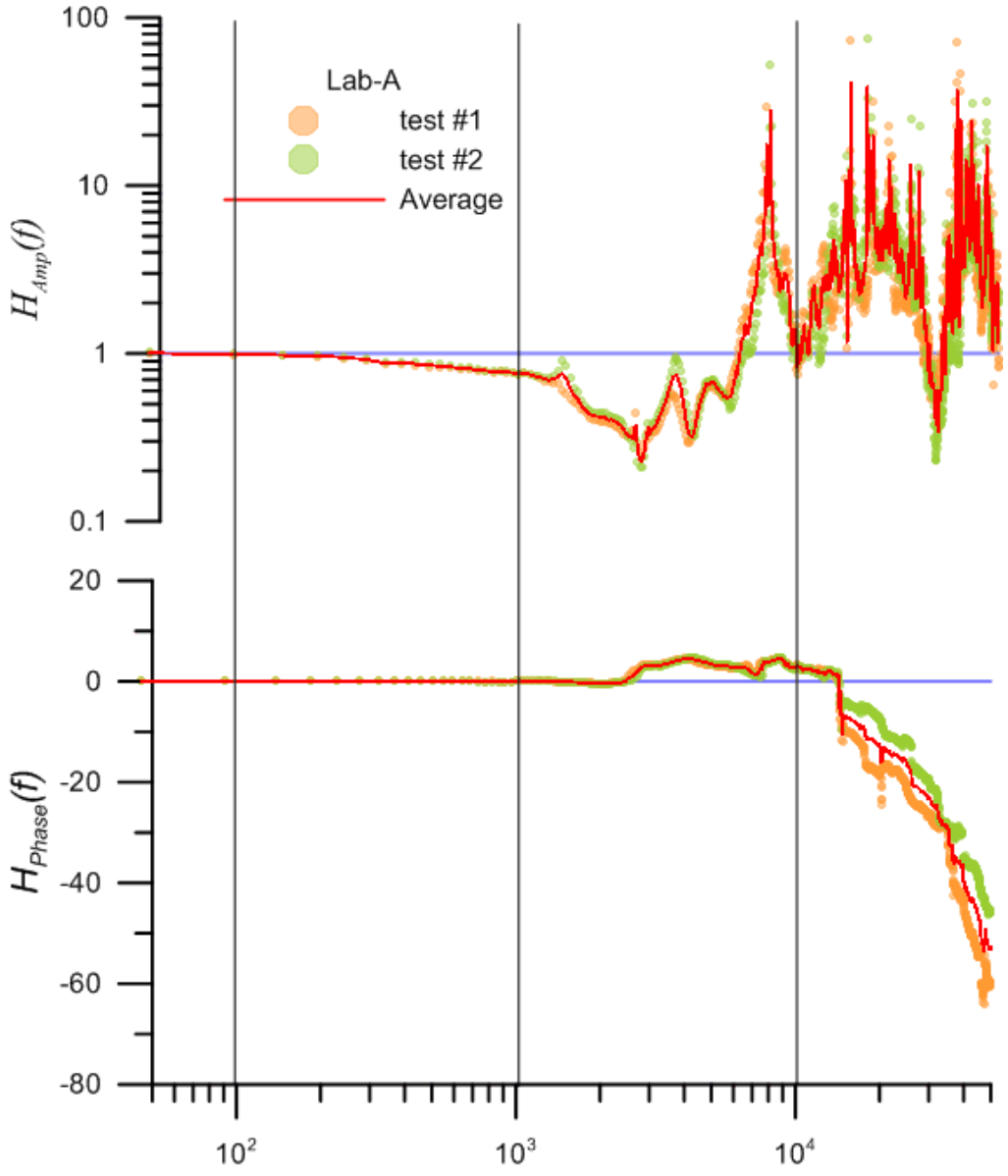

Figure 55. Empirical transfer functions for Laboratory A based on tests conducted at a speed of 187 in/s

The amplitude and phase information are used in the reconstruction of the signal in the time domain. In an ideal scenario, when there is no signal modulation, the transfer function must equal unity over the frequency range of interest. However, because of the vibrations associated with the load train, the transfer function deviates from unity past a certain frequency level (~ 1 kHz), which is dependent on the configuration of the load train. The empirical transfer functions for different test apparatuses were generated for the tests conducted at 180 in/s or higher. The transfer functions for different labs are compared in figures 56 and 57. Both amplitude and phase spectra reflect the significant differences in the load train configurations used by different laboratories. Caution must be exercised when using the transfer functions for data corrections, especially at higher frequencies at which the signal strength is weak and contaminated by noise. We observe that beyond 20 kHz,

the strength of the force signal based on tab gauges falls below -30 dB or 3% of the maximum amplitude. These signal levels will be in the error range (~ less than 1% of the full scale) of the load cells and, therefore, not reliable for development of transfer functions.

The transfer functions associated with the signal amplitudes were observed to be quite repeatable, as shown in figure 56. However, the phase information did not exhibit the same consistency and needs to be investigated further. Although this could be an impediment in the reconstruction of signals, the phase information from the strain-gauge signals could be used.

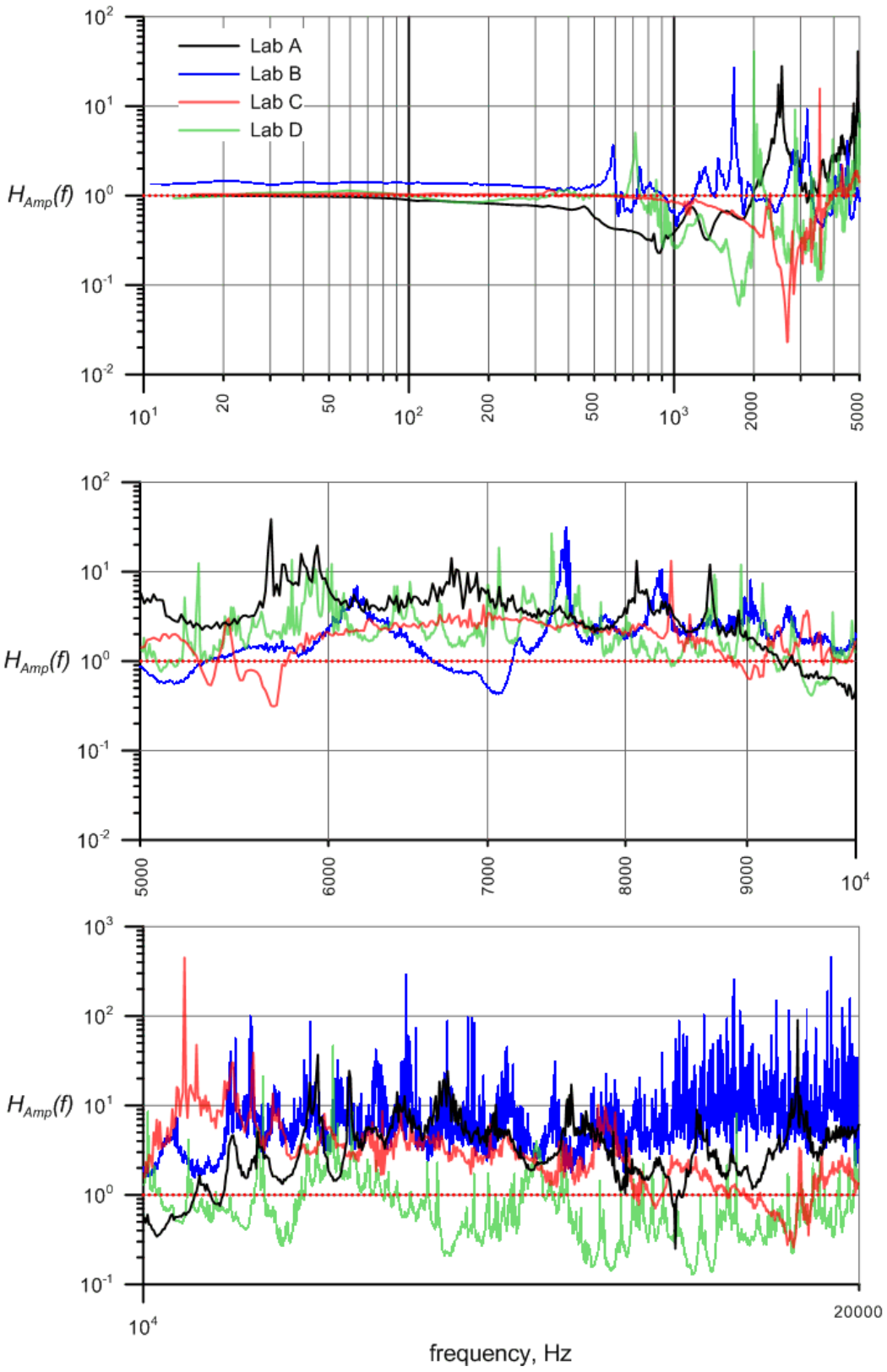

Figure 56. Comparison of transfer function amplitudes for different labs

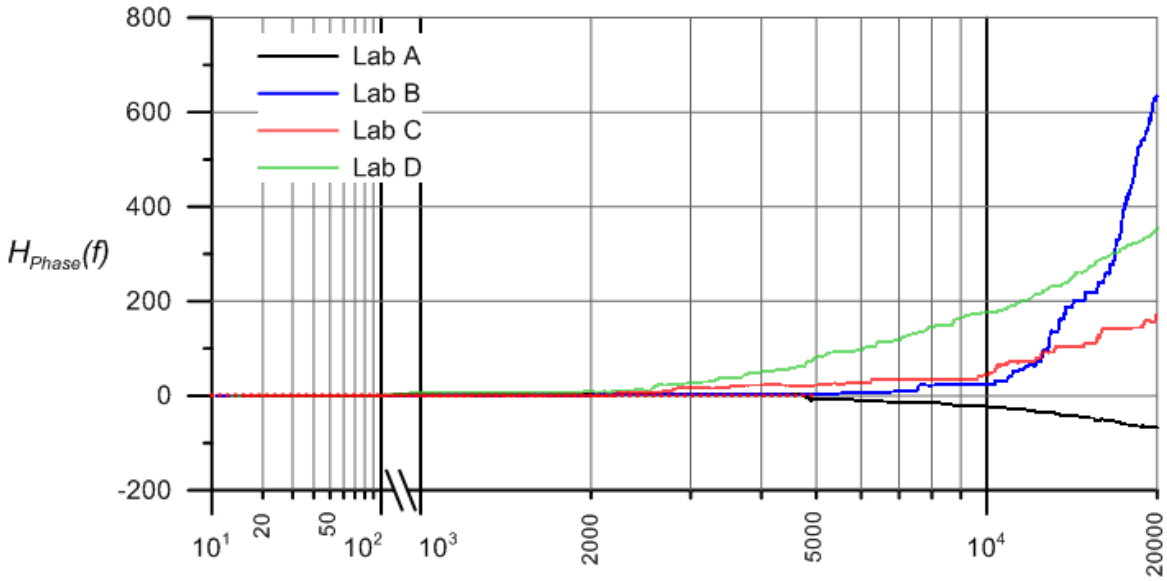

Figure 57. Comparison of phase shifts (in radians) for different frequency components of the transfer functions

4.3 CORRECTION AND RECONSTRUCTION OF SIGNALS USING EMPIRICAL TRANSFER FUNCTIONS

The empirical transfer functions were used to correct the load cell signals by modifying the amplitudes and phases in the frequency domain and subsequently reconstructing the signal in the time domain. The amplitudes and phases were corrected as:

$$H_{SENSOR}^{CORR} = H_{Amp} \times H_{SENSOR} \tag{7}$$

The corrected signal spectrum was subsequently used for generating the force signal in the time domain using the following equation:

$$F_{CORR}(t) = \sum_{i=0}^{n\max} H_{SENSOR}^{CORR}(f_i)\, Sin(2\pi f_i t + \phi_i) \tag{8}$$

where n_{max} corresponds to the bandwidth used for reconstruction. Although the above equation is straightforward to implement, the inconsistencies observed in the phase spectra introduce errors in the signal reconstruction. In addition, the well-known Gibbs phenomenon introduces high-frequency oscillations during reconstruction. To alleviate the Gibbs phenomenon, Lanczos smoothing was employed. This involves modification of each amplitude component by a value α_i, which is given by:

$$\alpha_i = \begin{cases} \dfrac{\sin\left(i\pi/n\right)}{\left(i\pi/n\right)} & i \le n \\ 0 & otherwise \end{cases} \tag{9}$$

This smoothing is equivalent to using a tapered frequency-domain window. The value of *n* in the equation corresponds to the frequency at the -30 dB limit.

To account for the phase corrections, the phase information from the strain gauge (gauge region) signals could be used. Because the pulse width of the strain and force signals must be identical, the phase information for the two signals will be the same, even though the amplitudes and pulse shapes are slightly different. This was verified by exploring different pulse shapes, albeit with same pulse widths. The phase spectra for the signals indicated only minor differences between them.

To demonstrate the correction methodology, the transfer function was applied to the load cell signal for an aluminum specimen tested at a cross-head speed of 75 in/s. The force signal recorded using the load cell and based on the tab strain gauge are compared with the corrected load cell signal in figure 58. The transfer function significantly reduces the high-frequency oscillations observed in the load cell signal. The stress-strain diagrams based on the different force signals are compared in the same figure. The transfer function method for correcting the data results in a stress-strain diagram with minimal oscillations compared to the curve based on raw data from the load cell.

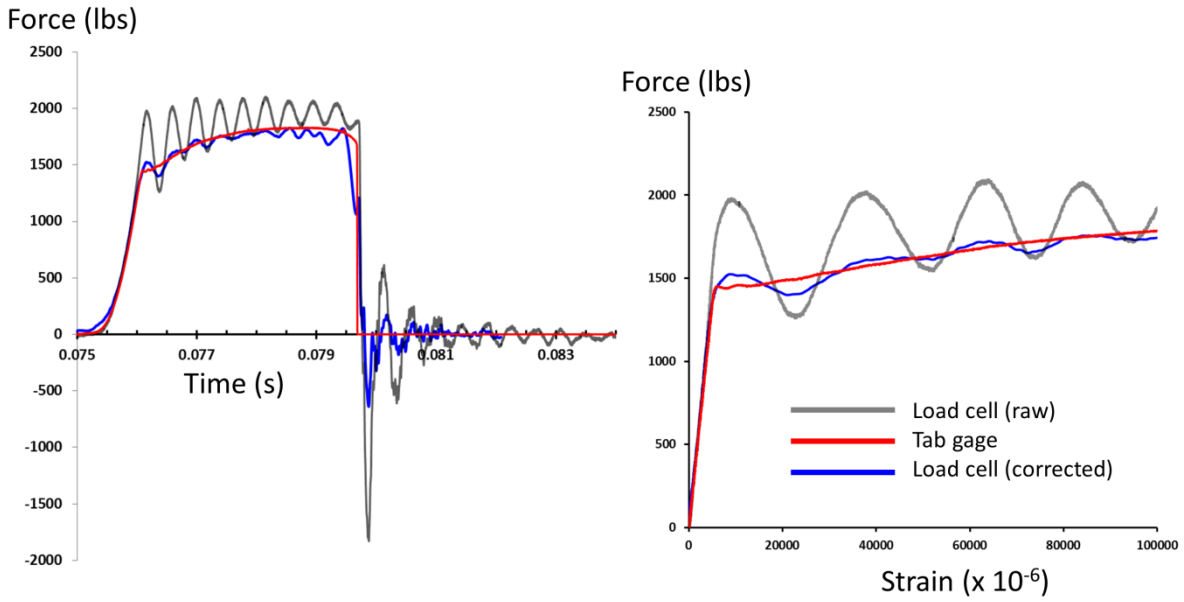

Figure 58. Comparison of raw and corrected signals with force signal based on tab-strain gauge

4.4 APPLICATION TO APPARENT RESULTS

Using the transfer function methodology generated in this investigation, a comparison of corrected and uncorrected tensile failure strength with increasing strain rate is also presented for each laboratory in figures 59–62. No data correction was required or applied for measurements taken at quasi-static rates. These plots provide an overview of the capability of generating repeatable results for each single laboratory. After correction, the apparent trend in tensile failure strength, increasing or decreasing depending on the laboratory, seems to vanish for material orientations [0°] and [90°]. However, the increasing trend observed for material orientation [45°] before correction is still noticeable across laboratories. Note that there is no corrected data for the [90° material orientation for Laboratory D. This is due to offset errors in the data and cannot be corrected.

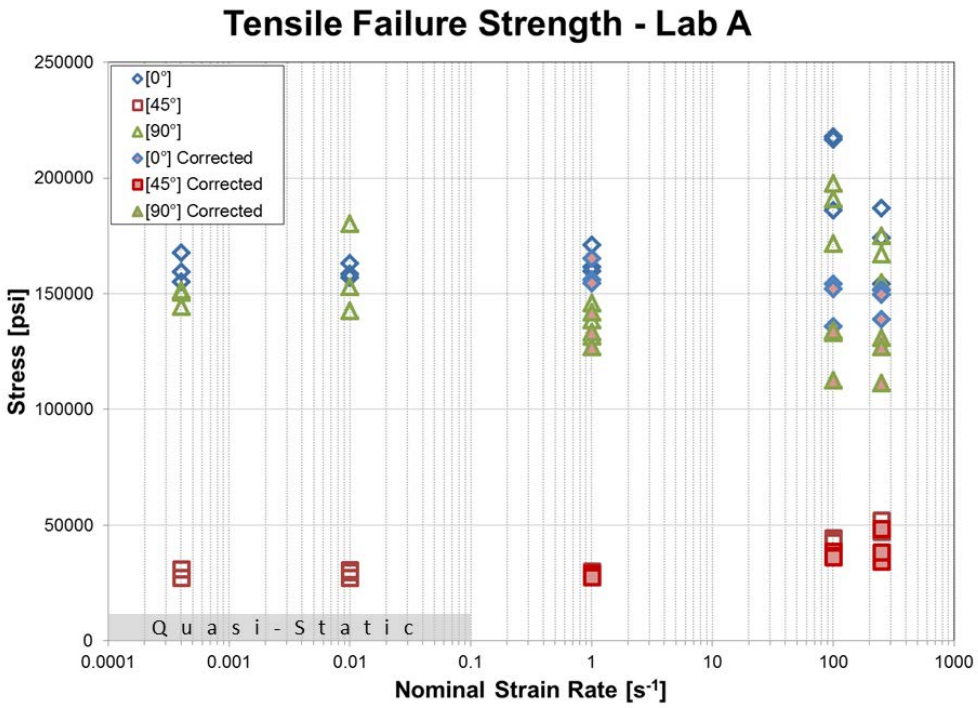

Figure 59. Corrected tensile failure strength of Toray T700G/2510 at various nominal strain rates for Laboratory A

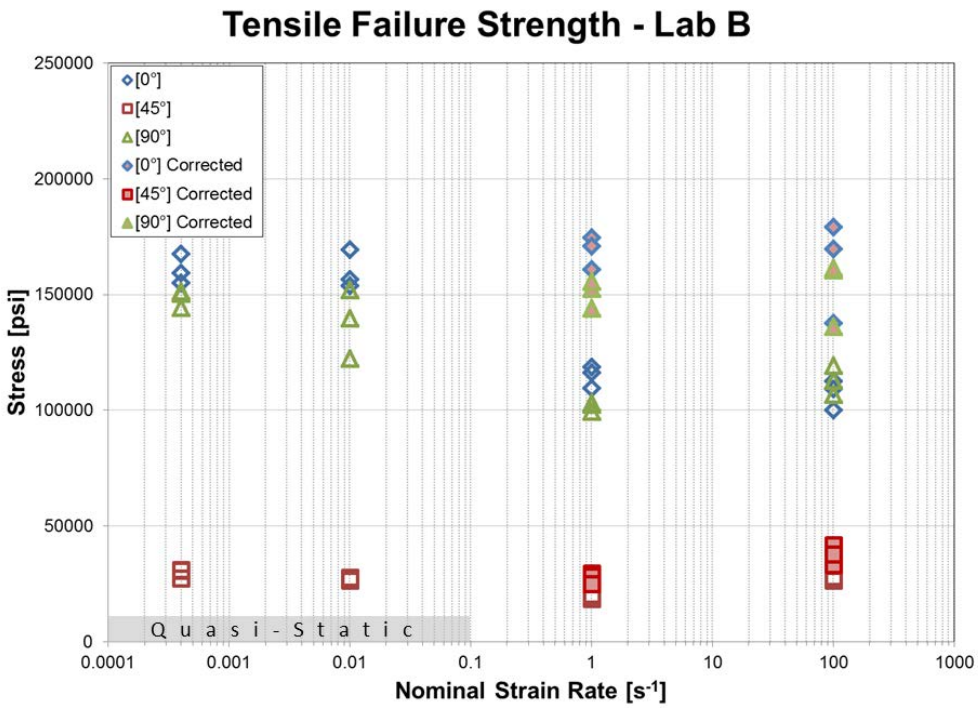

Figure 60. Corrected tensile failure strength of Toray T700G/2510 at various nominal strain rates for Laboratory B

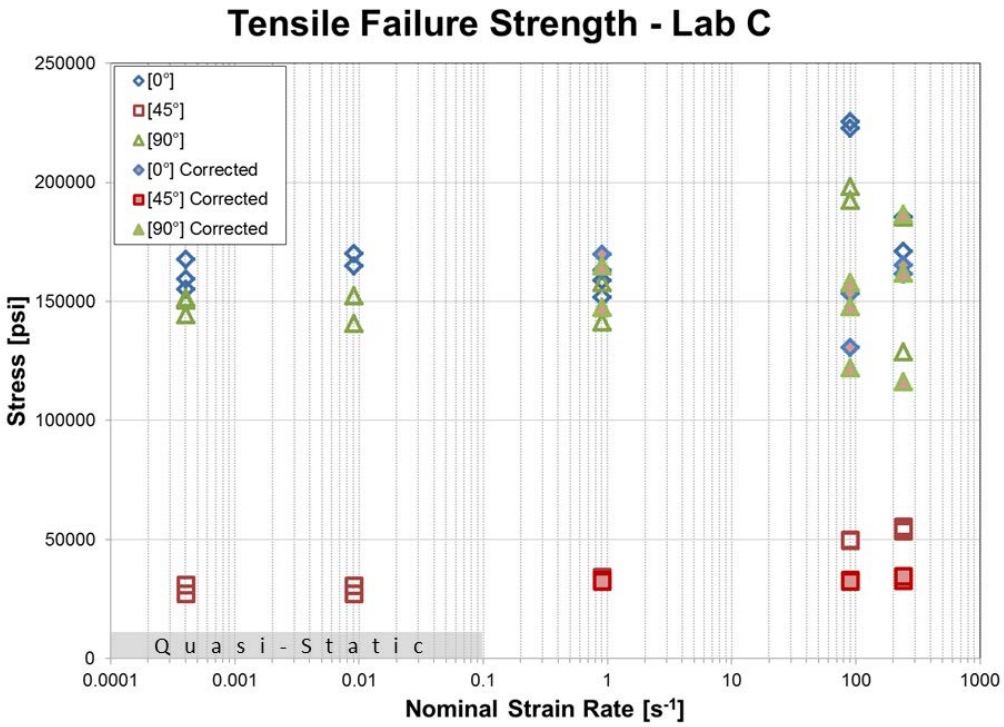

Figure 61. Corrected tensile failure strength of Toray T700G/2510 at various nominal strain rates for Laboratory C

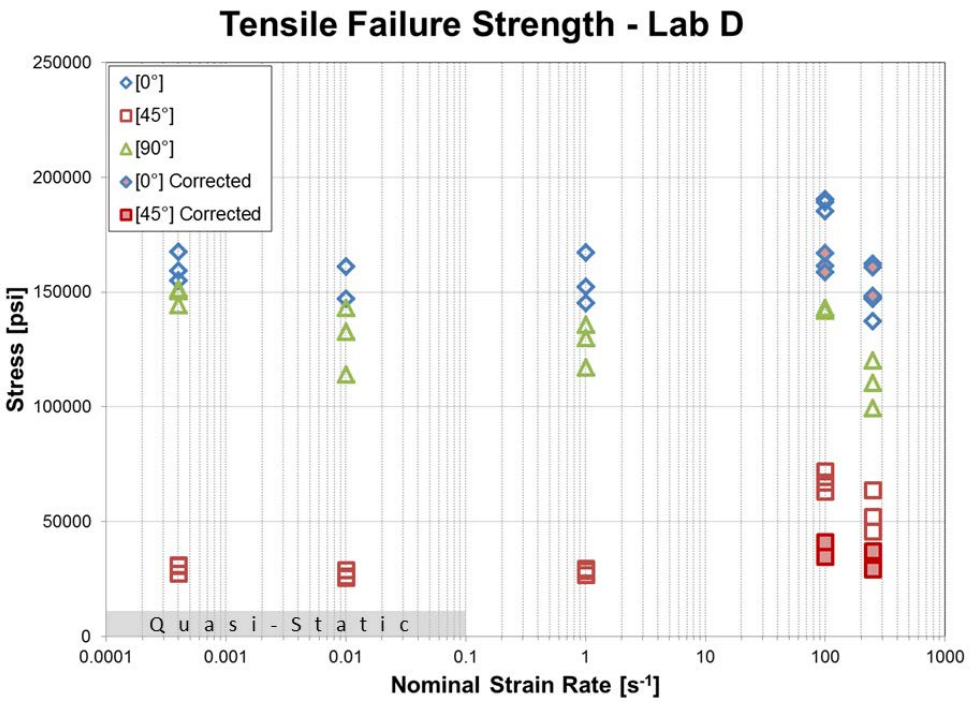

Figure 62. Corrected tensile failure strength of Toray T700G/2510 at various nominal strain rates for Laboratory D

4.5 LAB-TO-LAB VARIABILITY OF CORRECTED DATA

Corrected tensile failure strength is compared across laboratory per material orientation in figures 63–65 for each of the three material orientations. Quasi-static results from NIAR as well as the sub-size SHPB specimen data are included in these figures for reference. A conventional servo-hydraulic machine was used to test sub-sized SHPB specimens to generate quasi-static data. To add clarity to the plots in figures 62–64, the strain-rate data were shifted around the nominal strain rates (0.01, 1.0, 100, and 250) for each lab.

Corrected tensile failure strength results for [0°] and [90°] material orientations do not appear to be rate sensitive. However, there is an increasing trend in failure strength for [45°] material orientation with increasing nominal strain rate. These results exhibit the utility and necessity of employing the signal-correction methodology over the “apparent” raw data.

Figures 63-64 show increasing variability especially at the higher strain rates. The variability in the test data is a consequence of the test apparatus and sensors used in the experiments. It is a net effect of the wave propagation effects and the dynamics of the test apparatus. The variability can be reduced by minimizing the dynamic effects associated with the load measurement. The development of more compact grips with few intermediate components between the specimen and the load cell should be explored to address this problem.

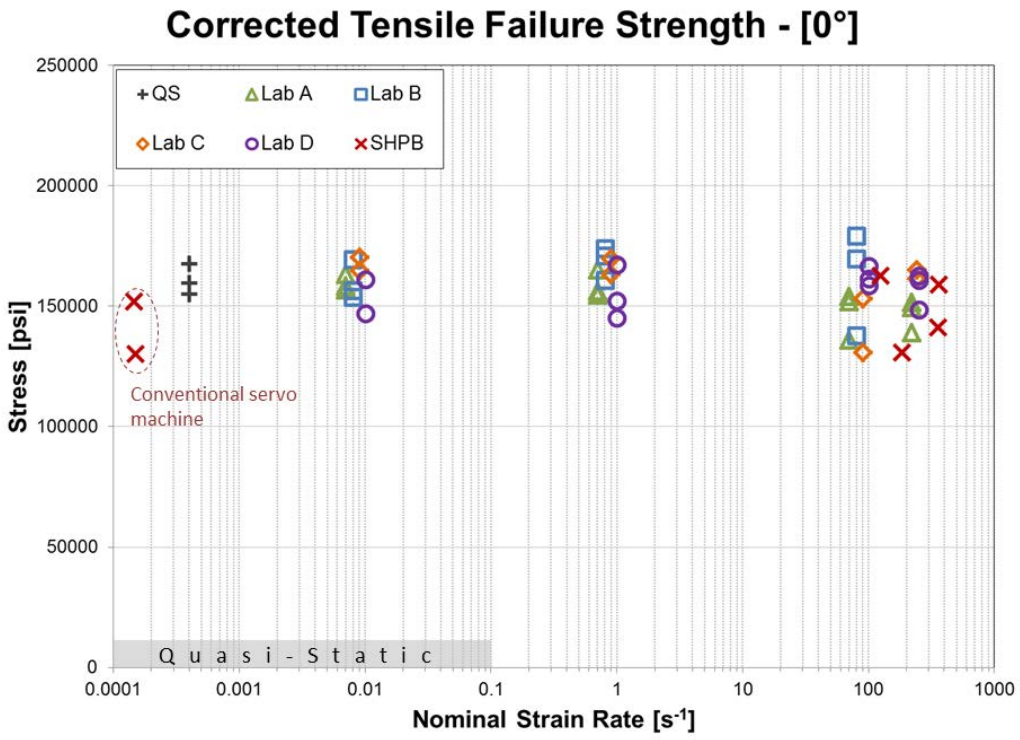

Figure 63. Servo-hydraulic data of corrected tensile failure strength of [0º] orientation of Toray T700G/2510 at various nominal strain rates for all laboratories and SHPB data

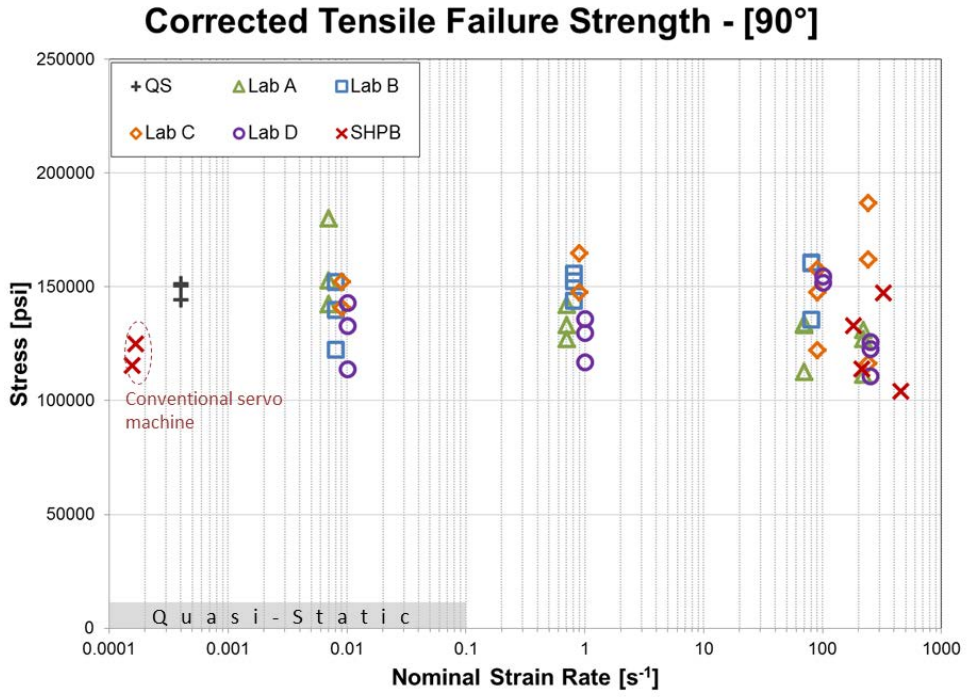

Figure 64. Servo-hydraulic data of corrected tensile failure strength of [90º] orientation of Toray T700G/2510 at various nominal strain rates for all laboratories and SHPB data

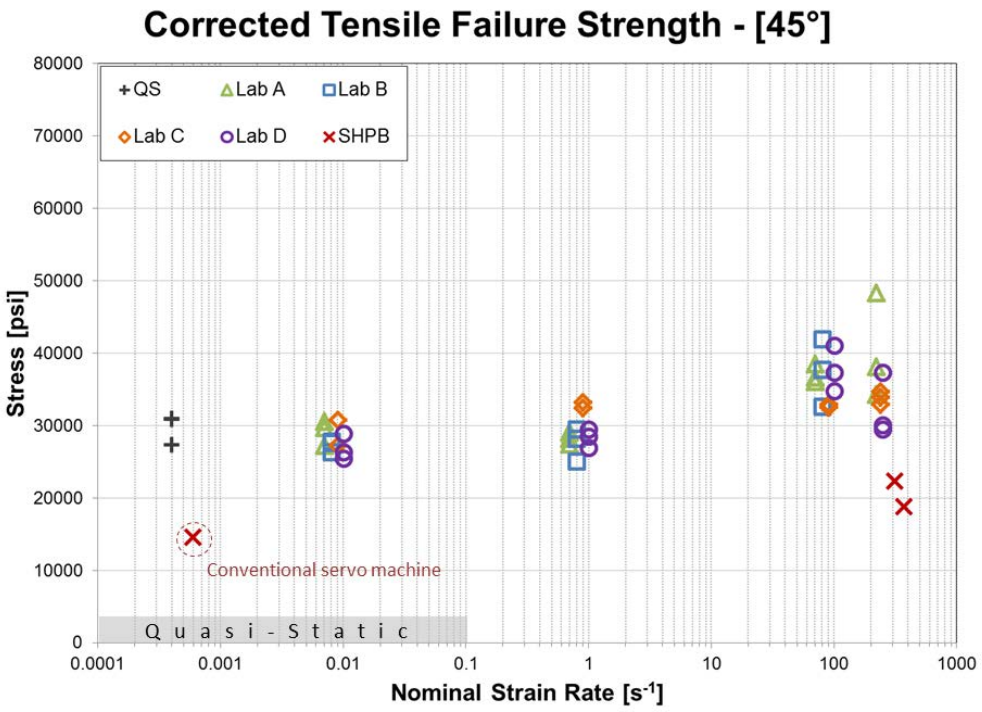

Figure 65. Servo-hydraulic data of corrected tensile failure strength of [45º] orientation of Toray T700G/2510 at various nominal strain rates for all laboratories and SHPB data

5. CONCLUSIONS AND RECOMMENDATIONS

The process of evaluating the test methods/apparatus and the force measurement methods employed by different laboratories when generating dynamic material properties is described in this report. Simultaneously, the tensile dynamic material response of a subject composite material is characterized. Dynamic testing of laminated composite materials was conducted by five different institutions. Two different types of test apparatuses were used for dynamic testing: servo-hydraulic machines and Split Hopkin Pressure Bar apparatus. Test methods/apparatuses and load measurement methods employed by the participating laboratories were comparatively evaluated using extended-tab metallic specimens.

Examination of the data revealed the following challenges and limitations associated with the use of servo-hydraulic load machines in the subject pursuit: non-constant test rates exist because of the use of open-loop control mode required to operate under the prescribed test conditions. Therefore, the load-frame actuator setting needs to be adjusted to achieve the desired stroke rate/speed when it engages the test specimen, not prior to engagement.

In addition, during dynamic loading conditions, the force measured using the hydraulic load-frame load cells are subject to load-frame oscillations. Therefore, post-test signal correction is required. A force signal correction methodology was developed and employed to correct for signal modulation resulting from the individual load-cell characteristics, unique load-train configuration behaviors (arising from aggregate effects of mass and material properties and modal

characteristics), and wave propagations and reflections. The correction methodology was used to correct the apparent tensile strength of the subject composite specimens.

After load correction, the material response of composite specimens in the principal directions [0˚] and [90˚] does not show significant sensitivity to the evaluated strain rates across laboratories. Because the response of carbon fibers when loaded in the fiber direction is linear elastic, they should not exhibit rate sensitivity. In contrast to principal directions, the response of the off-axis orientation [±45˚] showed larger failure-strength values with increasing strain rate. The rate sensitivity shown in off-axis specimens is due to the nonlinear response of the matrix constituent. This trend was consistent across laboratories, regardless of the scatter of the data.

The test procedure and test protocol developed for this investigation can be used as guidelines for dynamic tension testing. Baselines were generated for estimating the effect of strain rates as high as 250 s-1 and to address repeatability of experiments within each laboratory. Also, the overall intent of comparing laboratories was to assess the level of homogeneity found in apparatuses, methods, and output data. In reference to the test equipment, the load-correction methodology used in the current investigation helps the use of servo-machines to generate dynamic material properties from low-to-medium strain rates.

Major recommendations for future work should include shear and compression material properties for the subject composite material system. Shear and compression test methods should be developed to comprehensively generate material properties required for simulation of laminated composite material at the ply level. Also, given the variety of equipment apparatuses that could be used, and given the nature of the subject composite material systems in the consequent pursuit of repeatability, a comprehensive examination and error analysis of all likely sources of random and systemic error should be undertaken before actual test-data generation.

In the case of servo-hydraulic machines, conducting an advance determination of actuator velocity drop is recommended. Using the correct actuator velocity is necessary wherein signal transformation correction is anticipated to be employed in order to determine baseline system ringing characteristics.

Given the nature of high-strain rate testing of the subject composite material systems, the use of digital image correlation is highly indicated as beneficial augmentation to the use strain gauges. Larger deformations for equivalent load levels with less sensitivity to material discontinuities can be measured. This may improve failure detection and better account for damage progression in numerical material models used for simulation of crash events.

Variability in servo-hydraulic systems can be reduced by minimizing the dynamic effects associated with the load measurement. The development of more compact grips with few intermediate components between the specimen and the load cell should be explored to address this problem.

6. REFERENCES

1. FAA Report. (2017). Certification By Analysis – A Building Block Methodology for Composite and Metallic Aircraft Crashworthy Structures – Coupon Level (DOT/FAA/TC-16/21).

2. Chiem, C. Y., (1992). Material Deformation at High Strain Rates. In Meyers, M. A., Murr, L. E., and Staudhammer, K. P. (Eds.), *Shock-wave and High-strain-rate Phenomena in Materials*, (69-83). New York, NY: Marcel Dekker.

3. SAE International. (2008). *High Strain Rate Testing of Polymers* (SAE J2749).

4. FAA Report. (2009). Metallic Material Properties Development and Standardization (MMPDS-04).

5. AGATE. (2002). *A-Basis and B-Basis Design Allowables for Epoxy-Based Prepreg Toray T700SC-12K-50C/#2510 Plain Weave Fabric [SI Units]* (AGATE-WP3.3-033051-134). Wichita, KS: Tomblin, J., Sherraden, J., Seneviratne, W., and Raju, K.S.

6. AGATE. (2001). *B-Basis Design Allowables for Epoxy-Based Prepreg Newport E-Glass Fabric 7781/NB321* (AGATE-WP3.3-033051-097). Wichita, KS: Tomblin, J., McKenna, J., Ng, Y., and Raju, K.S.

7. ASTM E8 / E8M-13, "Standard Test Methods for Tension Testing of Metallic Materials," ASTM International, West Conshohocken, PA, 2013, DOI: 10.1520/E0008_E0008M, www.astm.org.

8. ASTM D3039 / D3039M-14, "Standard Test Method for Tensile Properties of Polymer Matrix Composite Materials," ASTM International, West Conshohocken, PA, 2014, DOI: 10.1520/D3039_D3039M-14, www.astm.org.

9. FAA Report. (2010) Crashworthiness of Composite Fuselage Structures – Material Dynamic Properties (Phase-I), (DOT/FAA/AR-09/8.

10. Kleiner, M., Tekkaya, A. E., Demir, O. K., Risch, D., and Psyk, V. (2009). A Drop-weight High-speed Tensile Testing Instrument. *Production Engineering, 3*(2), 175-190.

11. Barre, S., Chotard, T., and Benzeggagh, M. L. (1996). Comparative Study of Strain Rate Effects on Mechanical Properties of Glass Fibre-reinforced Thermoset Matrix Composites. *Composites Part A: Applied Science and Manufacturing, 27*(12), 1169-1181.

12. Harris, B., Beaumont, P. W. R., and Moncunill de Ferran, E. (1971). Strength and Fracture Toughness of Carbon Fibre Polyester Composites. *Journal of Materials Science, 6*(3), 238-251.

13. Hoggatt, C. R. and Recht, R. F. (1969). Stress-Strain Data Obtained at High Rates using an Expanding Ring. *Experimental Mechanics, 9*(10), 441–448.

14. Niordson, F. (1965). A Unit for Testing Materials at High Strain Rates. *Experimental Mechanics, 5*(1), 29-32.

15. Wang, Y., Xu, H., Erdman, D.L., Starbuck, M.J., Simunovic, S. (2011). Characterization of High Strain Rate Mechanical Behavior using 3D Digital Image Correlation. *Advanced Engineering Materials*, *13*(10), 943–948.

16. Dynamic Mechanics of Materials Laboratory, Dept. of Mechanical Engineering, The Ohio State University, http://www.mecheng.osu.edu/lab/dmm/node/35.

17. Staab, G. H. and Gilat, A. (1991). A Direct-tension Split Hopkinson Bar for High Strain Rate Testing. *Experimental Mechanics*, 31(3), 232-235.

18. Acosta, J.F., (2012). *Numerical and Experimental Studies on the Use of a Split Hopkinson Pressure Bar for High Strain Rate Tension Testing* (Ph.D. Dissertation). Wichita State University, KS.

19. Sierakowski, R. L. and Chaturvedi, S. K. (1997). Dynamic Properties. In *Dynamic Loading and Characterization of Fiber-reinforced Composites* (15–98). Hoboken, NJ: Wiley.

20. Montgomery, D. (2000). *Design and Analysis of Experiments* (5^{th} ed.). Hoboken, NJ: Wiley.

21. Zhu, D., Mobasher, B., Rajan, S. D., and Peralta, P. (2011). Characterization of Dynamic Tensile Testing Using Aluminum Alloy 6061-T6 at Intermediate Strain Rates. *Journal of Engineering Mechanics, 137*(10), 669-679.

22. International Iron and Steel Institute. (2005). Recommendations for Dynamic Tensile Testing of Sheet Steels. (1–25).

23. Rusinek, A., Cheriguene, R., Baumer, A., Klepaczko, J.R., and Larour, P. (2008). Dynamic Behavior of High-strength Sheet Steel in Dynamic Tension: Experimental and Numerical Analysis. *The Journal of Strain Analysis for Engineering Design 43*(1), 37-53.

24. Systat Software Inc. (2007). *TableCurve 2D*, San Jose, CA: Systat Software Inc.

APPENDIX A—LAB A RAW TESTING RESULTS

Laboratory A results using a conventional servo-hydraulic test machine.

ALUMINUM 2024-T3

Table A-1. Summary of test results for aluminum 2024-T3 at stroke rate of 0.0075 in/s

STROKE RATE [in/sec]	SPECIMEN NO.	TENSILE STRENGTH [psi]	MAXIMUM RECORDED STRAIN [in/in]	YOUNG'S MODULUS [Msi]	YIELD STRESS [psi]	AVERAGE STRAIN RATE [s^{-1}]
0.0075	R-0.0075-55	68651	0.0773	9.72	49535	0.00755
	R-0.0075-54	68373	0.0250	9.72	50301	0.00849
	R-0.0075-63	67045	0.1516	9.33	51953	0.00790
AVERAGE		68023	0.0847	9.59	50596	0.00798
STANDARD DEVIATION		858	0.0636	0.23	1236	0.00048
COEFFICIENT OF VARIATION [%]		1.26	75.16	2.35	2.44	5.96

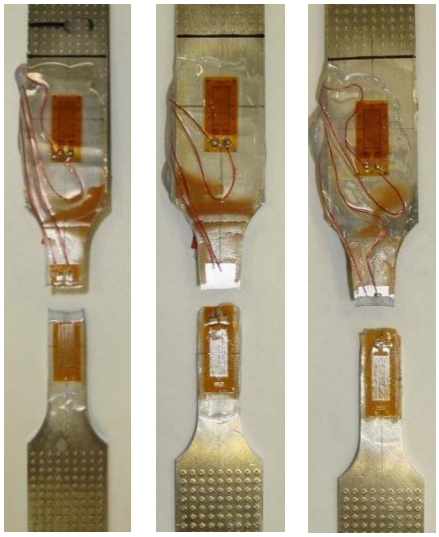

Figure A-1. Failure modes for aluminum 2024-T3 at stroke rate of 0.0075 in/s

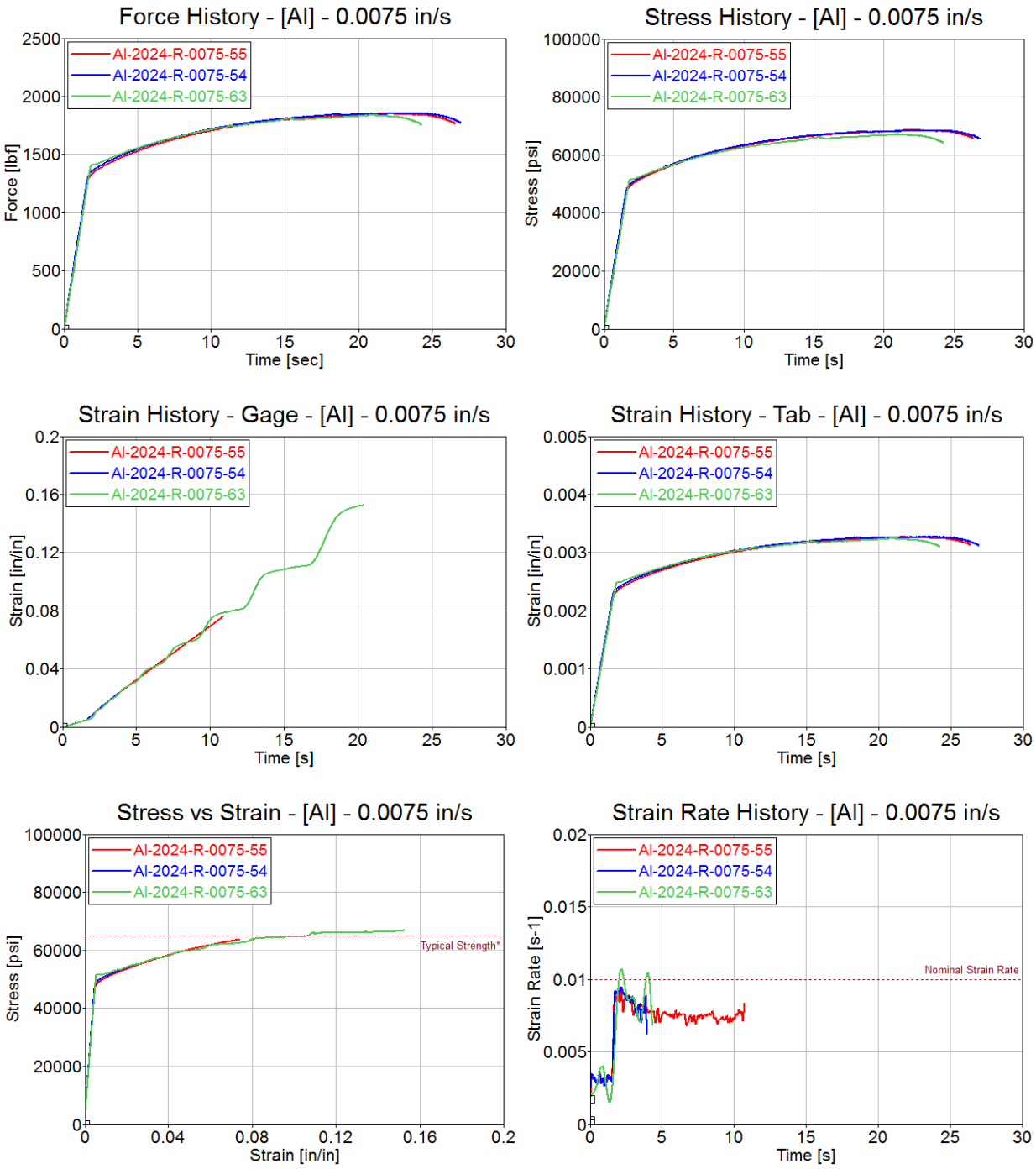

Figure A-2. Test results for aluminum 2024-T3 at stroke rate of 0.0075 in/s

Table A-2. Summary of test results for aluminum 2024-T3 at stroke rate of 0.75 in/s

STROKE RATE [in/sec]	SPECIMEN NO.	TENSILE STRENGTH [psi]	MAXIMUM RECORDED STRAIN [in/in]	YOUNG'S MODULUS [Msi]	YIELD STRESS [psi]	AVERAGE STRAIN RATE [s^{-1}]
0.75	R-0.75-47	69683	0.0970	11.43	53683	0.704
	R-0.75-82	62566	0.0900	9.01	50202	0.721
	R-0.75-65	68604	0.1275	9.97	51136	0.673
AVERAGE		66951	0.1049	10.14	51674	0.699
STANDARD DEVIATION		3836	0.0200	1.22	1802	0.024
COEFFICIENT OF VARIATION [%]		5.73	19.03	12.02	3.49	3.48

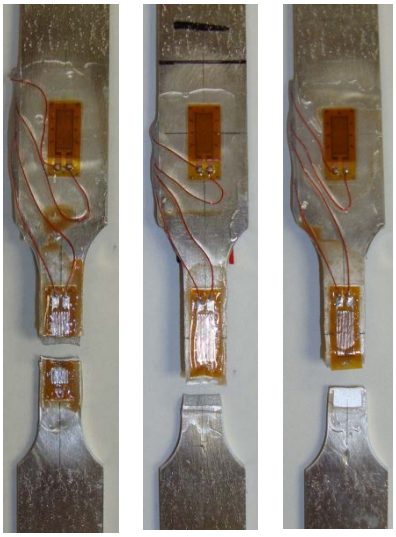

Figure A-3. Failure modes for aluminum 2024-T3 at stroke rate of 0.75 in/s

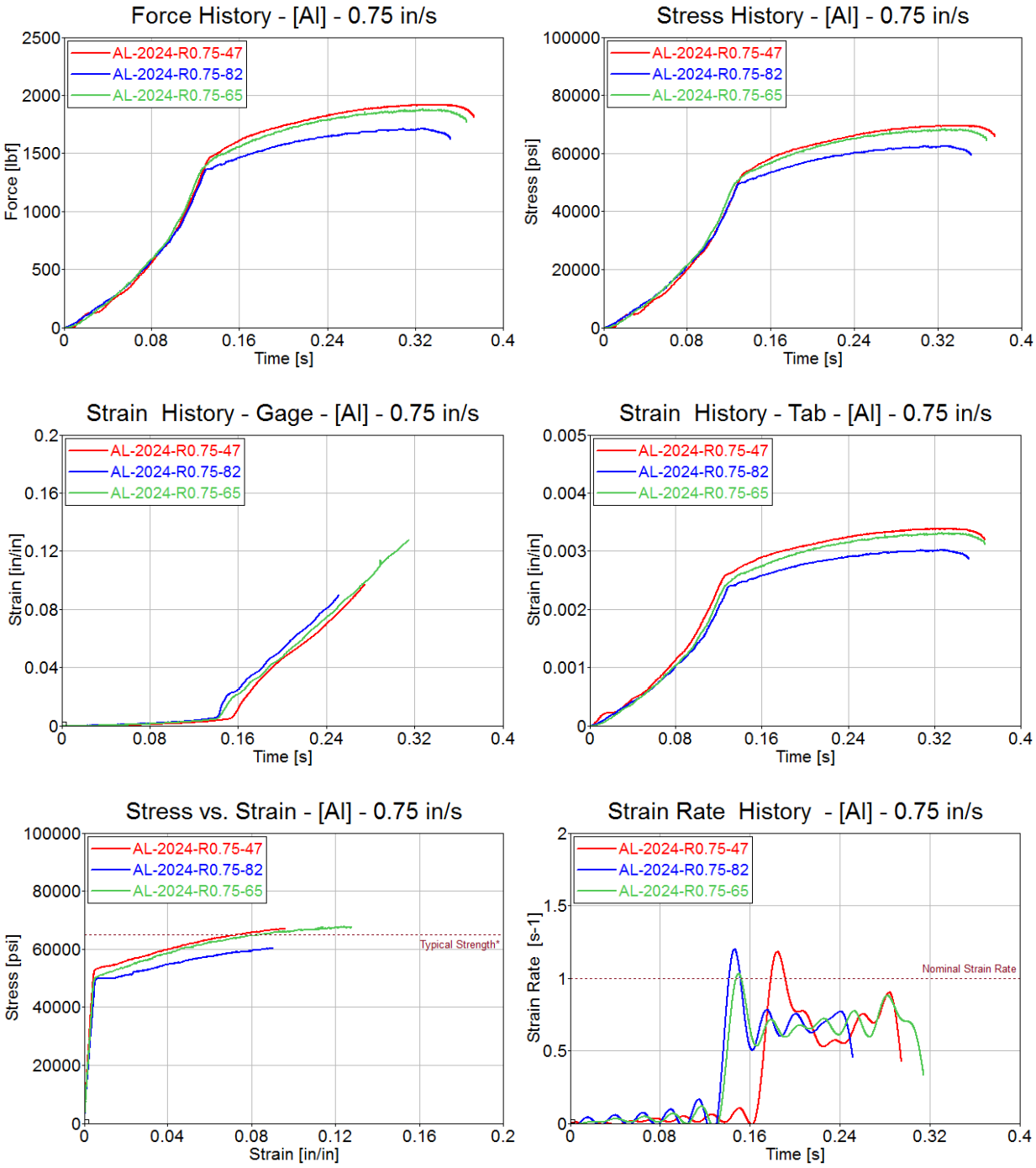

Figure A-4. Test results for aluminum 2024-T3 at stroke rate of 0.75 in/s

Table A-3. Summary of test results for aluminum 2024-T3 at stroke rate of 75 in/s

STROKE RATE [in/sec]	SPECIMEN NO.	TENSILE STRENGTH [psi]	MAXIMUM RECORDED STRAIN [in/in]	YOUNG'S MODULUS [Msi]	YIELD STRESS [psi]	AVERAGE STRAIN RATE [s^{-1}]
75	R-75-50	71290	0.1784	10.36	55931	67.45
	R-75-37	72085	0.1129	10.58	57132	65.61
	R-75-52	67593	0.1643	10.30	56505	72.77
AVERAGE		70323	0.1519	10.41	56523	68.61
STANDARD DEVIATION		2397	0.0345	0.15	601	3.72
COEFFICIENT OF VARIATION [%]		3.41	22.71	1.41	1.06	5.42

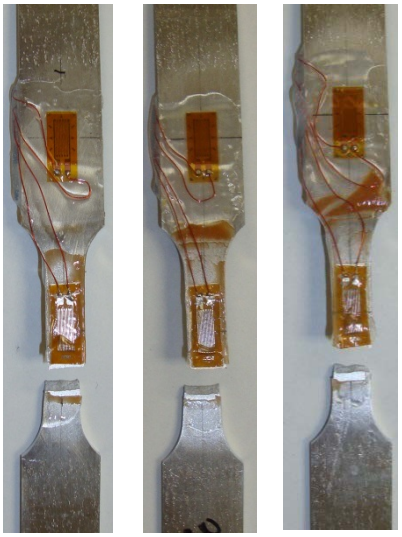

Figure A-5. Failure modes for aluminum 2024-T3 at stroke rate of 75 in/s

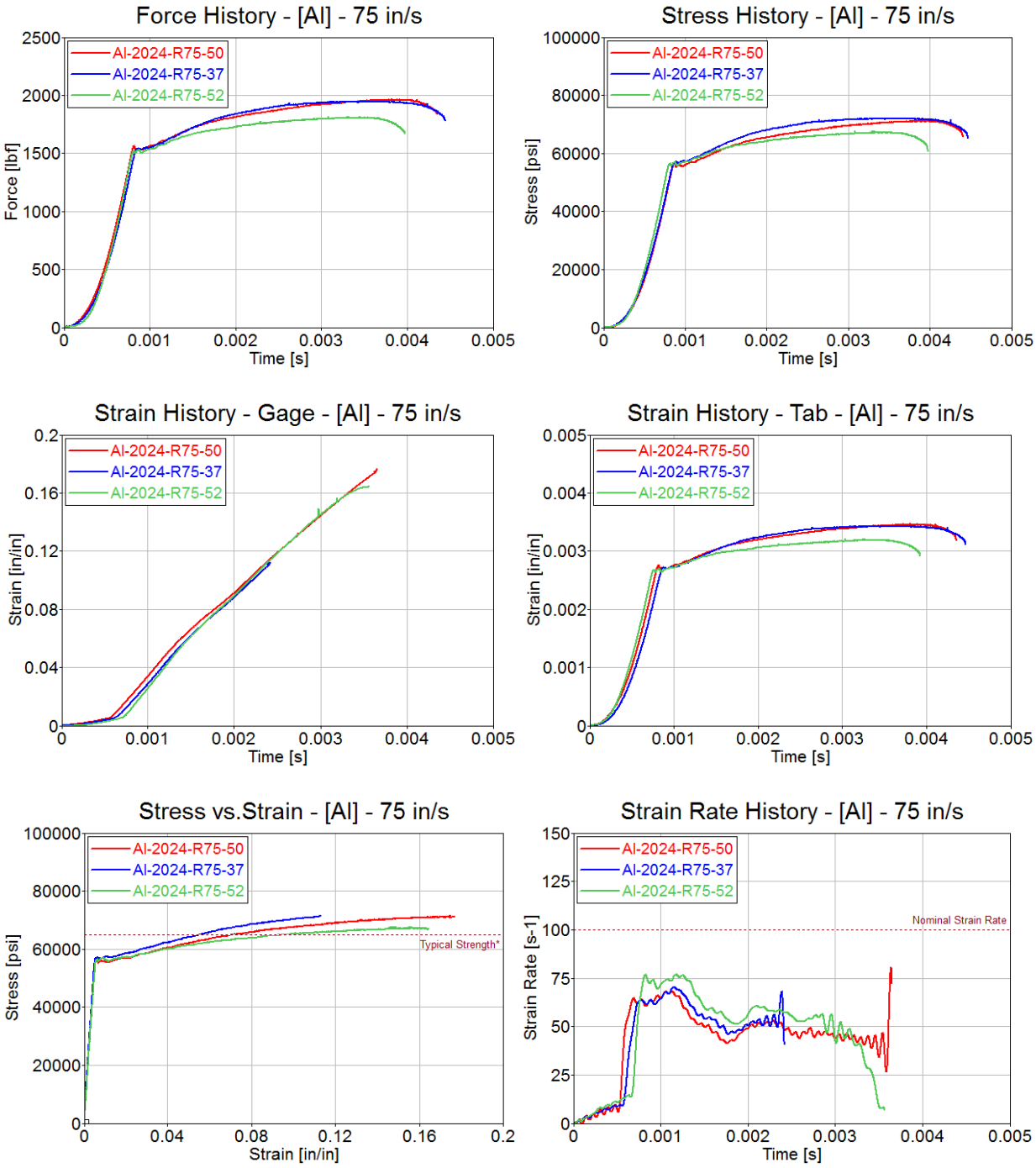

Figure A-6. Test results for aluminum 2024-T3 at stroke rate of 75 in/s

Table A-4. Summary of test results for aluminum 2024-T3 at stroke rate of 187.5 in/s

STROKE RATE [in/sec]	SPECIMEN NO.	TENSILE STRENGTH [psi]	MAXIMUM RECORDED STRAIN [in/in]	YOUNG'S MODULUS [Msi]	YIELD STRESS [psi]	AVERAGE STRAIN RATE [s^{-1}]
187.5	R-187.5-30	69597	0.1220	10.39	57761	321.28
	R-187.5-42	69282	0.1559	9.54	58224	330.16
	R-187.5-78	67675	0.0810	9.91	58972	322.08
AVERAGE		68851	0.1196	9.95	58319	324.51
STANDARD DEVIATION		1031	0.0375	0.43	611	4.91
COEFFICIENT OF VARIATION [%]		1.50	31.36	4.28	1.05	1.51

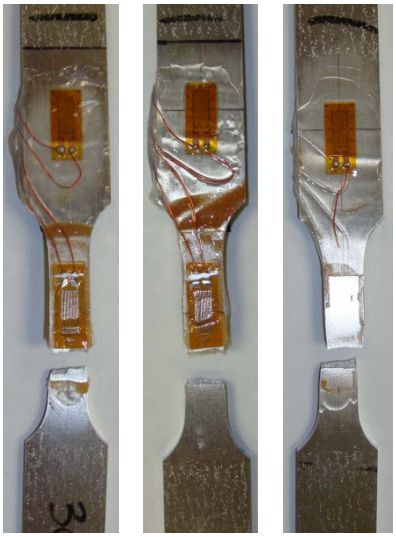

Figure A-7. Failure modes for aluminum 2024-T3 at stroke rate of 187.5 in/s

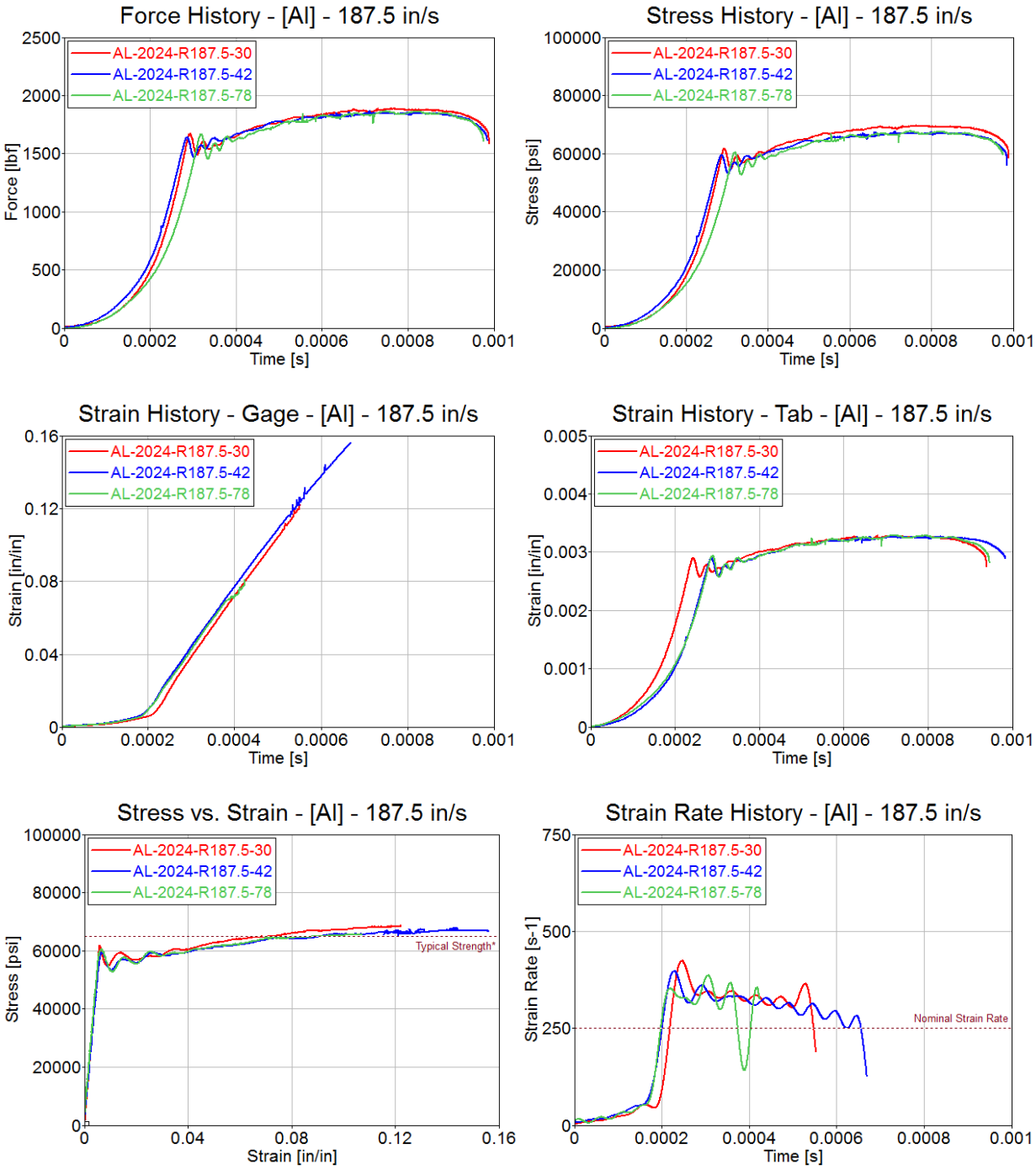

Figure A-8. Test results for aluminum 2024-T3 at stroke rate of 187.5 in/s

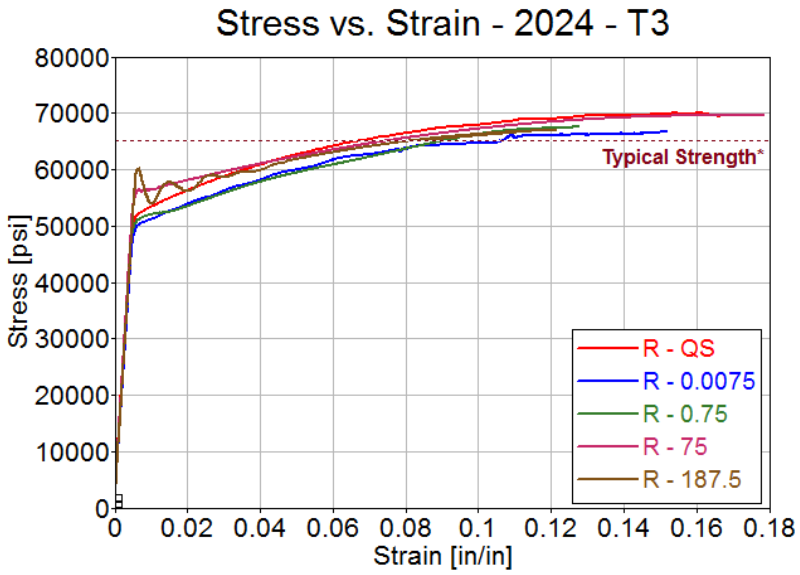

Figure A-9. Test results for aluminum 2024-T3: summary of all rates

TORAY [0°]$_4$

Table A-5. Summary of test results for Toray [0°]$_4$ at stroke rate of 0.02 in/s

STROKE RATE [in/sec]	SPECIMEN NO.	TENSILE STRENGTH [psi]	MAXIMUM RECORDED STRAIN [in/in]	YOUNG'S MODULUS [Msi]	AVERAGE STRAIN RATE [s^{-1}]
0.02	RR-P1-0-2-12-R02	163194	0.0177	8.78	0.00690
	RR-P1-0-4-3-R02	158461	0.0179	8.48	0.00658
	RR-P1-0-3-20-R02	156877	0.0181	8.86	0.00675
AVERAGE		159511	0.0179	8.71	0.00674
STANDARD DEVIATION		3287	0.0002	0.20	0.00016
COEFFICIENT OF VARIATION [%]		2.06	1.14	2.30	2.37

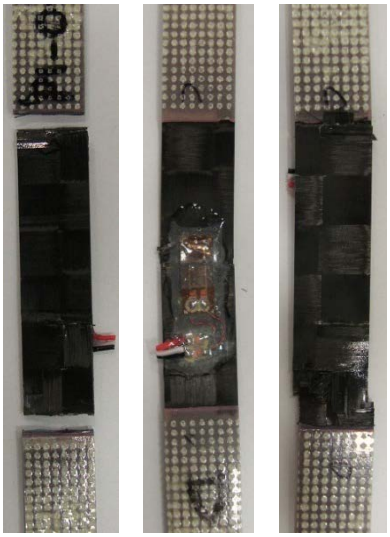

Figure A-10. Failure modes for Toray [0°]$_4$ at stroke rate of 0.02 in/s

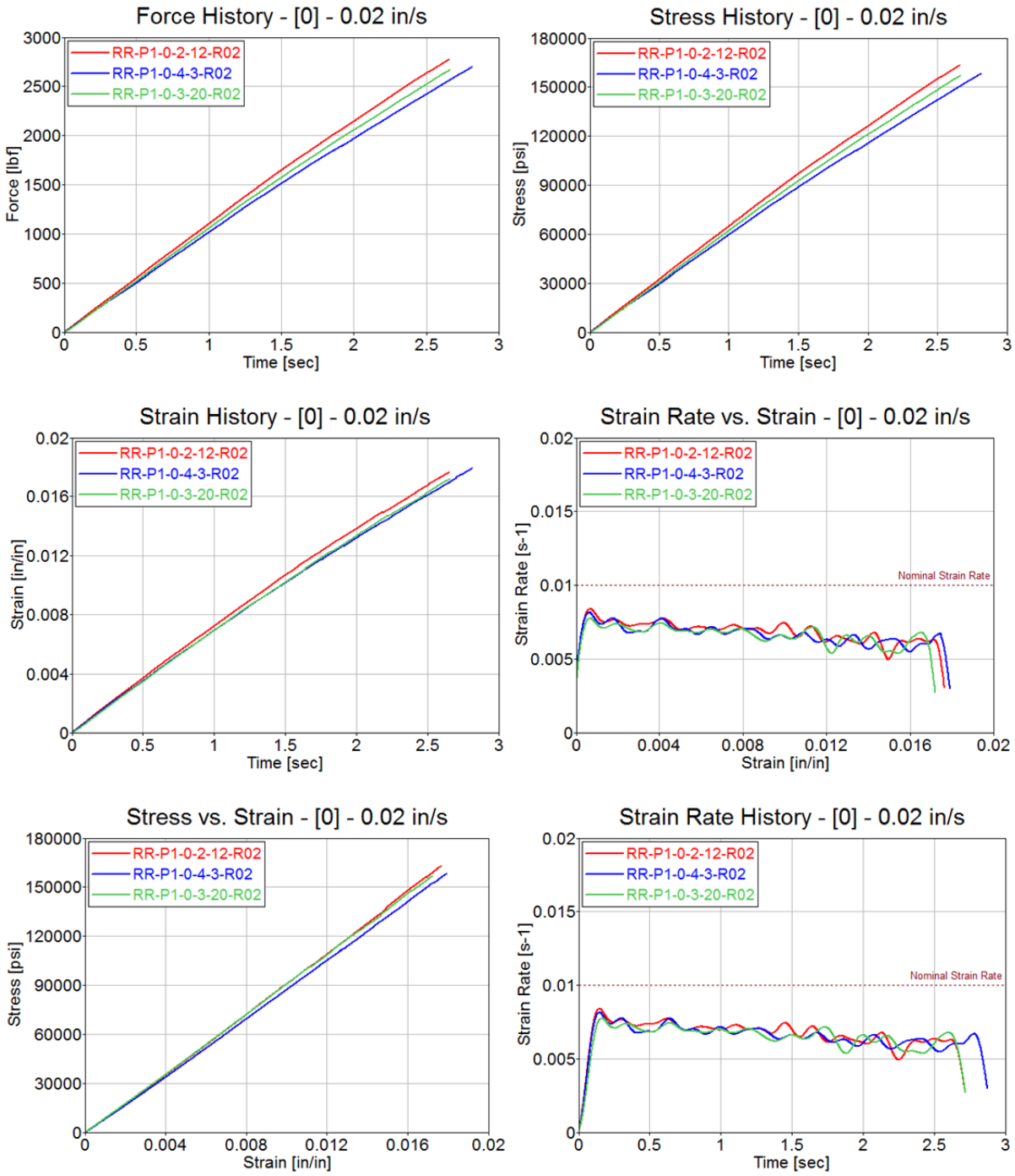

Figure A-11. Test results for Toray [0˚]4 at stroke rate of 0.02 in/s

Table A-6. Summary of test results for Toray $[0^{\circ}]_4$ at stroke rate of 2 in/s

STROKE RATE [in/sec]	SPECIMEN NO.	TENSILE STRENGTH [psi]	MAXIMUM RECORDED STRAIN [in/in]	YOUNG'S MODULUS [Msi]	AVERAGE STRAIN RATE [s^{-1}]
2	RR-P1-0-1-15-R2	161707	0.0172	9.78	0.193
	RR-P1-0-2-20-R2	159665	0.0167	9.87	0.191
	RR-P1-0-3-9-R2	171186	0.0180	9.44	0.204
AVERAGE		164186	0.0173	9.70	0.196
STANDARD DEVIATION		6147	0.0006	0.23	0.007
COEFFICIENT OF VARIATION [%]		3.74	3.70	2.34	3.57

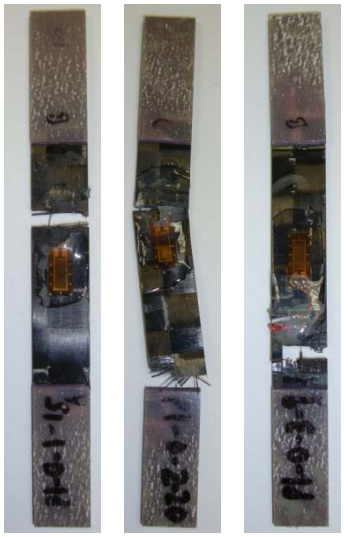

Figure A-12. Failure modes for Toray $[0^{\circ}]_4$ at stroke rate of 2 in/s

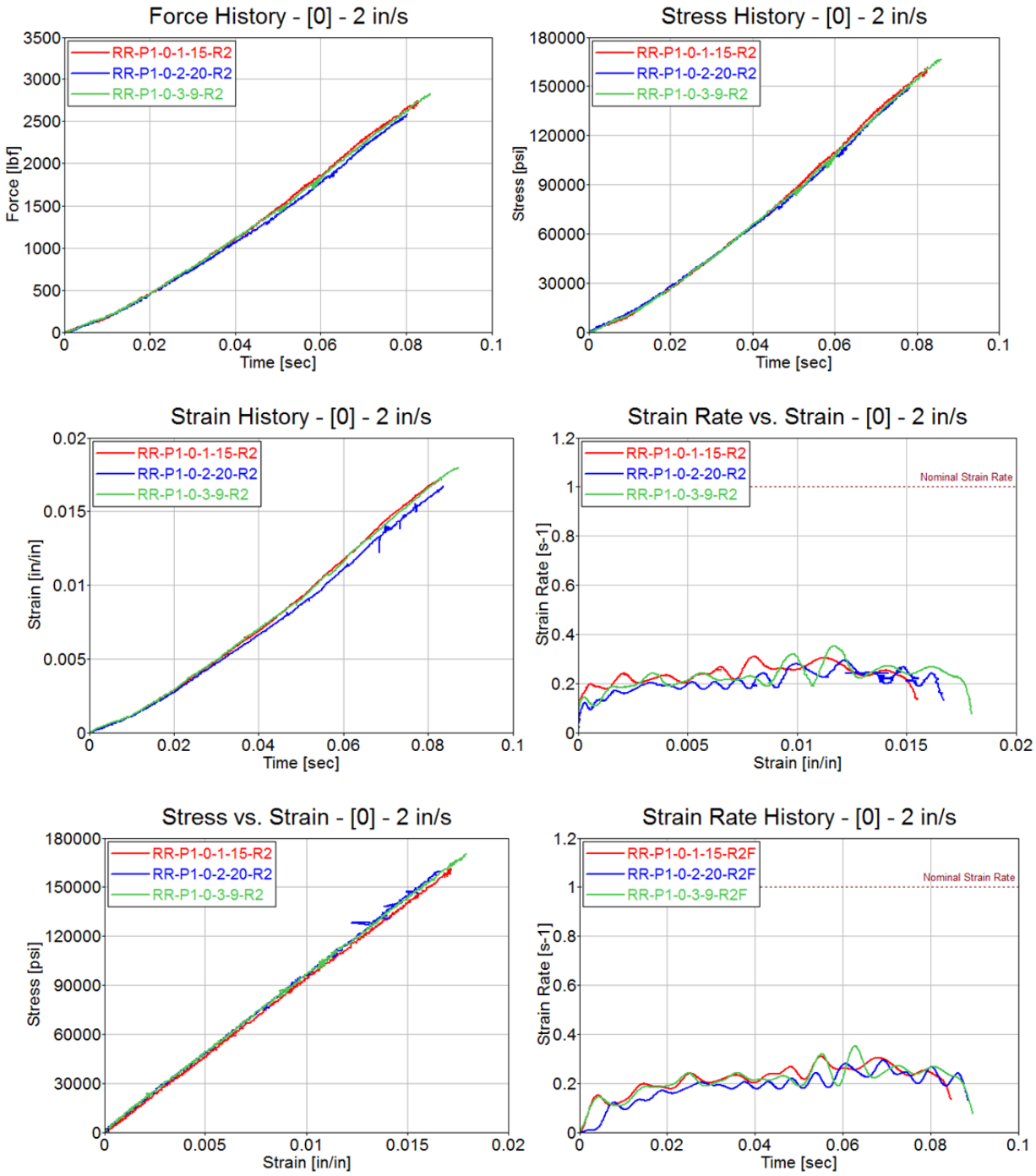

Figure A-13. Test results for Toray [0˚]$_4$ at stroke rate of 2 in/s

Table A-7. Summary of test results for Toray $[0^{\circ}]_4$ at stroke rate of 200 in/s

STROKE RATE [in/sec]	SPECIMEN NO.	TENSILE STRENGTH [psi]	MAXIMUM RECORDED STRAIN [in/in]	YOUNG'S MODULUS [Msi]	AVERAGE STRAIN RATE [s^{-1}]
200	RR-P1-0-1-2-R200	218003	0.0220	9.16	57.33
	RR-P1-0-1-20-R200	216708	0.0165	10.00	56.30
	RR-P1-0-1-23-R200	186089	0.0165	8.33	56.94
AVERAGE		206934	0.0183	9.16	56.86
STANDARD DEVIATION		18063	0.0032	0.84	0.52
COEFFICIENT OF VARIATION [%]		8.73	17.23	9.11	0.91

Figure A-14. Failure modes for Toray $[0^{\circ}]_4$ at stroke rate of 200 in/s

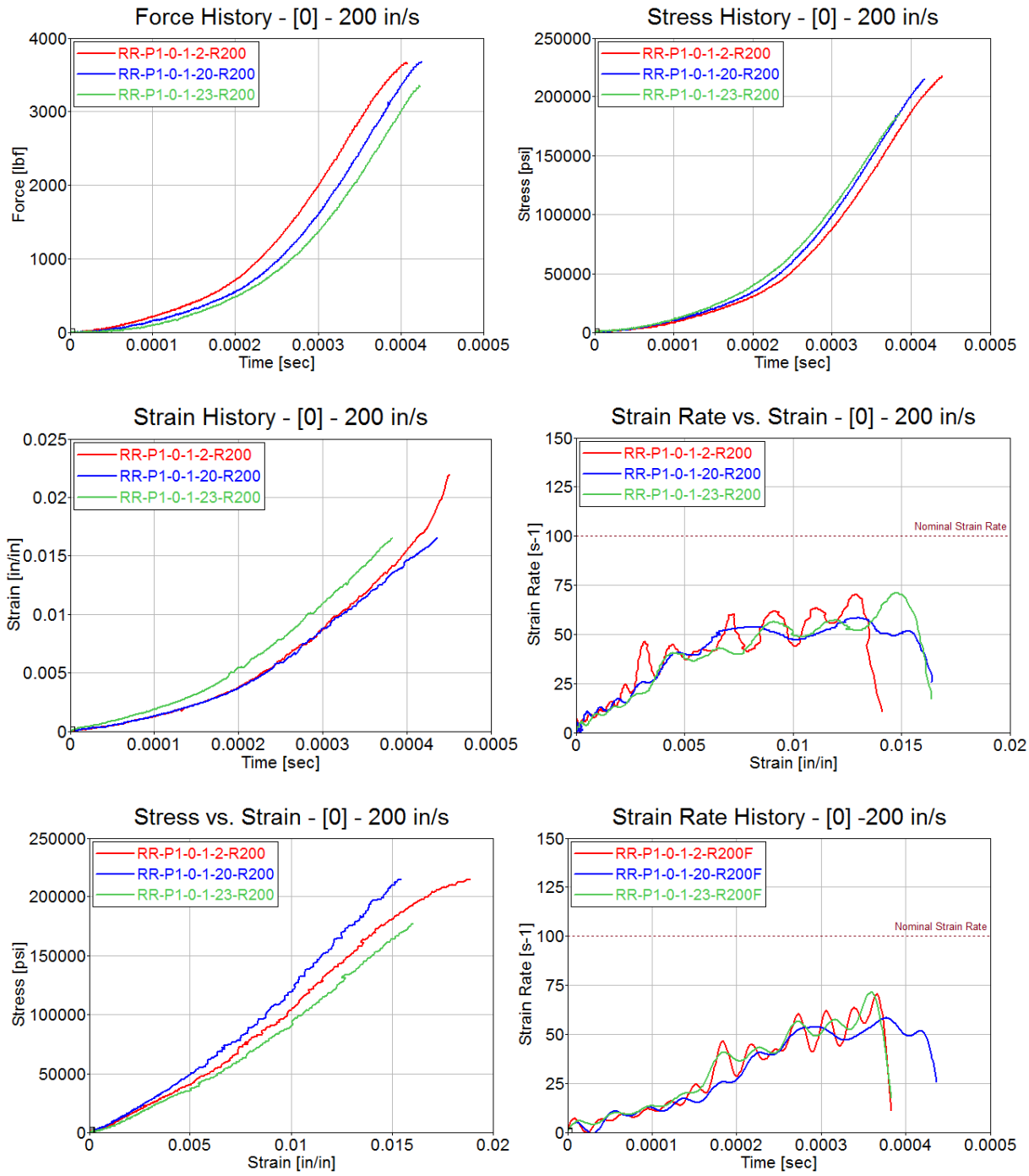

Figure A-15. Test results for Toray [0˚]$_4$ at stroke rate of 200 in/s

Table A-8. Summary of test results for Toray $[0^{\circ}]_4$ at stroke rate of 500 in/s

STROKE RATE [in/sec]	SPECIMEN NO.	TENSILE STRENGTH [psi]	MAXIMUM RECORDED STRAIN [in/in]	YOUNG'S MODULUS [Msi]	AVERAGE STRAIN RATE [s^{-1}]
500	RR-P1-0-1-24-R500	154117	0.0186	11.47	91.03
	RR-P1-0-2-4-R500	186896	0.0091	12.28	92.11
	RR-P1-0-3-19-R500	174058	0.0173	13.20	90.96
AVERAGE		171690	0.0150	12.32	91.37
STANDARD DEVIATION		16518	0.0051	0.87	0.64
COEFFICIENT OF VARIATION [%]		9.62	34.13	7.03	0.70

Figure A-16. Failure modes for Toray $[0^{\circ}]_4$ at stroke rate of 500 in/s

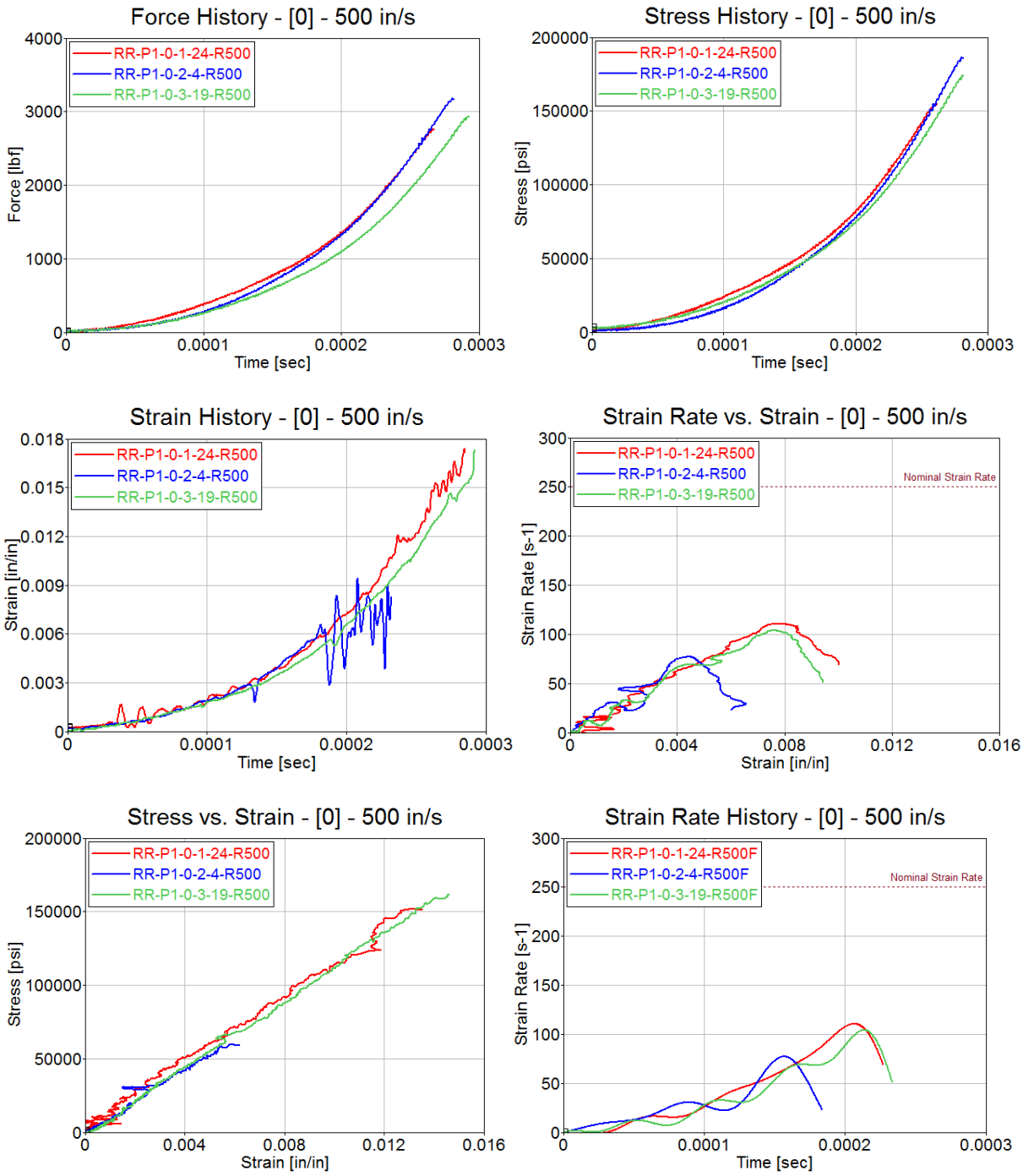

Figure A-17. Test results for Toray [0˚]$_4$ at stroke rate of 500 in/s

TORAY $[90]_4$

Table A-9. Summary of test results for Toray $[90^{\circ}]_4$ at stroke rate of 0.02 in/s

STROKE RATE [in/sec]	SPECIMEN NO.	TENSILE STRENGTH [psi]	MAXIMUM RECORDED STRAIN [in/in]	YOUNG'S MODULUS [Msi]	AVERAGE STRAIN RATE [s^{-1}]
0.02	RR-P2-90-2-2-R02	153004	0.0175	8.24	0.00705
	RR-P2-90-3-1-R02	180184	0.0184	9.63	0.00687
	RR-P2-90-3-4-R02	142516	0.0167	8.43	0.00676
AVERAGE		158568	0.0175	8.77	0.00689
STANDARD DEVIATION		19441	0.0009	0.75	0.00015
COEFFICIENT OF VARIATION [%]		12.26	5.02	8.61	2.16

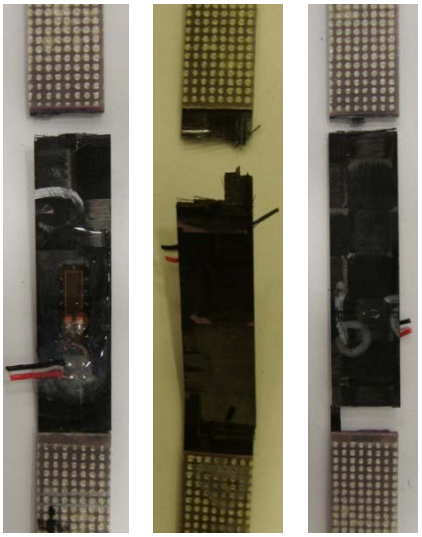

Figure A-18. Failure modes for Toray $[90^{\circ}]_4$ at stroke rate of 0.02 in/s

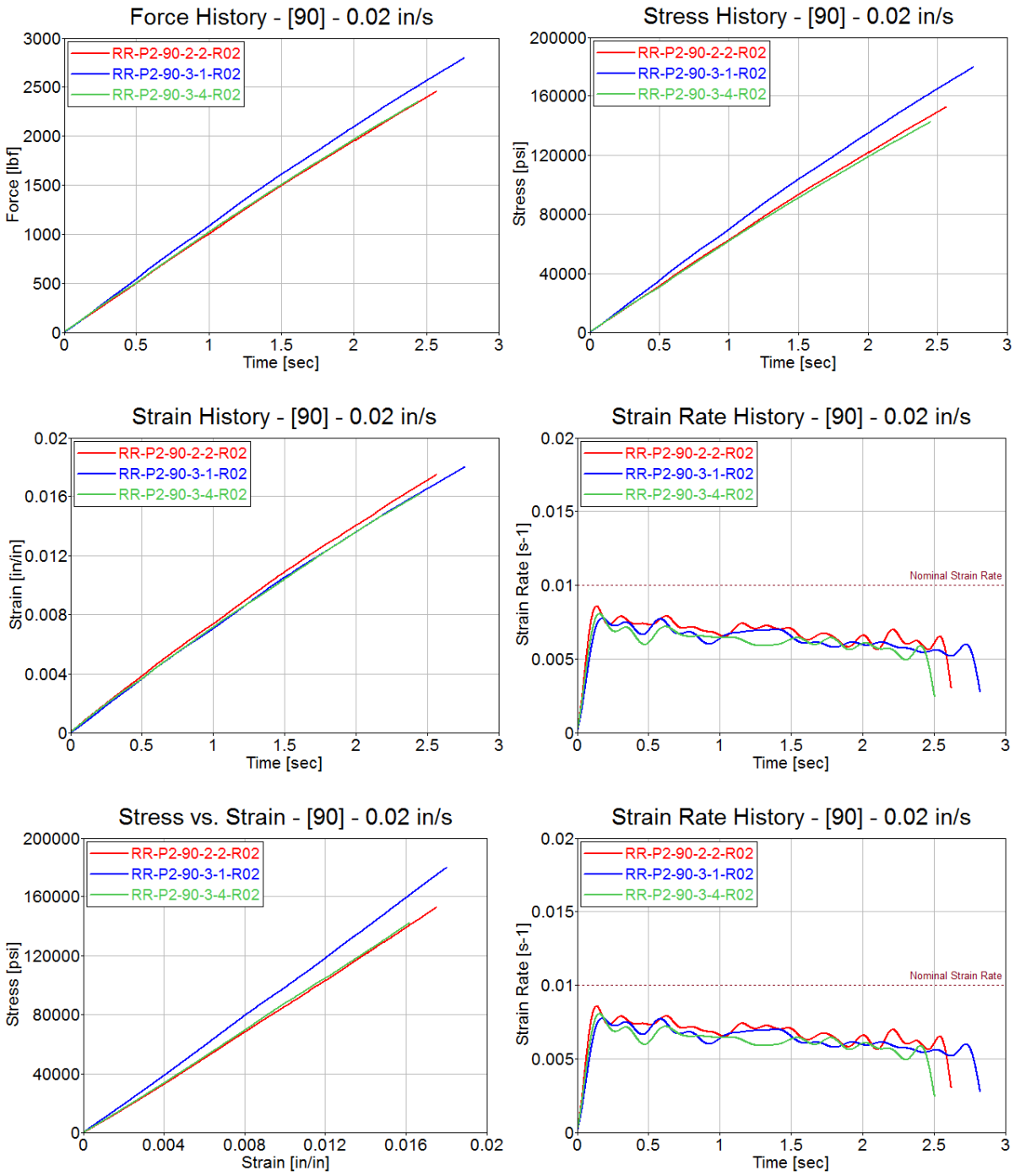

Figure A-19. Test results for Toray [90˚]$_4$ at stroke rate of 0.02 in/s

Table A-10. Summary of test results for Toray $[90^{\circ}]_4$ at stroke rate of 2 in/s

STROKE RATE [in/sec]	SPECIMEN NO.	TENSILE STRENGTH [psi]	MAXIMUM RECORDED STRAIN [in/in]	YOUNG'S MODULUS [Msi]	AVERAGE STRAIN RATE [s^{-1}]
2	RR-P2-90-1-12-R2	145897	0.0148	9.64	0.200
	RR-P2-90-3-7-R2	131549	0.0153	8.57	0.235
	RR-P2-90-3-18-R2	138729	0.0154	9.19	0.202
AVERAGE		138725	0.0152	9.13	0.212
STANDARD DEVIATION		7174	0.0003	0.54	0.019
COEFFICIENT OF VARIATION [%]		5.17	2.16	5.88	9.13

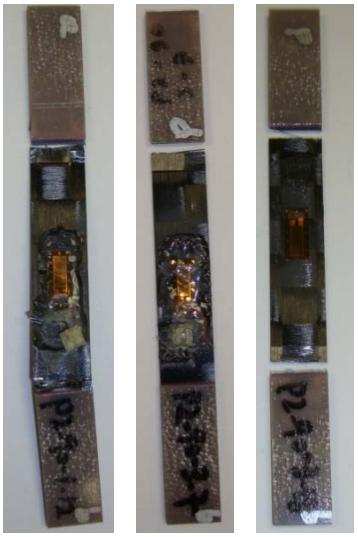

Figure A-20. Failure modes for Toray $[90^{\circ}]_4$ at stroke rate of 2 in/s

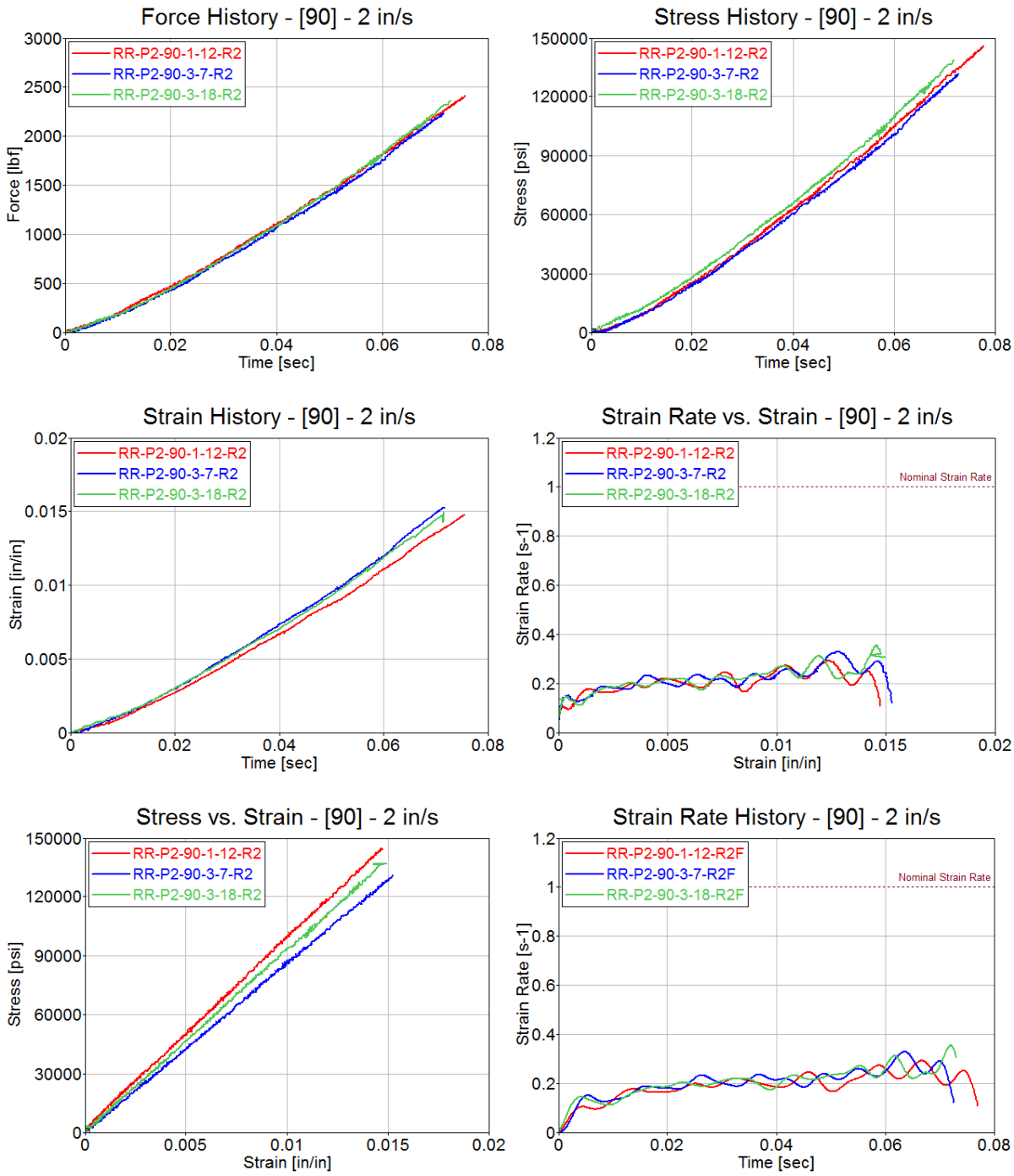

Figure A-21. Test results for Toray [90˚]$_4$ at stroke rate of 2 in/s

Table A-11. Summary of test results for Toray [90˚]$_4$ at stroke rate of 200 in/s

STROKE RATE [in/sec]	SPECIMEN NO.	TENSILE STRENGTH [psi]	MAXIMUM RECORDED STRAIN [in/in]	YOUNG'S MODULUS [Msi]	AVERAGE STRAIN RATE [s^{-1}]
200	RR-P2-90-2-15-R200	171704	0.0142	10.22	60.10
	RR-P2-90-3-3-R200	191083	0.0173	10.43	62.10
	RR-P2-90-3-10-R200	197610	0.0157	10.84	60.96
AVERAGE		186799	0.0157	10.50	61.05
STANDARD DEVIATION		13474	0.0016	0.31	1.00
COEFFICIENT OF VARIATION [%]		7.21	9.86	3.00	1.64

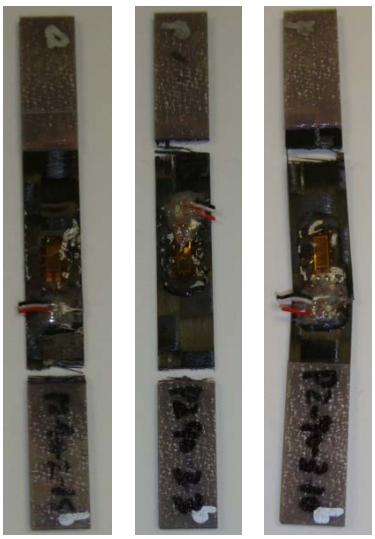

Figure A-22. Failure modes for Toray [90˚]$_4$ at stroke rate of 200 in/s

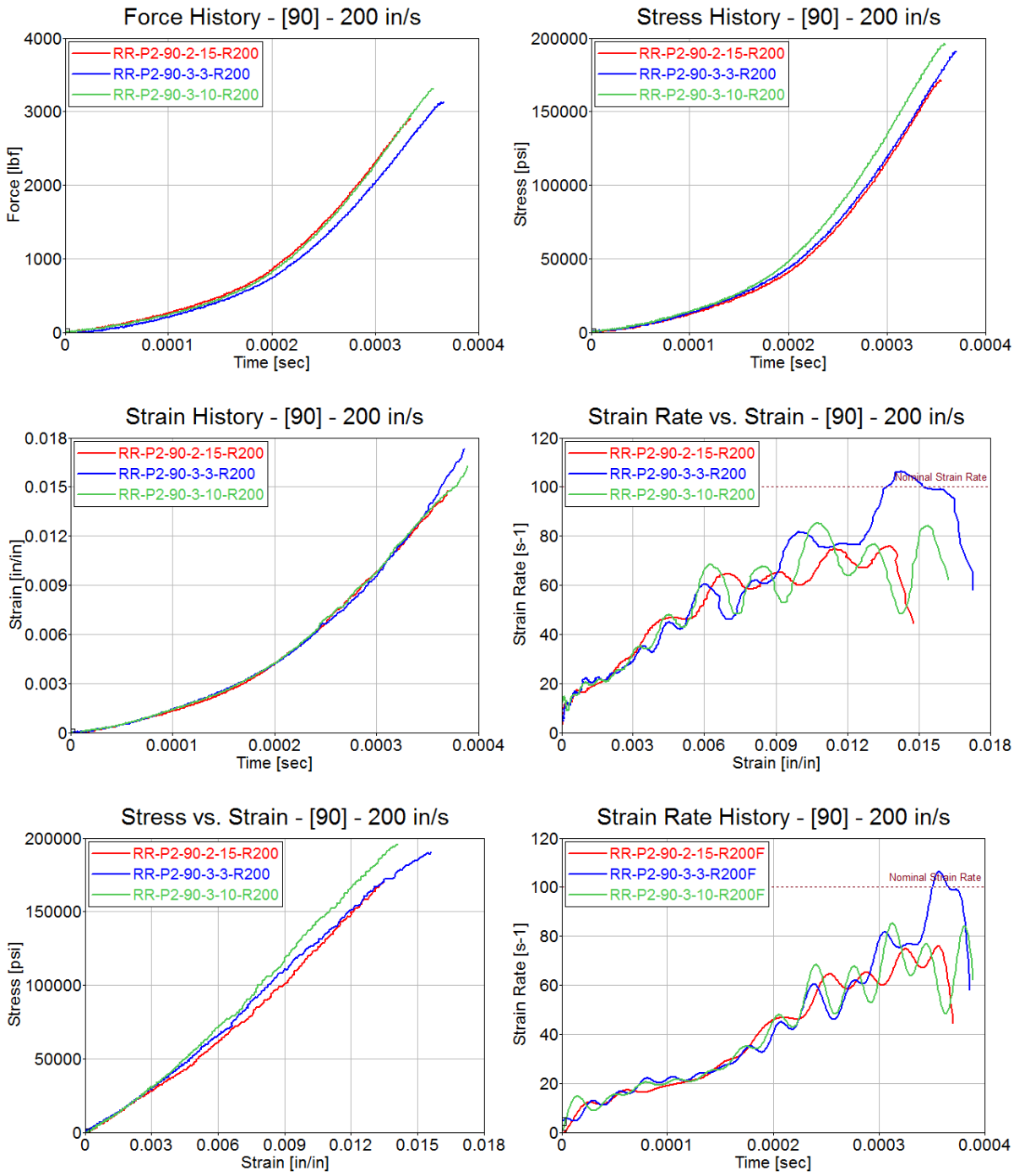

Figure A-23. Test results for Toray [90˚]$_4$ at stroke rate of 200 in/s

Table A-12. Summary of test results for Toray [90°]$_4$ at stroke rate of 500 in/s

STROKE RATE [in/sec]	SPECIMEN NO.	TENSILE STRENGTH [psi]	MAXIMUM RECORDED STRAIN [in/in]	YOUNG'S MODULUS [Msi]	AVERAGE STRAIN RATE [s^{-1}]
500	RR-P2-90-1-15-R500	175135	0.0173	13.94	77.53
	RR-P2-90-2-6-R500	154769	0.0119	12.65	83.35
	RR-P2-90-3-16-R500	167161	0.0097	12.81	82.70
AVERAGE		165688	0.0130	13.13	81.19
STANDARD DEVIATION		10262	0.0039	0.70	3.19
COEFFICIENT OF VARIATION [%]		6.19	29.92	5.36	3.93

Figure A-24. Failure modes for Toray [90°]$_4$ at stroke rate of 500 in/s

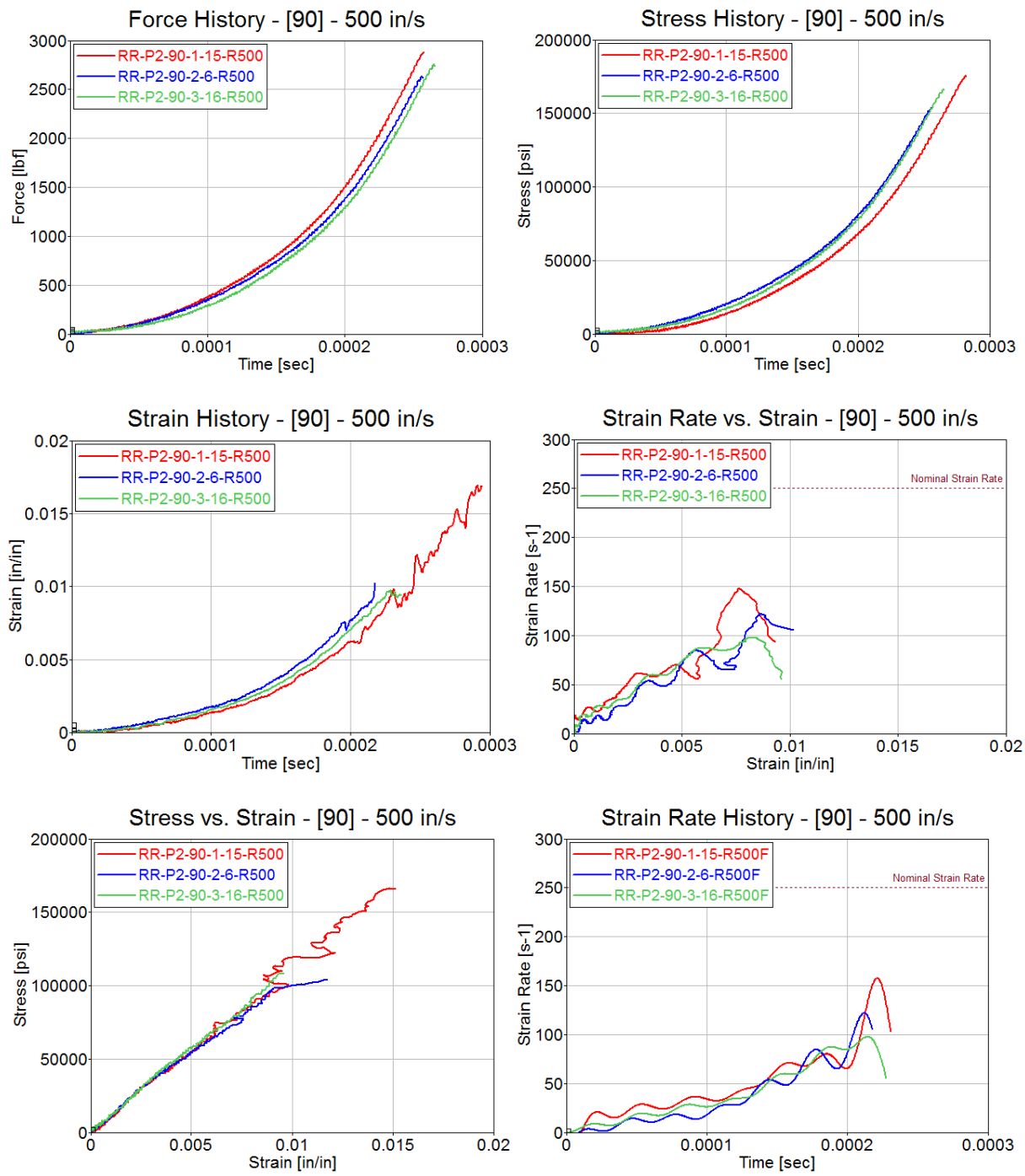

Figure A-25. Test results for Toray [90˚]$_4$ at stroke rate of 500 in/s

TORAY $[\pm 45^{\circ}]_4$

Table A-13. Summary of test results for Toray $[\pm 45^{\circ}]_4$ at stroke rate of 0.02 in/s

STROKE RATE [in/sec]	SPECIMEN NO.	TENSILE STRENGTH [psi]	MAXIMUM RECORDED STRAIN [in/in]	YOUNG'S MODULUS [Msi]	AVERAGE STRAIN RATE [s^{-1}]
0.02	RR-P3-45-1-12-R02	30566	*	2.25	0.00795
	RR-P4-45-1-11-R02	27238	*	2.18	0.00819
	RR-P4-45-1-20-R02	29678	*	2.07	0.00854
AVERAGE		29161	-	2.16	0.00823
STANDARD DEVIATION		1724	-	0.09	0.00029
COEFFICIENT OF VARIATION [%]		5.91	-	4.16	3.58

*Exceeded strain gauge capability of 0.03 in/in

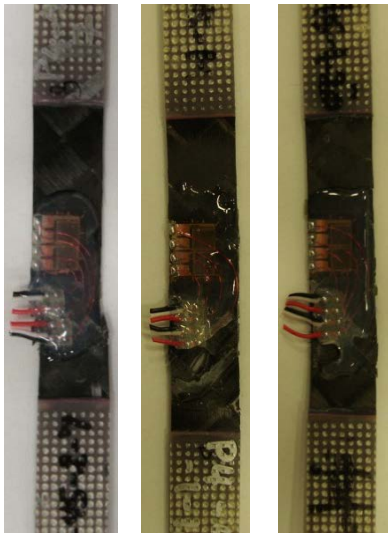

Figure A-26. Failure modes for Toray $[\pm 45^{\circ}]_4$ at stroke rate of 0.02 in/s

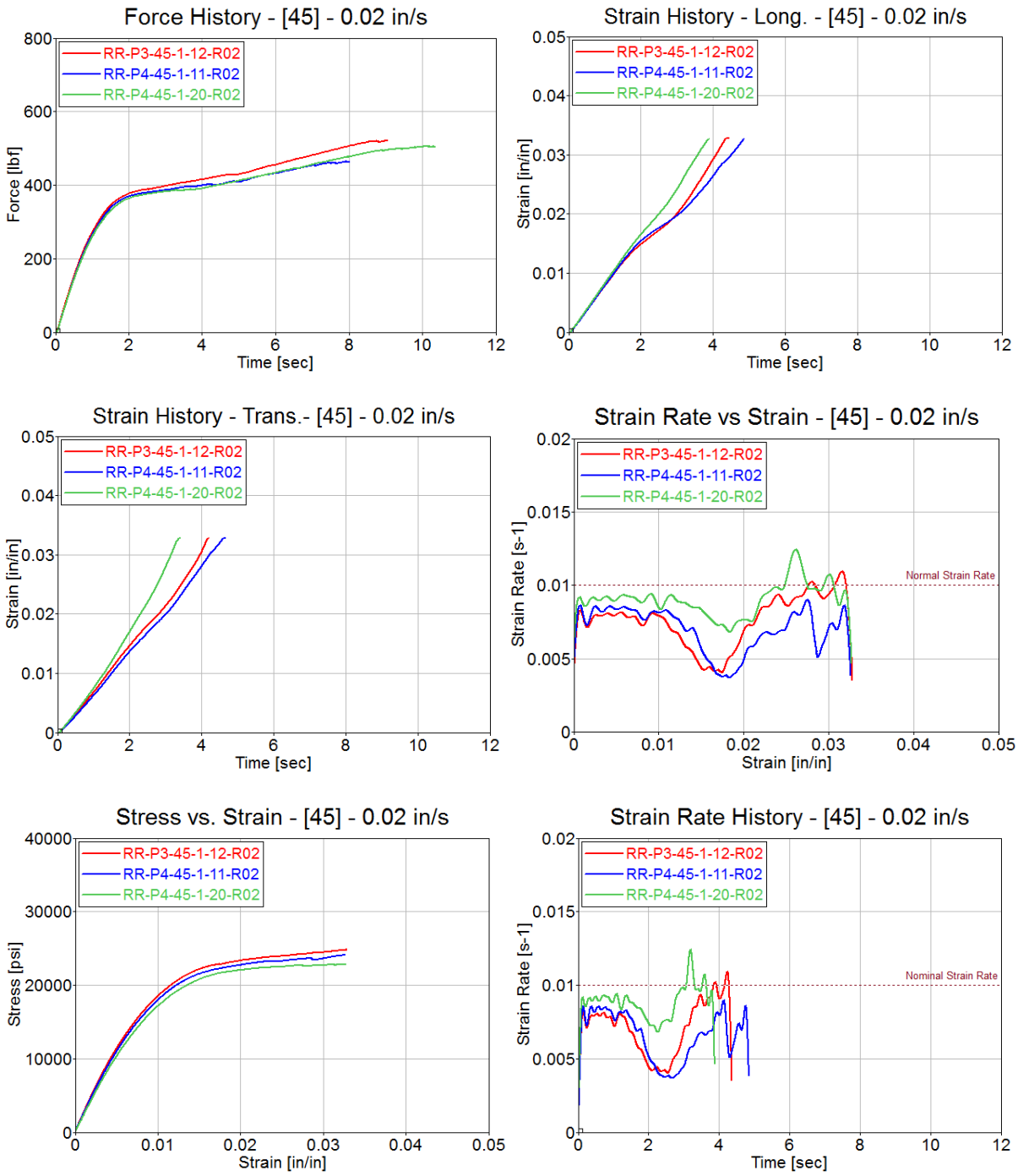

Figure A-27. Test results for Toray [±45˚]$_4$ at stroke rate of 0.02 in/s

Table A-14. Summary of test results for Toray [±45°]$_4$ at stroke rate of 2 in/s

STROKE RATE [in/sec]	SPECIMEN NO.	TENSILE STRENGTH [psi]	MAXIMUM RECORDED STRAIN [in/in]	YOUNG'S MODULUS [Msi]	AVERAGE STRAIN RATE [s^{-1}]
2	RR-P3-45-2-1-R2	28322	0.0299	2.38	0.604
	RR-P3-45-2-14-R2	28665	0.0299	2.34	0.570
	RR-P4-45-2-9-R2	29949	0.0300	2.63	0540
AVERAGE		28979	0.0299	2.45	0.571
STANDARD DEVIATION		857	0.0001	0.16	0.032
COEFFICIENT OF VARIATION [%]		2.96	0.2	6.41	5.60

Figure A-28. Failure modes for Toray [±45°]$_4$ at stroke rate of 2 in/s

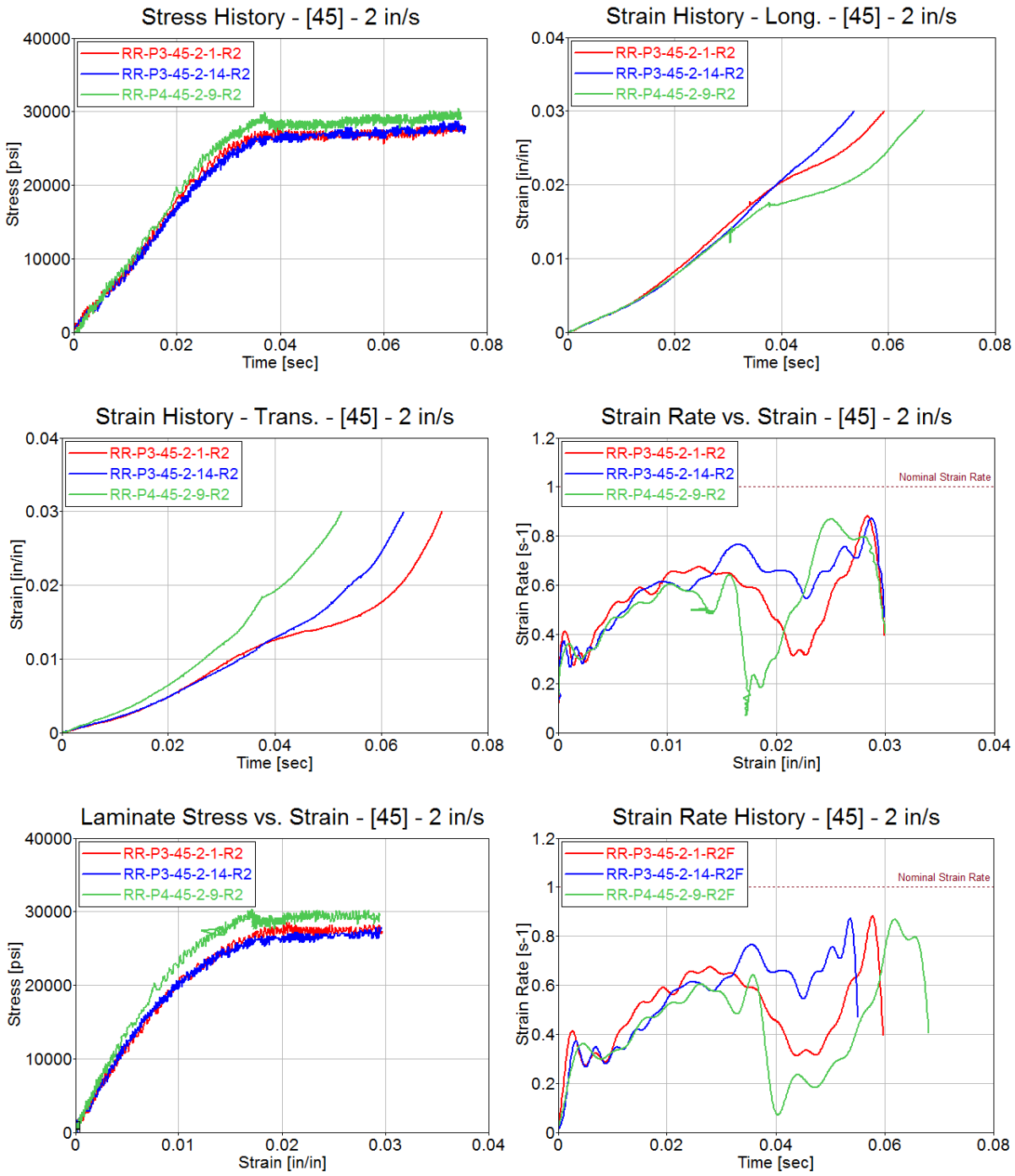

Figure A-29. Test results for Toray [±45°]$_4$ at stroke rate of 2 in/s

Table A-15. Summary of test results for Toray [±45°]$_4$ at stroke rate of 200 in/s

STROKE RATE [in/sec]	SPECIMEN NO.	TENSILE STRENGTH [psi]	MAXIMUM RECORDED STRAIN [in/in]	YOUNG'S MODULUS [Msi]	AVERAGE STRAIN RATE [s^{-1}]
200	RR-P3-45-1-11-R200	43858	0.0284	3.84	70.51
	RR-P3-45-2-5-R200	44431	0.0273	5.14	73.41
	RR-P3-45-2-18-R200	42626	0.0284	5.29	75.87
	RR-P3-45-2-19-R200	43858	0.0205	4.61	70.57
AVERAGE		43693	0.0262	4.72	72.59
STANDARD DEVIATION		761	0.0038	0.66	2.57
COEFFICIENT OF VARIATION [%]		1.74	14.61	13.89	3.54

Figure A-30. Failure modes for Toray [±45°]$_4$ at stroke rate of 200 in/s

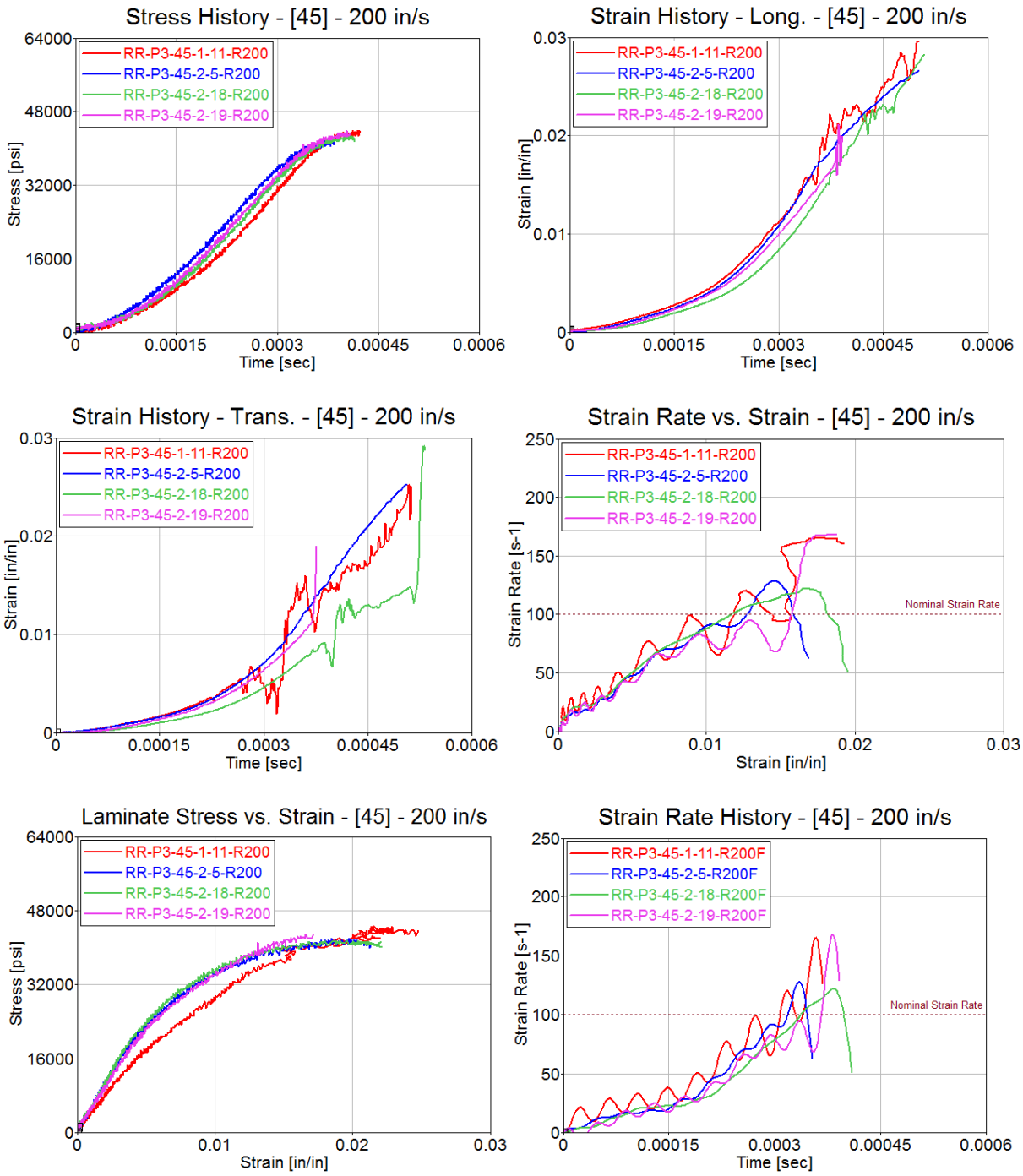

Figure A-31. Test results for Toray [±45˚]$_4$ at stroke rate of 200 in/s

Table A-16. Summary of test results for Toray [±45°]$_4$ at stroke rate of 500 in/s

STROKE RATE [in/sec]	SPECIMEN NO.	TENSILE STRENGTH [psi]	MAXIMUM RECORDED STRAIN [in/in]	YOUNG'S MODULUS [Msi]	AVERAGE STRAIN RATE [s^{-1}]
500	RR-P3-45-1-14-R500	47011	0.0243	3.45	132.09
	RR-P4-45-2-3-R500	52188	0.0193	3.06	131.56
	RR-P4-45-1-17-R500	47679	0.0127	3.69	113.09
AVERAGE		48959	0.0188	3.40	125.58
STANDARD DEVIATION		2816	0.0058	0.32	10.82
COEFFICIENT OF VARIATION [%]		5.75	31.00	9.35	8.62

Figure A-32. Failure modes for Toray [±45°]$_4$ at stroke rate of 500 in/s

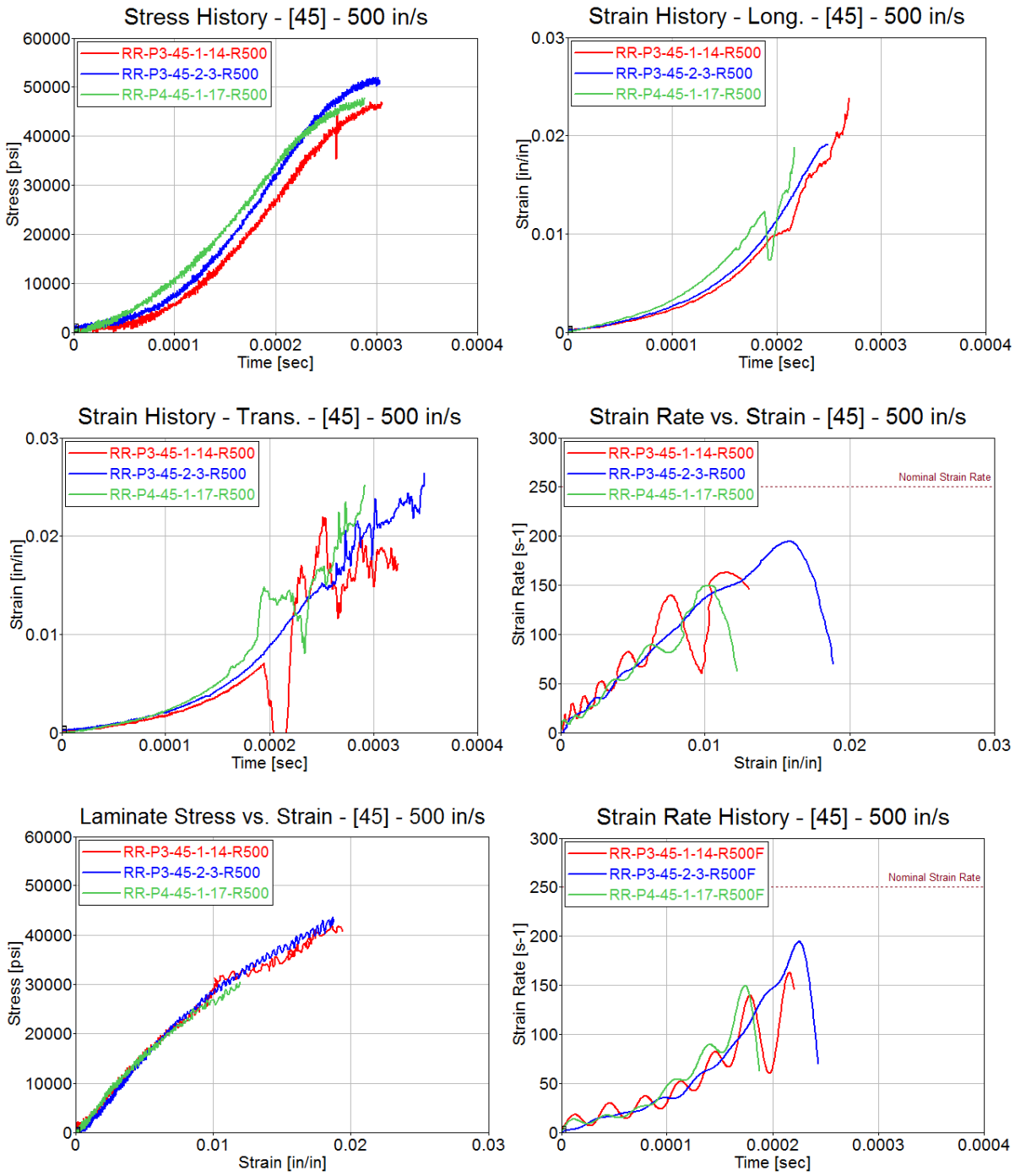

Figure A-33. Test results for Toray [±45˚]$_4$ at stroke rate of 500 in/s

APPENDIX B—LAB B RAW TESTING RESULTS

Laboratory B results using a conventional servo-hydraulic test machine.

TORAY $[0^{\circ}]_4$

Table B-1. Summary of test results for Toray $[0^{\circ}]_4$ at stroke rate of 0.02 in/s

STROKE RATE [in/sec]	SPECIMEN NO.	TENSILE STRENGTH [psi]	MAXIMUM RECORDED STRAIN [in/in]	YOUNG'S MODULUS [Msi]	AVERAGE STRAIN RATE [s^{-1}]
0.02	R-0.02-P1-0-1-18	156632	0.0194	7.90	0.00250
	R-0.02-P1-0-2-1	169554	0.0189	9.00	0.00256
	R-0.02-P1-0-3-6	153804	0.0185	8.07	0.00253
AVERAGE		159997	0.0189	8.32	0.00253
STANDARD DEVIATION		8397	0.0005	0.59	0.00003
COEFFICIENT OF VARIATION [%]		5.25	2.51	7.11	1.15

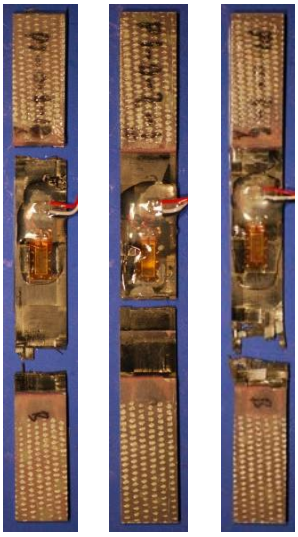

Figure B-1. Failure modes for Toray $[0^{\circ}]_4$ at stroke rate of 0.02 in/s

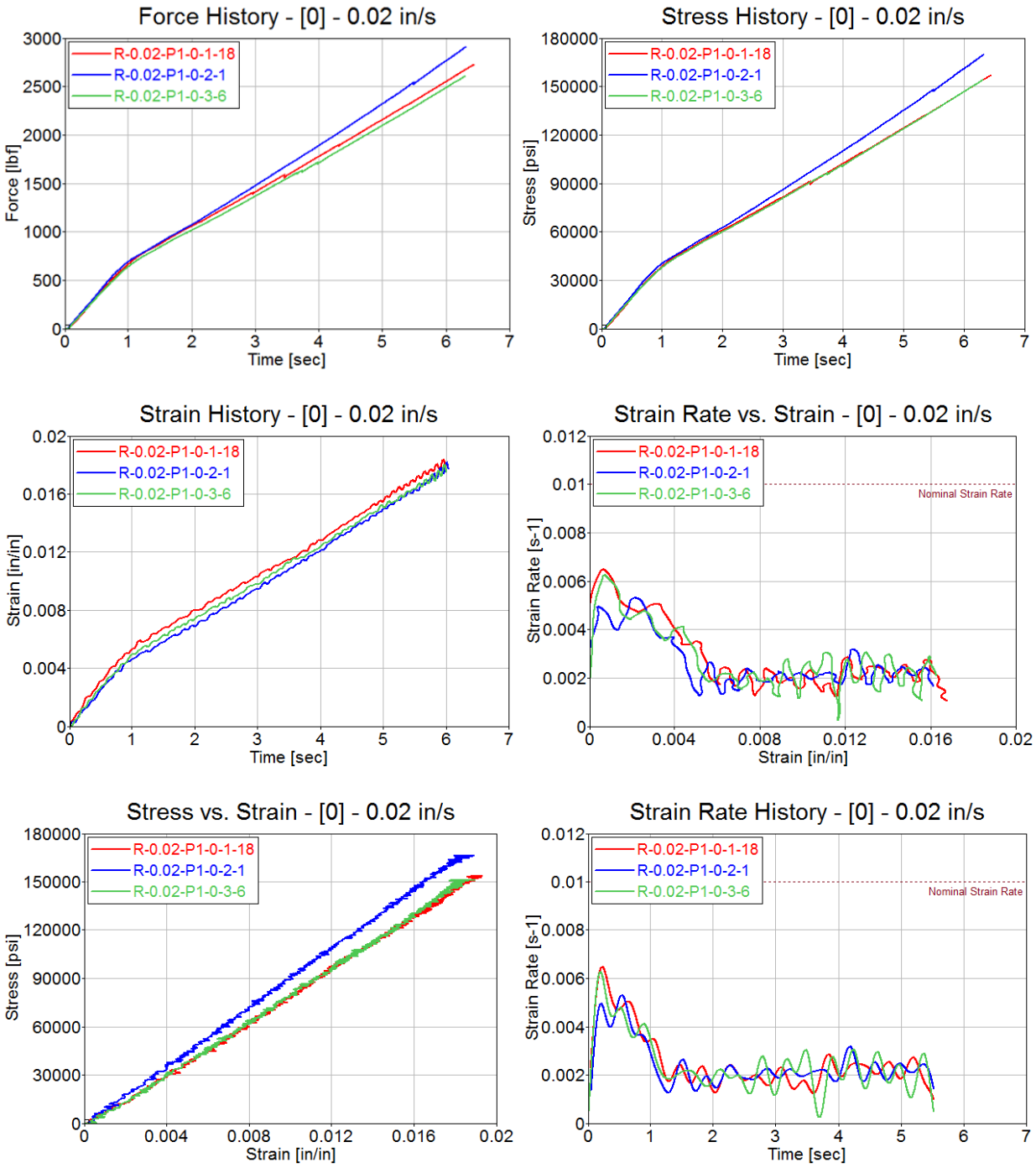

Figure B-2. Test results for Toray [0˚]$_4$ at stroke rate of 0.02 in/s

Table B-2. Summary of test results for Toray [0°]4 at stroke rate of 2 in/s

STROKE RATE [in/sec]	SPECIMEN NO.	TENSILE STRENGTH [psi]	MAXIMUM RECORDED STRAIN [in/in]	YOUNG'S MODULUS [Msi]	AVERAGE STRAIN RATE [s^{-1}]
2	R-2-P1-0-1-5	118703	0.0187	6.01	0.186
	R-2-P1-0-1-6	116195	0.0198	5.51	0.167
	R-2-P1-0-1-19	109680	0.0179	5.86	0.180
AVERAGE		114859	0.0188	5.79	0.178
STANDARD DEVIATION		4657	0.0009	0.26	0.010
COEFFICIENT OF VARIATION [%]		4.05	5.02	4.43	5.47

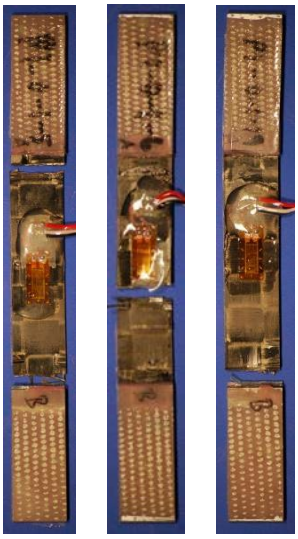

Figure B-3. Failure modes for Toray [0°]4 at stroke rate of 2 in/s

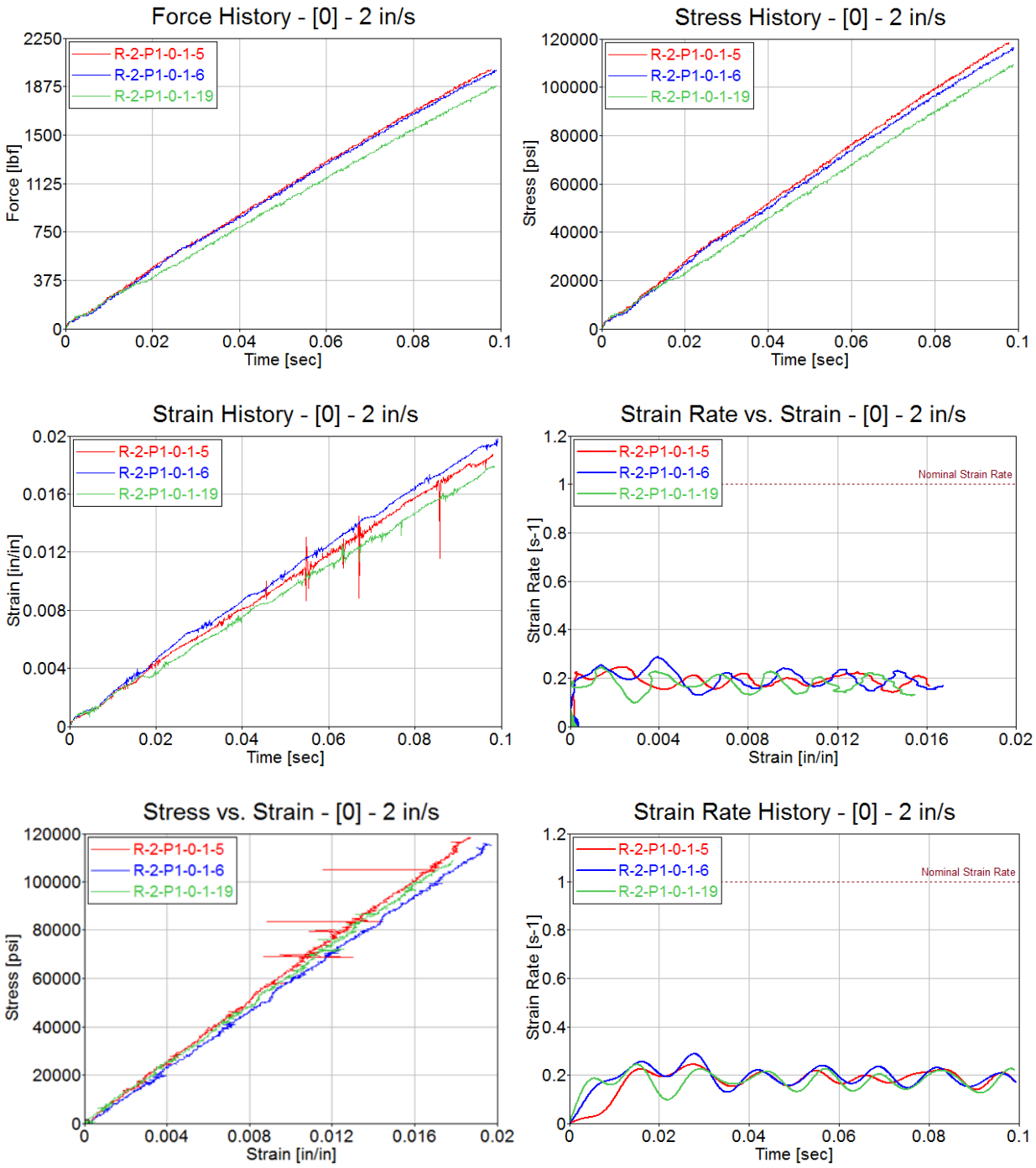

Figure B-4. Test results for Toray [0°]$_4$ at stroke rate of 2 in/s

Table B-3. Summary of test results for Toray [0°]$_4$ at stroke rate of 200 in/s

STROKE RATE [in/sec]	SPECIMEN NO.	TENSILE STRENGTH [psi]	MAXIMUM RECORDED STRAIN [in/in]	YOUNG'S MODULUS [Msi]	AVERAGE STRAIN RATE [s^{-1}]
200	R-200-P1-0-1-8	112630	0.0184	5.52	32.16
	R-200-P1-0-1-14	109314	0.0196	5.08	29.82
	R-200-P1-0-3-17	100038	0.0180	5.63	33.62
AVERAGE		107327	0.0187	5.41	31.87
STANDARD DEVIATION		6527	0.0008	0.29	1.92
COEFFICIENT OF VARIATION [%]		6.08	4.50	5.38	6.02

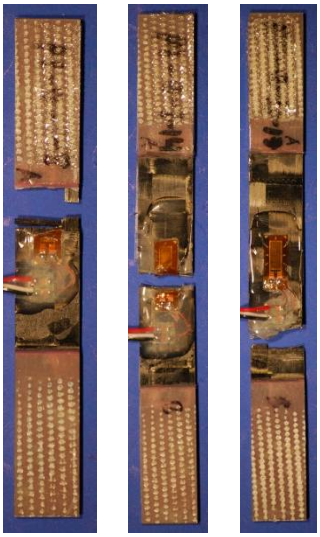

Figure B-5. Failure modes for Toray [0°]$_4$ at stroke rate of 200 in/s

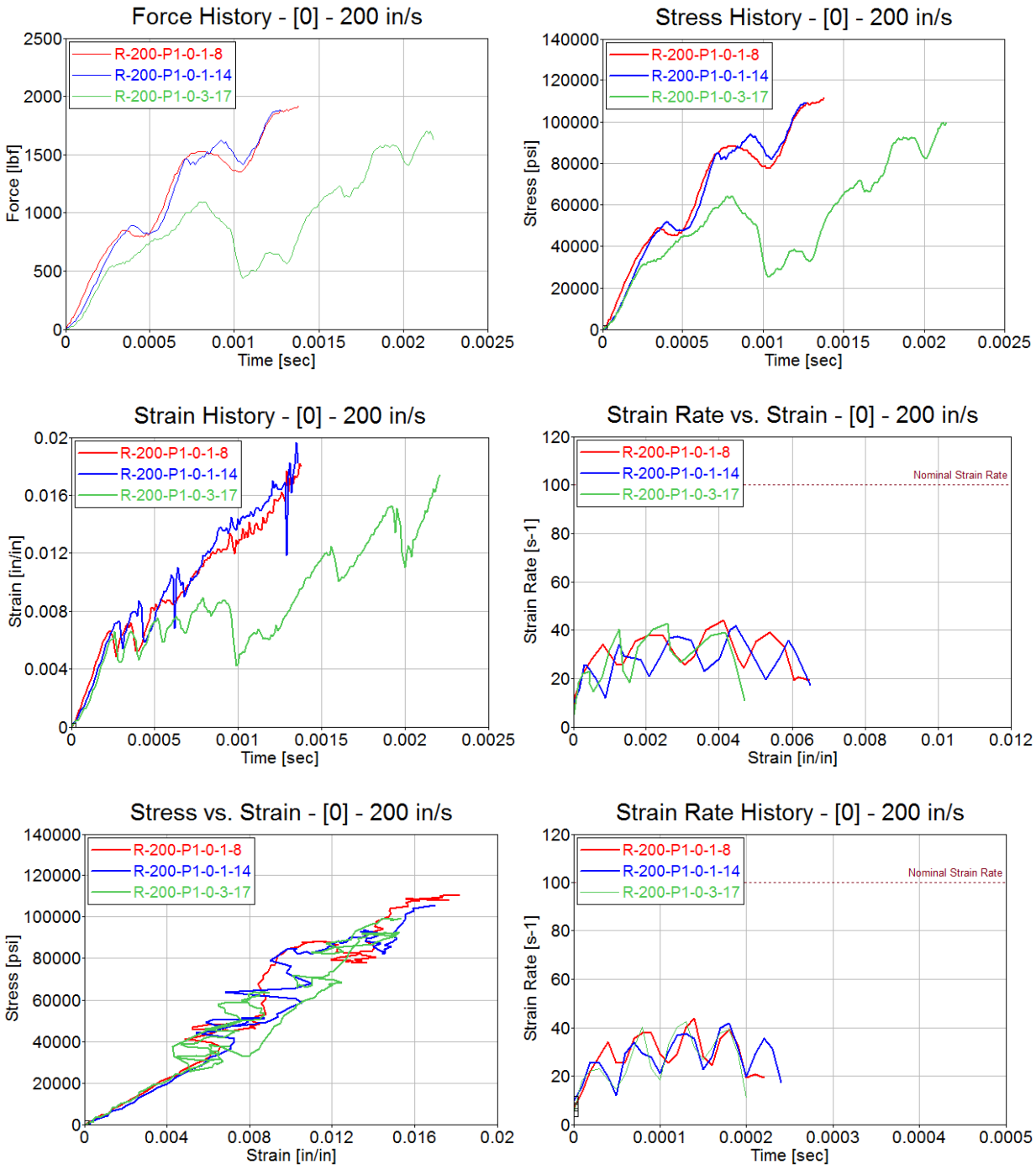

Figure B-6. Test results for Toray $[0^{\circ}]_4$ at stroke rate of 200 in/s

TORAY $[90]_4$

Table B-4. Summary of test results for Toray $[90^{\circ}]_4$ at stroke rate of 0.02 in/s

STROKE RATE [in/sec]	SPECIMEN NO.	TENSILE STRENGTH [psi]	MAXIMUM RECORDED STRAIN [in/in]	YOUNG'S MODULUS [Msi]	AVERAGE STRAIN RATE [s^{-1}]
0.02	R-0.02-P2-90-1-13	139858	0.0173	8.72	0.00238
	R-0.02-P2-90-2-12	122515	0.0154	7.92	0.00288
	R-0.02-P2-90-4-16	152093	0.0179	8.88	0.00234
AVERAGE		138155	0.0169	8.51	0.00253
STANDARD DEVIATION		14863	0.0013	0.51	0.00030
COEFFICIENT OF VARIATION [%]		10.76	7.67	6.05	11.74

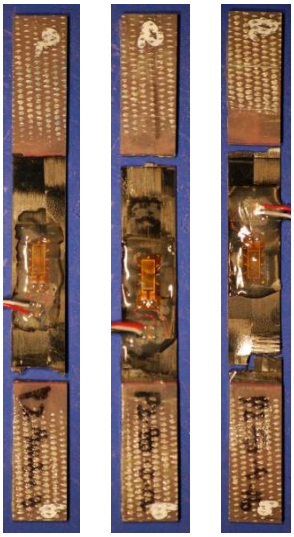

Figure B-7. Failure modes for Toray $[90^{\circ}]_4$ at stroke rate of 0.02 in/s

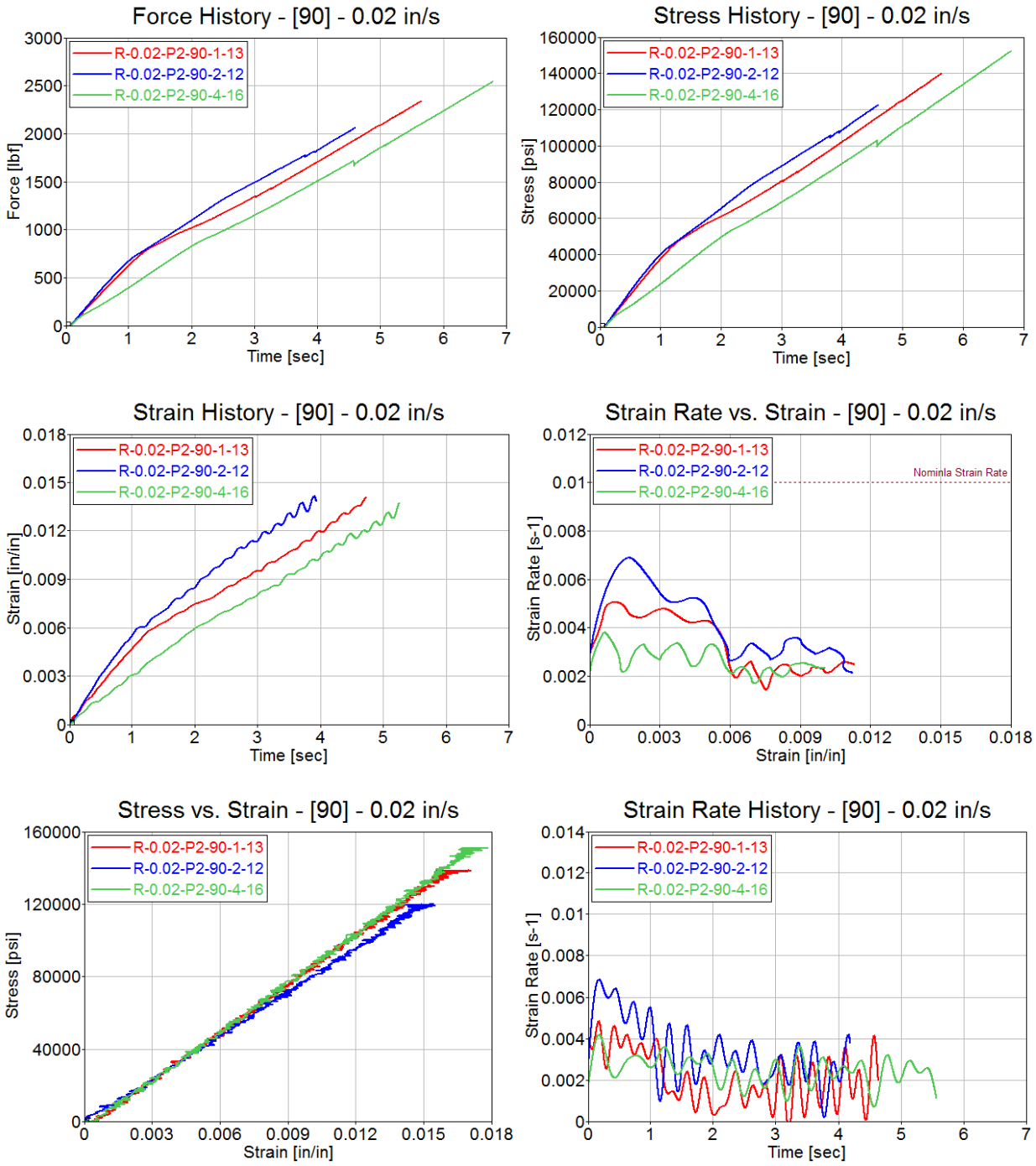

Figure B-8. Test results for Toray [90˚]$_4$ at stroke rate of 0.02 in/s

Table B-5. Summary of test results for Toray [90°]$_4$ at stroke rate of 2 in/s

STROKE RATE [in/sec]	SPECIMEN NO.	TENSILE STRENGTH [psi]	MAXIMUM RECORDED STRAIN [in/in]	YOUNG'S MODULUS [Msi]	AVERAGE STRAIN RATE [s^{-1}]
2	R-2-P2-90-1-4	103234	0.0165	6.06	0.174
	R-2-P2-90-2-4	99394	0.0170	5.07	0.194
	R-2-P2-90-4-8	102577	0.0179	5.49	0.193
AVERAGE		101735	0.0171	5.54	0.187
STANDARD DEVIATION		2054	0.0007	0.50	0.012
COEFFICIENT OF VARIATION [%]		2.02	4.16	8.97	6.20

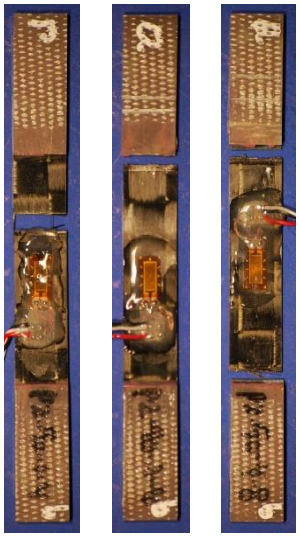

Figure B-9. Failure modes for Toray [90°]$_4$ at stroke rate of 2 in/s

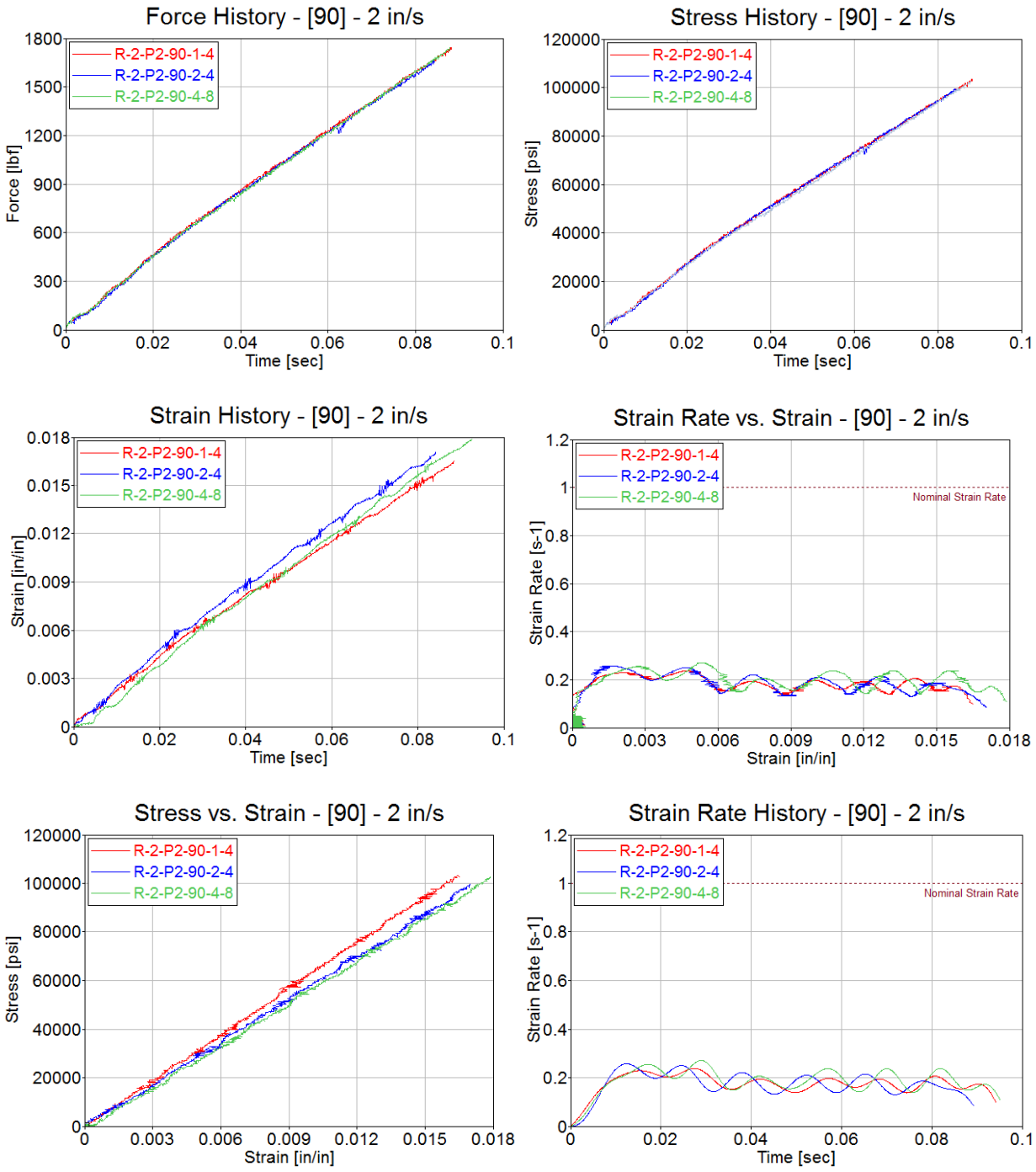

Figure B-10. Test results for Toray [90˚]$_4$ at stroke rate of 2 in/s

Table B-6. Summary of test results for Toray [90˚]$_4$ at stroke rate of 200 in/s

STROKE RATE [in/sec]	SPECIMEN NO.	TENSILE STRENGTH [psi]	MAXIMUM RECORDED STRAIN [in/in]	YOUNG'S MODULUS [Msi]	AVERAGE STRAIN RATE [s^{-1}]
200	R-200-P2-90-1-16	119194	0.0181	5.35	30.15
	R-200-P2-90-3-11	113038	0.0165	4.97	36.40
	R-200-P2-90-4-7	106756	0.0176	4.02	37.08
AVERAGE		112996	0.0174	4.78	34.54
STANDARD DEVIATION		6219	0.0008	0.69	3.82
COEFFICIENT OF VARIATION [%]		5.50	4.73	14.33	11.06

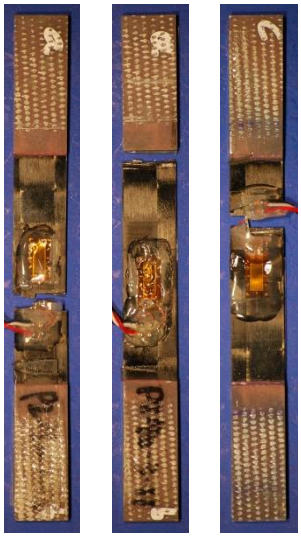

Figure B-11. Failure modes for Toray [90˚]$_4$ at stroke rate of 200 in/s

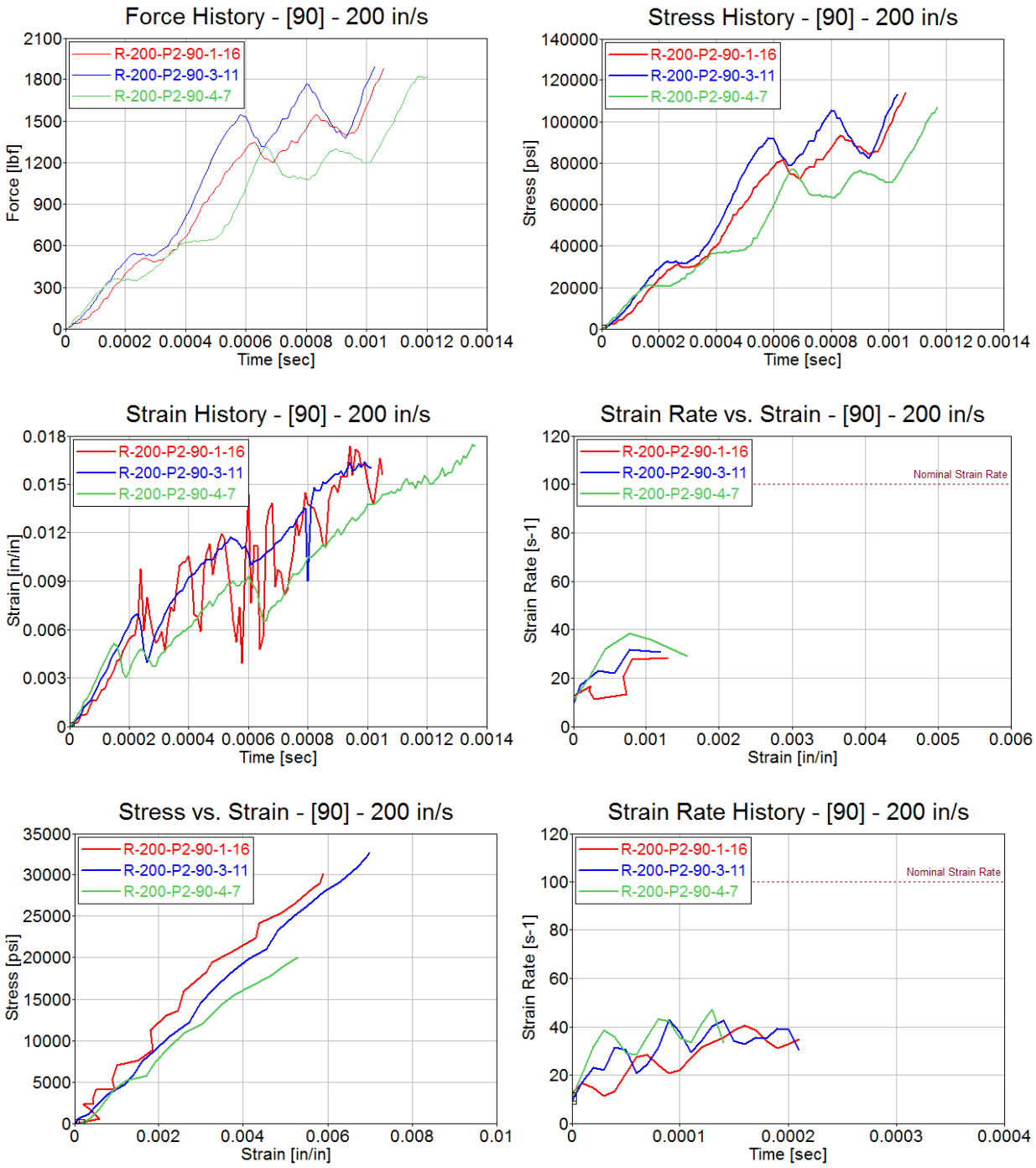

Figure B-12. Test results for Toray [90˚]$_4$ at stroke rate of 200 in/s

TORAY [±45°]$_4$

Table B-7. Summary of test results for Toray [±45°]$_4$ at stroke rate of 0.02 in/s

STROKE RATE [in/sec]	SPECIMEN NO.	TENSILE STRENGTH [psi]	MAXIMUM RECORDED STRAIN [in/in]	YOUNG'S MODULUS [Msi]	AVERAGE STRAIN RATE [s^{-1}]
0.02	R-0.02-P3-45-2-6	27659	0.0328	2.15	0.00785
	R-0.02-P3-45-2-12	26376	0.0327	1.87	0.00870
	R-0.02-P4-45-1-6	27853	0.0329	2.08	0.00858
AVERAGE		27296	0.0328	2.03	0.00838
STANDARD DEVIATION		802	0.0001	0.15	0.00046
COEFFICIENT OF VARIATION [%]		2.94	0.30	7.17	5.51

Figure B-13. Failure modes for Toray [±45°]$_4$ at stroke rate of 0.02 in/s

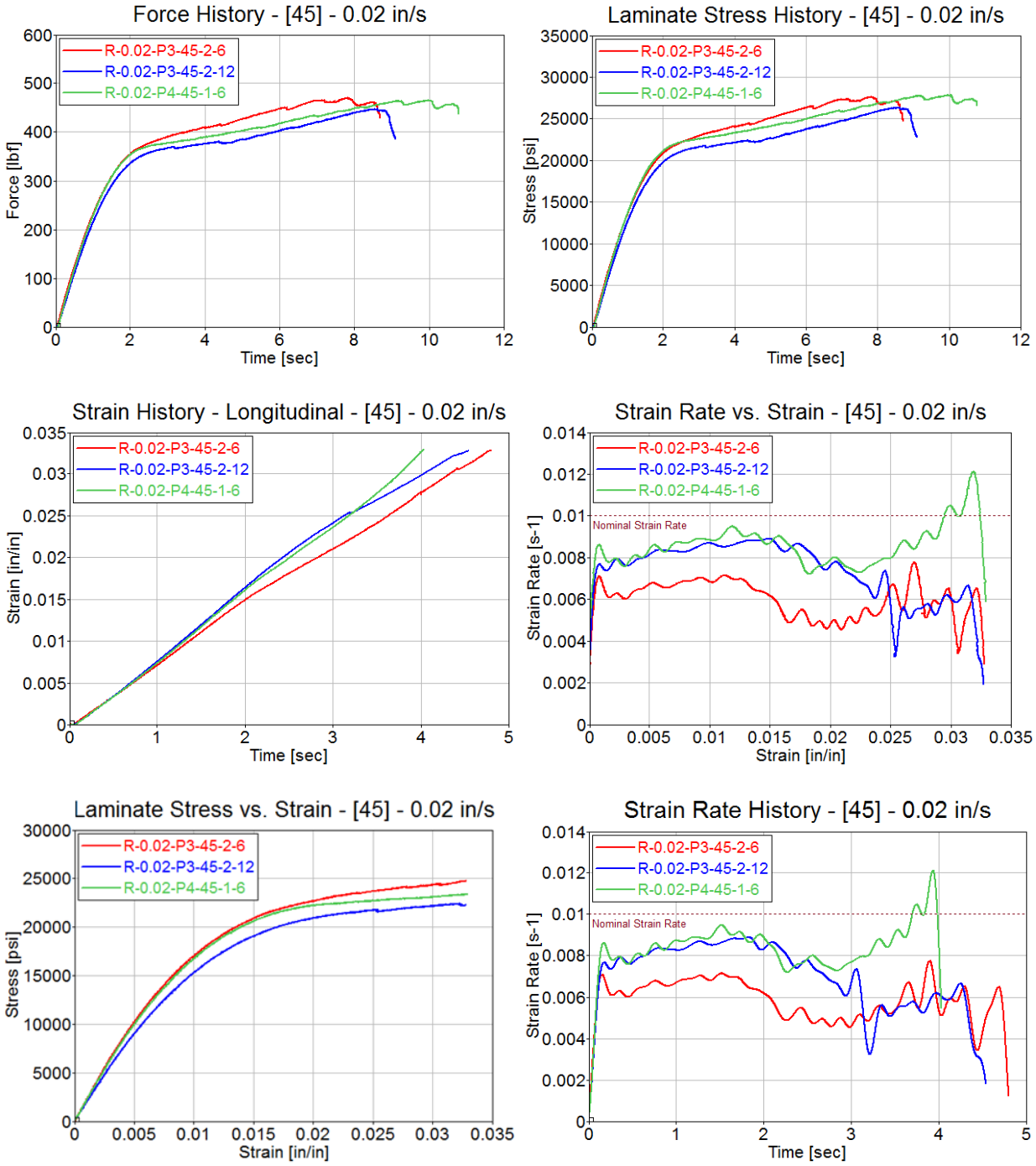

Figure B-14. Test results for Toray [±45˚]$_4$ at stroke rate of 0.02 in/s

Table B-8. Summary of test results for Toray [±45°]$_4$ at stroke rate of 2 in/s

STROKE RATE [in/sec]	SPECIMEN NO.	TENSILE STRENGTH [psi]	MAXIMUM RECORDED STRAIN [in/in]	YOUNG'S MODULUS [Msi]	AVERAGE STRAIN RATE [s^{-1}]
2	R-2-P3-45-1-13	20273	0.0299	1.48	0.521
	R-2-P3-45-2-11	19587	0.0301	1.52	0.579
	R-2-P4-45-1-21	18616	0.0300	1.48	0.618
AVERAGE		19492	0.0300	1.49	0.573
STANDARD DEVIATION		833	0.0001	0.02	0.048
COEFFICIENT OF VARIATION [%]		4.27	0.20	1.55	8.46

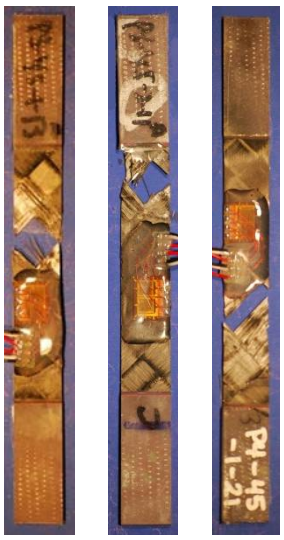

Figure B-15. Failure modes for Toray [±45°]$_4$ at stroke rate of 2 in/s

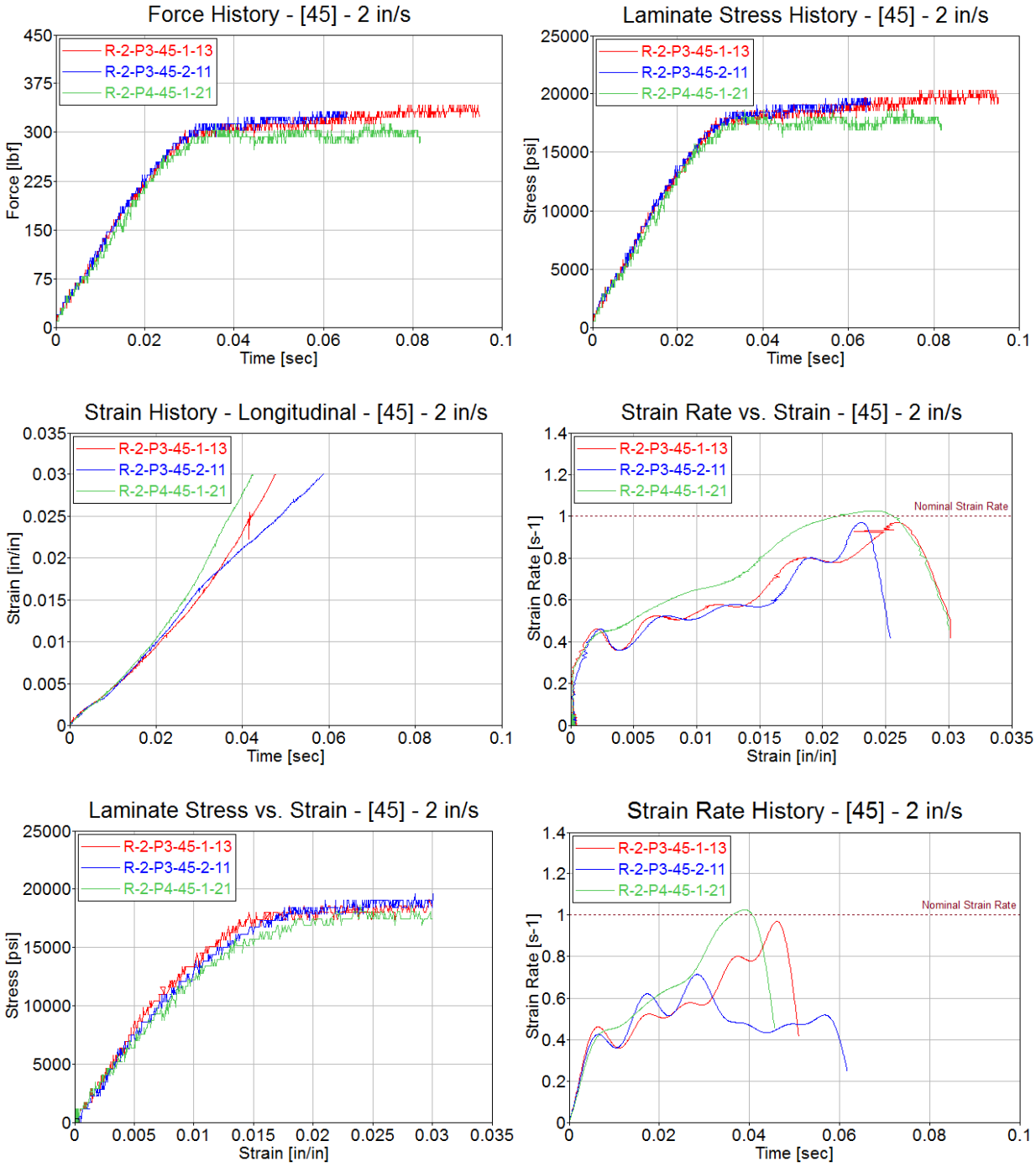

Figure B-16. Test results for Toray [±45°]$_4$ at stroke rate of 2 in/s

Table B-9. Summary of test results for Toray [±45°]$_4$ at stroke rate of 200 in/s

STROKE RATE [in/sec]	SPECIMEN NO.	TENSILE STRENGTH [psi]	MAXIMUM RECORDED STRAIN [in/in]	YOUNG'S MODULUS [Msi]	AVERAGE STRAIN RATE [s^{-1}]
200	R-200-P4-45-2-5	27656	0.0301	2.20	55.68
	R-200-P4-45-2-6	26502	0.0279	1.99	47.83
	R-200-P4-45-2-11	27901	0.0288	2.72	51.41
AVERAGE		27353	0.0289	2.30	51.64
STANDARD DEVIATION		747	0.0011	0.38	3.93
COEFFICIENT OF VARIATION [%]		2.73	3.77	16.32	7.61

Figure B-17. Failure modes for Toray [±45°]$_4$ at stroke rate of 200 in/s

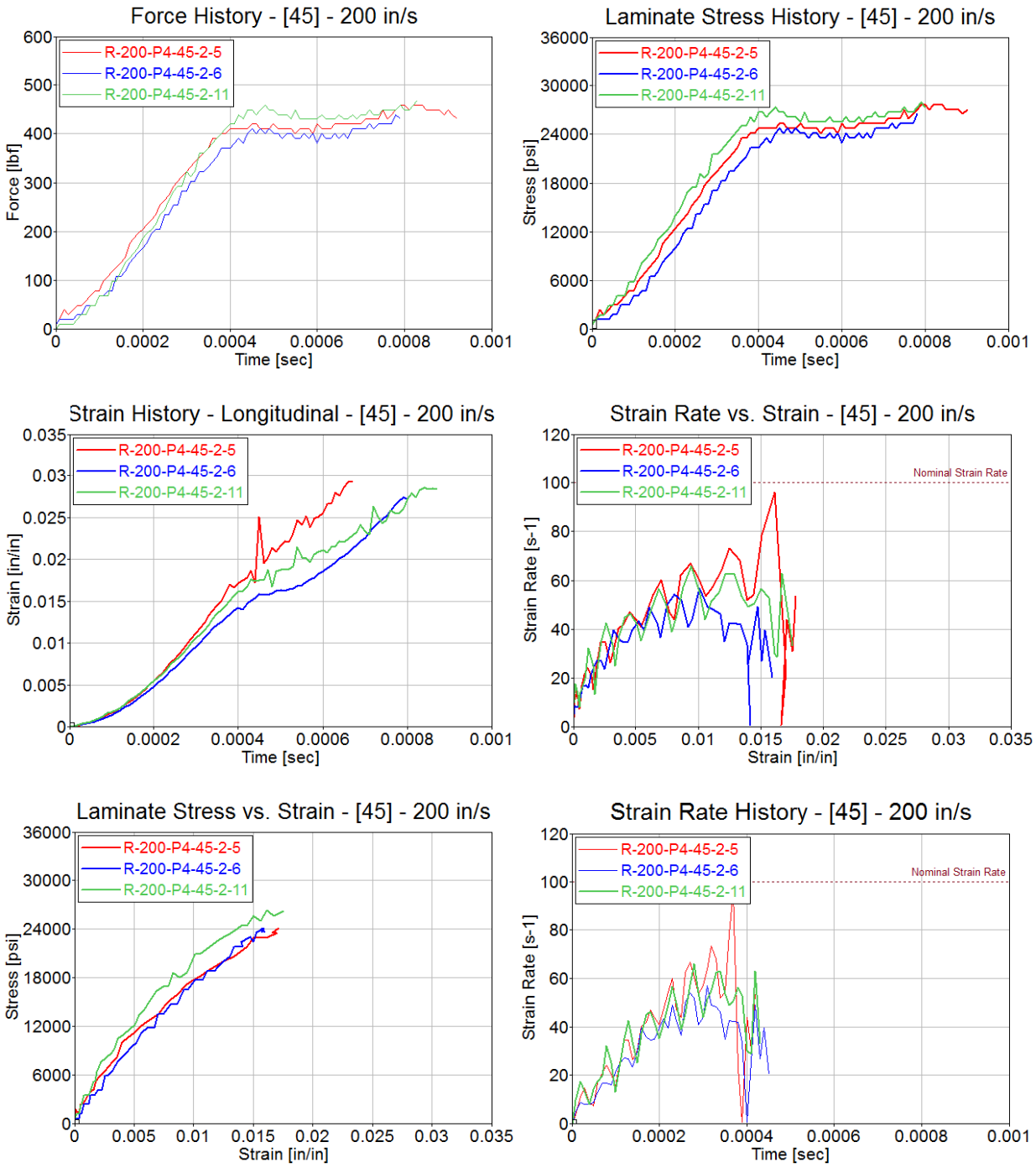

Figure B-18. Test results for Toray [±45˚]$_4$ at stroke rate of 200 in/s

APPENDIX C—LAB C RAW TESTING RESULTS

Laboratory C results using a conventional servo-hydraulic test machine.

TORAY $[0^{\circ}]_4$

Table C-1. Summary of test results for Toray $[0^{\circ}]_4$ at stroke rate of 0.02 in/s

STROKE RATE [in/sec]	SPECIMEN NO.	TENSILE STRENGTH [psi]	MAXIMUM RECORDED STRAIN [in/in]	YOUNG'S MODULUS [Msi]	AVERAGE STRAIN RATE [s^{-1}]
0.02	R-0.02-P1-0-1-3	164967	0.0187	8.19	0.00510
	R-0.02-P1-0-3-12	170250	0.0186	8.21	0.00589
AVERAGE		167608	0.0186	8.20	0.00550
STANDARD DEVIATION		3736	0.0001	0.01	0.00056
COEFFICIENT OF VARIATION [%]		2.23	0.50	0.17	10.12

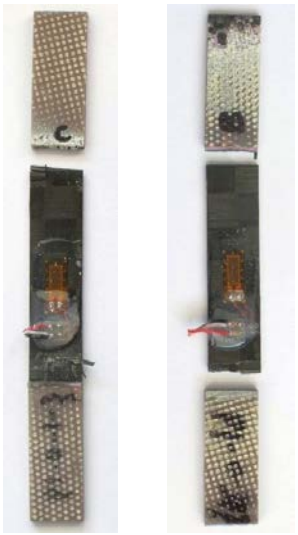

Figure C-1. Failure modes for Toray $[0^{\circ}]_4$ at stroke rate of 0.02 in/s

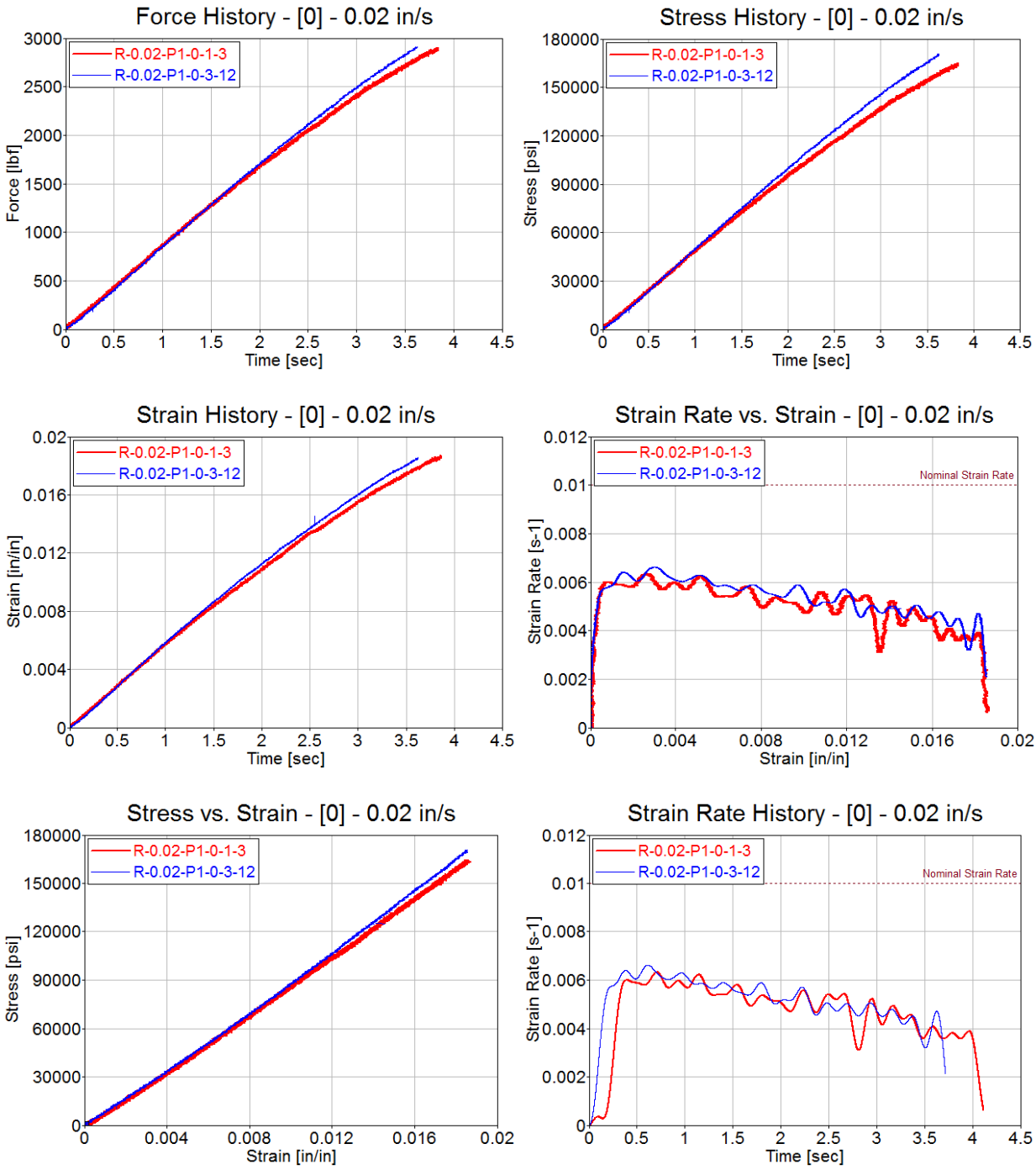

Figure C-2. Test results for Toray [0˚]$_4$ at stroke rate of 0.02 in/s

Table C-2. Summary of test results for Toray $[0^{\circ}]_4$ at stroke rate of 2 in/s

STROKE RATE [in/sec]	SPECIMEN NO.	TENSILE STRENGTH [psi]	MAXIMUM RECORDED STRAIN [in/in]	YOUNG'S MODULUS [Msi]	AVERAGE STRAIN RATE [s^{-1}]
2	R-2-P1-0-3-11	151865	0.0167	8.37	0.465
	R-2-P1-0-3-14	158994	0.0173	7.91	0.525
AVERAGE		155429	0.0170	8.14	0.495
STANDARD DEVIATION		5041	0.0004	0.33	0.043
COEFFICIENT OF VARIATION [%]		3.24	2.59	4.00	8.61

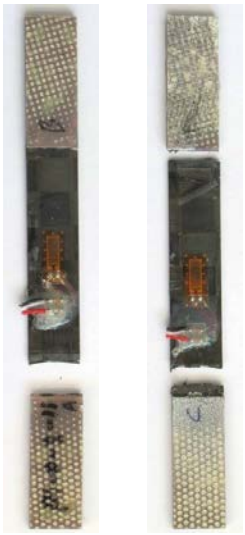

Figure C-3. Failure modes for Toray $[0^{\circ}]_4$ at stroke rate of 2 in/s

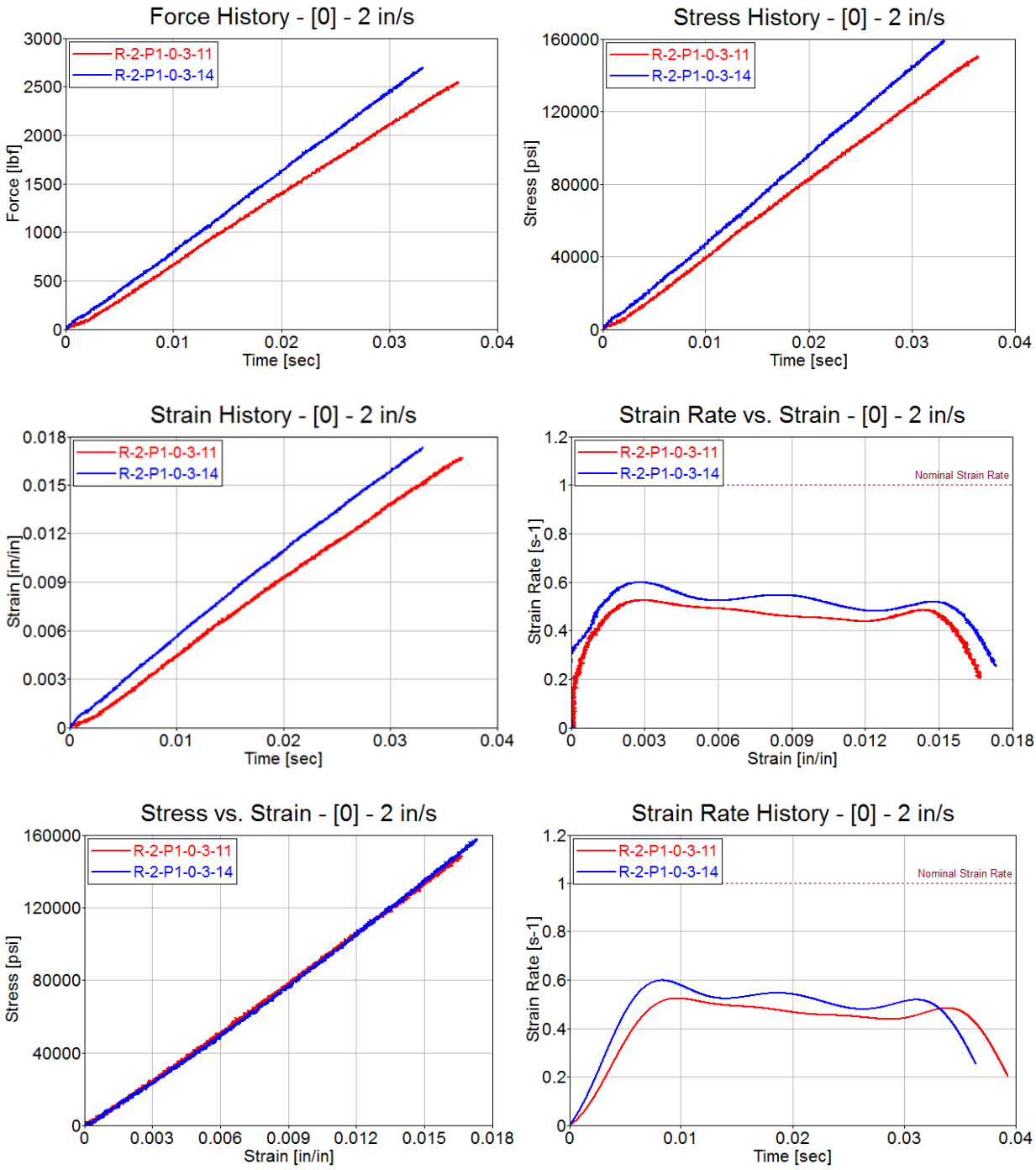

Figure C-4. Test results for Toray [0°]$_4$ at stroke rate of 2 in/s

Table C-3. Summary of test results for Toray [0˚]$_4$ at stroke rate of 200 in/s

STROKE RATE [in/sec]	SPECIMEN NO.	TENSILE STRENGTH [psi]	MAXIMUM RECORDED STRAIN [in/in]	YOUNG'S MODULUS [Msi]	AVERAGE STRAIN RATE [s^{-1}]
200	R-200-P1-0-2-14	222946	0.0233	11.17	70.18
	R-200-P1-0-2-18	225508	0.0186	8.99	82.55
AVERAGE		224227	0.0209	10.08	76.37
STANDARD DEVIATION		1812	0.0034	1.54	8.75
COEFFICIENT OF VARIATION [%]		0.81	16.04	15.29	11.45

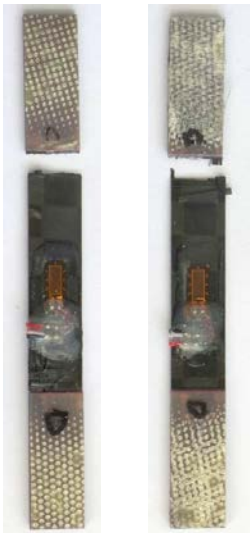

Figure C-5. Failure modes for Toray [0˚]$_4$ at stroke rate of 200 in/s

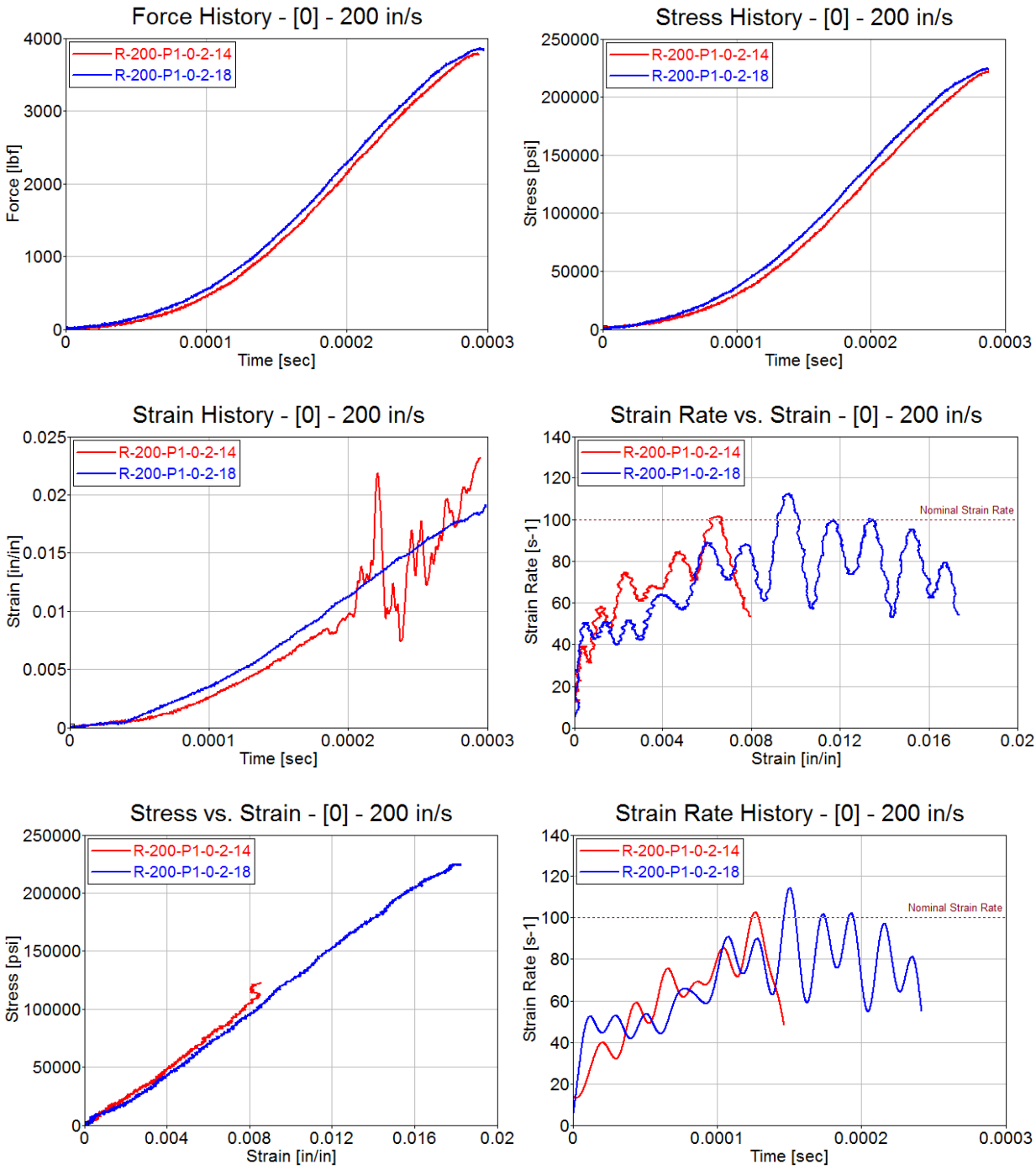

Figure C-6. Test results for Toray [0˚]4 at stroke rate of 200 in/s

Table C-4. Summary of test results for Toray $[0^{\circ}]_4$ at stroke rate of 500 in/s

STROKE RATE [in/sec]	SPECIMEN NO.	TENSILE STRENGTH [psi]	MAXIMUM RECORDED STRAIN [in/in]	YOUNG'S MODULUS [Msi]	AVERAGE STRAIN RATE [s^{-1}]
500	R-500-P1-0-1-13	185566	0.0204	10.46	102.40
	R-500-P1-0-2-24	171060	0.0192	8.64	125.12
AVERAGE		178313	0.0198	9.55	113.76
STANDARD DEVIATION		10257	0.0009	1.29	16.07
COEFFICIENT OF VARIATION [%]		5.75	4.33	13.48	14.12

Figure C-7. Failure modes for Toray $[0^{\circ}]_4$ at stroke rate of 500 in/s

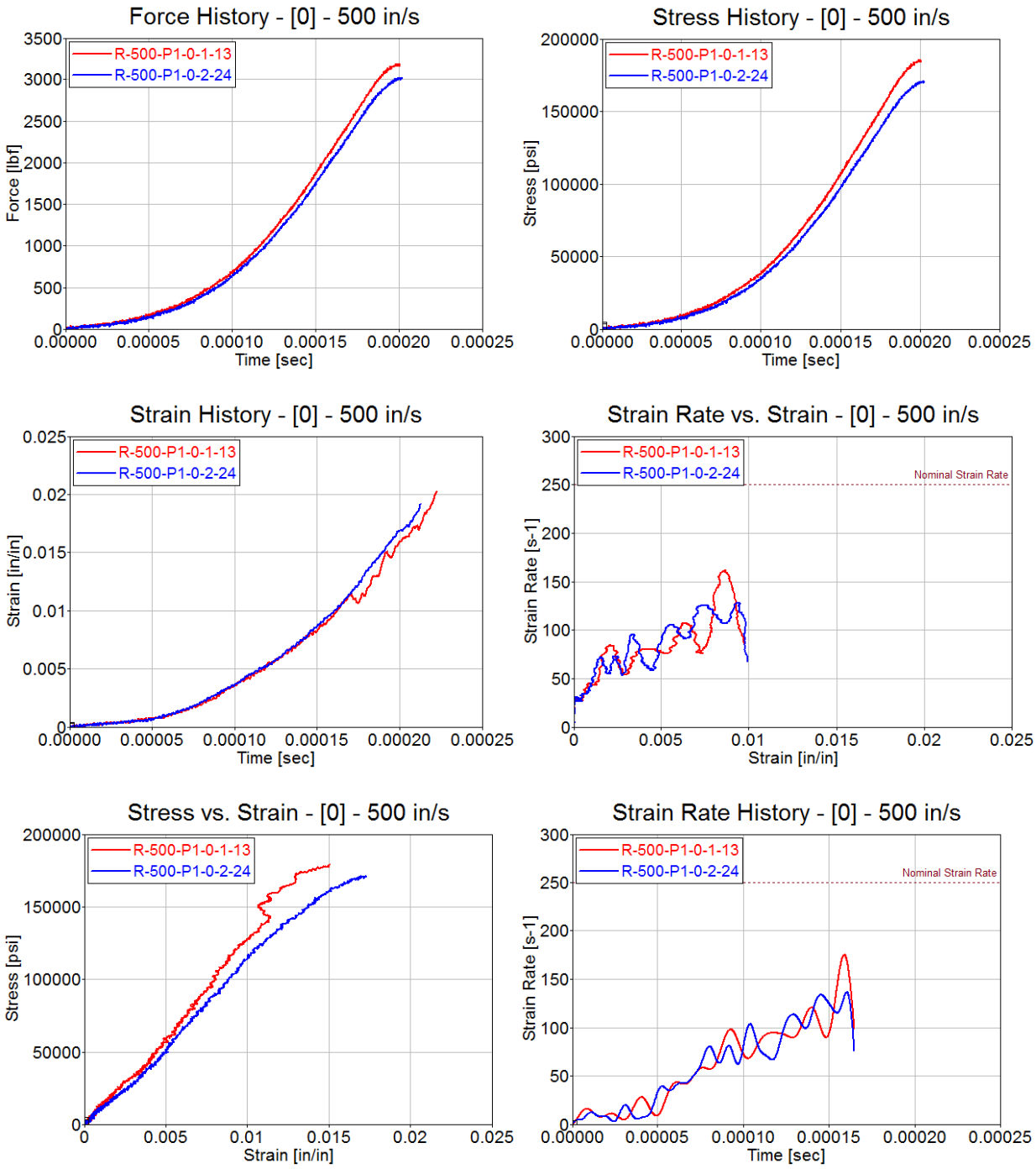

Figure C-8. Test results for Toray [0˚]$_4$ at stroke rate of 500 in/s

TORAY $[90]_4$

Table C-5. Summary of test results for Toray $[90^{\circ}]_4$ at stroke rate of 0.02 in/s

STROKE RATE [in/sec]	SPECIMEN NO.	TENSILE STRENGTH [psi]	MAXIMUM RECORDED STRAIN [in/in]	YOUNG'S MODULUS [Msi]	AVERAGE STRAIN RATE [s^{-1}]
0.02	R-0.02-P2-90-4-6	152368	0.0169	8.63	0.00494
	R-0.02-P2-90-1-20	140899	0.0152	8.83	0.00429
AVERAGE		146634	0.0160	8.73	0.00462
STANDARD DEVIATION		8110	0.0012	0.14	0.00046
COEFFICIENT OF VARIATION [%]		5.53	7.17	1.62	9.91

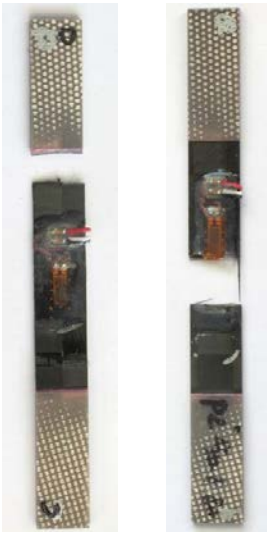

Figure C-9. Failure modes for Toray $[90^{\circ}]_4$ at stroke rate of 0.02 in/s

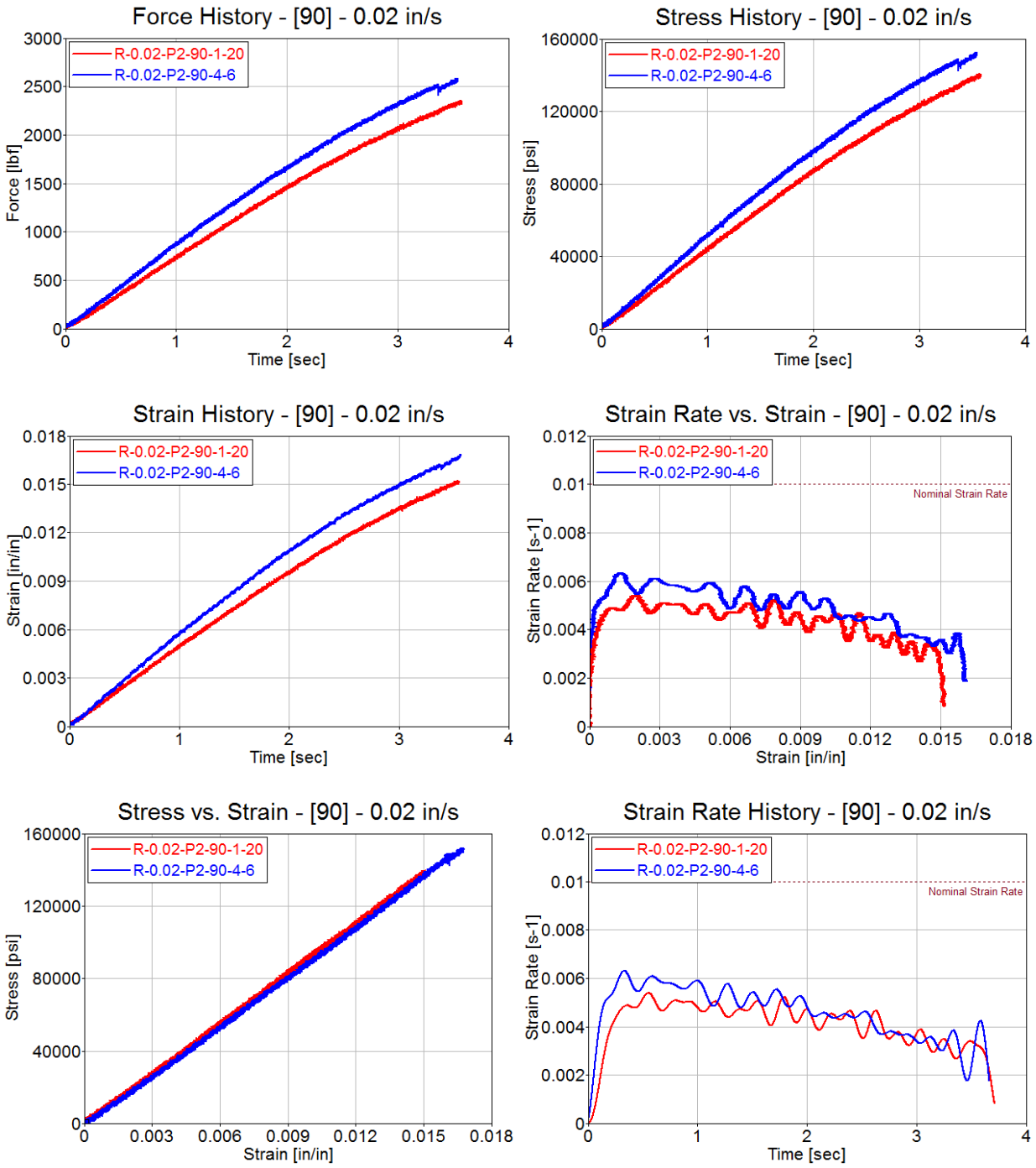

Figure C-10. Test results for Toray [90˚]$_4$ at stroke rate of 0.02 in/s

Table C-6. Summary of test results for Toray $[90^{\circ}]_4$ at stroke rate of 2 in/s

STROKE RATE [in/sec]	SPECIMEN NO.	TENSILE STRENGTH [psi]	MAXIMUM RECORDED STRAIN [in/in]	YOUNG'S MODULUS [Msi]	AVERAGE STRAIN RATE [s^{-1}]
2	R-2-P2-90-1-2	157872	0.0176	8.33	0.478
	R-2-P2-90-1-5	141366	0.0166	7.76	0.504
AVERAGE		149619	0.0171	8.05	0.491
STANDARD DEVIATION		11672	0.0007	0.40	0.018
COEFFICIENT OF VARIATION [%]		7.80	4.14	5.01	3.75

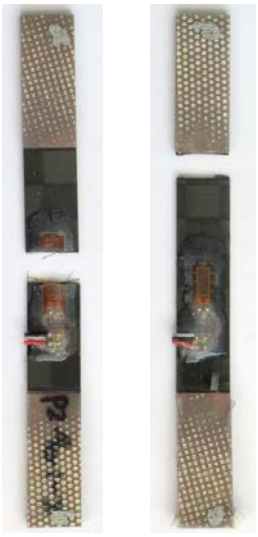

Figure C-11. Failure modes for Toray $[90^{\circ}]_4$ at stroke rate of 2 in/s

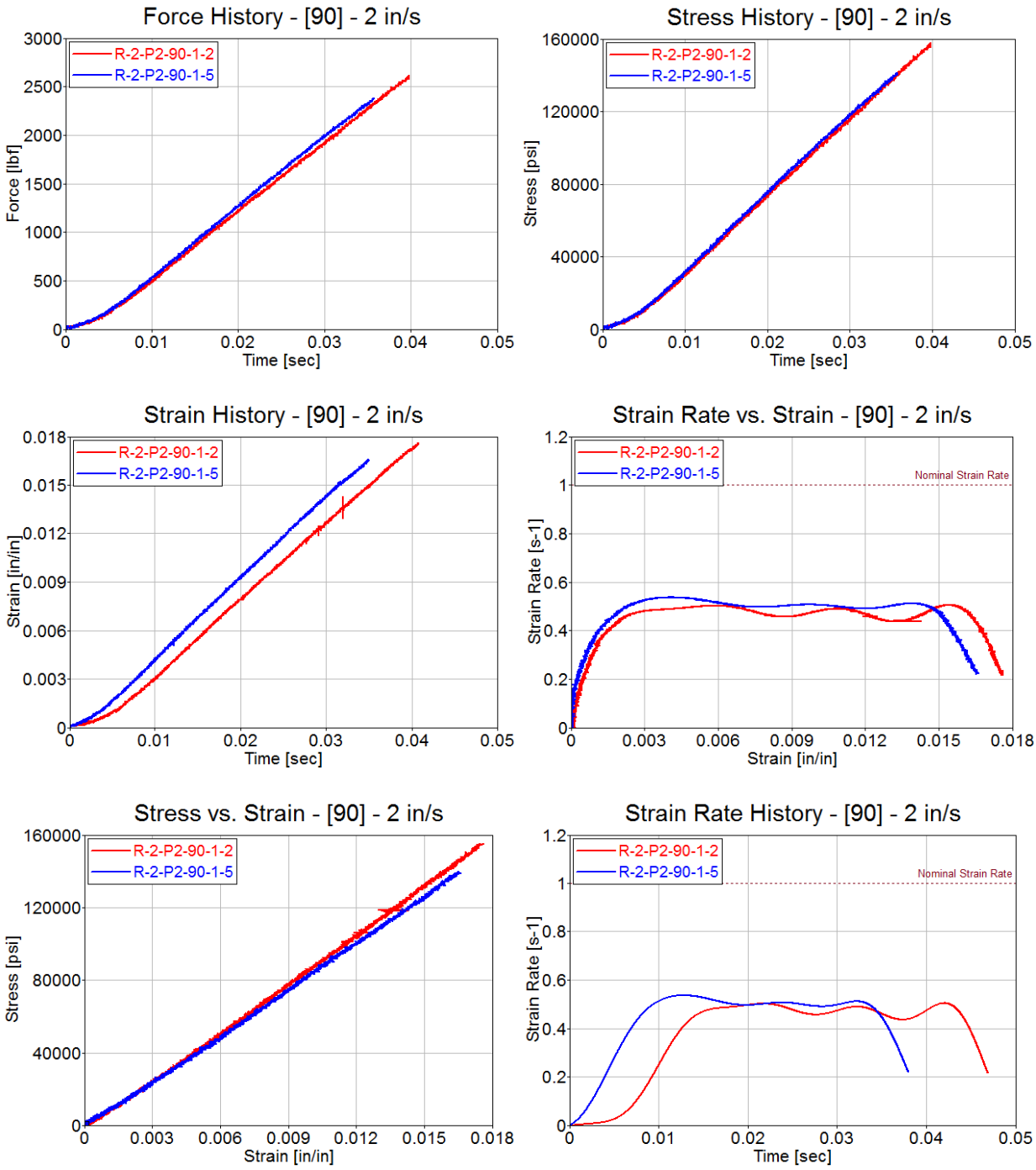

Figure C-12. Test results for Toray [90˚]$_4$ at stroke rate of 2 in/s

Table C-7. Summary of test results for Toray [90˚]$_4$ at stroke rate of 200 in/s

STROKE RATE [in/sec]	SPECIMEN NO.	TENSILE STRENGTH [psi]	MAXIMUM RECORDED STRAIN [in/in]	YOUNG'S MODULUS [Msi]	AVERAGE STRAIN RATE [s^{-1}]
200	R-200-P2-90-2-13	198235	0.0168	12.74	74.46
	R-200-P2-90-2-14	192424	0.0167	10.44	77.42
	R-200-P2-90-4-11	157949	0.0155	12.60	83.94
AVERAGE		182870	0.0163	11.93	78.61
STANDARD DEVIATION		21776	0.0007	1.29	4.85
COEFFICIENT OF VARIATION [%]		11.91	4.20	10.81	6.17

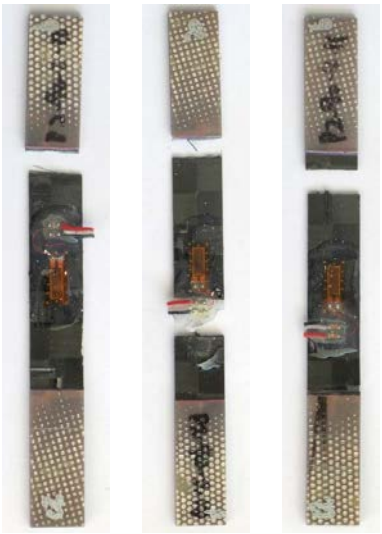

Figure C-13. Failure modes for Toray [90˚]$_4$ at stroke rate of 200 in/s

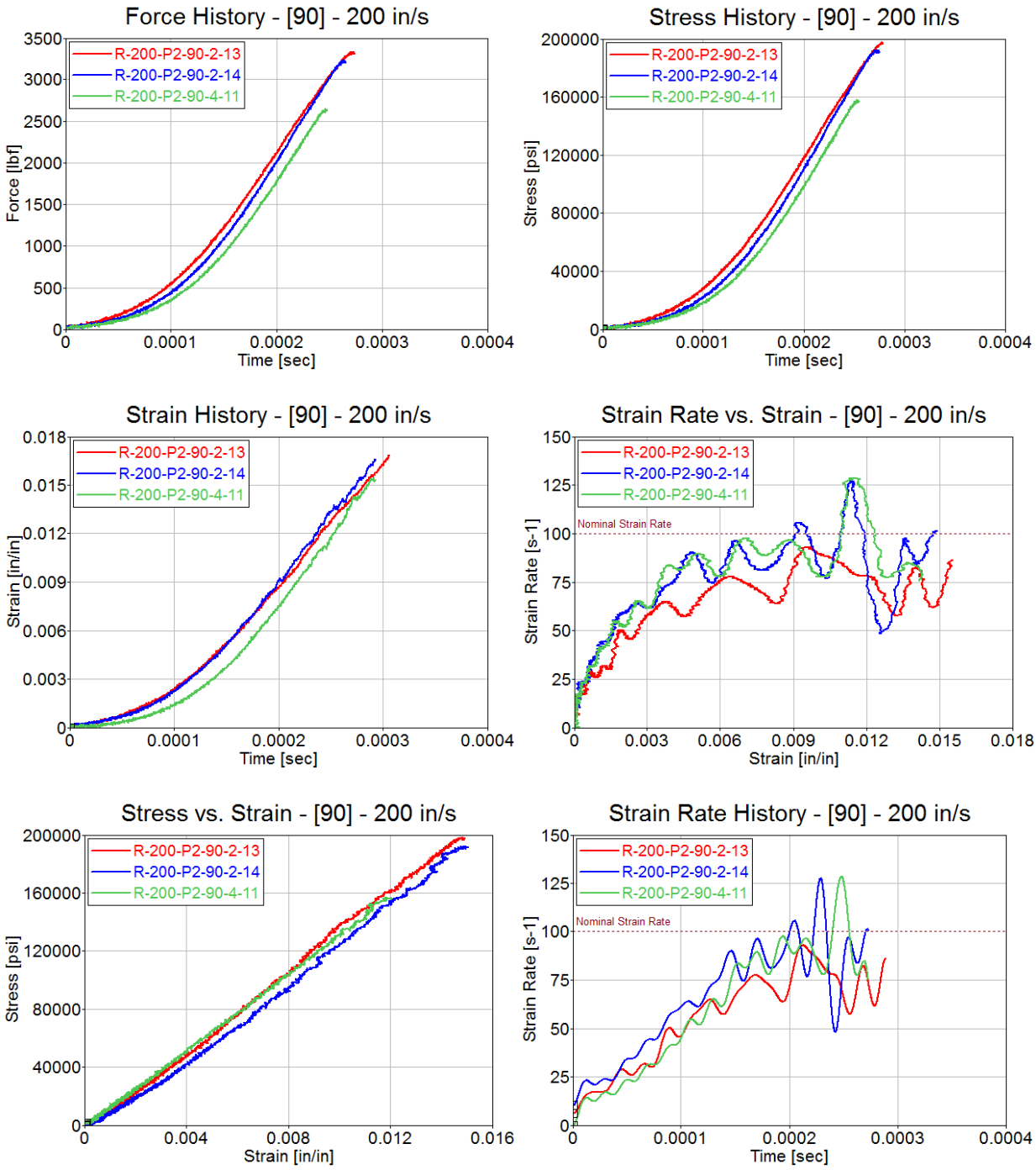

Figure C-14. Test results for Toray [90˚]$_4$ at stroke rate of 200 in/s

Table C-8. Summary of test results for Toray [90˚]$_4$ at stroke rate of 500 in/s

STROKE RATE [in/sec]	SPECIMEN NO.	TENSILE STRENGTH [psi]	MAXIMUM RECORDED STRAIN [in/in]	YOUNG'S MODULUS [Msi]	AVERAGE STRAIN RATE [s^{-1}]
500	R-500-P2-90-3-2	185552	0.0159	8.19	111.86
	R-500-P2-90-3-12	128845	0.0160	9.79	117.70
	R-500-P2-90-4-9	186400	0.0185	8.27	111.11
AVERAGE		166932	0.0168	8.75	113.56
STANDARD DEVIATION		32987	0.0015	0.90	3.61
COEFFICIENT OF VARIATION [%]		19.76	8.80	10.30	3.18

Figure C-15. Failure modes for Toray [90˚]$_4$ at stroke rate of 500 in/s

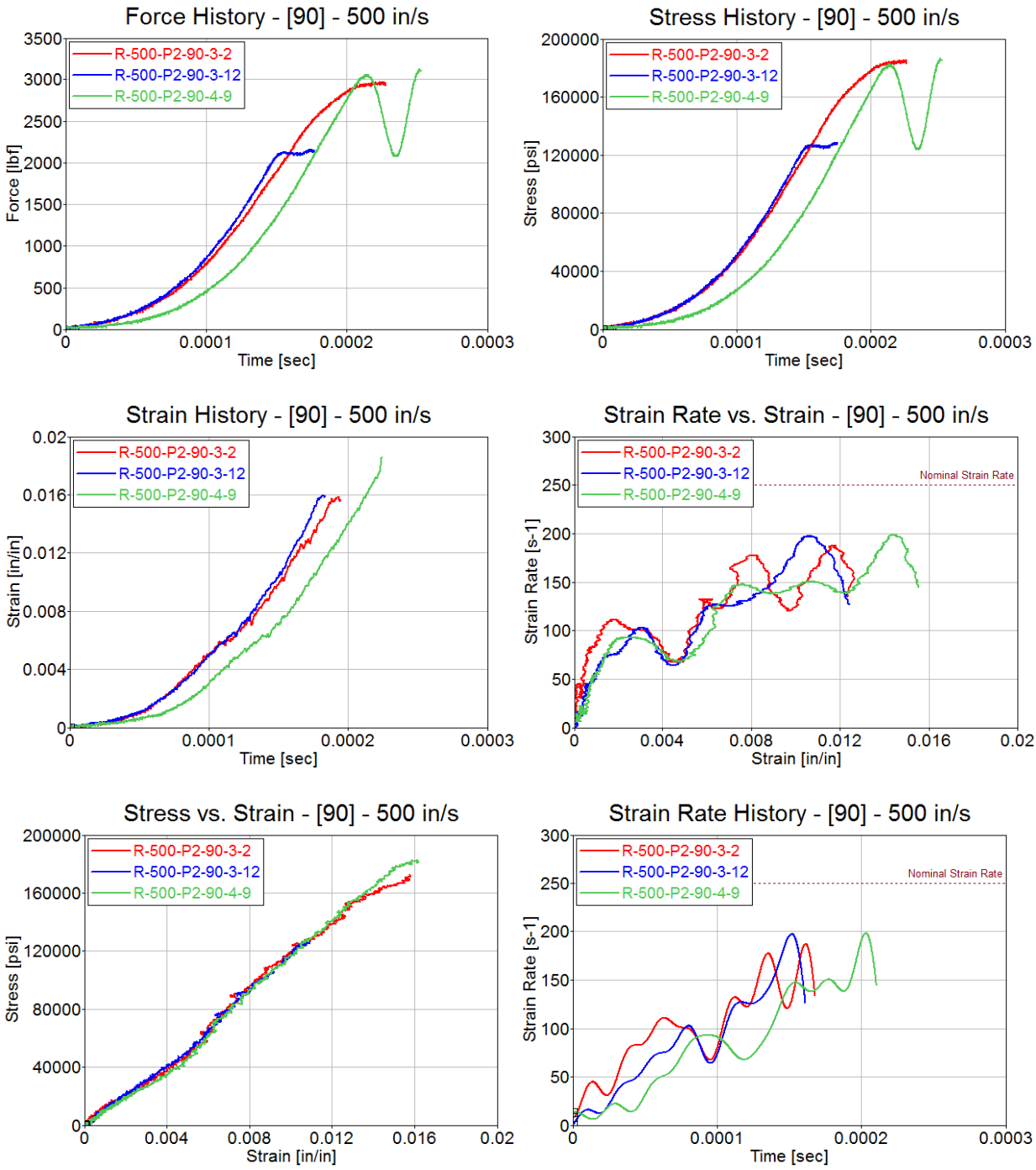

Figure C-16. Test results for Toray [90˚]$_4$ at stroke rate of 500 in/s

TORAY $[\pm 45^{\circ}]_4$

Table C-9. Summary of test results for Toray $[\pm 45^{\circ}]_4$ at stroke rate of 0.02 in/s

STROKE RATE [in/sec]	SPECIMEN NO.	TENSILE STRENGTH [psi]	MAXIMUM RECORDED STRAIN [in/in]	YOUNG'S MODULUS [Msi]	AVERAGE STRAIN RATE [s^{-1}]
0.02	R-0.02-P4-45-1-20	30766	0.0726	2.30	0.00794
	R-0.02-P3-45-2-13	27254	0.0719	2.17	0.00762
AVERAGE		29010	0.0722	2.24	0.00778
STANDARD DEVIATION		2483	0.0005	0.09	0.00022
COEFFICIENT OF VARIATION [%]		8.56	0.63	4.11	2.88

Figure C-17. Failure modes for Toray $[\pm 45^{\circ}]_4$ at stroke rate of 0.02 in/s

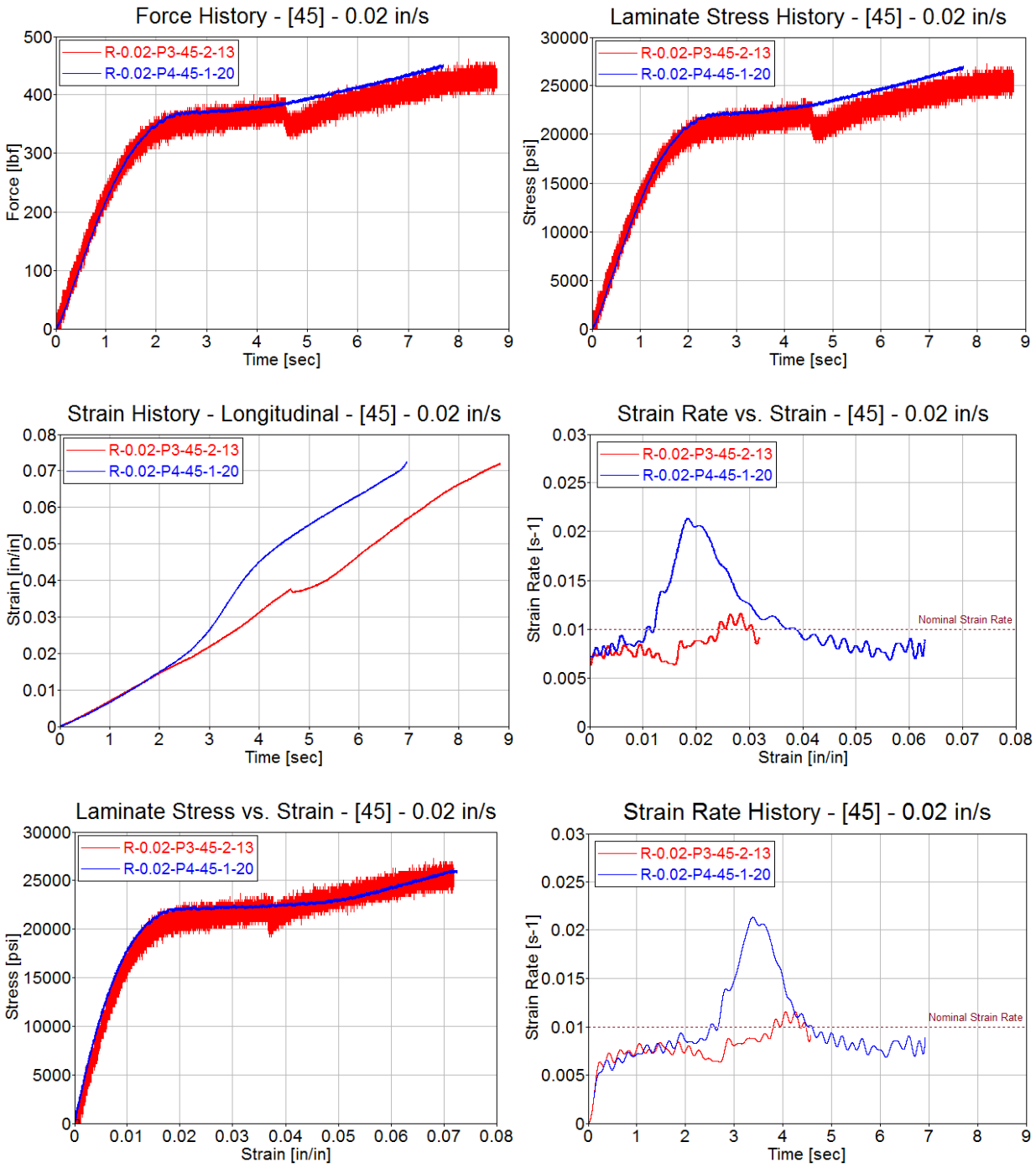

Figure C-18. Test results for Toray [±45˚]$_4$ at stroke rate of 0.02 in/s

Table C-10. Summary of test results for Toray [±45°]$_4$ at stroke rate of 2 in/s

STROKE RATE [in/sec]	SPECIMEN NO.	TENSILE STRENGTH [psi]	MAXIMUM RECORDED STRAIN [in/in]	YOUNG'S MODULUS [Msi]	AVERAGE STRAIN RATE [s^{-1}]
2	R-2-P4-45-1-4	34180	0.0526	2.37	0.675
	R-2-P4-45-2-10	33583	0.0721	1.92	0.654
AVERAGE		33881	0.0624	2.15	0.665
STANDARD DEVIATION		422	0.0138	0.32	0.015
COEFFICIENT OF VARIATION [%]		1.25	22.14	14.83	2.23

Figure C-19. Failure modes for Toray [±45°]$_4$ at stroke rate of 2 in/s

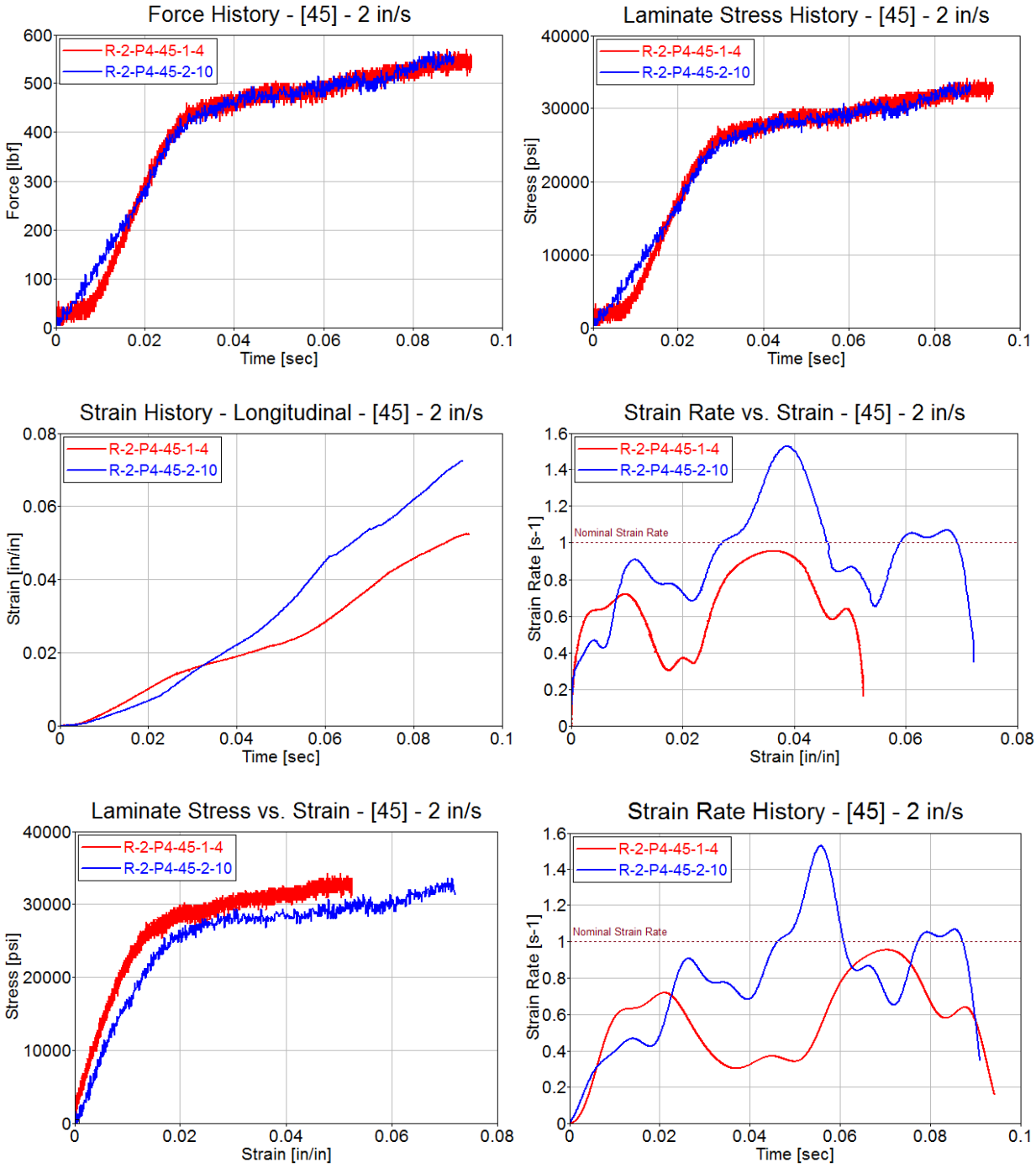

Figure C-20. Test results for Toray [±45°]$_4$ at stroke rate of 2 in/s

Table C-11. Summary of test results for Toray [±45°]$_4$ at stroke rate of 200 in/s

STROKE RATE [in/sec]	SPECIMEN NO.	TENSILE STRENGTH [psi]	MAXIMUM RECORDED STRAIN [in/in]	YOUNG'S MODULUS [Msi]	AVERAGE STRAIN RATE [s^{-1}]
200	R-200-P3-45-1-12	49707	0.0175	3.91	101.73
	R-200-P4-45-1-19	49806	0.0327	3.21	107.69
AVERAGE		49756	0.0251	3.56	104.71
STANDARD DEVIATION		70	0.0107	0.49	4.21
COEFFICIENT OF VARIATION [%]		0.14	42.69	13.90	4.02

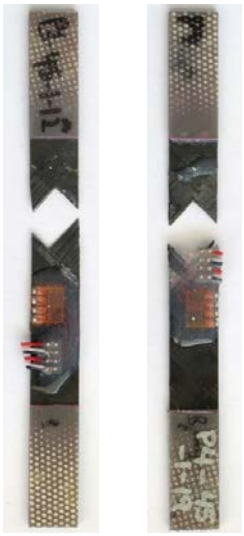

Figure C-21. Failure modes for Toray [±45°]$_4$ at stroke rate of 200 in/s

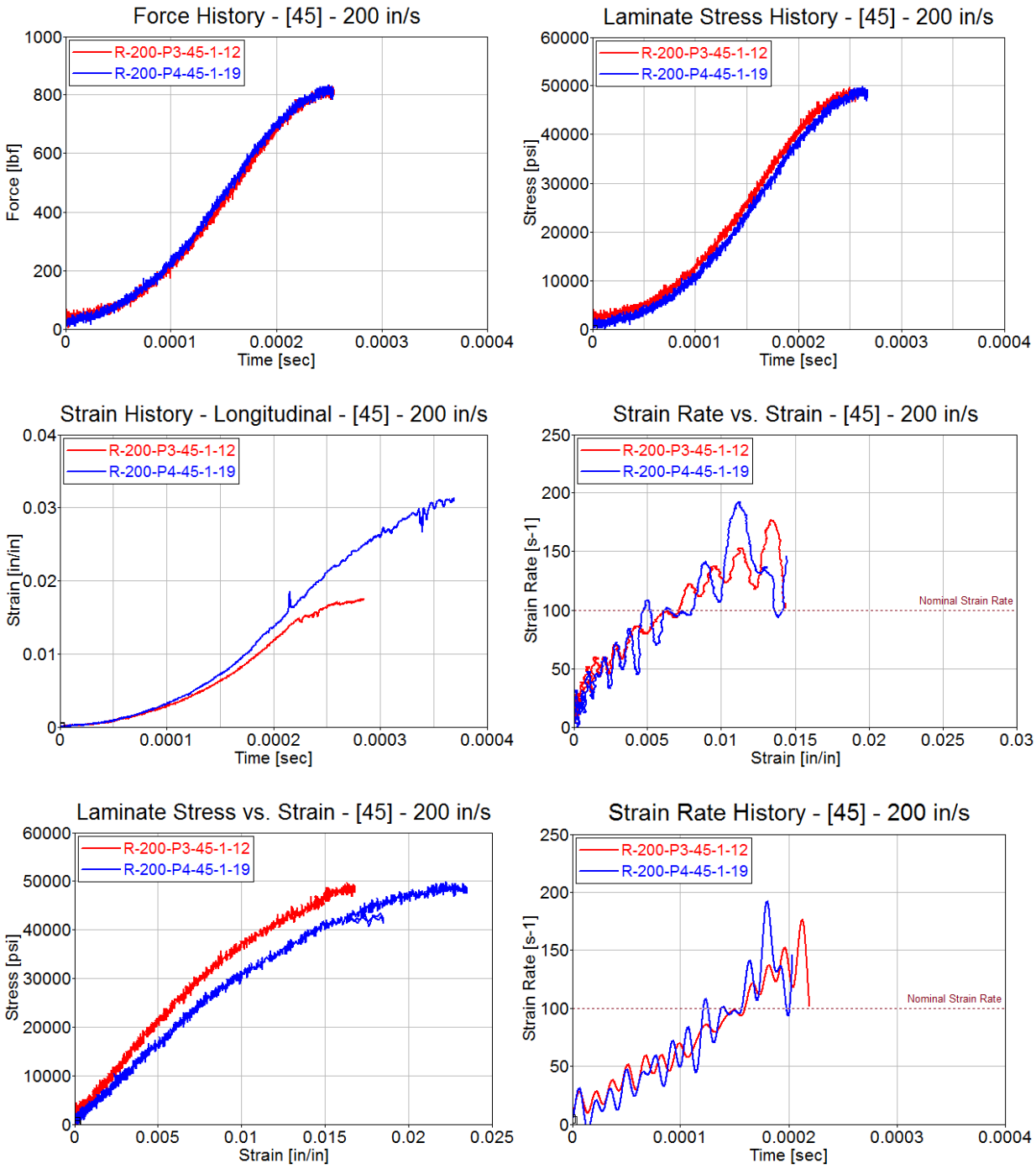

Figure C-22. Test results for Toray [±45˚]$_4$ at stroke rate of 200 in/s

Table C-12. Summary of test results for Toray [±45°]$_4$ at stroke rate of 500 in/s

STROKE RATE [in/sec]	SPECIMEN NO.	TENSILE STRENGTH [psi]	MAXIMUM RECORDED STRAIN [in/in]	YOUNG'S MODULUS [Msi]	AVERAGE STRAIN RATE [s^{-1}]
500	R-500-P3-45-1-3	54775	0.0364	3.69	154.10
	R-500-P4-45-1-8	53678	0.0267	2.81	137.31
	R-500-P4-45-1-13	55424	0.0401	3.10	146.17
AVERAGE		54626	0.0344	3.20	145.86
STANDARD DEVIATION		883	0.0069	0.45	8.40
COEFFICIENT OF VARIATION [%]		1.62	20.12	14.01	5.76

Figure C-23. Failure modes for Toray [±45°]$_4$ at stroke rate of 500 in/s

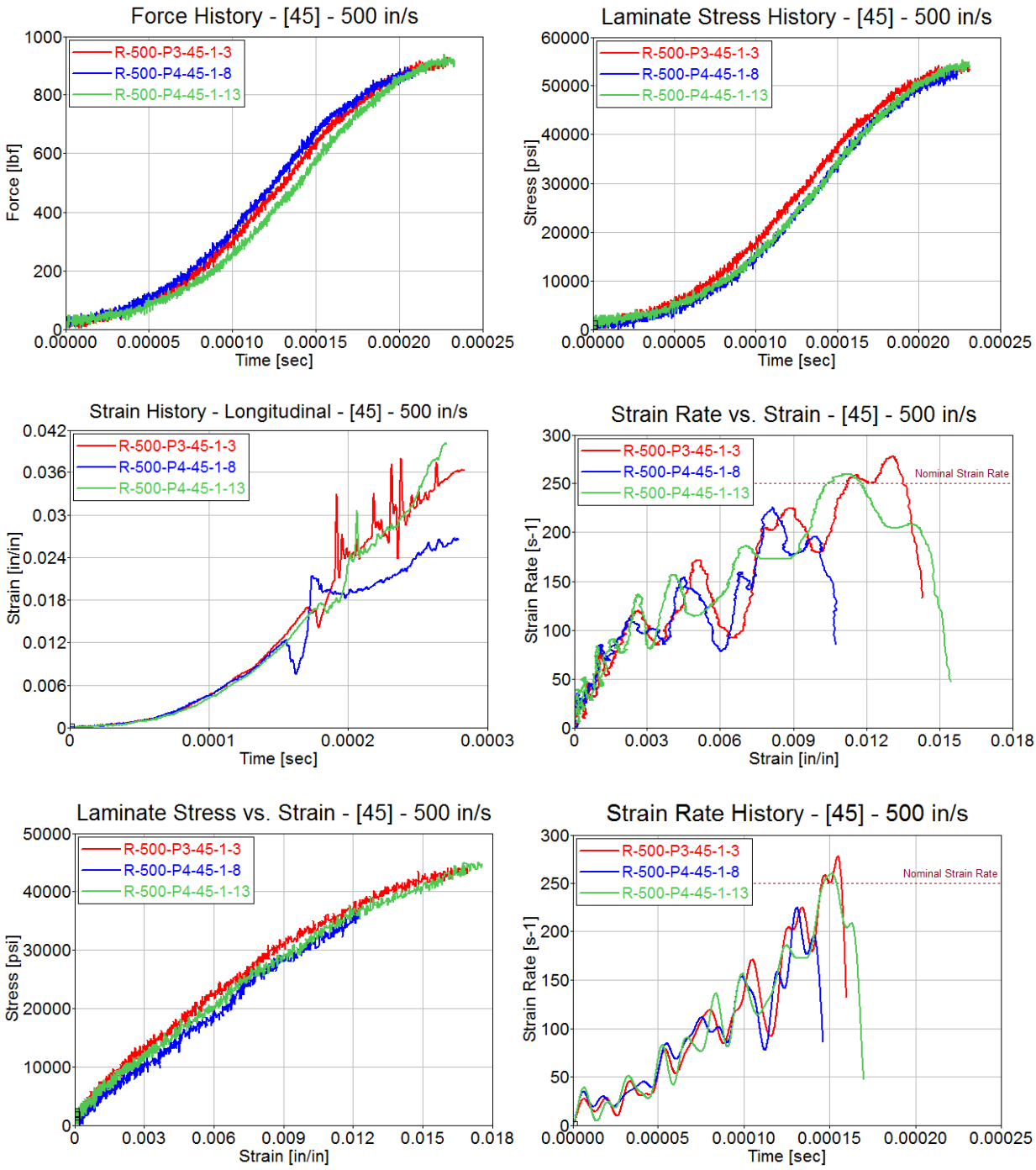

Figure C-24. Test results for Toray [±45˚]$_4$ at stroke rate of 500 in/s

APPENDIX D—LAB D RAW TESTING RESULTS

Laboratory D results using a conventional servo-hydraulic test machine.

TORAY $[0^{\circ}]_4$

Table D-1. Summary of test results for Toray $[0^{\circ}]_4$ at stroke rate of 0.02 in/s

STROKE RATE [in/sec]	SPECIMEN NO.	TENSILE STRENGTH [psi]	MAXIMUM RECORDED STRAIN [in/in]	YOUNG'S MODULUS [Msi]	AVERAGE STRAIN RATE [s^{-1}]
0.02	R-0.02-P1-0-1-21	147153	0.0170	8.36	0.00268
	R-0.02-P1-0-2-7	161237	0.0180	8.35	0.00264
AVERAGE		154195	0.0175	8.36	0.00266
STANDARD DEVIATION		9959	0.0007	0.01	0.00003
COEFFICIENT OF VARIATION [%]		6.46	4.14	0.08	1.06

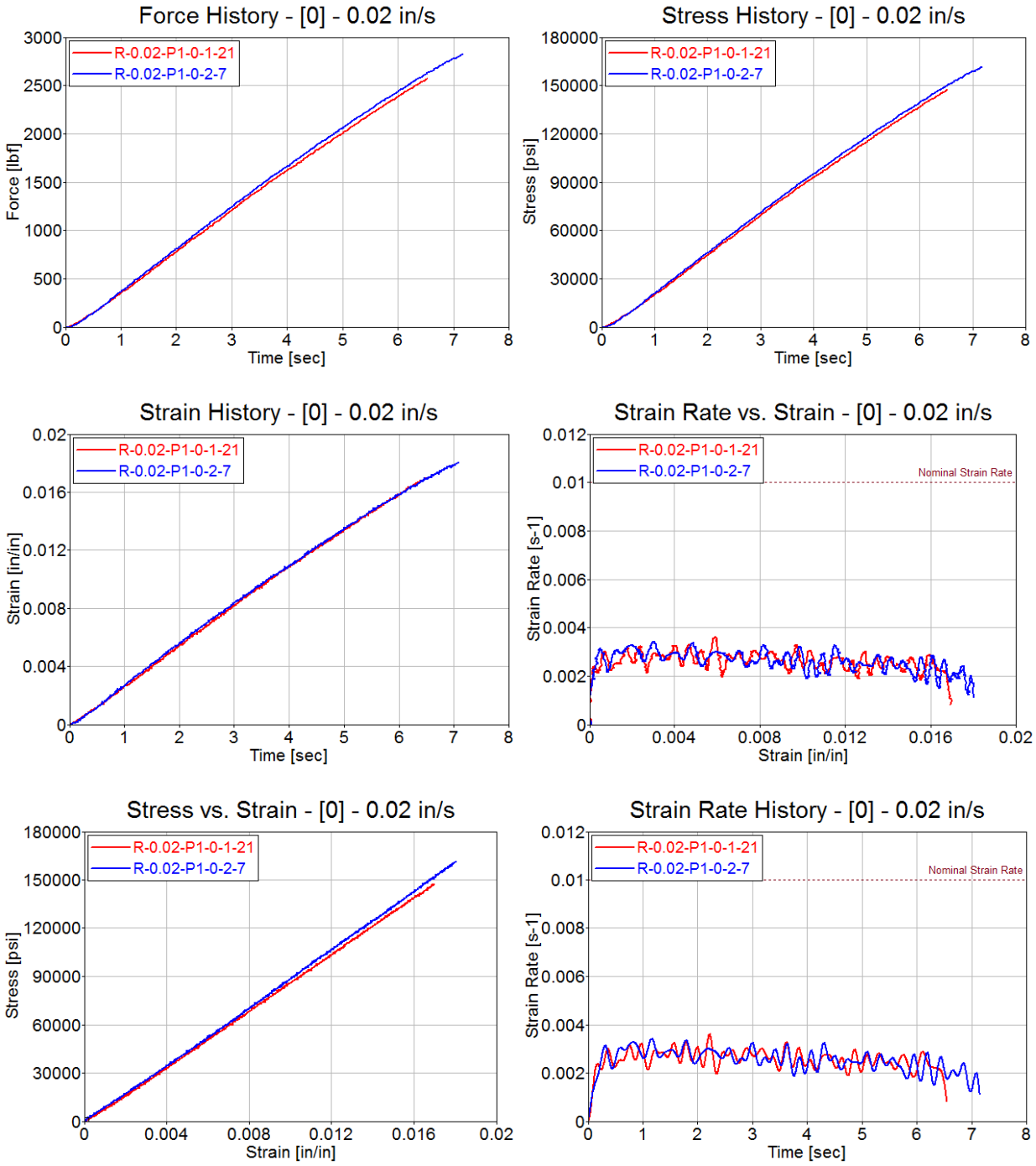

Figure D-1. Test results for Toray [0˚]$_4$ at stroke rate of 0.02 in/s

Table D-2. Summary of test results for Toray $[0^{\circ}]_4$ at stroke rate of 2 in/s

STROKE RATE [in/sec]	SPECIMEN NO.	TENSILE STRENGTH [psi]	MAXIMUM RECORDED STRAIN [in/in]	YOUNG'S MODULUS [Msi]	AVERAGE STRAIN RATE [s^{-1}]
2	R-2-P1-0-1-22	152360	0.0179	7.62	0.265
	R-2-P1-0-2-9	167315	0.0193	7.85	0.269
	R-2-P1-0-2-21	145345	0.0170	8.15	0.263
AVERAGE		155006	0.0181	7.87	0.265
STANDARD DEVIATION		11222	0.0011	0.27	0.003
COEFFICIENT OF VARIATION [%]		7.24	6.35	3.38	1.09

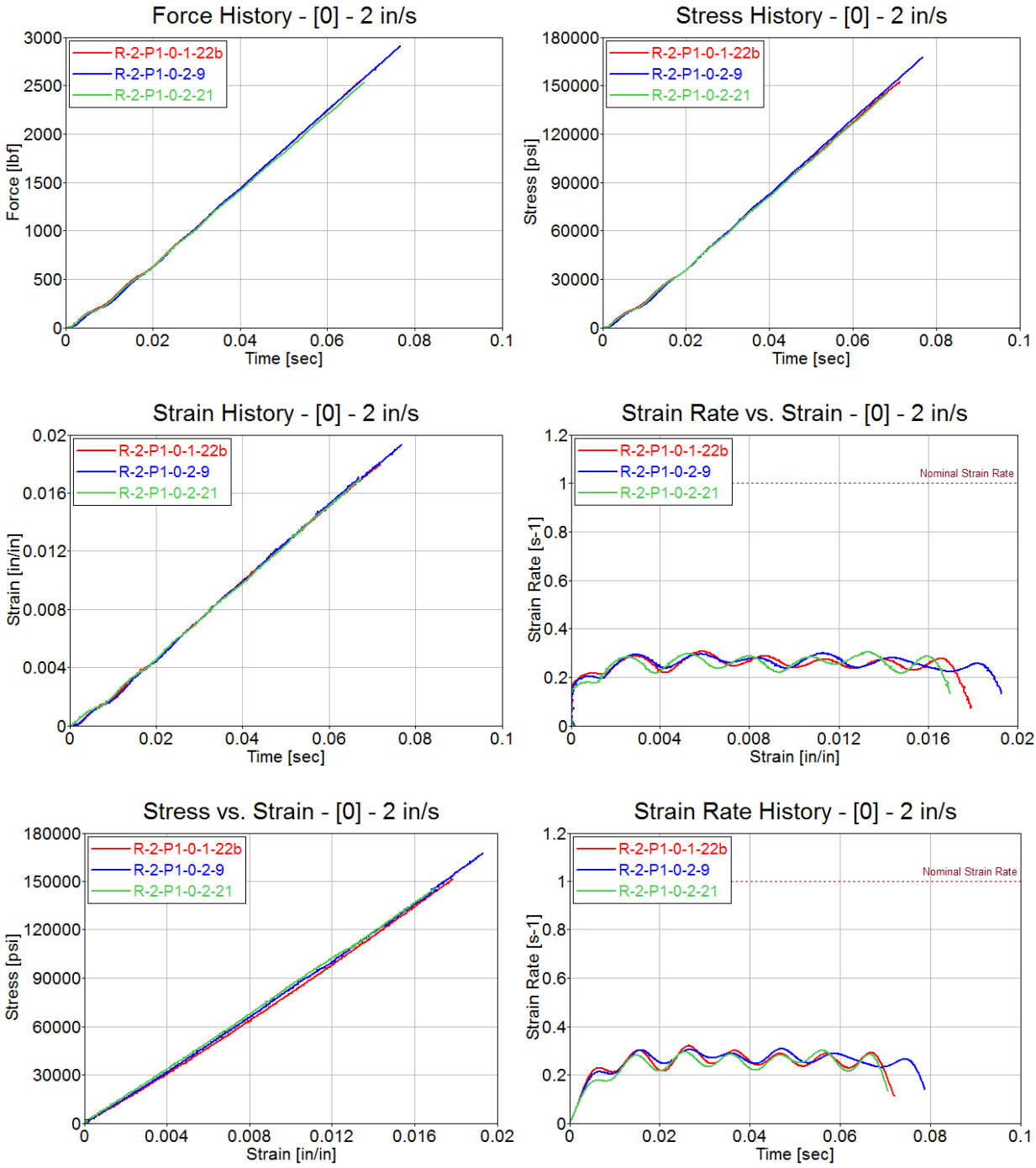

Figure D-2. Test results for Toray [0°]4 at stroke rate of 2 in/s

Table D-3. Summary of test results for Toray $[0^{\circ}]_4$ at stroke rate of 200 in/s

STROKE RATE [in/sec]	SPECIMEN NO.	TENSILE STRENGTH [psi]	MAXIMUM RECORDED STRAIN [in/in]	YOUNG'S MODULUS [Msi]	AVERAGE STRAIN RATE [s^{-1}]
200	R-200-P1-0-1-16	189128	0.0186	6.97	111.20
	R-200-P1-0-2-17	190512	0.0186	8.31	110.40
	R-200-P1-0-4-5	185249	0.0168	7.58	105.78
AVERAGE		188296	0.0180	7.62	109.13
STANDARD DEVIATION		2728	0.0011	0.67	2.93
COEFFICIENT OF VARIATION [%]		1.45	5.94	8.80	2.68

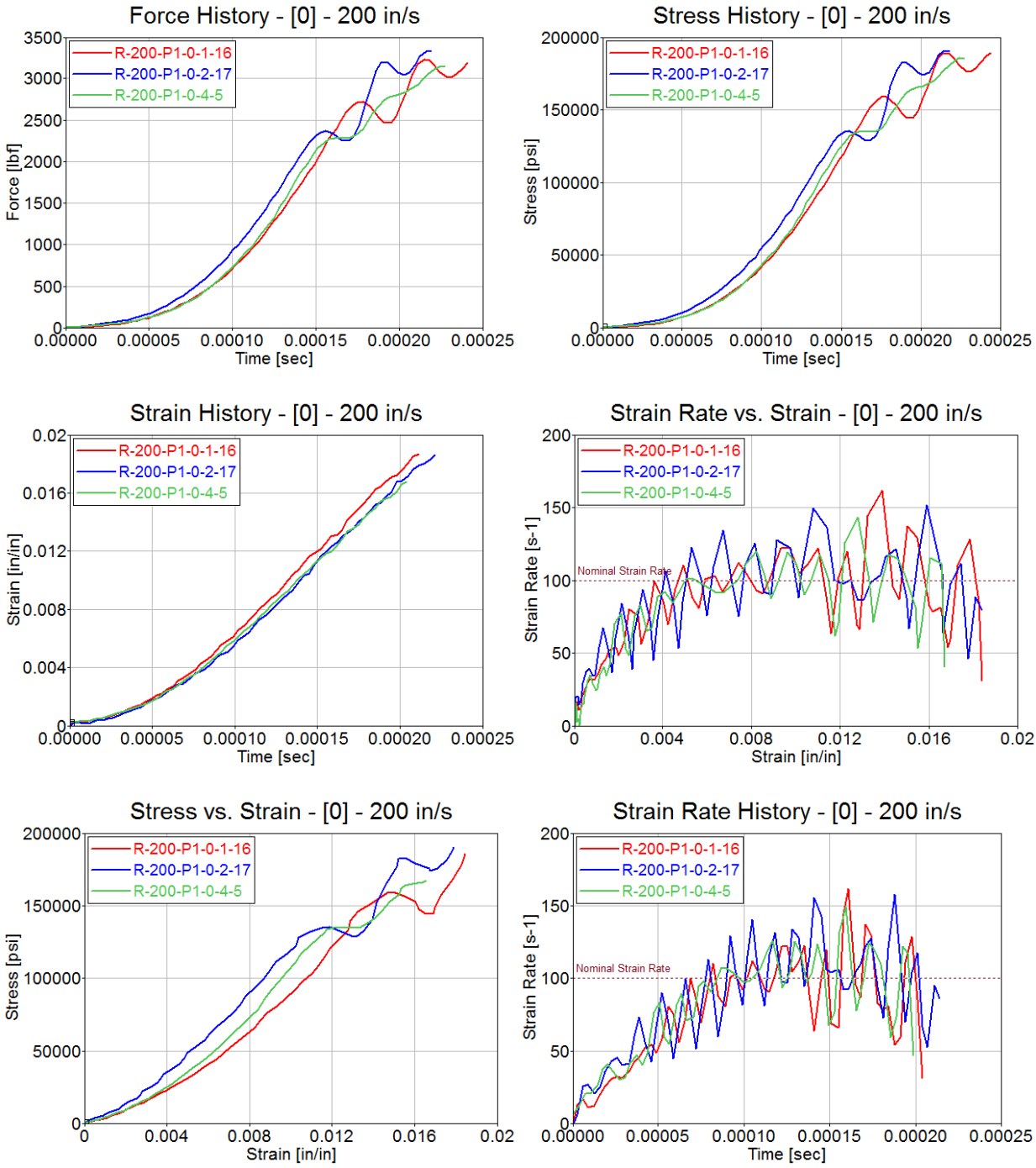

Figure D-3. Test results for Toray [0˚]$_4$ at stroke rate of 200 in/s

Table D-4. Summary of test results for Toray $[0^{\circ}]_4$ at stroke rate of 500 in/s

STROKE RATE [in/sec]	SPECIMEN NO.	TENSILE STRENGTH [psi]	MAXIMUM RECORDED STRAIN [in/in]	YOUNG'S MODULUS [Msi]	AVERAGE STRAIN RATE [s^{-1}]
500	R-500-P1-0-1-7	147607	0.0176	9.34	152.26
	R-500-P1-0-2-5	147110	0.0186	10.87	147.10
	R-500-P1-0-2-10	137337	0.0198	7.56	168.06
AVERAGE		144018	0.0187	9.26	155.81
STANDARD DEVIATION		5791	0.0011	1.66	10.92
COEFFICIENT OF VARIATION [%]		4.02	5.95	17.90	7.01

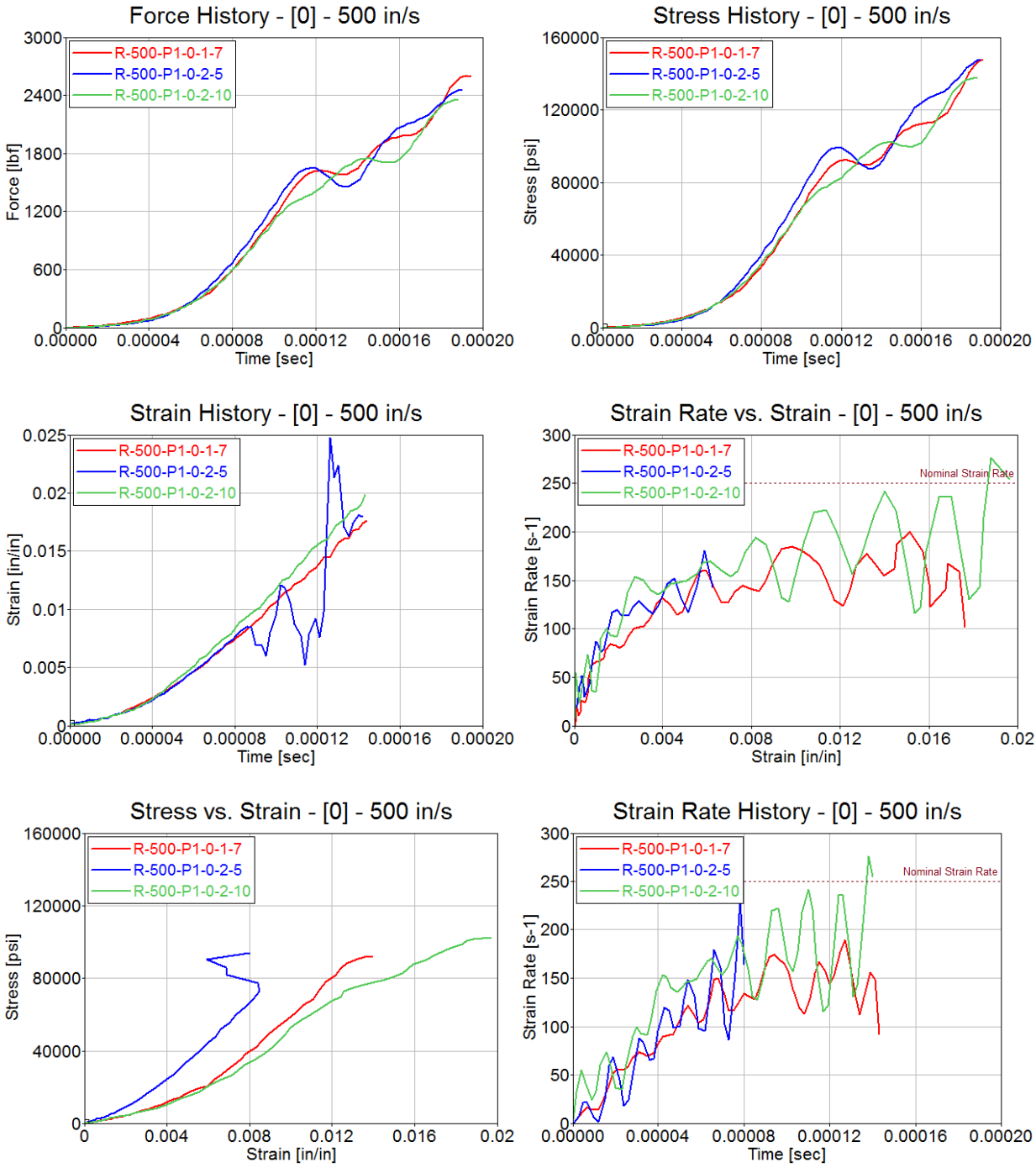

Figure D-4. Test results for Toray [0˚]$_4$ at stroke rate of 500 in/s

TORAY $[90]_4$

Table D-5. Summary of test results for Toray $[90^{\circ}]_4$ at stroke rate of 0.02 in/s

STROKE RATE [in/sec]	SPECIMEN NO.	TENSILE STRENGTH [psi]	MAXIMUM RECORDED STRAIN [in/in]	YOUNG'S MODULUS [Msi]	AVERAGE STRAIN RATE [s^{-1}]
0.02	R-0.02-P2-90-1-3	132920	0.0157	8.14	0.00280
	R-0.02-P2-90-1-11	114039	0.0131	8.45	0.00277
	R-0.02-P2-90-4-17	143091	0.0168	8.17	0.00258
AVERAGE		130016	0.0152	8.25	0.00272
STANDARD DEVIATION		14742	0.0019	0.17	0.00012
COEFFICIENT OF VARIATION [%]		11.34	12.28	2.07	4.33

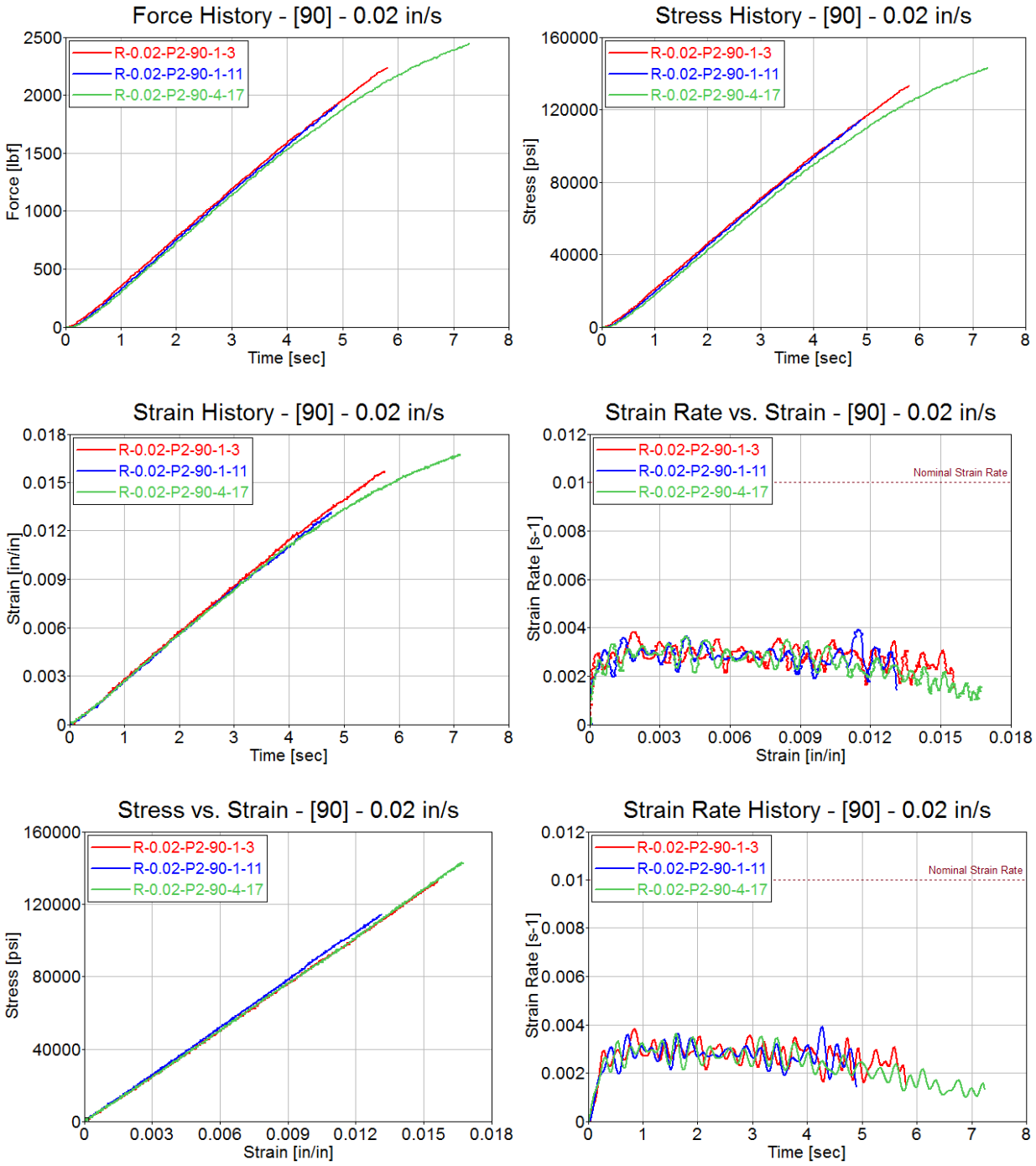

Figure D-5. Test results for Toray [90˚]$_4$ at stroke rate of 0.02 in/s

Table D-6. Summary of test results for Toray $[90^{\circ}]_4$ at stroke rate of 2 in/s

STROKE RATE [in/sec]	SPECIMEN NO.	TENSILE STRENGTH [psi]	MAXIMUM RECORDED STRAIN [in/in]	YOUNG'S MODULUS [Msi]	AVERAGE STRAIN RATE [s^{-1}]
2	R-2-P2-90-1-6	130005	0.0146	8.73	0.255
	R-2-P2-90-3-15	117065	0.0147	7.56	0.283
	R-2-P2-90-4-18	135905	0.0157	8.39	0.254
AVERAGE		127658	0.0150	8.23	0.264
STANDARD DEVIATION		9637	0.0006	0.60	0.016
COEFFICIENT OF VARIATION [%]		7.55	3.86	7.32	6.17

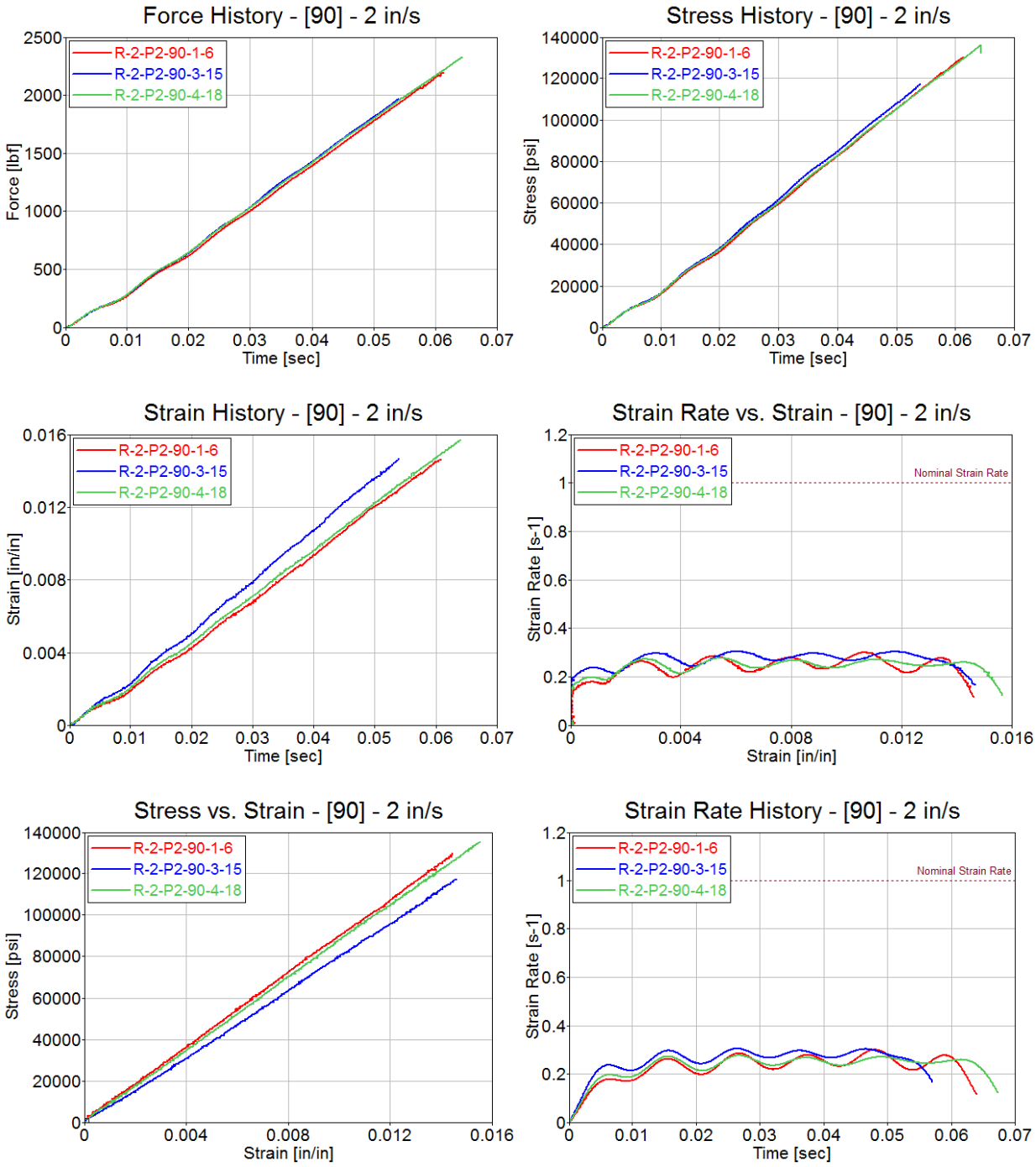

Figure D-6. Test results for Toray [90˚]$_4$ at stroke rate of 2 in/s

Table D-7. Summary of test results for Toray $[90^{\circ}]_4$ at stroke rate of 200 in/s

STROKE RATE [in/sec]	SPECIMEN NO.	TENSILE STRENGTH [psi]	MAXIMUM RECORDED STRAIN [in/in]	YOUNG'S MODULUS [Msi]	AVERAGE STRAIN RATE [s^{-1}]
200	R-200-P2-90-2-9	141909	0.0151	9.18	108.43
	R-200-P2-90-2-20	143245	0.0168	8.62	113.01
AVERAGE		142577	0.0160	8.90	110.72
STANDARD DEVIATION		945	0.0012	0.40	3.24
COEFFICIENT OF VARIATION [%]		0.66	7.67	4.45	2.92

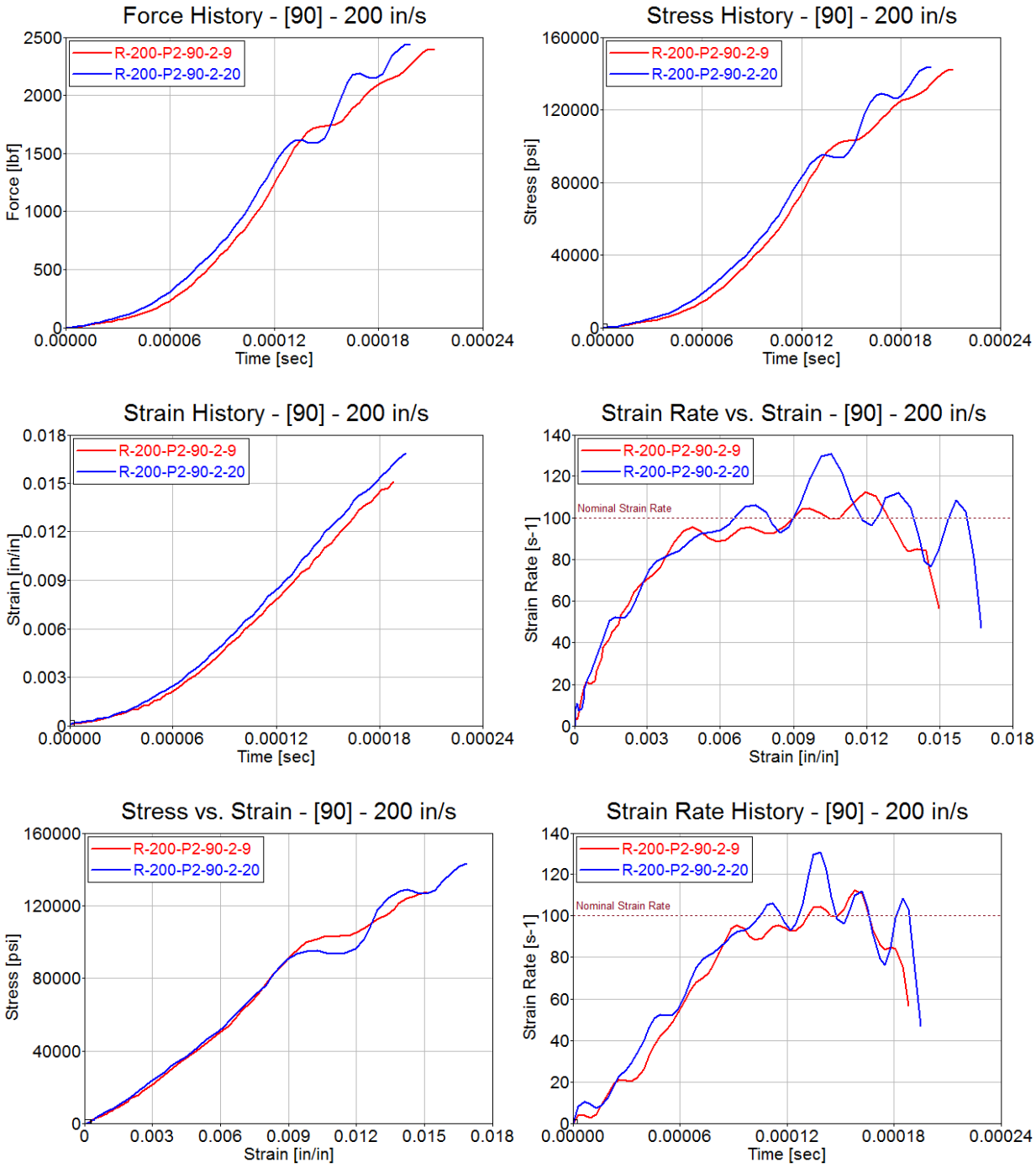

Figure D-7. Test results for Toray [90˚]$_4$ at stroke rate of 200 in/s

Table D-8. Summary of test results for Toray $[90^{\circ}]_4$ at stroke rate of 500 in/s

STROKE RATE [in/sec]	SPECIMEN NO.	TENSILE STRENGTH [psi]	MAXIMUM RECORDED STRAIN [in/in]	YOUNG'S MODULUS [Msi]	AVERAGE STRAIN RATE [s^{-1}]
500	R-500-P2-90-1-9	99515	0.0168	9.38	168.01
	R-500-P2-90-2-19	120191	0.0204	10.13	164.13
	R-500-P2-90-3-19	110340	0.0177	9.45	160.47
AVERAGE		110016	0.0183	9.65	164.20
STANDARD DEVIATION		10342	0.0018	0.41	3.77
COEFFICIENT OF VARIATION [%]		9.40	10.05	4.29	2.30

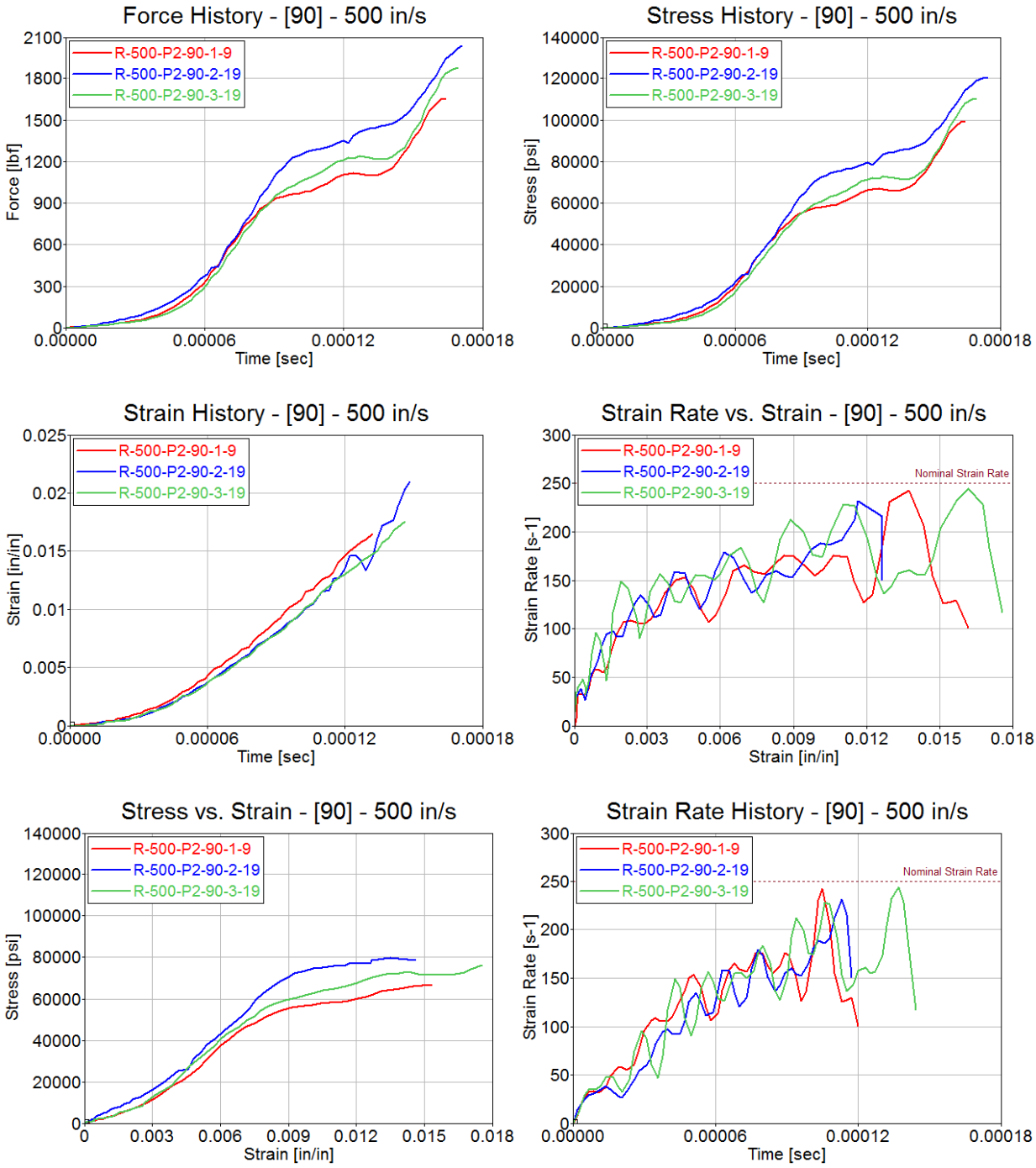

Figure D-8. Test results for Toray [90˚]$_4$ at stroke rate of 500 in/s

TORAY $[\pm 45^{\circ}]_4$

Table D-9. Summary of test results for Toray $[\pm 45^{\circ}]_4$ at stroke rate of 0.02 in/s

STROKE RATE [in/sec]	SPECIMEN NO.	TENSILE STRENGTH [psi]	MAXIMUM RECORDED STRAIN [in/in]	YOUNG'S MODULUS [Msi]	AVERAGE STRAIN RATE [s^{-1}]
0.02	R-0.02-P3-45-2-4	25485	0.0675	2.31	0.00617
	R-0.02-P3-45-2-18	28929	0.0625	2.52	0.00543
	R-0.02-P4-45-2-12	26312	0.0827	2.04	0.00755
AVERAGE		26908	0.0709	2.29	0.00638
STANDARD DEVIATION		1798	0.0105	0.24	0.00108
COEFFICIENT OF VARIATION [%]		6.68	14.86	10.51	16.87

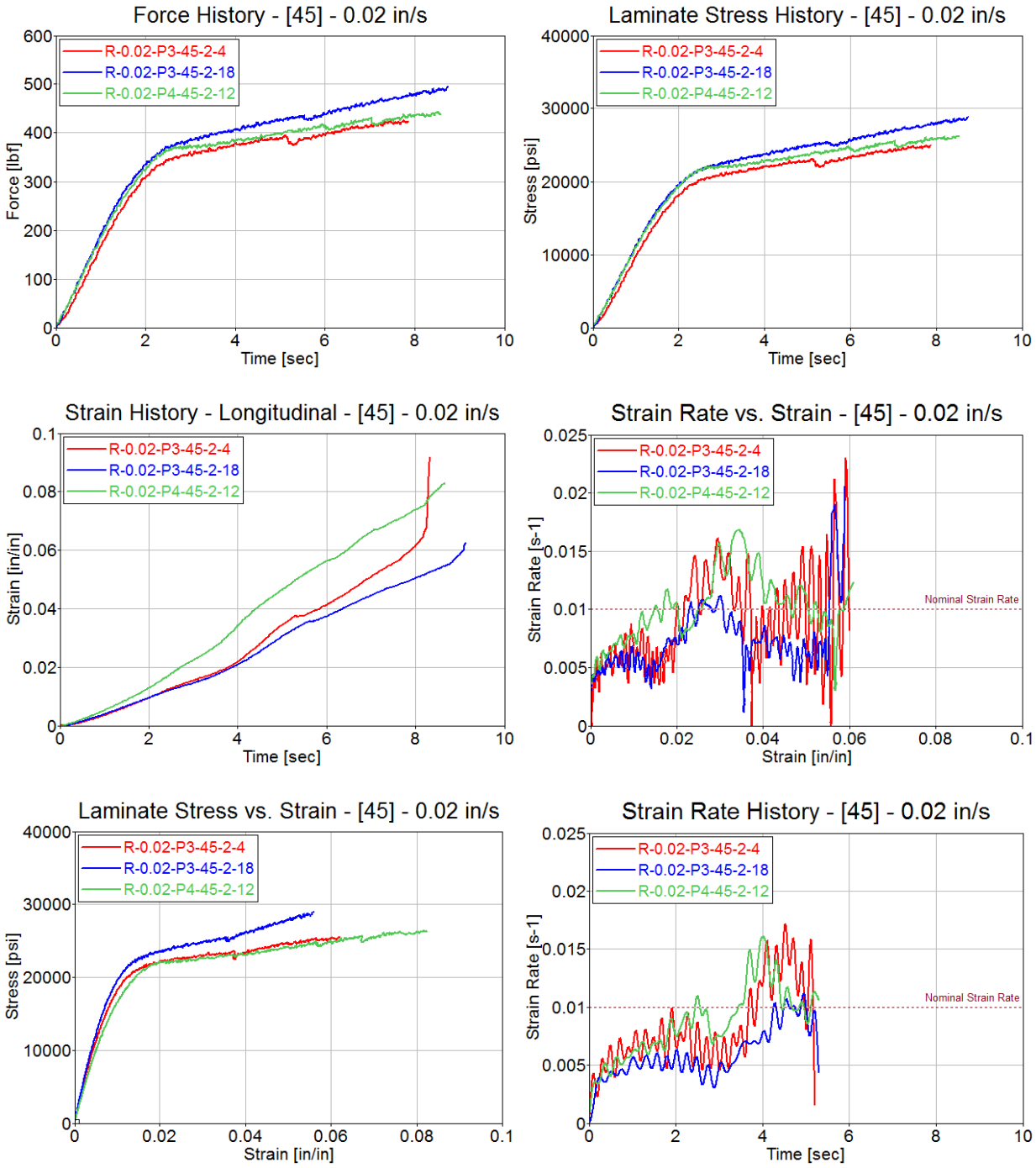

Figure D-9. Test results for Toray [±45°]$_4$ at stroke rate of 0.02 in/s

Table D-10. Summary of test results for Toray [±45°]$_4$ at stroke rate of 2 in/s

STROKE RATE [in/sec]	SPECIMEN NO.	TENSILE STRENGTH [psi]	MAXIMUM RECORDED STRAIN [in/in]	YOUNG'S MODULUS [Msi]	AVERAGE STRAIN RATE [s^{-1}]
2	R-2-P3-45-2-16	28502	0.0556	2.02	0.703
	R-2-P4-45-1-3	26953	0.0306	2.34	0.604
	R-2-P4-45-2-16	29512	0.0618	2.22	0.627
AVERAGE		28322	0.0493	2.19	0.645
STANDARD DEVIATION		1289	0.0165	0.16	0.052
COEFFICIENT OF VARIATION [%]		4.55	33.49	7.37	8.04

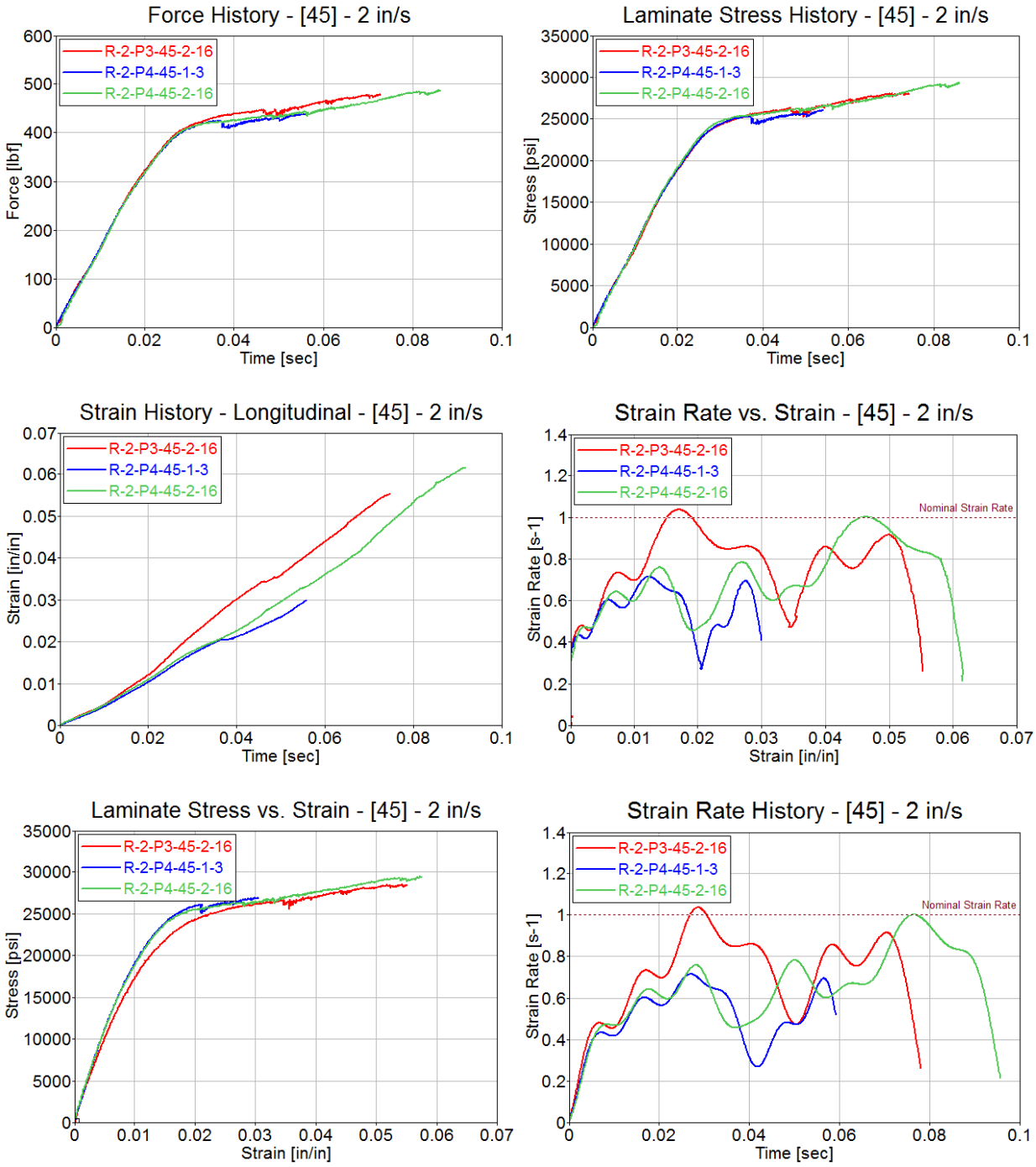

Figure D-10. Test results for Toray [±45°]$_4$ at stroke rate of 2 in/s

Table D-11. Summary of test results for Toray $[\pm 45^{\circ}]_4$ at stroke rate of 200 in/s

STROKE RATE [in/sec]	SPECIMEN NO.	TENSILE STRENGTH [psi]	MAXIMUM RECORDED STRAIN [in/in]	YOUNG'S MODULUS [Msi]	AVERAGE STRAIN RATE [s^{-1}]
200	R-200-P3-45-1-2	63299	0.0750	2.05	163.40
	R-200-P3-45-2-7	71964	0.0528	3.17	156.48
	R-200-P4-45-1-18	67078	0.0599	2.47	173.71
AVERAGE		67447	0.0626	2.56	164.53
STANDARD DEVIATION		4345	0.0113	0.57	8.67
COEFFICIENT OF VARIATION [%]		6.44	18.10	22.07	5.27

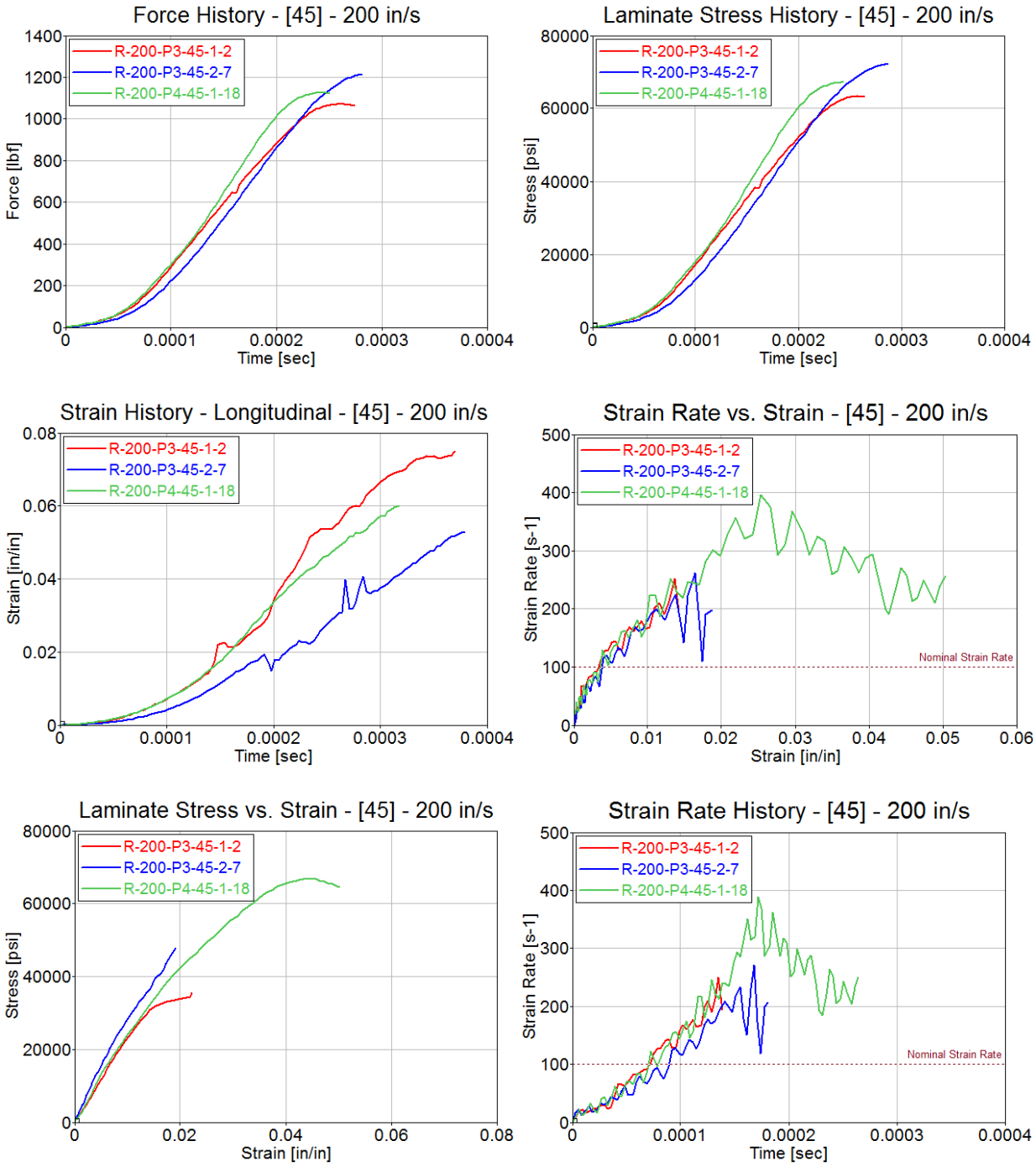

Figure D-11. Test results for Toray [±45˚]$_4$ at stroke rate of 200 in/s

Table D-12. Summary of test results for Toray $[\pm 45^{\circ}]_4$ at stroke rate of 500 in/s

STROKE RATE [in/sec]	SPECIMEN NO.	TENSILE STRENGTH [psi]	MAXIMUM RECORDED STRAIN [in/in]	YOUNG'S MODULUS [Msi]	AVERAGE STRAIN RATE [s^{-1}]
500	R-500-P3-45-1-15	52280	0.0497	1.19	257.10
	R-500-P4-45-1-10	45905	0.0545	1.03	227.58
	R-500-P4-45-2-14	63741	0.0593	0.62	199.09
AVERAGE		53975	0.0545	0.95	227.92
STANDARD DEVIATION		9038	0.0048	0.29	29.01
COEFFICIENT OF VARIATION [%]		16.74	8.81	31.06	12.73

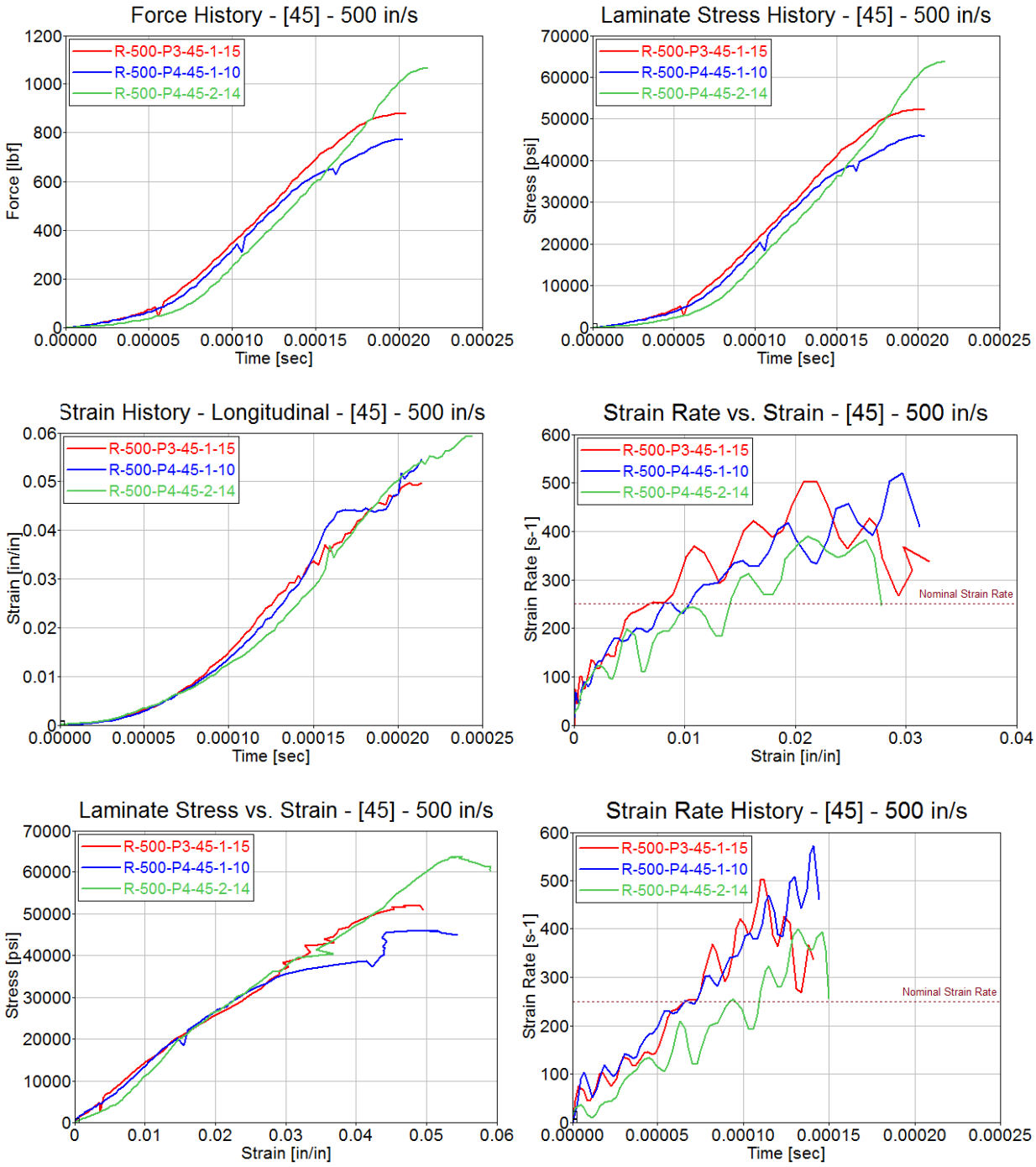

Figure D-12. Test results for Toray [±45˚]$_4$ at stroke rate of 500 in/s

APPENDIX E—TESTING RESULTS FOR SPLIT HOPKINSON PRESSURE BAR

Strain rate 1 (SR1) was approximately 0.00015 s^{-1} and was generated using a servo-hydraulic machine and the sub-sized Split Hopkinson Pressure Bar specimen. Strain rate 2 (SR2) was approximately 150 s^{-1} and strain rate 3 (SR3) approximately 360 s^{-1}.

TORAY $[0^{\circ}]_4$

Table E-1. Summary of test results for Toray $[0^{\circ}]_4$ at SR1

TEST RATE	SPECIMEN NO.	TENSILE STRENGTH [psi]	MAXIMUM RECORDED STRAIN [in/in]	YOUNG'S MODULUS [Msi]	AVERAGE STRAIN RATE [s^{-1}]
SR1	[0]-SR1-N1	130222	0.0171	7.12	0.000150
	[0]-SR1-N2	151985	0.0182	8.04	0.000146
AVERAGE		141104	0.0177	7.58	0.000148
STANDARD DEVIATION		15389	0.0008	0.65	0.000003
COEFFICIENT OF VARIATION [%]		10.91	4.39	8.58	1.91

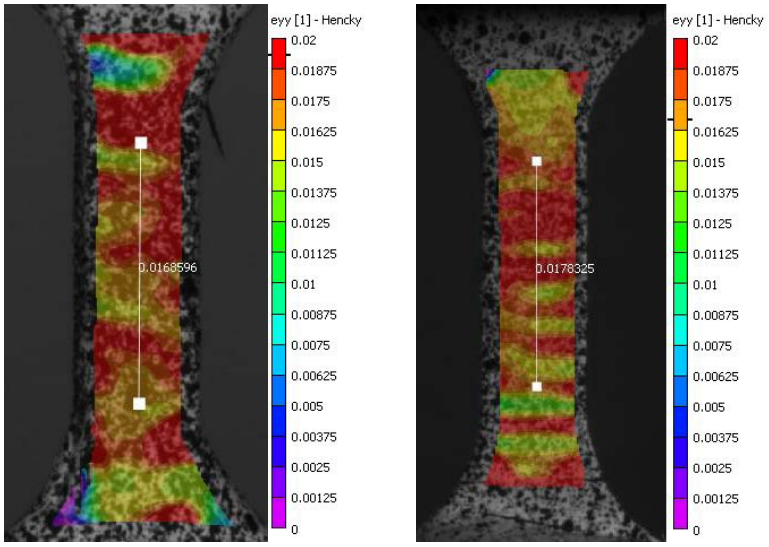

Figure E-1. Strain distribution before failure of Toray $[0^{\circ}]_4$ at test rate SR1

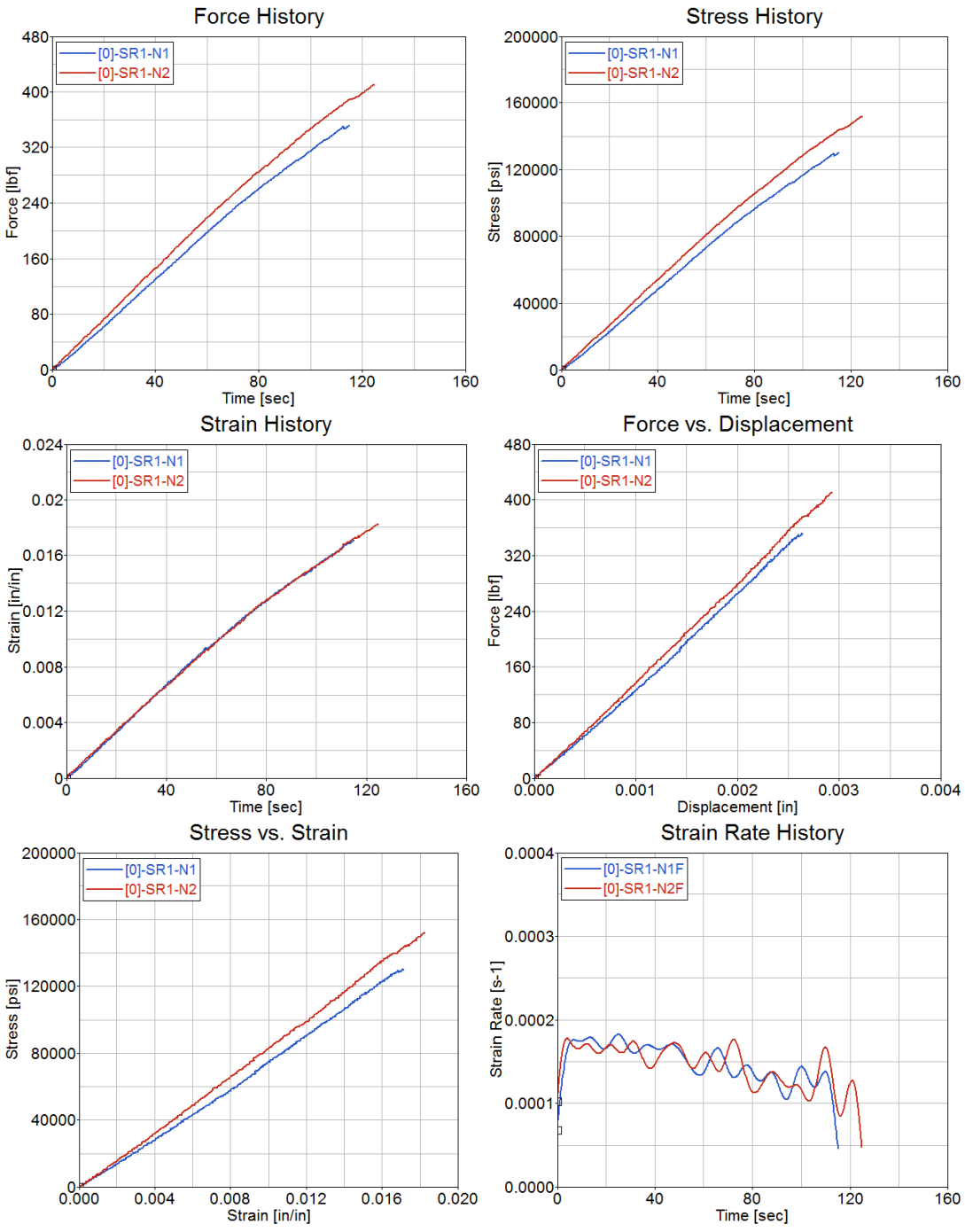

Figure E-2. Test results for Toray $[0^{\circ}]_4$ at test rate SR1

Table E-2. Summary of test results for Toray $[0^{\circ}]_4$ at test rate SR2

TEST RATE	SPECIMEN NO.	TENSILE STRENGTH [psi]	MAXIMUM RECORDED STRAIN [in/in]	YOUNG'S MODULUS [Msi]	AVERAGE STRAIN RATE [s^{-1}]
SR2	[0]-SR2-N1	162723	0.0198	6.89	125.44
	[0]-SR2-N2	130852	0.0181	6.99	185.24
AVERAGE		146788	0.0190	6.94	155.34
STANDARD DEVIATION		22537	0.0012	0.07	42.28
COEFFICIENT OF VARIATION [%]		15.35	6.46	1.02	27.22

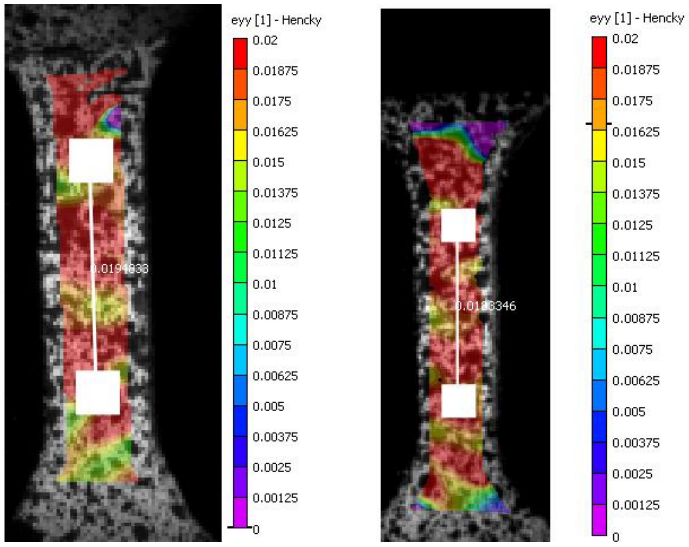

Figure E-3. Strain distribution before failure of Toray $[0^{\circ}]_4$ at test rate SR2

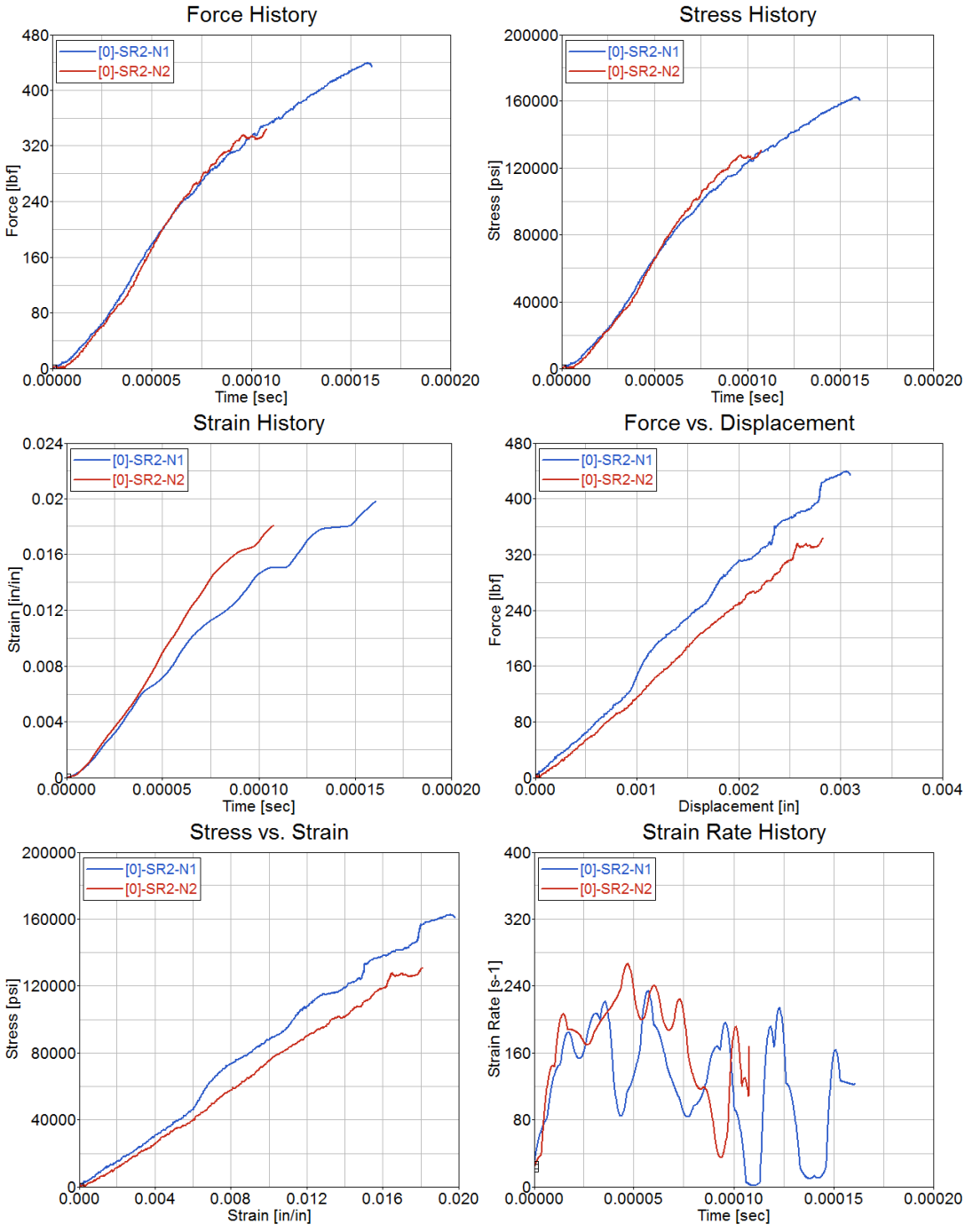

Figure E-4. Test results for Toray $[0^{\circ}]_4$ at test rate SR2

Table E-3. Summary of test results for Toray [0°]$_4$ at test rate SR3

TEST RATE	SPECIMEN NO.	TENSILE STRENGTH [psi]	MAXIMUM RECORDED STRAIN [in/in]	YOUNG'S MODULUS [Msi]	AVERAGE STRAIN RATE [s^{-1}]
SR3	[0]-SR3-N1	158933	0.0177	9.00	363.73
	[0]-SR3-N2	141206	0.0188	6.29	356.00
AVERAGE		150070	0.0182	7.65	359.87
STANDARD DEVIATION		12535	0.0008	1.92	5.47
COEFFICIENT OF VARIATION [%]		8.35	4.56	25.07	1.52

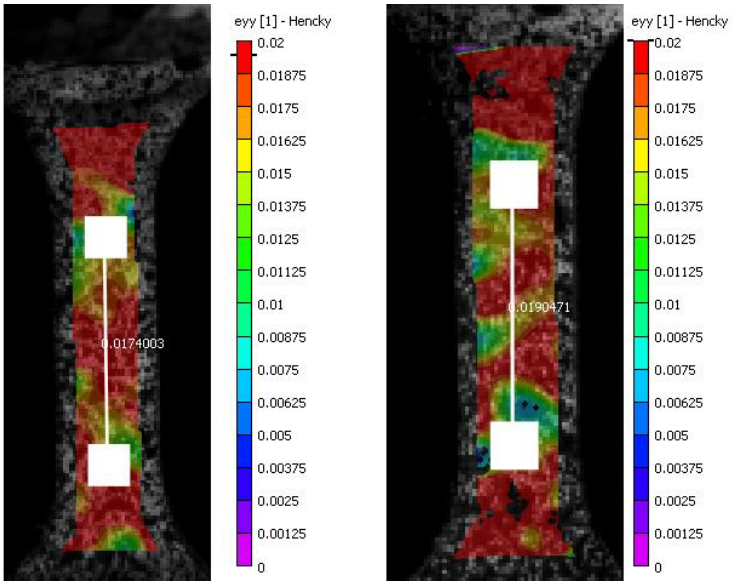

Figure E-5. Strain distribution before failure of Toray [0°]$_4$ at test rate SR3

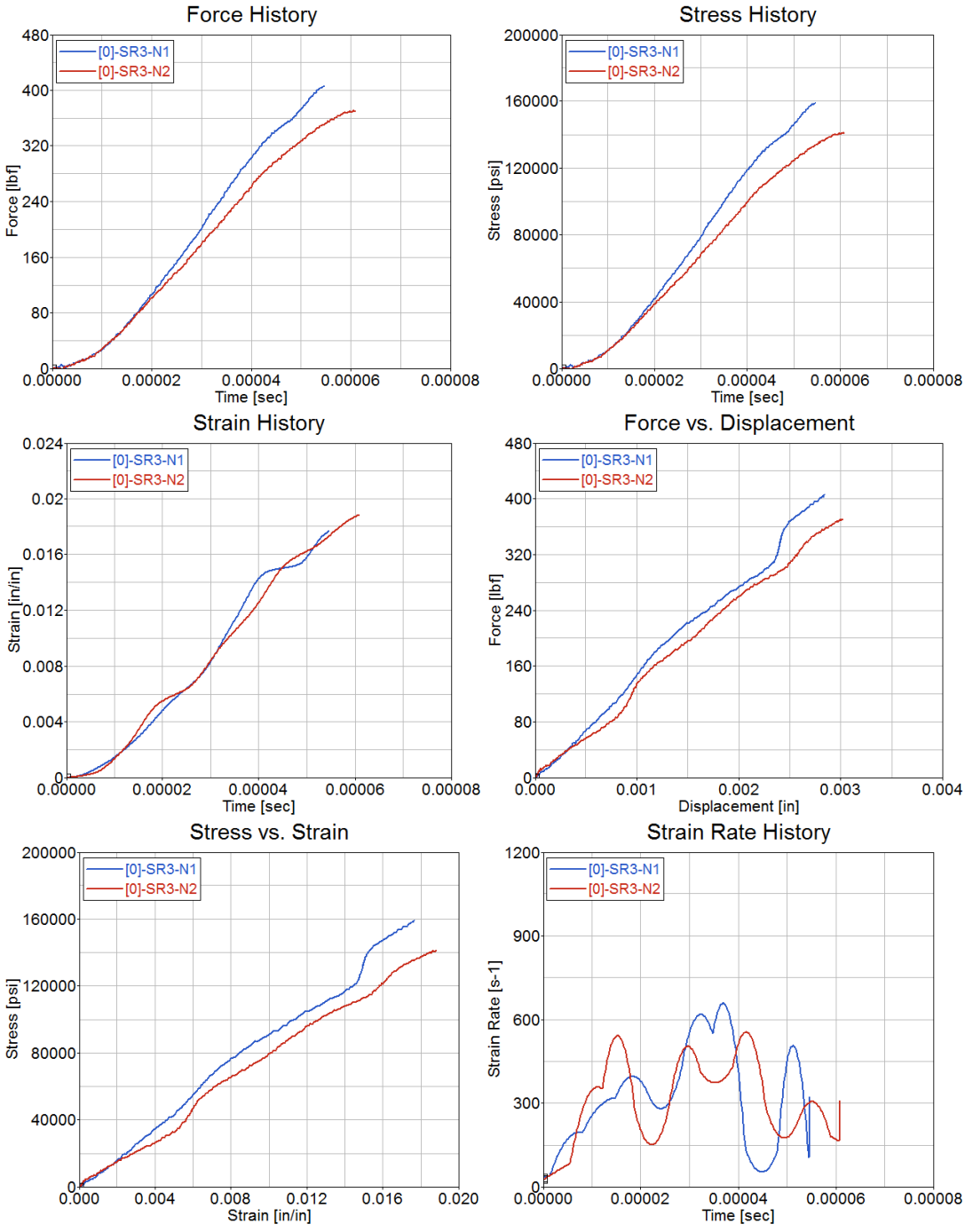

Figure E-6. Test results for Toray [0˚]$_4$ at test rate SR3

TORAY $[90]_4$

Table E-4. Summary of test results for Toray $[90^{\circ}]_4$ at test rate SR1

TEST RATE	SPECIMEN NO.	TENSILE STRENGTH [psi]	MAXIMUM RECORDED STRAIN [in/in]	YOUNG'S MODULUS [Msi]	AVERAGE STRAIN RATE [s^{-1}]
SR1	[90]-SR1-N1	124823	0.0176	7.02	0.000167
	[90]-SR1-N2	115459	0.0144	8.16	0.000155
AVERAGE		120141	0.0160	7.59	0.000161
STANDARD DEVIATION		6622	0.0023	0.81	0.000009
COEFFICIENT OF VARIATION [%]		5.51	14.07	10.62	5.50

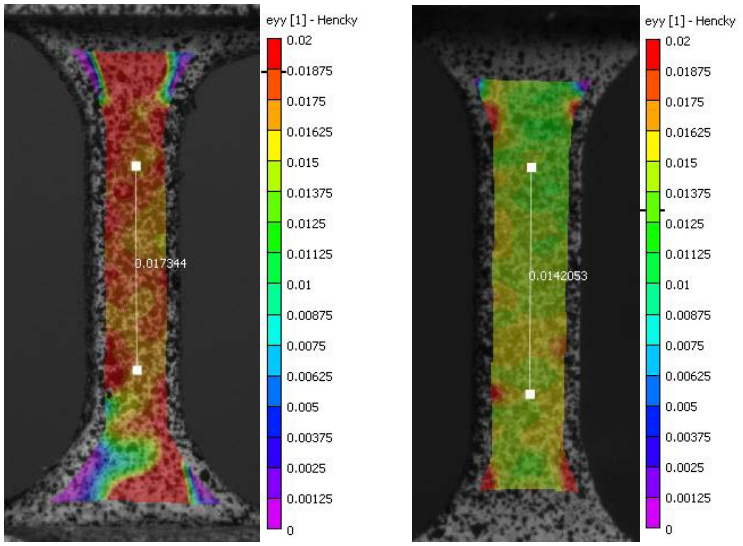

Figure E-7. Strain distribution before failure of Toray $[90^{\circ}]_4$ at test rate SR1

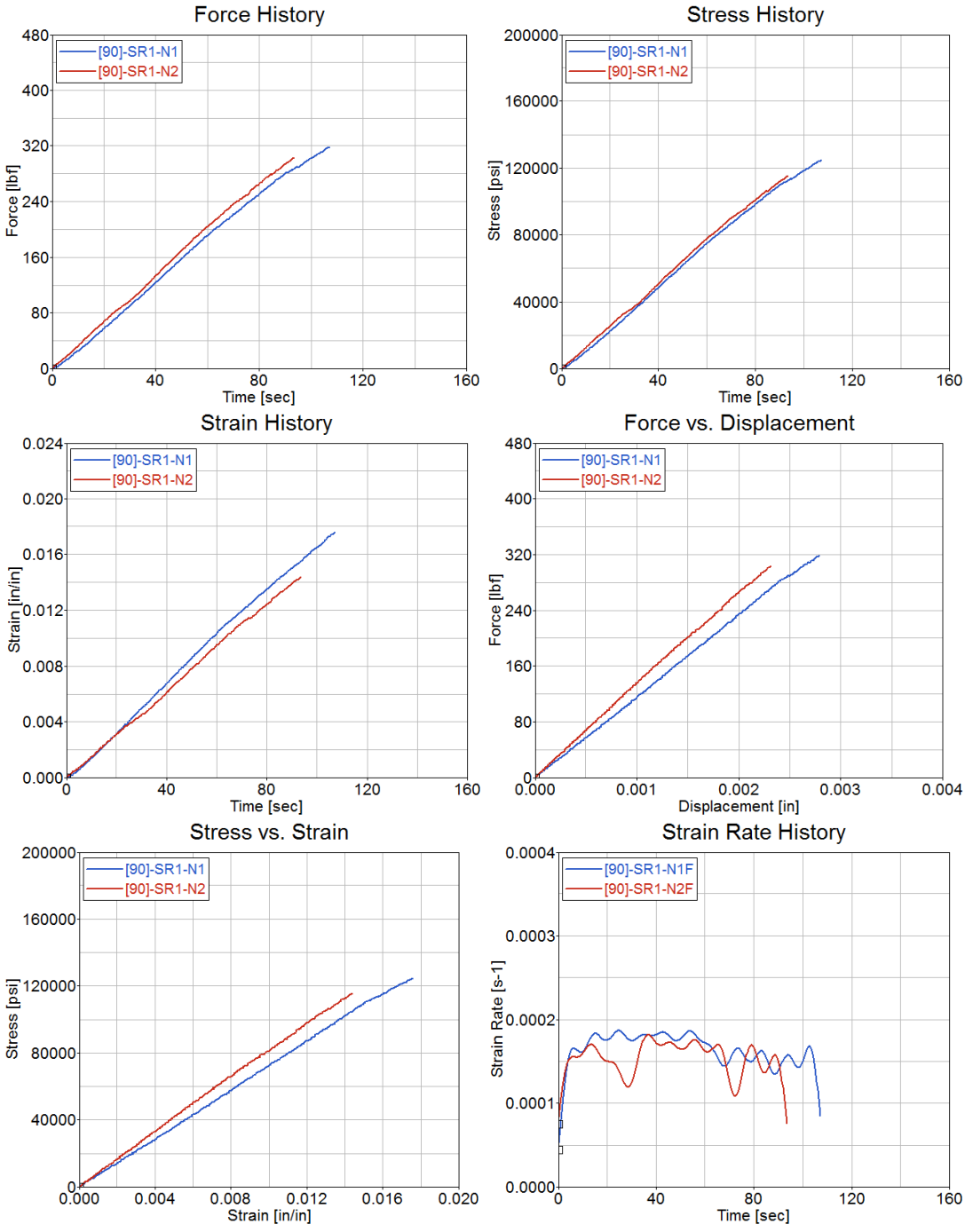

Figure E-8. Test results for Toray [90˚]$_4$ at test rate SR1

Table E-5. Summary of test results for Toray [90˚]$_4$ at test rate SR2

TEST RATE	SPECIMEN NO.	TENSILE STRENGTH [psi]	MAXIMUM RECORDED STRAIN [in/in]	YOUNG'S MODULUS [Msi]	AVERAGE STRAIN RATE [s^{-1}]
SR2	[90]-SR2-N1	132953	0.0164	7.29	181.03
	[90]-SR2-N2	113914	0.0149	7.57	213.94
AVERAGE		123433	0.0157	7.43	197.49
STANDARD DEVIATION		13462	0.0010	0.20	23.27
COEFFICIENT OF VARIATION [%]		10.91	6.64	2.66	11.78

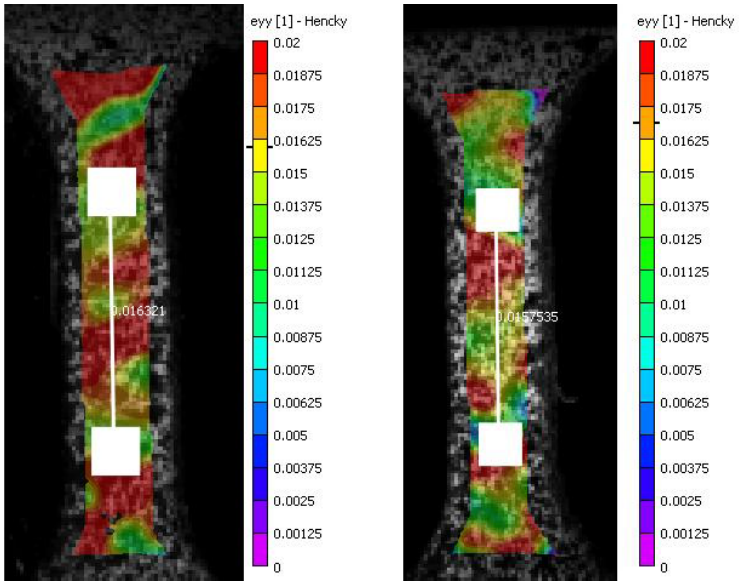

Figure E-9. Strain distribution before failure of Toray [90˚]$_4$ at test rate SR2

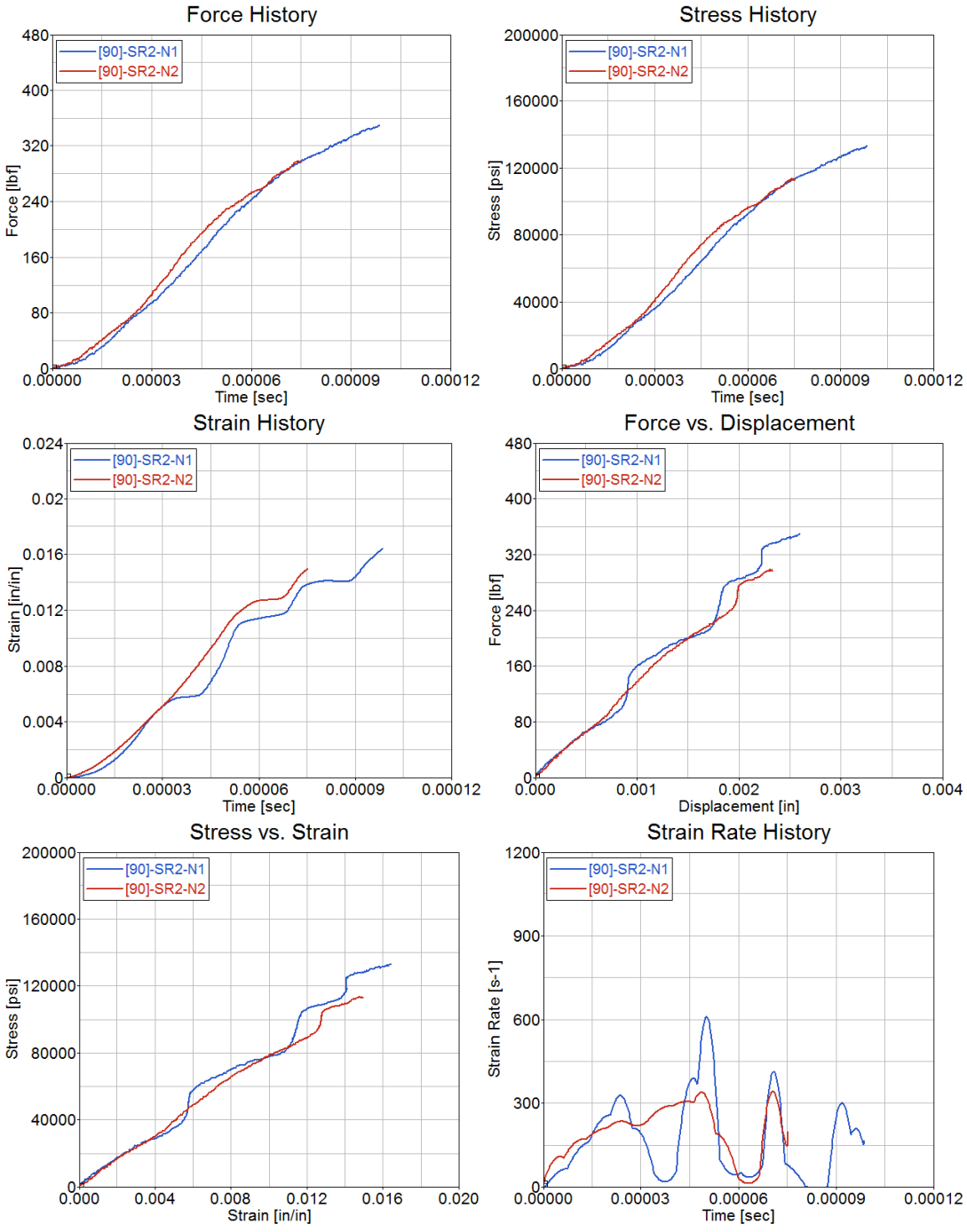

Figure E-10. Test results for Toray [90˚]$_4$ at test rate SR2

Table E-6. Summary of test results for Toray [90˚]$_4$ at test rate SR3

TEST RATE	SPECIMEN NO.	TENSILE STRENGTH [psi]	MAXIMUM RECORDED STRAIN [in/in]	YOUNG'S MODULUS [Msi]	AVERAGE STRAIN RATE [s^{-1}]
SR3	[90]-SR3-N1	147387	0.0164	5.34	323.76
	[90]-SR3-N2	103991	0.0149	4.67	454.65
AVERAGE		125689	0.0156	5.01	389.21
STANDARD DEVIATION		30685	0.0011	0.47	92.55
COEFFICIENT OF VARIATION [%]		24.41	7.06	9.47	23.78

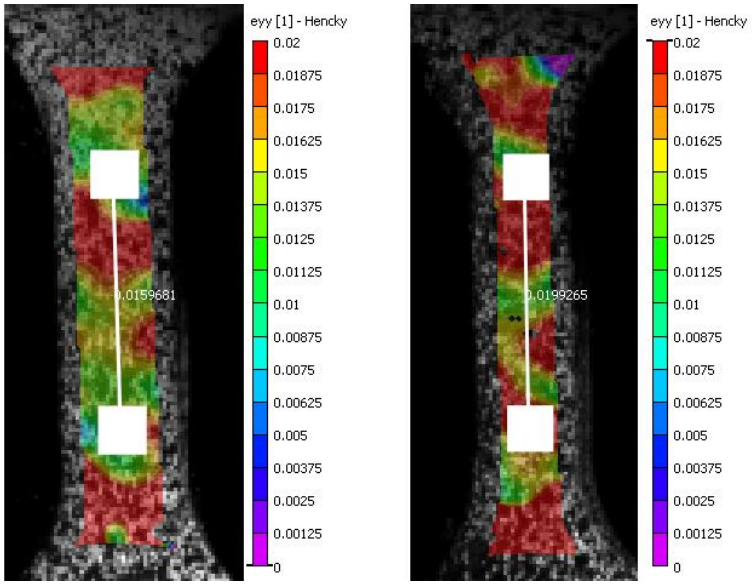

Figure E-11. Strain distribution before failure of Toray [90˚]$_4$ at test rate SR3

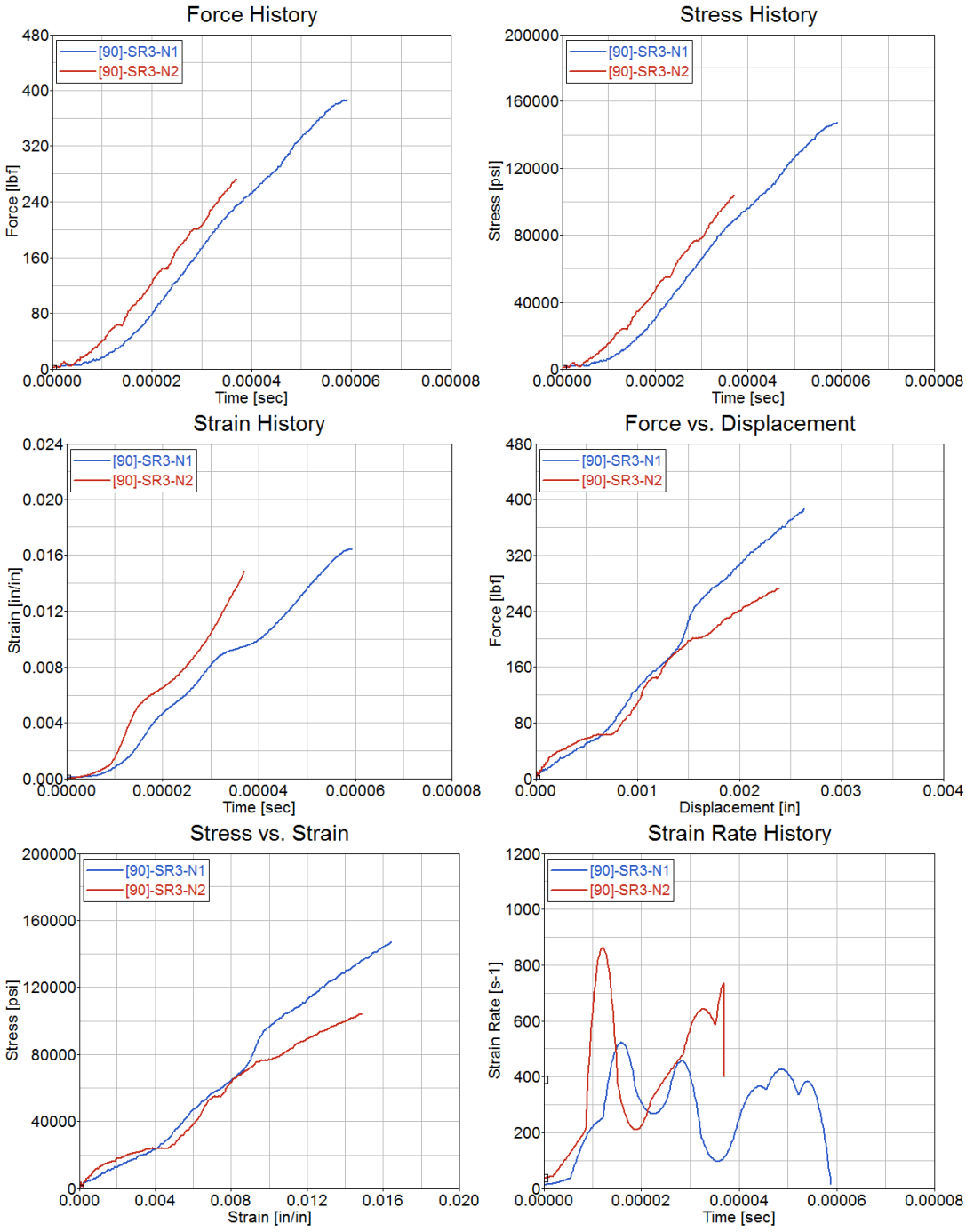

Figure E-12. Test results for Toray [90˚]$_4$ at test rate SR3

TORAY [±45°]$_4$

Table E-7. Summary of test results for Toray [±45°]$_4$ at test rate SR1

TEST RATE	SPECIMEN NO.	TENSILE STRENGTH [psi]	MAXIMUM RECORDED STRAIN [in/in]	YOUNG'S MODULUS [Msi]	AVERAGE STRAIN RATE [s^{-1}]
SR1	[45]-SR1-N1	14583	0.0242	1.69	0.000595
AVERAGE		-	-	-	-
STANDARD DEVIATION		-	-	-	-
COEFFICIENT OF VARIATION [%]		-	-	-	-

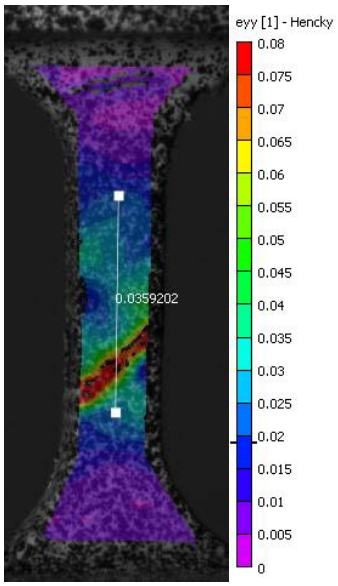

Figure E-13. Strain distribution before failure of Toray [±45°]$_4$ at test rate SR1

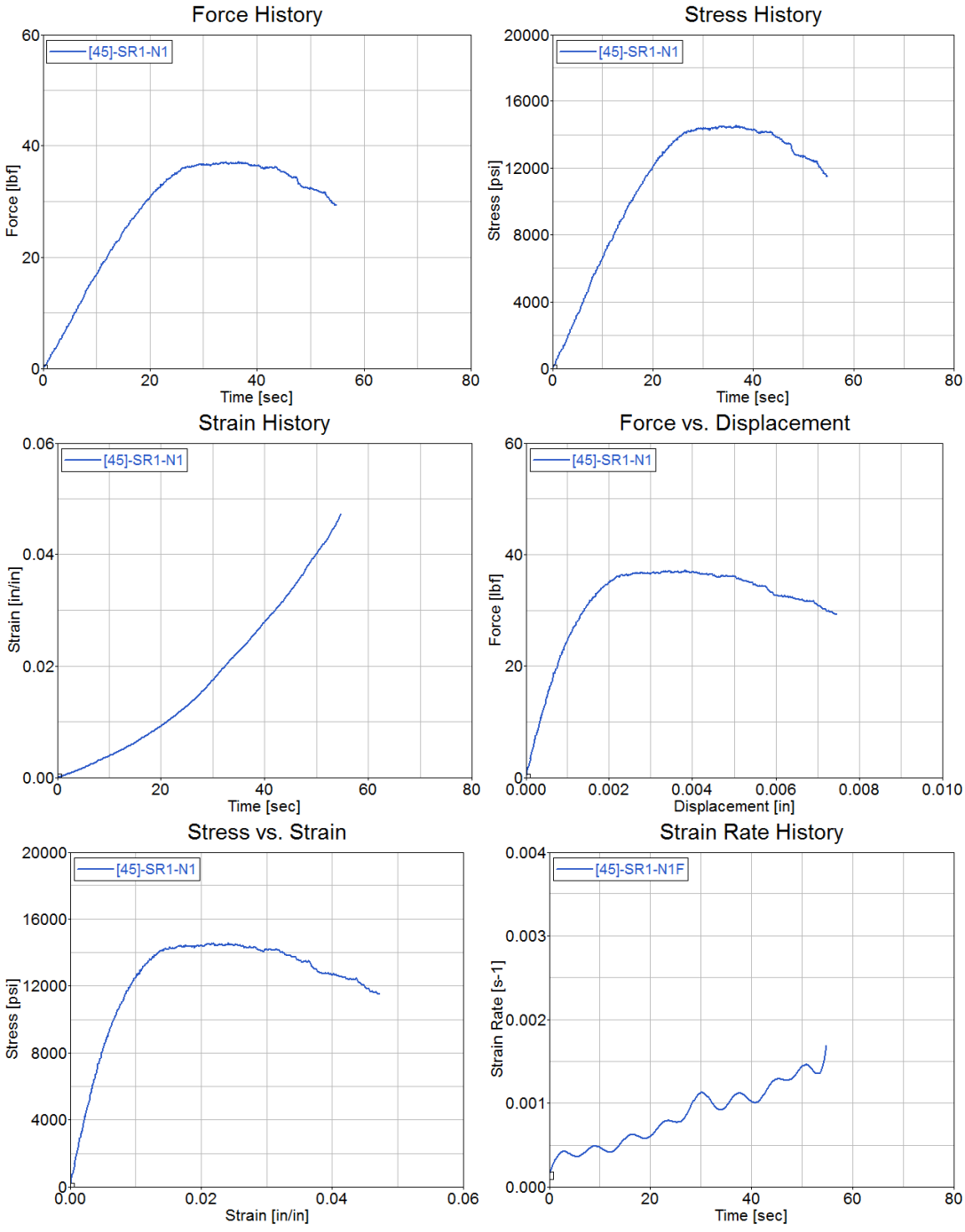

Figure E-14. Test results for Toray [±45˚]$_4$ at test rate SR1

Table E-8. Summary of test results for Toray [±45°]$_4$ at test rate SR2

TEST RATE	SPECIMEN NO.	TENSILE STRENGTH [psi]	MAXIMUM RECORDED STRAIN [in/in]	YOUNG'S MODULUS [Msi]	AVERAGE STRAIN RATE [s^{-1}]
SR2	[45]-SR2-N1	18776	0.0217	1.66	369.46
	[45]-SR2-N2	22348	0.0220	1.37	310.98
AVERAGE		20562	0.0219	1.52	340.22
STANDARD DEVIATION		2525	0.0002	0.21	41.35
COEFFICIENT OF VARIATION [%]		12.28	0.98	13.54	12.16

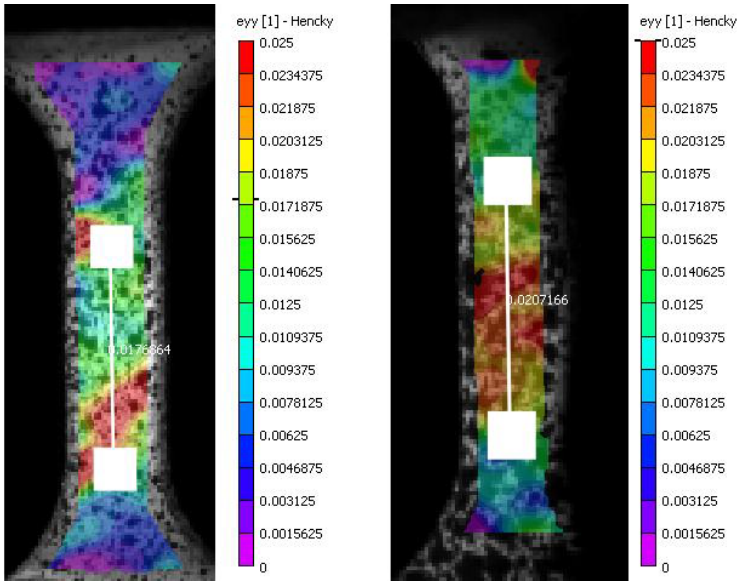

Figure E-15. Strain distribution before failure of Toray [±45°]$_4$ at test rate SR2

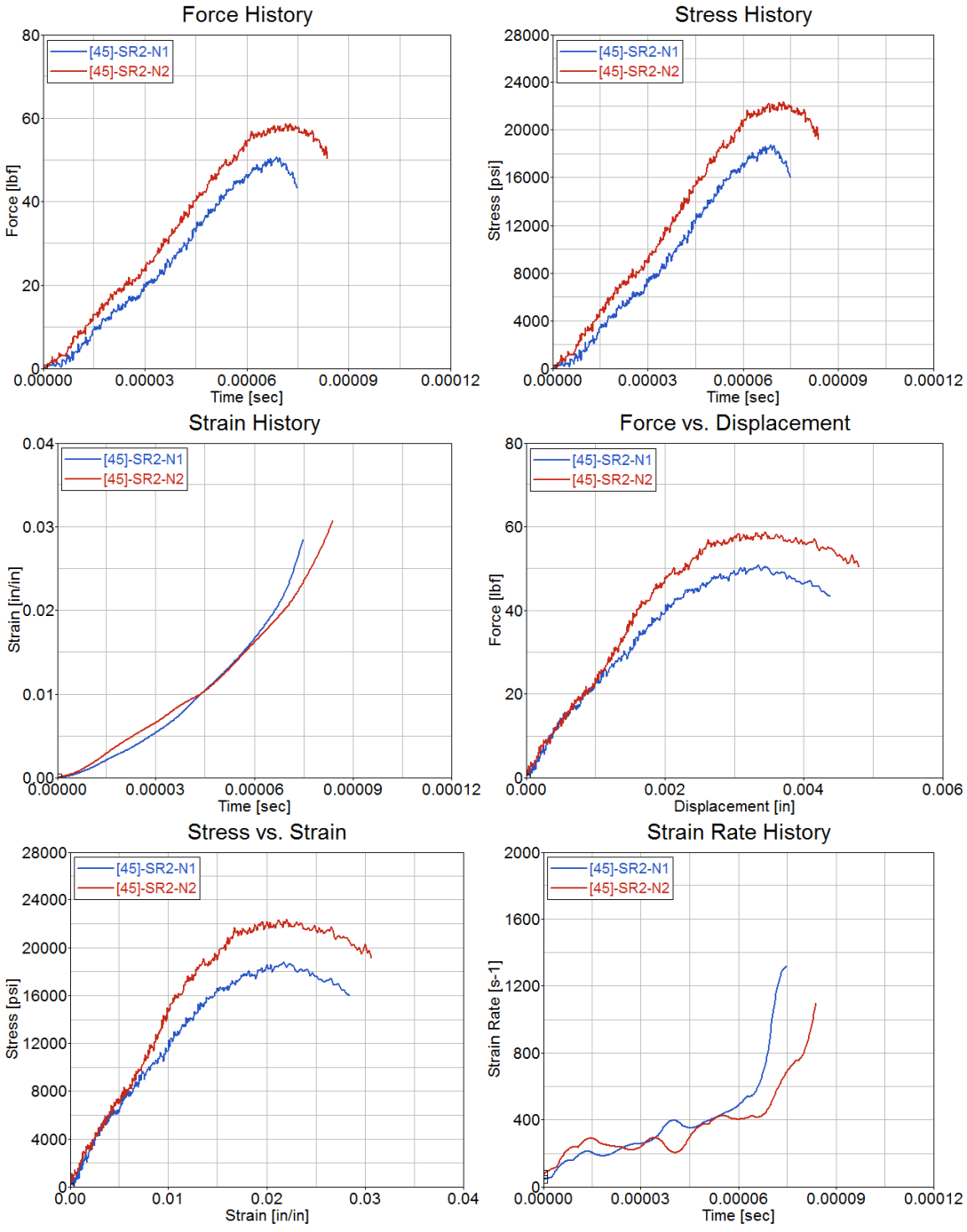

Figure E-16. Test results for Toray [±45˚]$_4$ at test rate SR2

APPENDIX F—NIAR QUASI-STATIC RAW TESTING RESULTS

Tests were conducted at the National Institute of Aviation Research at Wichita State University using a conventional servo-hydraulic testing machine.

ALUMINUM 2024-T3

Table F-1. Summary of test results for aluminum 2024-T3 at stroke rate of 0.00083 in/s

STROKE RATE [in/sec]	SPECIMEN NO.	TENSILE STRENGTH [psi]	MAXIMUM RECORDED STRAIN [in/in]	YOUNG'S MODULUS [Msi]	YIELD STRESS [psi]	AVERAGE STRAIN RATE [s^{-1}]
0.00083	R-QS-24	69906	0.1120	9.96	52633	0.000853
	R-QS-79	69953	0.1682	9.84	54164	0.000861
	R-QS-58	70061	0.1505	9.95	51296	0.000843
	R-QS-16	70895	0.1957	9.77	55378	0.000867
AVERAGE		70204	0.1566	9.88	53368	0.000856
STANDARD DEVIATION		465	0.0351	0.09	1781	0.000010
COEFFICIENT OF VARIATION [%]		0.66	22.40	0.92	3.34	1.21

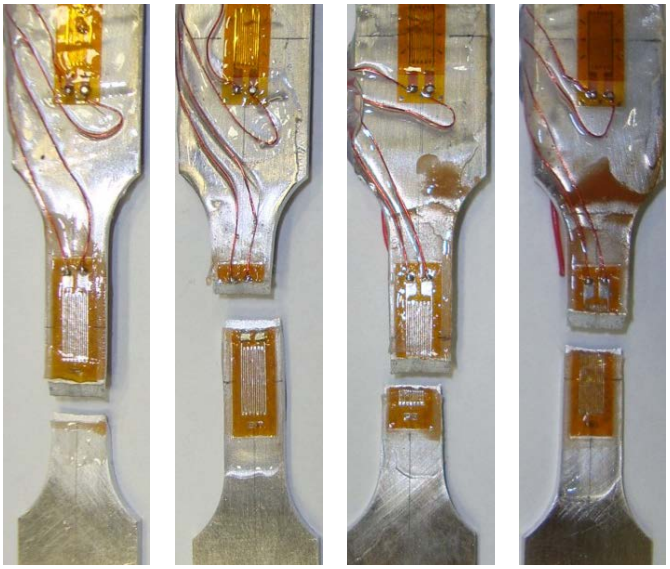

Figure F-1. Failure modes for aluminum 2024-T3 at stroke rate of 0.00083 in/s

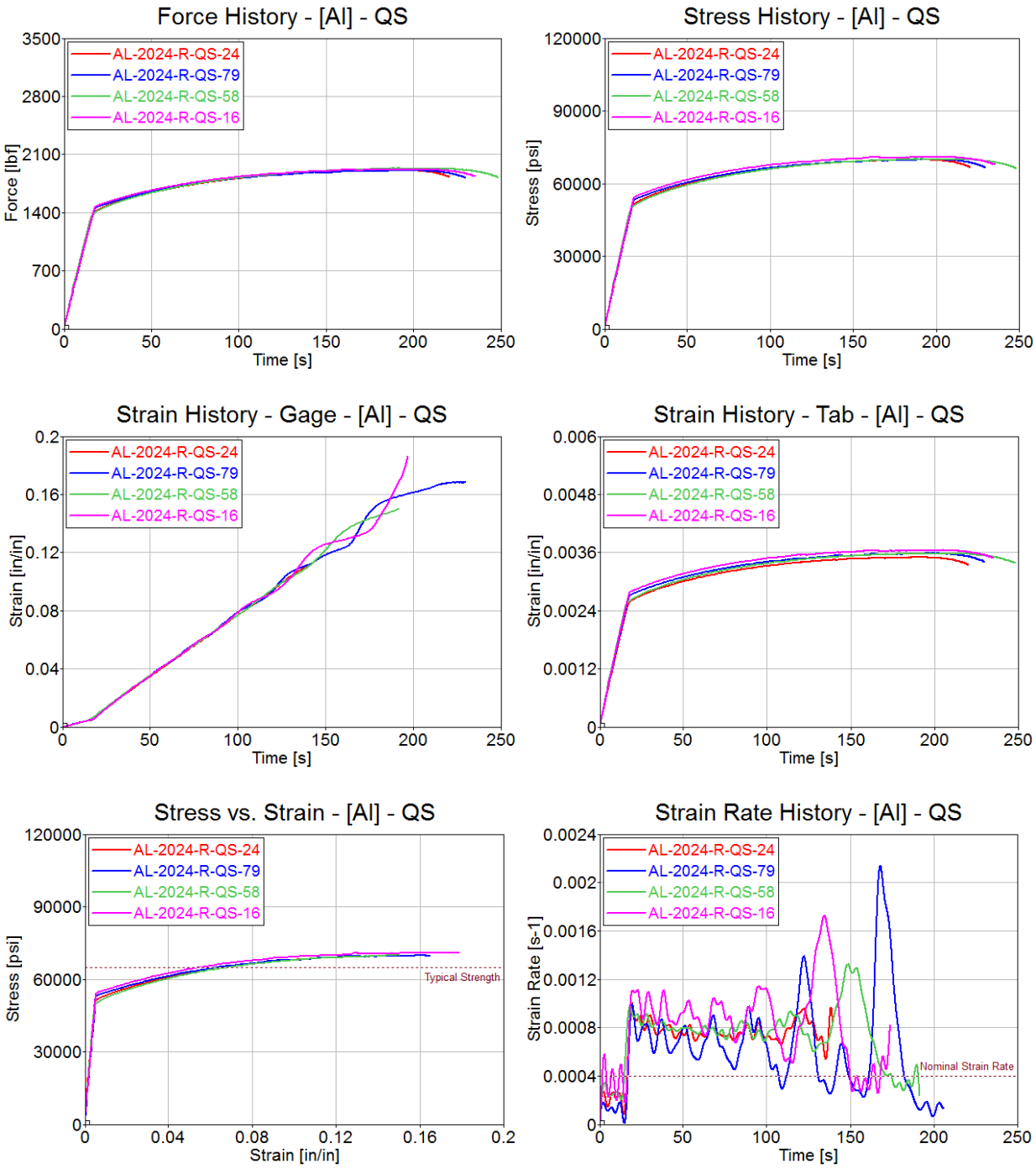

Figure F-2. Test results for aluminum 2024-T3 at stroke rate of 0.00083 in/s

TORAY $[0^{\circ}]_4$

Table F-2. Summary of test results for Toray $[0^{\circ}]_4$ at stroke rate of 0.00083 in/s

STROKE RATE [in/sec]	SPECIMEN NO.	TENSILE STRENGTH [psi]	MAXIMUM RECORDED STRAIN [in/in]	YOUNG'S MODULUS [Msi]	AVERAGE STRAIN RATE [s^{-1}]
0.00083	RR-P1-0-1-12-QS	155075	0.0173	8.62	0.000257
	RR-P1-0-2-13-QS	167571	0.0189	8.23	0.000282
	RR-P1-0-3-23-QS	159459	0.0183	7.91	0.000264
AVERAGE		160701	0.0182	8.25	0.000268
STANDARD DEVIATION		6340	0.0008	0.36	0.000013
COEFFICIENT OF VARIATION [%]		3.95	4.49	4.30	4.82

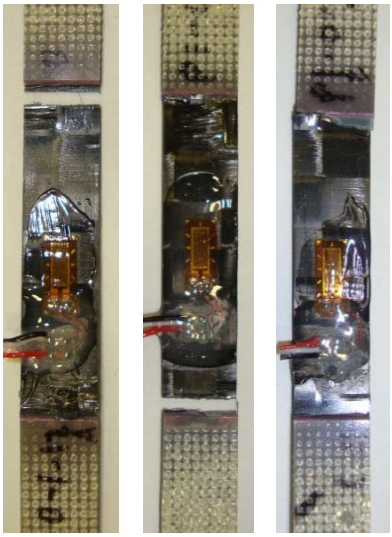

Figure F-3. Failure modes for Toray $[0^{\circ}]_4$ at stroke rate of 0.00083 in/s

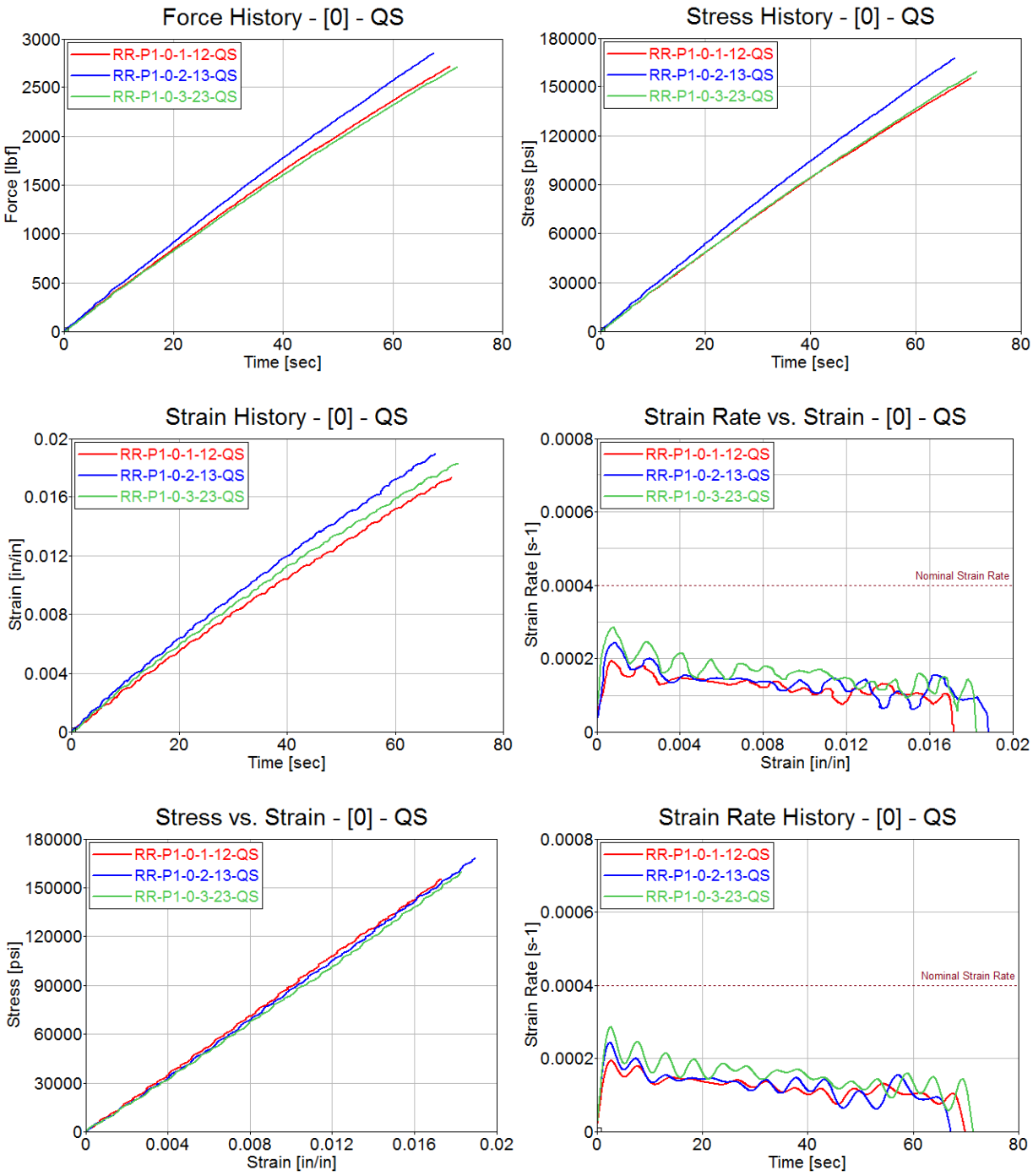

Figure F-4. Test results for Toray [0˚]$_4$- at stroke rate of 0.00083 in/s

TORAY $[90]_4$

Table F -3. Summary of test results for Toray $[90^{\circ}]_4$ at stroke rate of 0.00083 in/s

STROKE RATE [in/sec]	SPECIMEN NO.	TENSILE STRENGTH [psi]	MAXIMUM RECORDED STRAIN [in/in]	YOUNG'S MODULUS [Msi]	AVERAGE STRAIN RATE [s^{-1}]
0.00083	RR-P2-90-3-16-QS	144412	0.0158	8.97	0.000245
	RR-P2-90-4-3-QS	150485	0.0164	9.12	0.000235
	RR-P2-90-4-12-QS	151466	0.0171	8.23	0.000245
AVERAGE		148788	0.0164	8.77	0.000242
STANDARD DEVIATION		3821	0.0006	0.48	0.000006
COEFFICIENT OF VARIATION [%]		2.57	3.90	5.44	2.39

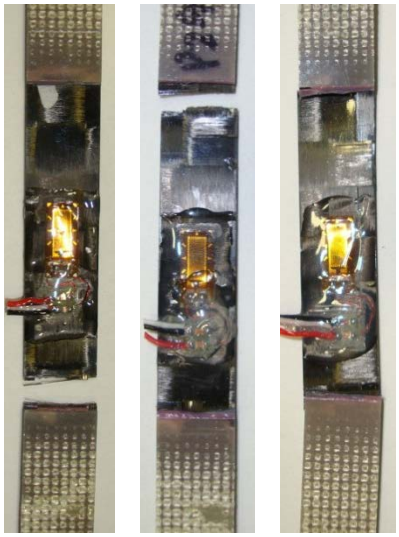

Figure F-5. Failure modes for Toray $[90^{\circ}]_4$ at stroke rate of 0.00083 in/s

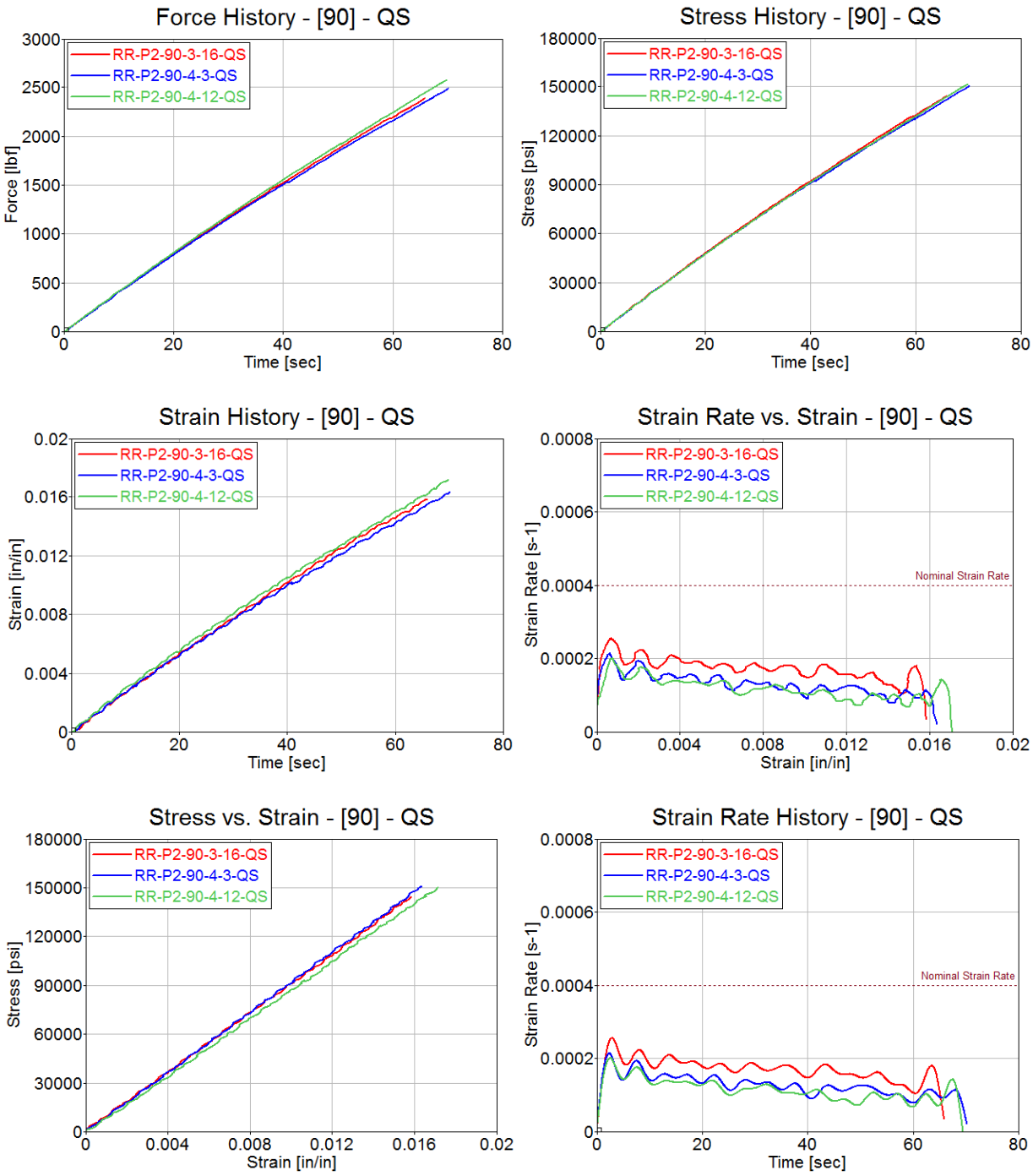

Figure F-6. Test results for Toray [90˚]$_4$ at stroke rate of 0.00083 in/s

TORAY $[\pm 45^{\circ}]_4$

Table F -4. Summary of test results for Toray $[\pm 45^{\circ}]_4$ at stroke rate of 0.00083 in/s

STROKE RATE [in/sec]	SPECIMEN NO.	TENSILE STRENGTH [psi]	MAXIMUM RECORDED STRAIN [in/in]	YOUNG'S MODULUS [Msi]	AVERAGE STRAIN RATE [s^{-1}]
0.00083	RR-P4-45-1-6-QS	30884	*	1.93	0.000382
	RR-P4-45-2-17-QS	27380	*	1.85	0.000408
	RR-P4-45-2-19-QS	30981	*	2.13	0.000335
AVERAGE		29748	-	1.97	0.000375
STANDARD DEVIATION		2051	-	0.14	0.000037
COEFFICIENT OF VARIATION [%]		6.90	-	7.30	9.87

*Exceeded strain gauge capability of 0.03 in/in

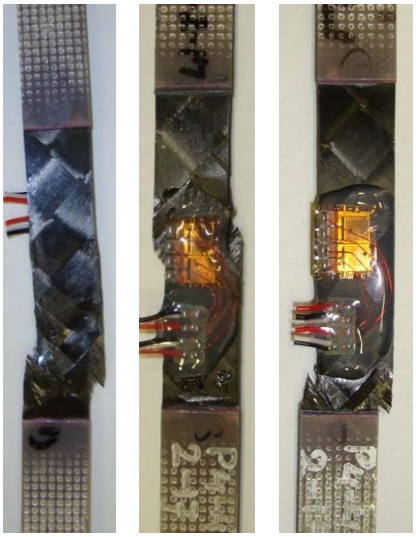

Figure F-7. Failure modes for Toray $[\pm 45^{\circ}]_4$ at stroke rate of 0.00083 in/s

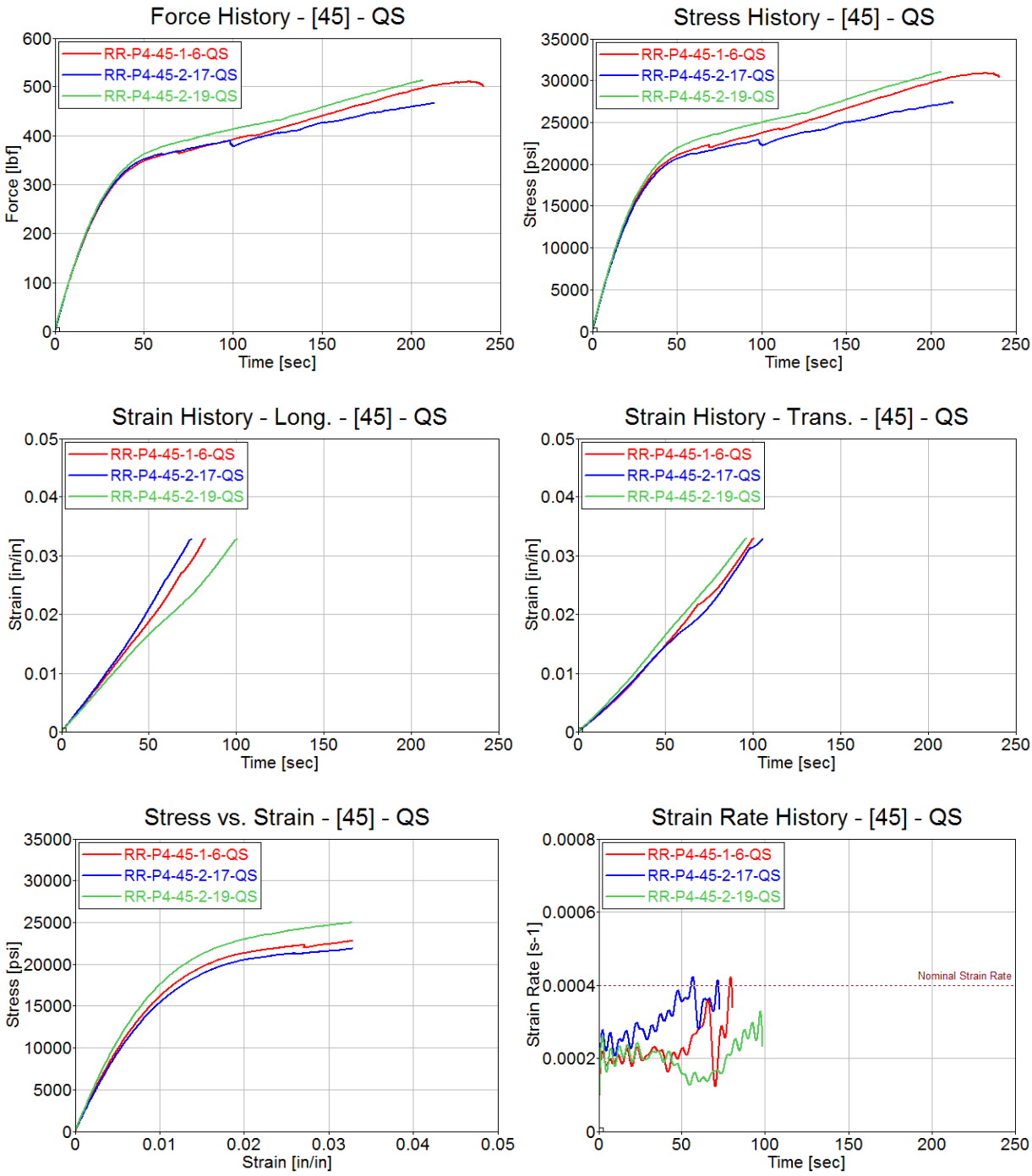

Figure F-8. Test results for Toray [±45°]$_4$ at stroke rate of 0.00083 in/s

APPENDIX G—TEST PROCEDURE FOR USE OF NIAR SLACK INDUCER APPARATUS

This section describes the test procedure/guidelines to be followed when using the National Institute of Aviation Research (NIAR) slack-inducer apparatus. Any deviations must be described in the final report.

A description of the procedure for mounting the slack adapter, wedges, and test specimen follows. Refer to figures 5 and 10 in section 2.6.1 for illustrations of the same.

i. Fasten the slack adapter tube to the actuator using an appropriate all-thread rod (figure G-1). The slack adapter has a 1-14 UNS thread for attachment to the actuator. Use of lock washers between the slack tube and actuator is optional. However, the ends of the slack tube and actuator must be flush with each other.

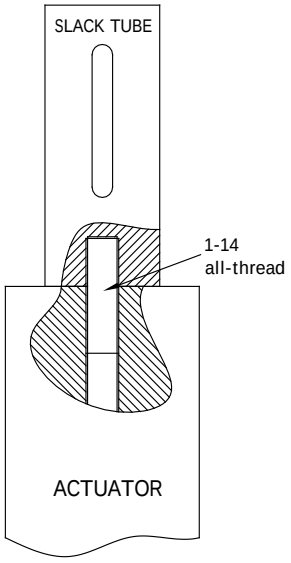

Figure G-1. Connecting slack tube to the actuator

ii. Insert the damping washer around the slack rod head (figure G-2).

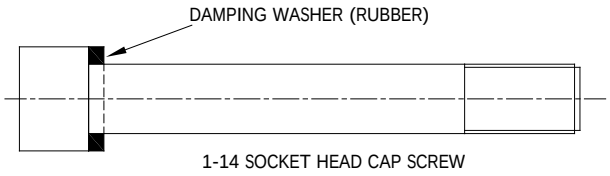

Figure G-2. Slack rod with damping washer

iii. Insert the slack rod in the slack tube.

iv. Fasten the bearing/arrest block to the slack-adapter tube. The threaded end of the slack rod should protrude out of the bearing/arrest block and should slide easily through the bearing (figure G-3).

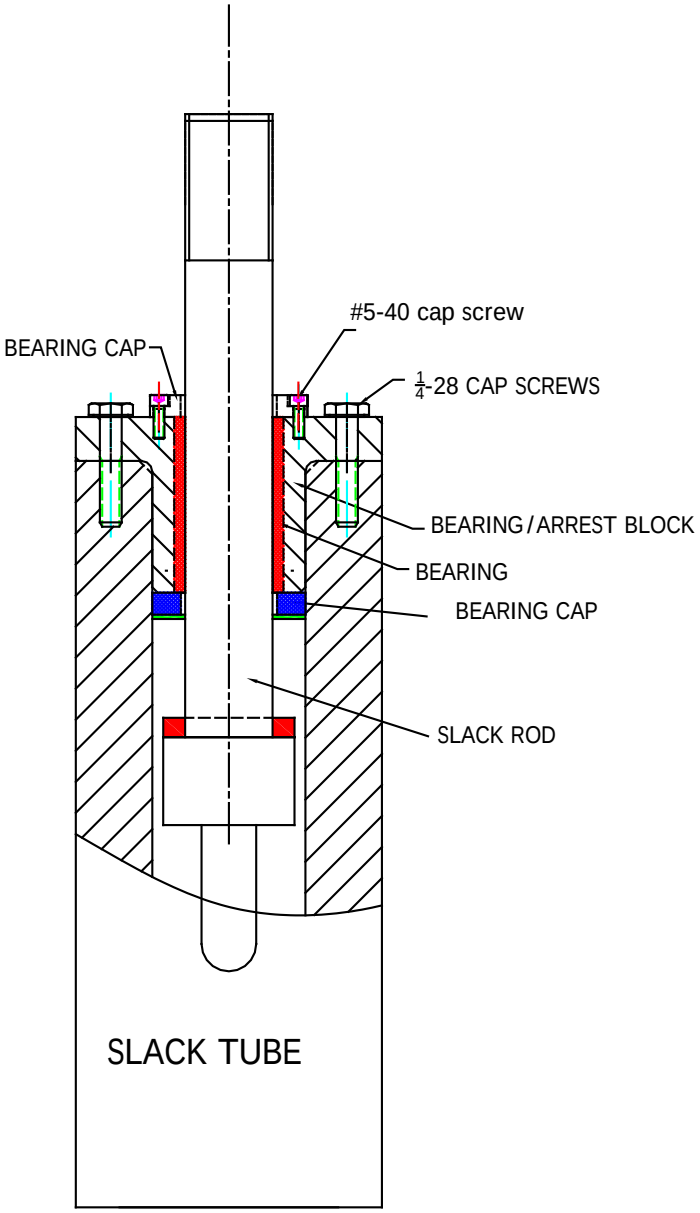

Figure G-3. Slack inducer assembly

v. Fasten the grip attach block for the lower grips to the threaded end of the slack rod (figure G-4).

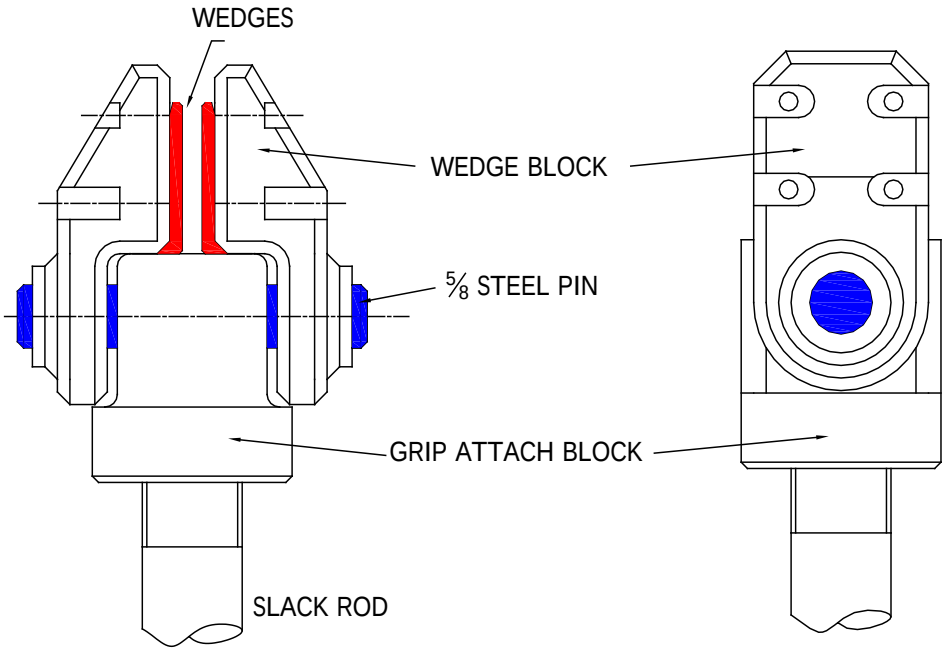

Figure G-4. Wedge grip assembly

vi. Mount the load cell (not provided by NIAR) to the fixed end of the testing machine (figure G-5).

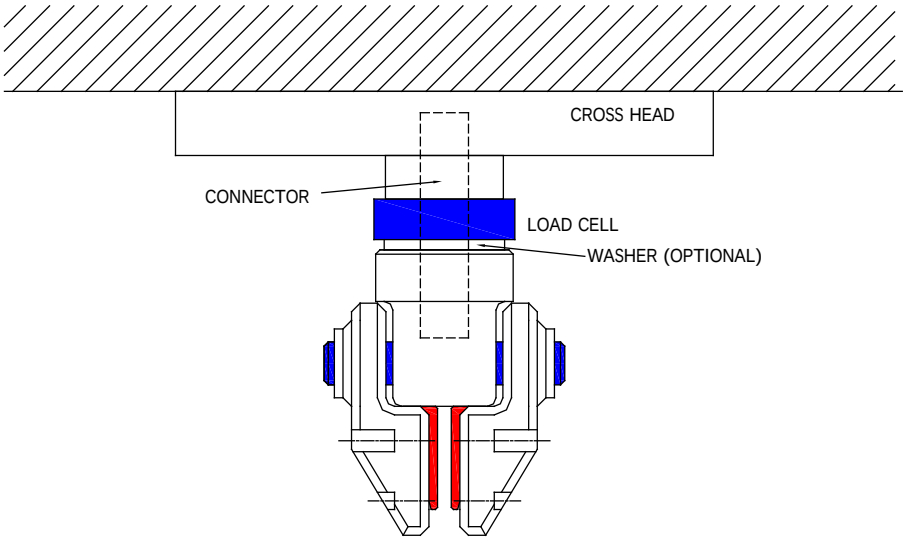

Figure G-5. Load-cell and upper-grip assembly

vii. Fasten the grip attach block for the upper grips to the load cell. Appropriate torque may be applied to preload the load cell (piezoelectric) if necessary.

viii. Mount the wedge blocks to the grip-attach blocks using the pins provided.

ix. Apply a thin layer of grease on the inclined surface of the wedges that come into contact with the wedge blocks.

x. Insert the gripping fasteners through the holes in the pair of wedge blocks.

xi. Mount the extended length nuts on the fasteners, but do not tighten (figure G-6).

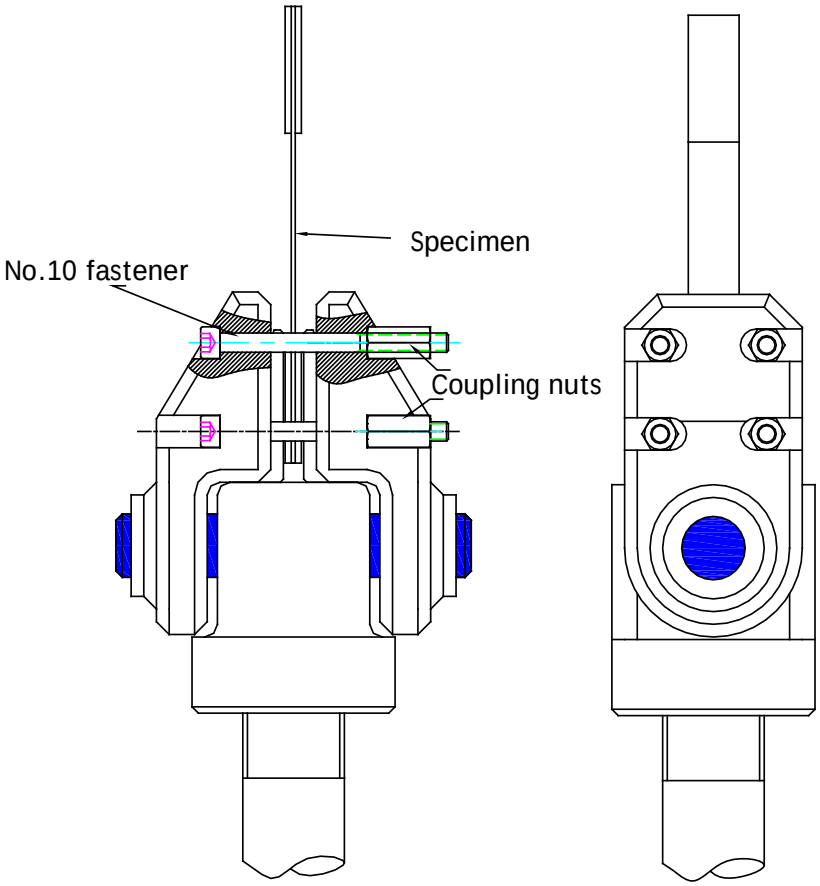

Figure G-6. Wedge grip block with gripping fastener and nut installed

xii. Insert specimen end between the wedges. Center the specimen across the width using the alignment tool (figure G-7). The wedges are 0.6 inches wide, and the composite specimens are 0.5 inches wide. The alignment tool facilitates centering of the composite specimen across the width. When mounting the aluminum specimen, whose grip regions is 0.6 inches wide, the centering tool may not be necessary. The edge of the aluminum specimen should be flush with that of the wedges.

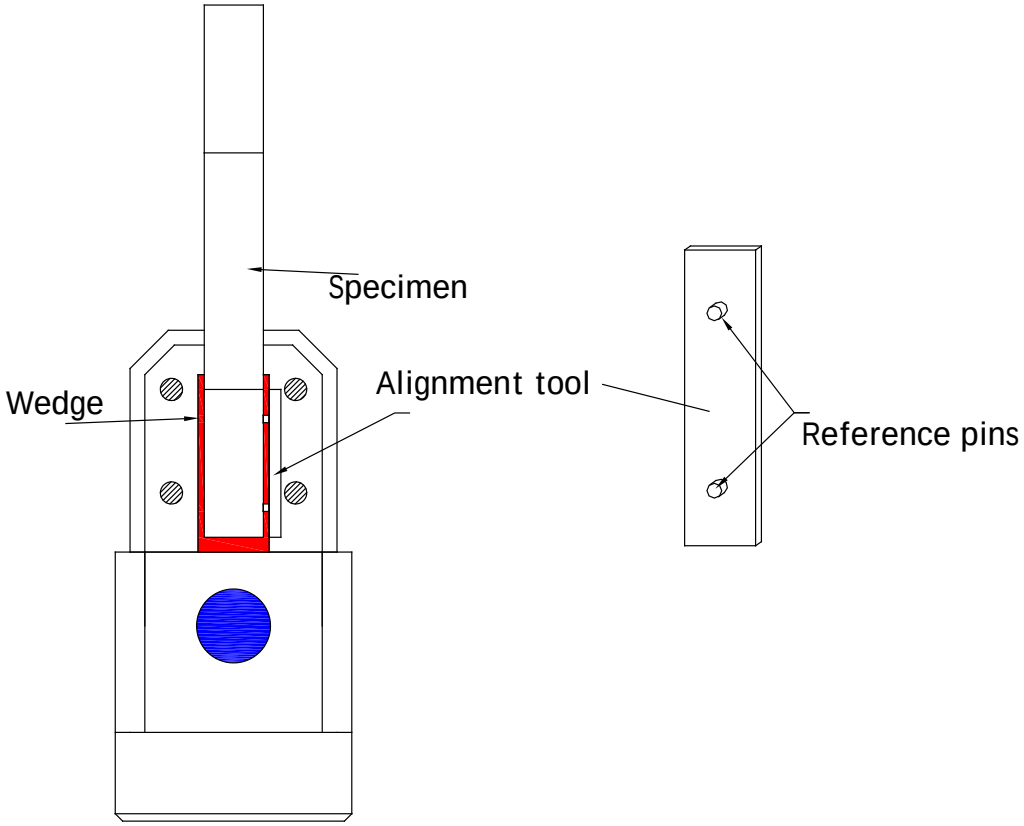

Figure G-7. Alignment of specimens in the grips

xiii. Clamp the specimen by tightening the fasteners using a minimum torque of **40 in-lbs**. The specimen may be clamped between the lower grips first and followed by the upper grips. Tighten the socket-head cap screws incrementally to avoid "pinching" of the specimen tabs, which could lead to undesirable failure modes.

xiv. When gripping the aluminum specimens, the extended tab should be gripped using the wedge grips attached to the load cell, as shown in figure G-8.

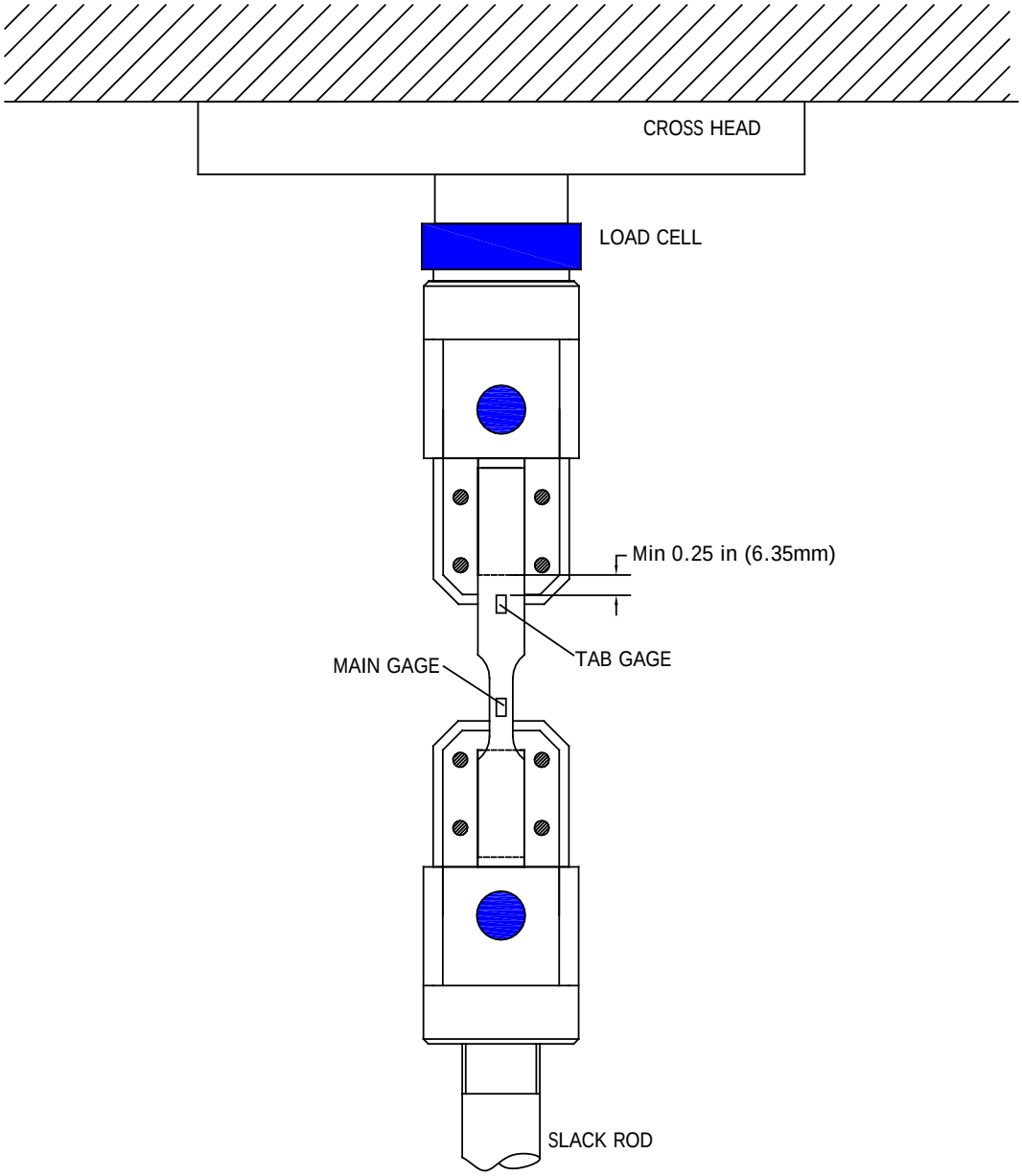

Figure G-8. Specimen orientation for extended tab aluminum specimens

REPORT FORMAT

The test report should contain the following information about the test apparatus, data acquisition and, signal conditioner, preferably in the following format:

Table G-1. Test report format

NO	ITEM	DESCRIPTION	COMMENTS
1	Testing machine	<model number, make>	
2.	Signal conditioning (strain gauge)	<signal conditioner model>, excitation voltage, gain, signal conditioner bandwidth, filter bandwidth	
3.	Signal conditioner (load cell)	<signal conditioner model>, excitation voltage, gain, signal conditioner bandwidth, filter bandwidth	
3.	Data acquisition	<Data acquisition card > <Resolution> <data acquisition rate>	
4.	Test environment	Temperature/humidity	
5.	Load cell	Model number, type (strain gauge based/piezoelectric), Load range, natural frequency	
6.	Stroke-measurement method	Linear variable differential transformer model number	
7.	Grips used	NIAR supplied/Other* Weight of the grip assembly	*Provide grip drawings
8.	Slack adapter	NIAR supplied/Other* <Weight of the slack rod>	*Provide drawings

The test data, which include time histories of force, stroke, and strain(s) must be submitted in electronic format for individual tests. Refer to section 2.3 for the time span over which the test data must be provided.